Dynamic mucus penetrating nanoparticles for controlled pulmonary drug delivery

Chen, Hanpeng

Awarding institution:
King's College London

Dynamic mucus penetrating nanoparticles for controlled pulmonary drug delivery

Hanpeng Chen

In fulfilment of the requirement

for the degree of Doctor of Philosophy (PhD)

Institute of Pharmaceutical Science

King’s College London

August 2016

Acknowledgements

I would like to express my gratitude to Dr Stuart Jones and Prof Ben Forbes for their exemplary supervision over the course of this project. Their ready guidance, support and encouragement have fuelled my interest, enthusiasm and understanding in this area. I am also extremely grateful for their kindness and patience whilst I came to terms with particularly difficult personal circumstances outside of work. I am also grateful to Dr Arcadia Woods for her insightful and detailed comments when proof reading this thesis.

I would like to thank the technical team of KCL, especially Dan, Bea, Dave and Steve, who provided various forms of support during this PhD. Thanks to all my colleagues, for their company over the last four years and for creating such a friendly and enjoyable atmosphere in which to work. Special thanks to Jesmine, Jasminder, Ricardo, Simon, Richard, Aateka, Magda and Abhinav.

Last but certainly not least, none of this would have been possible without the support and patience of my parents– my constant source of love, support and strength.

Abstract

Nanoparticles are promising carriers for the purpose of controlled pulmonary drug delivery because they can reside in the airways and slowly release a drug into the lung tissue. However, development into the clinic of nanoparticle products for pulmonary delivery has been limited to date due to the lack of control over the drug release process from these small carriers. In this work the feasibility of generating an inhaled nanoparticle system that could be administered to the airways, penetrate the respiratory mucus and act as a reservoir from which drug release could be controlled was explored.

Nanoparticle systems were fabricated using an emulsion phase inversion technique and a nanoprecipitation method to produce lipid nanoparticle (LNPs) and polymer nanoparticles (PVA NPs), respectively. The LNPs had a particle size of ca. 50 nm and the PVA NPs had a size of ca. 250 nm respectively. Rifampicin was loaded into nanoparticles and the release was controlled using 2 different permeabilisation strategies that were designed to encourage the drug liberation from the particles. Both permeabilisation strategies involved mixing a chemical agent with the nanoparticles to induce a carrier structural change to occur. Both LNP and PVA particles were shown to be capable of controlling the release of rifampicin using their permeabilisation agents. However, using a multidimensional diffusion model the LNPs were shown to penetrate through the mucus barrier more quickly with a rate of $30.08 \pm 2.49 \times 10^4$ nm^2/s, compared to the PVA NPs ($1.64 \pm 0.37 \times 10^4$ nm^2/s). Therefore, the LNPs were used in all the subsequent work. A novel spray drying technique was designed to fabricate microparticles to deliver the LNPs into the lung using a dry powder inhaler. The LNPs were loaded with drug and the agent that initiated the permeabilisation mechanism was incorporated into with the LNPs in micropartcles with a suitable size for airway deposition. The incorporation of LNPs with the permeabiliser into the microparticles did not diminish the ability of the LNPs to control drug release. The fate of labelled LNPs was tracked following their administration to respiratory epithelial Calu-3 cells and macrophage U937 cell lines. LNPs were found to persist at the cell surface over 8 h when delivered to a Calu-3 cell monolayer, with less than 10% of the applied particles being internalised into the cells. The permeabilisation process increased the particle uptake by both cell types which was thought to be a consequence of the particles distending upon exposure the permeabiliser. A co-culture model was developed containing the airway epithelial cells and macrophages. When the co-culture was exposed to the LNPs, the particles were found in both cell types, with a great proportion internalisated by macrophage cells.

The ability of the LNP to distend upon exposure to a chemical permeabiliser controlled release, penetrate mucus and gain preferential entry into macrophage cells in the lung suggested they could be an attractive means to deliver therapeutic agents such as rifampicin into the lung.

Table of contents

List of Publications

Journal articles

H. Chen, E. Mansfield, A. Woods, V. Khutoryanskiy, B. Forbes, S.A. Jones. Understanding the diffusion restriction of nanomaterials by mucus barriers using static and mobile gels. *Biomaterials*, in preparation.

H. Chen, A. Woods, B. Forbes, S.A. Jones. Controlled drug release from lung-targeted nanocarriers via chemically mediated shell permeabilisation. *International Journal of Pharmaceutics*, (511) 2016, 1033-1041

H. Chen, R. Amison, S. Cleary, A. Woods, B. Forbes, S.A. Jones. Understanding the cellular bio-distribution of nanocarriers in the airways of the lung. *European Journal of* Pharmaceutics and *Biopharmaceutics, i*n preparation.

A. Morgan, D. Spina, Y. Vasquez, A. Patel, H. Chen, A. Starr, E. Lau, S. Jones, B. Forbes, K. Sunassee, S. Clark, R. Rosales, C. Page, L. Dailey. Longitudinal assessment of lung health in mice following oropharyngeal aspiration of poly(vinyl acetate) nanoparticles using non-invasive computed tomography. *ACS Nano*, under review, 2015.

Conference abstracts

H. Chen, B. Forbes, S.A. Jones. Tracking nanoparticle transport through mucus. American Thoracic Society International Conference, San Diego, USA (2014).

K. Vandera, H. Chen, J. Cai, S. Baba Hamed, M.B. Baba Hamed, S.M.E.A. Abi-ayad, S.A. Jones. Novel inhaled medicines fabricated using natural cellulose nanocarriers (PP12). 1st CRS International Congress Greek Local Chapter in Small Molecules (Original-Generics) and Biotechnological Drugs (Biosimilars), Athens, Greece (2015).

J.Y.Tai, H. Chen, S.A. Jones.Controlled Delivery to the Lung – Nanoparticle Penetration through Mucus. BPSA 73rd Annual Conference, Liverpool, UK (2015).

H. Chen, E. Mansfield, A. Woods, V. Khutoryanskiy, B. Forbes, S.A. Jones. Understanding the fate of distensible lipid nanocapsules in the lung using a multidimensional mucus diffusion model. Crossing Biological Barriers - Advances in Nanocarrier Design for Targeted Drug Delivery, Dresden, Germany (2015).

List of Figures

List of Tables

List of Equations

List of Abbreviations

ANOVA	Analysis of variance
ATDs	Antitubercular drugs
BNF	British National Formulary
BSA	Bovine serum albumin
CFC	Chlorofluorocarbons
CFM	Cystic fibrosis mucus
CLSM	Confocal laser scanning microscopy
CMC	Critical micelle concentration
COPD	Chronic obstructive pulmonary disease
CVM	Cervicovaginal mucus
CV	Coefficient of variation
DMF	Dimethyl formamide
DMPE	1,2-dimyristoyl-sn-glycero-3-phosphoethanolamine
DMSO	Dimethyl sulphoxide
DPI	Dry powder inhaler
DTPA	Diethylene triaminepentaacetic acid
EDTA	Ethylene diamine tetraacetic acid
EO	Ethylene oxide
FACS	Fluorescence-activated cell sorting
FBS	Fetal bovine serum
FDA	Food and Drug Administration

FTIR	Fourier transform infrared spectroscopy
HA	Hyaluronic acid
HBSS	Hank’s balanced salt solution
HFA	Hydrofluoroalkanes
HIC	Hydrophobic interaction chromatography
HPLC	High performance liquid chromatography
LNP	Lipid nanoparticle
LOD	Limit of detection
LOQ	Limit of quantification
LPP	Large porous particle
MCC	Mucociliary clearance
MDR	Multidrug-resistant
MMAD	Mass median aerodynamic diameter
MP	Microparticle
MPT	Multiple particle tracking
MTT	3-(4,5-Dimethylthiazol-2-yl)-2,5-diphenyltetrazolium bromide
NP	Nanoparticle
PBS	Phosphate buffered saline
PCS	Photon correlation spectroscopy
PEG	Polyethylene glycol
PGM	Porcine gastric mucus
PLGA	Poly(glycolic-co-lactic-acid)

pMDI	Pressurised metered dose inhaler
PNAP	Porous nanoparticle-aggregate particle
PO	Propylene oxide
PS	Polystyrene
PVA	Poly(vinyl alcohol)
SBS	Salbutamol sulfate
SDS	Sodium dodecyl sulphate
SD	Standard deviation
SEM	Scanning electron microscopy
SPSS	Statistical Package for Social Sciences
TB	Tuberculosis
TEM	Transmission electron microscopy
TER	Transepithelial electrical resistance
WHO	World Health Organization

CHAPTER ONE

Introduction

1.1 General introduction

Drug delivery refers to the approach taken to transport a pharmaceutical agent to its desired site of action in the body (Park, 2014). Various routes of drug administration can be used and hence a number of different formulations and devices have been developed for drug delivery (Jain, 2014).

There is increasing interest in the delivery of drugs viathe lungs to treat a variety of diseases. The large surface areas of the airways, abundant blood supply and thin epithelial layer render this route of delivery attractive to several types of therapeutic agents (Patton and Byron, 2007). Inhaled medicines are most frequently characterized by a rapid onset of activity. This may be due to the rapid absorption of molecules across the respiratory epithelium and subsequent systemic exposure. This enables some parenterally administrated therapies to be delivered to the airways for either local or systemic action. The recent use of inhaled anti-microbial therapiesis a good example of injectable agents being delivered via the lungs (Zhou et al., 2015). In the case of antibiotics, lung delivery results in a potent local action and minimal systemic exposure. However, the rapid clearance of molecules from the airways of the lung does limit the applicability of the inhaled route to some agents that would benefit from sustained local tissue or plasma concentrations. This could be solved if a good controlled release system could be developed for the lungs.

The small size of nanomaterials provides the opportunity to generate controlled drug delivery in the lung (Ibrahim and Garcia-Contreras, 2013). However, nanomaterials must be non-immunogenic and biocompatible if they are to reside in the airways for a sufficient length of time to provide controlled drug release (Kumari et al., 2010). The context of the lung airways offers particular challenges for nanosystem residence because the airways are highly sensitive to inflammation and they are highly efficient at clearing deposited materials. Achieving sustained therapeutic effects using a nanocarier requires the carrier to pass through the mucus after deposition in the airways, avoid mucocilliary clearance and rapid absorption. This challenge has yet to be overcome in a clinical setting and as a result there are no commercial systems that have managed to achieve controlled drug delivery via this mechanism in the pulmonary system.

The most promising nanocarrier systems for lung delivery developed to date appear to be the lipid nanocarriers. This is because they have been shown to be easily produced and they do

not stimulate an acute immune response upon administration. However, loading a drug into these carriers and controlling the drug release out of them remains a challenge. For example, it was difficult to encapsulate poorly soluble compounds such as saquinavir into the carriers (< 1% loading) (Beloqui et al., 2013) and an initial burst release (20% within 1 h) was observed when ibuprofen was loaded into the nanocarriers (Lamprecht et al., 2004).

The use of an active drug release system may offer a solution to the problems experienced with nanosystems during inhaled drug delivery (Ganta et al., 2008). Stimuli responsive nanosystems can be induced to release their drug pay load in response to exogenous or endogenous triggers (Mura et al., 2013). Endogenous stimuli-responsive nanocarriers often respond to pathological triggers that generate a specific change inpH, redox or chemical microenvironment, which can be target as the release stimuli. For example, anticancer drug-delivery systems take advantage of the slight difference of pH existing between healthy tissues (~7.4) and the extracellular environment of solid tumours (6.5–7.2) (Deng et al., 2011). This offers an interesting opportunity for drug delivery where the delivery system becomes an active participant in the process. However, the process of trigger release via endogenous systems can be patient specific due to the complex microenvironments encountered by the nanosystems. As a consequence exogenous triggers tend to be favoured in this field of research. External stimuli such as magnetic fields (Carregal et al., 2015) or ultrasound have been shown to be an effective means to induce payload release from nanocarriers (Yan et al., 2013). As a consequence two stimuli-responsive nanosystems (using heat and a magnetic field) have reached the early stages of clinical trials (Mura et al., 2013), but issues associated with tissue-penetration depth and focusing (to avoid damage to healthy tissues) have hampered the development of these triggered delivery systems. For pulmonary administration, it is very desirable to design chemically triggered nanocarriers that have good degradability and biocompatibility. Ideally a chemical trigger would only mix with the nanocarrier upon administration and this mixing would lead to nanocarrier premeabilisation and drug release through the leaky nanocarrier. However, to design such a system consideration must be given to administration of such a carrier to the lung and its fate within the lung and this requires detailed knowledge of the lung anatomy, physiology and aerosol science.

1.2 Lung structure and physiology

The human respiratory track can be divided into two functional regions: the conducting zone and respiratory zone (Weibel and Gomez, 1962). The conducting zone consists of the pharynx, larynx, the trachea, bronchi and terminal bronchioles, a branching system with branches becoming progressively smaller in diameter and length (Patton, 1996). The respiratory zone consists of respiratory bronchioles, the alveolar ducts and alveolar sacs, where gas exchange occurs. With each division from the trachea (generation 0) to the respiratory airways (generation 17 onward), the number of airway branches is doubled, with marked increases in cross sectional area. The airways bifurcate an average of 23 times from the trachea to the alveolar sacs (Figure 1.1) (Weibel and Gomez, 1962), presenting a tortuous path for the inhaled air and any aerosolised ambient or therapeutic matter carried within it.

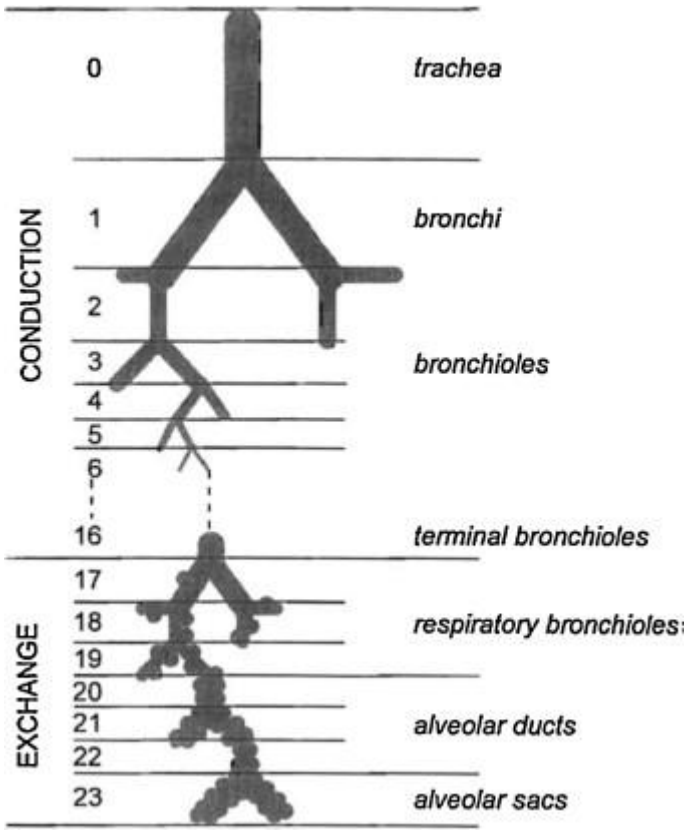

Figure 1.1: Model of airways described by Weibel (Weibel and Gomez, 1962).

The airway and alveolar epithelia line the lumen of the respiratory tract, and form an important primary barrier between the external environment and the internal physiology of the body. Progressive changes in the epithelial lining are observed along the length of the respiratory tract (Figure 1.2) (Patton and Byron, 2007). As the airway progresses from the

conducting to the respiratory zone, the cell types alter to accommodate the specific functions and defence mechanisms for each region. The pseudo-stratified columnar epithelium of the airways is composed of three major cell types: basal (stem or progenitor cells), goblet (mucus secreting cells) and ciliated (involved in mucocillary clearance) (B éruB é et al., 2010). In the bronchioles, the ciliated cells are interspersed mainly by club cells. The epithelium becomes more cuboidal in nature as the bronchioles are approached. The alveolar epithelium is composed of two type cells; broad and thin squamous Type I cells (95%) provide a thin absorptive membrane for gas exchange, and compact Type II cells (5%) are responsible for lung surfactant production as well as vectorial transport of sodium from the apical to the basolateral surface(Matthay et al., 2005).

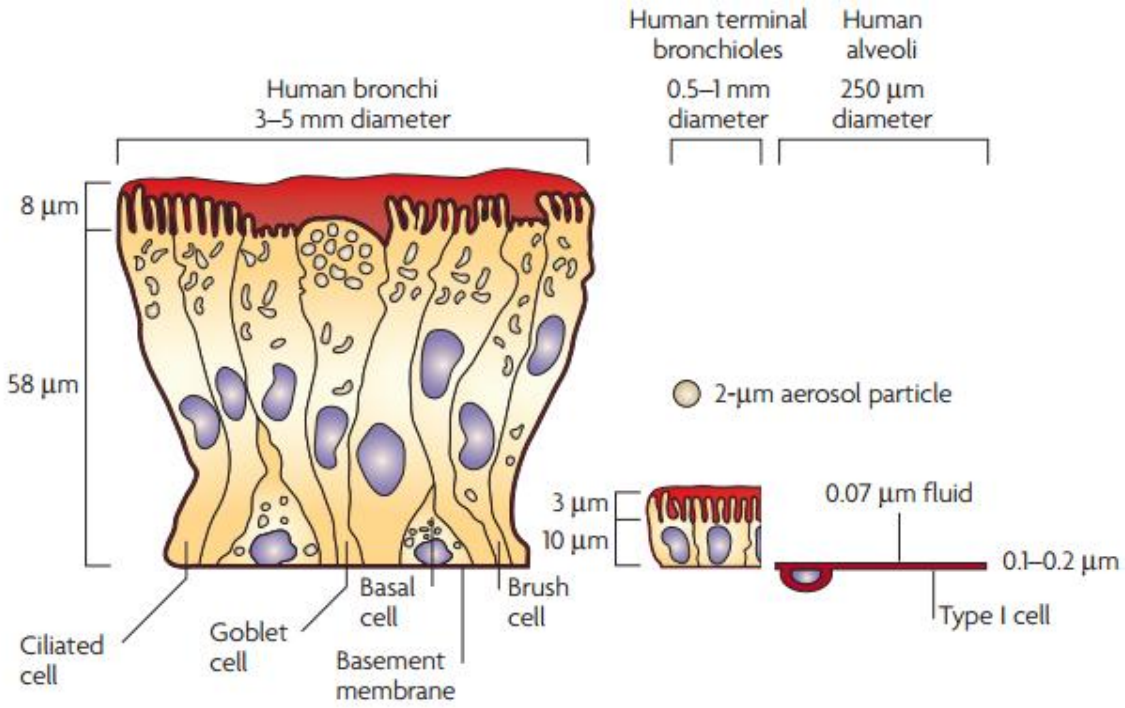

Figure 1.2: Comparison of the lung epithelium at different sites within the lungs. From (Patton and Byron, 2007)

The composition of the lung surface lining fluid also varies between the conducting and respiratory regions. In the conducting airways the lining fluid consists of two layers; a watery 'sol' in direct contact with the ciliated epithelial surface which is covered by a second patchy viscoelastic mucus gel layer (Lansley, 1993). The viscous mucus, comprising mainly water, glycoproteins, (mucins), proteins, electrolytes and lipids (Widdicombe and Widdicombe, 1995), is secreted directly into the lumen by goblet cells and sub-mucosal glands, and can be up to 10 µm thick in the upper airways (Lansley, 1993). This layer becomes thinner when

reaching the bronchioles and terminal bronchioles, around 3 μm in height. The mucus is absent in the respiratory regions, where a much thinner layer of surface lining fluid exists (0.1 μm), to facilitate their function of gas exchange. In both regions the lining fluid is topped with a monolayer of highly surface active lung surfactant, comprising mainly phospholipids (85%), which serves to reduce the surface tension at the air liquid interface (Pérez-Gil, 2008).

1.3 Particle deposition in the lungs

Drug formulations, whether intended for local or systemic effect, must be effectively aerosolised to be administered to the lungs via inhalation (Dolovich and Dhand, 2011). This involves the generation of a fine dispersion of drug-containing particles or droplets which must be entrained within the inspired air. A proportion of the particles travelling through the respiratory system will be trapped after coming into contact with the wet airspace surfaces, a phenomenon with is known as deposition. Three types of devices,namely dry powder inhalers (DPI), pressurised metered dose inhalers (pMDI) and nebulisers are used routinely in clinical practice to generate aerosols (Thompson, 1998). Device parameters are critical in determining performance of the resultant aerosol. Typically delivery of 40-50% of the nominal dose to the pulmonary tree is considered a highly efficient system (Dolovich and Dhand, 2011). However, the drug formulations must themselves be optimised to achieve reproducible aerosolisation. As such the active pharmaceutical ingredient is often combined with excipients to facilitate its dispersion. Common inhaled excipients include lactose, hydrofluoroalkane propellants, surfactants (such as sorbitantrioleate) and co-solvents (such as ethanol) (Pilcer and Amighi, 2010). Selection of the appropriate device and formulation will depend on several factors, including the clinical indication, patient dexterity, treatment schedule and portability.

There are three principal mechanisms that lead to pulmonary deposition: inertial impaction, gravitational sedimentation and Brownian diffusion, as summarized in Table 1.1. The relative contributions for a given formulation are dependent on aerodynamic particle diameter (Courrier et al., 2002). The aerodynamic diameter of a particle is equivalent to the diameter of a unit density sphere that has the same terminal velocity in still air as particle (Hinds, 2012). The inertial impaction occurs during the passage through the oropharynx and large conducting airways if the particles possess a mass median aerodynamic diameter (MMAD) more than 5 μm. Particle ranges from 1 to 5 μm are predominantly influenced by gravitational force that occurs in smaller airways and respiratory bronchioles, where air

velocity is lower. The deposition of particles smaller than 0.5 μm is governed significantly by diffusion, based on Brownian motion and can occur in the alveoli where air is more stationary and resides for longer periods, however very small particles can also be extensively exhaled (Labiris and Dolovich, 2003a). The effect of particle size on the deposition of aerosol particles in the human respiratory tract following slow inhalation is summarized in Figure 1.3. However it was proved that gravitational sedimentation was the main mechanism of particle deposition and dispersion when experiment was carried out under the microgravity condition (Darquenne et al., 2000).

Table1.1: Mechanism of aerosol deposition. From (Yang et al., 2008)

Site	Size (μm)	Mechanism of deposition	Comment
Large airways	>5	Impaction	Mostly deposition in segmental airways
Smaller airways	1-5	Gravitational sedimentation	Improved with slow and deep breathe
Respiratory bronchioles	1-3	Gravitational sedimentation	Improved with slow and deep breathe
Alveoli	≤0.5	Brownian diffusion	Mostly exhaled

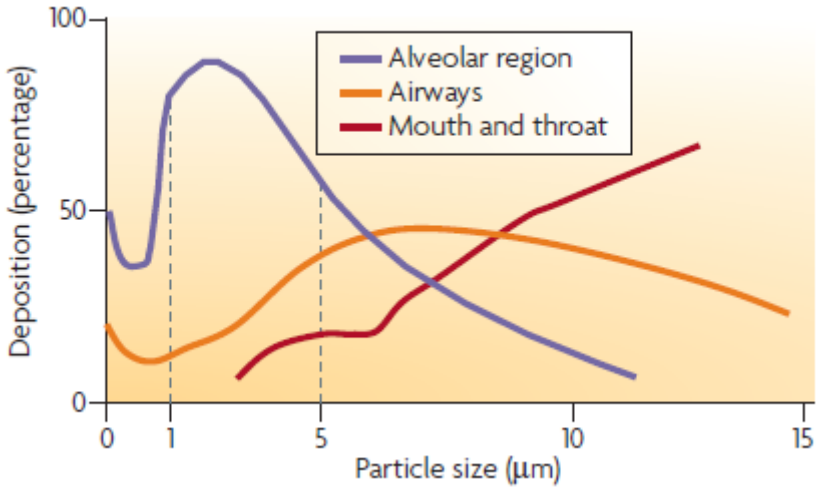

Figure 1.3: The effect of particle size on the deposition of aerosol particles in the human respiratory tract following slow inhalation (From Patton & Byron, 2007)

Targeting therapeutics to achieve preferential lung deposition for systemic or local delivery can be accomplished by altering the aerosol properties and physiology including particle size, density, surface properties or shapes to direct them to the peripheral or central regions of the

lungs as required. However, the site, extent and efficacy of particle deposition after inhalation is also influenced primarily by other ventilatory factors like breath pattern, flow rates and tidal volume, determining the airflow velocity and the residence time in the respiratory tract (Byron and Patton, 1994). Depending on the particle size, shape and ventilation parameters, deposition occurs in all regions of the lung: the airways and the alveoli (Heyder et al., 1986; Patton et al., 2010).

1.4 The fate of inhaled drugs

Once deposited on the surface of airways, the fate of an aerosolised drug formulation depends on their solubility and their landing site, because deposition within the lung is a complex function of kinetics of absorption and non-absorptive clearance mechanisms (Sakagami, 2006). Drugs in the particulate forms first undergo wetting in the lung surface lining fluids, regardless of the nature of the materials surfaces (Geiser et al., 2003). The surfactant will then help particulate matter to sink into the fluid, passing first through the gel phase and then the sol phase. If the deposited matter is fairly soluble in body fluids, it can undergo dissolution and enter this will make the agent available for cellular absorption. For particulates that are relatively insoluble, clearance is governed mainly by the mechanical removal by mucociliary clearance and phagocytosis by alveolar macrophages. Importantly, these mechanisms occur simultaneously, which makes it more difficult to study each of them individually (Ibrahim and Garcia-Contreras, 2013). Diseases of the lung can alter the fate of inhaled agents, eg it can modify the mucus production which determines the pharmacokinetics and pharmacodynamics of the administered medicines (Wang et al., 2014).

1.4.1 Absorption

Solubilised drug molecules can be rapidly cleared from the airways across the epithelial barrier, either transcellularly through the epithelial cells, or paracellularly between adjacent cells of the respiratory tract into the interstitium and then to blood and lymph (Ferin and Oberdörster, 1992; Patton, 1996). Transcellular drug transport occurs primarily through passive diffusion, but can involve active carrier mediated processes (including by P-glycoprotein or multi drug resistance proteins) for certain drug substrates (Schmid et al., 2009). Transcytosis can also occur and this process is important for large macromolecules and nanosized particulates (Bosquillon, 2010; Gumbleton, 2001). For example, inhaled human insulin has been suggested to achieve and maintain effective glycaemic control as a

result of absorption across epithelia cells due to transcytosis (DeFronzo et al., 2005). Passive transcellular diffusion for all molecules depends on drug physiochemical properties, such as molecular weight, charge and hydrophobicity (log P). Small lipophilic molecules tend to readily diffuse through the lipid bilayers of cells. The alternative paracellular route is commonly used by hydrophilic molecules that are small enough to filter through the cellular junctions (Patton and Byron, 2007). The junctional complex between adjacent cells includes the tight junction and the adherens junction, which together form a selective permeability barrier at the apical border of the epithelium, with a molecular weight cut off of 40 kDa (Patton, 1996). Once molecules have translocated to the blood circulation, they can be distributed throughout the body.

1.4.2 Mucociliary clearance (MCC)

Insoluble particles that deposit in the conducting airways (from generations 0 to 16) can become entrapped in the upper viscous mucus layer and removed from the respiratory tree in a host defence mechanism known as mucociliary clearance (Lansley, 1993). Driven by ciliary beating, inhaled particulate materials that consist of slowly dissolving or insoluble materials are most often trapped in the mucus layer and moved up to the larynx where they are swallowed into the gastro-intestinal tract (Fulford and Blake, 1986). Cilia beat in coordination and adjust their frequency and phase of beating in response to neighbouring cilia, which is an important parameter for mucociliary transport (Sleigh et al., 1988). The average transport velocity in the human trachea has been estimated at 3-10 mm/min (Yeates et al., 1975). Previous work showed that insoluble particles larger than 6 μm are cleared from the bronchial airways by MCC in 24 h, while relatively long retention of smaller particles in the conducting airways has been observed (Kreyling et al., 2006).

1.4.3 Macrophage uptake

Clearance of the slowly dissolving and insoluble particulates not removed by mucociliary clearance from the respiratory region is predominantly by macrophage phagocytosis. Where mucociliary clearance is absent, macrophages patrol the alveolar surface as the predominant clearance mechanism. According to the anatomical location, four populations of macrophages in lungs can be distinguished: pleural macrophages, intravascular macrophages, interstitial and surface macrophages, which all have specific phenotypes and different functions (Geiser, 2010). Macrophages scavenge and engulf particulate matter, a process which is facilitated by

the adsorption of complement proteins and opsonisation factors onto the surface of the particles (Geiser, 2010). Macrophage uptake of material deposited in the airways is rapid and believed to complete in 6-12 h after deposition of particles in the alveoli, however this process depends on the particle size, potential and composition of coating material (He et al., 2010). The optimal particle size for phagocytosis by alveolar macrophages has been estimated to be 1-3 μm. Larger particles can still be removed by these cells but the rate of phagocytosis is progressively slower as the particle size increases beyond 3 μm (Chono et al., 2006). Particles that deposit in the airways of the lung with sizes less than 0.26 μm can escape from phagocytosis by macrophages (Sharma et al., 2010). It appears that there are significant particle landing site-dependent effects on the effectiveness of this process (Geiser, 2010). Once internalized in the macrophages, the particulates will be either disintegrated or accumulated in the lymphatic system. A small fraction of the particle carrying macrophages will migrate to the ciliated airways where they are removed by the MCC (Schmid et al., 2009).

1.5 Controlled drug delivery

Despite the number of effective clearance mechanisms encountered by inhaled medicines, inhalation therapy represents an attractive application route for the targeted delivery of a number of active agents. The local application of therapeutic agents to the respiratory system in particular has several advantages over other routes of administration, like increased selectivity, high local concentration and lower systemic exposure. For these reasons the local delivery of inhaled agents is theprevalent approach in the treatment of respiratory diseases (Courrier et al., 2002). There are a wide range of inhalation products that have been commercialised (Table 1.2). The majority of these products administer locally acting drugs for treatment of lung diseases. However, in addition, as inhalation represents an attractive non-invasive alternative for systemic delivery of biopharmaceuticals (e.g. peptides and proteins) there is an emerging market for these products. The lower enzymatic activity (compared to the oral route), large alveolar surface area and thin epithelial air-blood barrier allow rapid absorption of macromolecules from the alveolar airspace (Patton and Byron, 2007), but as their development is time-consuming and costly there arerelatively few commercial products that currently exist.

Table 1.2: Commercial inhalation products

Therapeutic usage	Drug classifications	Drugs	Inhalation device
COPD and asthma	Short-acting beta-2 agonist	Salbutamol	Nebulizer, pMDI, DPI
	Long-acting beta-2 agonist	Salmeterol	pMDI, DPI
	Anticholinergic agents	Ipratropium bromide	Nebulizer, pMDI
	Inhaled corticosteroids	Beclomethasone dipropionate	Nebulizer, pMDI, DPI
Cystic fibrosis	Antibiotics	Tobramycin	Nebulizer, DPI
	Mucus mobilizers	Dornase alfa	Nebulizer
Respiratory distress syndrome	Pulmonary surfactant	Phospholipids	Endo-tracheal tube
Analgesia	Opioids	Fentanyl	Novel inhaler
Diabetes	Peptides	Insulin	DPI
Parkinson's disease	Psychoactive drug	Levodopa	DPI

Despite their routine clinical use, existing inhaled formulations suffer from rapid elimination from the airways which decreases the initial high local concentrations in lung tissue and results in repeated administration and poor patient compliance (Gessler et al., 2008). This places a significant burden on the patient, especially where the disease state is chronic in nature. Controlled release formulations that are able to regulate the delivery of therapeutic agents over time would be highly advantageous for the treatment of both local and systemic disease states (Hickey, 2014; Loira-Pastoriza et al., 2014).

1.5.1 Drug modification

Increasing a compound hydrophobicity, encouraging tissue binding and increasing an agents molecular mass can be considerated as molecular engineering stratagies to prolong the duration of therapeutic agents in the lung. The prolonged absorption of fluticasone propionate relative to the other inhaled corticosteriods was a consequence of molecular engineering to

make the compound more hydrophobic through a prodrug (Winkler et al., 2004). Long acting beta agonists, e.g salmeterol is an example of an agent that has been structurally modified from the shorter acting salbutamol to provide sustained bronchodilation (lasting up to 12 hours) through an increased tissue binding (Kips and Pauwels, 2001). Furthermore, modification of the lipophilic compound, pentamidine has been shown to increase binding to the lung tissue (Byron, 1993). Conjugating positive charge to a drug with a water-soluble inert ligand such as polyethylene glycol (PEG) is another strategy that can increase the agents molecular weight, which reduces clearance (Veronese and Pasut, 2005). A recent study demonstrated that conjugation of antibody fragments to PEG increased pulmonary residence time through mucoadhesion and bypass of alveolar macrophages (Koussoroplis et al., 2014). However, all these afforementioned approaches are based on specific modifications to individual active agents. Generating a drug delivery platform technology that could be applied to a range of active agents is more desirable.

1.5.2 Microparticulate carriers

The use of microsized carriers can enhance lung retention. This strategy avoids chemical modification, which may cause adverse effects or modify the pharmacology of a drug. A number of polymer carriers have demonstrated slow dissolution in lung fluid. Carriers typically slow drug dissolution down by forming a barrier, which protects the drug from interacting with the dissolution fluid (Pilcer and Amighi, 2010). Of all the polymer systems developed for inhaled delivery poly(lactic-co-glycolic acid) (PLGA) represents the most investigated system for the preparation of sustained-release drug profile (Beck-Broichsitter et al., 2012; Ungaro et al., 2012). PLGA has a number of advantages over other polymers used in drug delivery because it is biodegradable and biocompatible (Anderson and Shive, 2012). Chitosan is another polymer employed to improve drug absorption and control drug release. Chitosan has the added advantage that it has mucoadhesive properties, but it also can act as a penetration enhancer and this is seen to be problematic (Takeuchi et al., 2001). The rate of drug release can be tailored by selecting an appropriate molecular weight of chitosan as a drug release modifier in the formulation (Learoyd et al., 2008). Hyaluronic acid (HA) has also attracted the attention of scientists working on sustained respiratory delivery. Inhaled sodium hyaluronate insulin-containing microparticles were shown to prolong insulin release, resulting from the polymer's mucoadhesive and viscosity enhancing effects (Morimoto et al., 2001; Surendrakumar et al., 2003). However, an inhaled controlled release microparticulate

formulation is yet to be commercialised. This may be attributed to concerns over the long-term use of relatively new excipients in the lungs and the associated regulatory challenge this entails.

The use of large porous particles (LPPs) was an innovative strategy to provide a drug carrier that avoids rapid pulmonary clearancedue to relatively lower mass densities (0.4 g/cm^3) and larger diameter (> 5 μm) (Edwards et al., 1997). Large porous particles are readily dispersed due to the large geometric size, but theirsmall aerodynamic size allows the particles to escape impaction in upper airways and penetrate into deep lung. Furthermore, large geometric size prevents their uptake by alveolar macrophages (Cook et al., 2005). Previous work showed doxorubicin release from PLGA microparticles over 2 weeks, suggesting that porous large PLGA microparticles have great potential as a long-term inhalation agent for the treatment of lung cancer (Kim et al., 2012). This technique has been widely used using various porogens and preparation techniques for controlled release profiles (Kim et al., 2006; Rawat et al., 2008; Ungaro et al., 2006;Yang et al., 2009). Additionally, nanoparticles can be encapsulated into porous particles for drug delivery to specific sites of the body, known as porous nanoparticle-aggregate particles (PNAP) (Tsapis et al., 2002). The merits of nanoparticle and large porous particles were innovatively combined in this formulation. Sung et al. (2009) showed that *in vitro* release of rifampicin-loaded PNAPs resulted in an initial burst followed by a sustained release over 8 h. Similarly, prolonged systemic levels of rifampicin were observed after delivery to guinea pigs by insufflation compared with porous particles containing free rifampicin (Sung et al., 2009). Despite the achievement of LPPs for controlled pulmonary drug delivery, there are some difficulties in adjusting drug release, assessing the risk of polymer accumulation within the lungs and scaling up manufacture. Consequently, more efforts are needed to eventually realize this delivery system from bench to bedside.

Swellable microparticles are another promising strategy to sustain pulmonary release. Once deposited on the lung fluid lining, their size increases significantly by swelling and drug can be released in a controlled manner. El-Sherbiny, Smyth et al. (2010) synthesized PEG-grafted N-phthaloyl chitosan (NPHC) copolymer, which self-assembled into drug-loaded nanoparticles and were encapsulated in sodium alginate semi-interpenetrating microspheres (El-Sherbiny and Smyth, 2010). They found that increasing alginate content in the microspheres tended to decrease the percentage of bovine serum albumin (BSA) released.

1.5.3 Nanocarriers for pulmonary drug delivery

a) Liposomes

Liposomes are colloidal vesicles formed of lipid bilayers that have been shown as suitable drug carrier systems. Liposomes can encapsulate both hydrophilic and hydrophobic drugs. As lipids are used to prepare liposomes they have a good compatibiliy with the lung tissue. A range of different drugs have been encapsulated in liposomes and released over a sustained period (Beck-Broichsitter et al., 2013; Hajos et al., 2008). For example, a liposome systems have been used to retard the rapid absorption of insulinin mouse alveoli and this reduced drug induced side-effects (Huang and Wang, 2006). More recently, pulmonary delivery of liposomes in a rat model showed that the liposomes were effectively distributed in the respiratory tract and lungs, and that the release of salbutamol sulfate (SBS) from liposomes was sustained for at least 48 hours (Chen et al., 2012). Pharmacodynamic analysis in a guinea pig model showed that the anti-asthmatic effect of SBS liposomes persisted for up to 18 hours, whereas that of free SBS solution was less than 8 hours. Another inhaled liposomal ciprofloxacin formulation, known as Pulmaquintm is in phase 3 clinical studies for treatment of non-cystic fibrosis bronchiectasis (Serisier et al., 2013). It has been shown to provide a burst release followed by a sustained release over 24 h. However, a major challenge associated with conventional liposomal formulations, particularly for pulmonary delivery, is long-term instability (Allen and Cullis, 2013). Physicochemical property changes during the dehydration process that are used to store these formulations can create problems (He et al., 2010). Therefore the use of a colloidal system with similar material properties to liposomes, but greater structural stability could prove to be highly advantageous in the context of controlled pulmonary delivery.

b) Micelles/dendrimers

Micelles are self-assembling nanosized colloidal particles with a hydrophobic core and hydrophilic shell (Torchilin, 2007). At low concentrations, the amphiphiles exist as monomers. Above the critical micelle concentration (CMC), the monomers self-assemble to form micelles. Micelles are used as carriers of poorly soluble compounds where solubilization occurs in the micelle core. Gill et al. (2011) evaluated the potential of paclitaxel loaded micelles fabricated from PEG_{5000} as a sustained release system following pulmonary delivery (Gill et al., 2011). The results showed the micelles retarded paclitaxel release over 8 h *in vitro*. More recently, Hu et al. (2014) showed aerosolized PEG–PLGA

micelles were a promising carrier for pulmonary sustained release of labile drugs (Hu et al., 2014). Dendrimers are three-dimensional structures similar to micelles, also known as unimolecular micelles, which have been proved as successful carriers in different routes of drug administration (Cheng et al., 2008). Several studies have shownthat dendrimers can sustain drug release within the airway tract. Kaminskas et al. (2014) explored the conjugation of a 56 kDa PEGylated polylysine dendrimer to doxorubicin to promote the controlled and prolonged exposure of lung-resident cancers to cytotoxic drug (Kaminskas et al., 2014). The dendrimer sustained doxorubicin in the lungs for 7 days compared to rapid absorption of free drug.

c) Nanoparticles

Nanoparticles for medical applications are defined as solid colloidal particles of 1 to 1000 nm in diameter (Duncan and Gaspar, 2011). In the area of drug delivery nanoparticles are generally 50 nm or larger in size (De Jong and Borm, 2008). The active therapeutic agent is either dissolved, entrapped or encapsulated within the nanocarrier, or alternatively absorbed or attached to the surface of the matrix (Sahoo and Labhasetwar, 2003). Depending on their structures and morphologies, nanoparticles can be further classified as matrix (nanosphere) or vesicular structures (nanocapsule). Nanospheres are matrix systems in which the therapeutic agent is physically and uniformly dispersed, whereas nanocapsules are vesicular systems in which drug is usually contained within a cavity surrounded by a solid or liquid core that is encapsulated by an outer shell. The advantages of using nanoparticles for drug delivery result from their small size that can penetrate through mucus and from their degradation if made from biodegradable materials which can allow sustained drug release within the target site over a period of time (Thomas and Klibanov, 2003). A wide range of materials have been used to fabricate nanoparticles for various applications with different properties and release characteristics for the encapsulated therapeutic agent (Zhang et al., 2008). The materials employed to fabricate nanocarriers for drug delivery can broadly be categorised as inorganic (elements such as silica and alumina) or polymeric (naturally occurring such as gelatin and albumin, or synthetic such as poly(cyanoacrylate)) (Parveen et al., 2012). When considering their use in inhaled formulations it is imperative that the materials used do not elicit an acute inflammatory response or accumulate following chronic dosing (Dailey et al., 2006). Although inorganic nanoparticles possess good stability and demonstrated successes in imaging and treatment of tumors (Huang et al., 2006), they are not well biodegraded and

hence raise concerns over their biopersistence and long term toxicity (Huang et al., 2011). Biodegradable polymers are thought to be more attractive when considering repeat human exposure. Polymers can undergo hydrolysis upon implantation into the body, forming biologically compatible and metabolizable moieties that are eventually removed from the body. There are various potential applications of nanoparticles for delivery of therapeutic agents to the cells and tissue (Panyam and Labhasetwar, 2003). Biodegradable nanoparticles formulated from PLGA have been extensively investigated for sustained and targeted/localized delivery of different agents including plasmid DNA, proteins and peptides and low molecular weight compounds (Ungaro et al., 2012).

Nanoparticles offer several advantages over larger particles due to their small size. Compared to micro-sized carriers, nanoparticles can penetrate through small capillaries and access individual cells, thus allowing drug accumulation at the required site (Panyam and Labhasetwar, 2003). Therefore, theoretically the unwanted side effects and the toxicity of the therapeutic agent is reduced and the therapeutic efficacy is enhanced. Another study demonstrated that pulmonary epithelial cells internalize particles 0.5 μm or smaller 10 times more than 1 μm particles and 100 times more than 2 or 3 μm particles (Foster et al., 2001). In addition, nanoparticle formulations have been used to enhance the bioavailability of poorly soluble drugs due to their large surface area to volume ratio (Gonçalves et al., 2016). Passive targeting has also been attempted following the inhalation of nanoparticles as a means to treat lung diseases (Azarmi et al., 2008). Furthermore, the use of biodegradable materials for nanoparticle preparation allows the potential for prolonged drug release (Gu et al., 2008). Many applications of nanoparticles have been designed to exploit the body's normal or pathological states, depending on the desired therapeutic target. For example, the enhanced permeation and retention effect is well described in the literature and results in passive targeting by nanoparticles through 'leaky' vasculature, for example in and around tumour sites (Peer et al., 2007). When compared to other nanocarriers, such as liposomes, nanoparticles confer the advantages of high payload encapsulation efficiency, good stability and a capacity to resist solvent entry over prolonged storage periods (Hans and Lowman, 2002). Furthermore, nanoparticles can be used to protect the loaded therapeutic agent from degradation (Chalasani et al., 2007). The advantages and disadvantages are summarized in Table 1.3. To accomplish controlled pulmonary delivery, innovative carriers that possess good release properties are needed to overcome the airway clearance machanisms.

Table 1.3: Comparison of different drug delivery systems for controlled pulmonary release

Delivery systems	Merits	Demerits
Conventional microparticles	• Simple and practical manufacture process with mature preparation techniques	• Unflavorable fluidization and dispersibility • Prone to be phagocytosed by alveolar macrophages
Large porous particles	• Decreased tendency to aggregation and decreased phagocytosis by alveolar macrophages • Higher aerosolization efficiency	• Lack of universal preparation method and poor control of encapsulation efficiency and release profile
Swellable microparticles	• Diminished phagocytosis by alveolar macrophages	• Unfavorablefluidization and dispersibility • Challenging to customize drug release pattern
Liposomes	• Tremendous versatility in particle size and physical characteristics • Solubilize poorly soluble drugs, facilitate alveolar macrophage delivery	• High production cost • Drug leakage owing to the relative instability during storage and nebulisation • Instability during the dehydration process
Polymeric nanoparticles	• Hightargeting • Escape alveolar macrophage clearance	• Unclear pulmonary nanotoxicity
Solid lipid nanoparticles	• Biocompatible, more stable than liposomes under nebulization, easy to scale-up	• Poor drug loading, elusive drug release behavior and the possibility of gelation
Porous nanoparticle-aggregate particles	• Decreased tendency to aggregate • Escape alveolar macrophage clearance	• Undesirable redispersibillity

1.6 Administration of inhaled nanocarriers

The respirable fraction of an inhalable powder is generally the fraction of particles with an aerodynamic diameter ranging between 1 and 5 μm (Patton and Byron, 2007). Most nanoparticles used for inhaled delivery find it difficult to deposit in the respiratory tract. These small particles can be subjected to exhalation, making the direct adminstration of nanoparticles for pulmonary delivery problematic. In addition, it is difficult to physically stabililse nanoparticles during the aerosolisation process (Abdelwahed et al., 2006). Generally, to try and overcome these issues nanoparticles are dispersed in a liquid or solid formulation for inhaled delivery. The simplest means of achieving this is via nebulisation of a nanoparticle suspension (McCallion et al., 1996).

During nebulisation a liquid is broken up by compressed gas flow into anaerosol with useful size for airway deposition. The advantage of nebulizers is that no special inhalation techniques are needed for optimum delivery (Labiris and Dolovich, 2003b). Another associated advantage is the rapid liberation of nanoparticles from the micro-droplets upon contact with the lung surface lining fluids, as the spreading of the aqueous vehicle would be immediate. However, the nanoparticles must be resilient enough to withst and the shear forces experienced during the nebulisation process. A major drawback is that many nebulisers need compressed gas or a compressor to operate and the delivery process is relatively time consuming. Furthermore, the poor efficiency of nebulising drug suspensions is a major limitation to their use (Knoch and Keller, 2005).

An alternative approach to enable effective pulmonary administration of nanoparticles is to formulate nanoparticle-containing microparticles of respirable size for inclusion in dry powder/ pressurised metered dose inhalers. Pressurised metered-dose inhaler (pMDIs) are portable, convenient, multi-dose devices that use a propellant such as hydrofluoroalkanes (HFAs) under pressure to generate a metered dose of an aerosol through an atomisation nozzle. No safety concerns have been identified with their use in healthy individuals or patients with asthma as hydrofluoroalkanes are non-toxic, non-flammable, and chemically stable. However, typically less than 50% of the emitted dose has been reported to deposite in the lung (Nyambura et al., 2009), which limitsthe administertation of high doses. A variety of parameters affect the delivery efficiency of an pMDI, such as a patient's breathing pattern, inspiratory flow rate and hand–mouth co-ordination (Smyth, 2003). Dry powder inhalers (DPIs) are the most innovative devices for both local and systematic effect and for delivery

of a range of drugs. There is a wide range of DPI devices on the market, from single-dose devices loaded by the patient to multiunit dose devices (Ninane et al., 2015). DPIs eliminate the co-ordination difficulties associated with the pMDI. However, DPIs in use today are breath actuated and are dependent on a patient's inspiratory flow rate. Active DPIs are being developed that reduce the importance of a patient's inspiratory effort so that the generation of a respirable aerosol becomes independent of inspiratory flow rate but these systems are not yet very popular as they remain expensive (Dolovich and Dhand, 2011). Strageties to enhance delivery efficiency have been studied. For example, a dry powder inhaler with the potential to control particle deposition and sustain release to the lung by encapsulating nanoparticle in large porous PLGA particles has been formulated (Arnold et al., 2007). Also mannitol microparticles containing chitosan nanoparticles were reported to allow efficient nanoparticle liberation upon incubation with aqueous media (Grenha et al., 2007).

1.7 Fate of inhaled nanocarriers

The fate of nanoparticles after landing in the respiratory tract is difficult to study *in vivo*. Generally, the first barrier nanoparticles encounter is the surfactant on top of the airway lining fluid. It is important to understand whether the nanoparticle properties are retained upon their suspension in such biological fluids as physical instability and aggregation will result in the loss of their size specific advantages and may have deleterious effects on drug delivery (Madlova et al., 2009). It has previously been shown that small metal oxide nanoparticles rapidly agglomerated in biological fluids, which could be due to a high number density (Limbach et al., 2005). Similarly, polystyrene nanoparticles (300 nm) were found to aggregate in cell culture medium despite being physically stable in aqueous media (Madlova et al., 2009). On the other hand, there is interaction between nanoparticles and pulmonary surfactant system, which could significantly impact on biophysical surfactant function, surfactant metabolism, particle clearance, and particle-induced toxicity (Schleh and Hohlfeld, 2009). Following wetting in the lung surface lining fluid there are several competing pathways that nanoparticles may follow, including mucociliary and phagocytic clearance, as well as prolonged retention, cellular uptake and epithelial barrier penetration (Figure 1.4). Two major mechanisms,the mucociliary escalator and macrophage clearanceare involved in the clearance of particles in the lungs. The mucociliary escalator eliminates particles deposited in the airways.

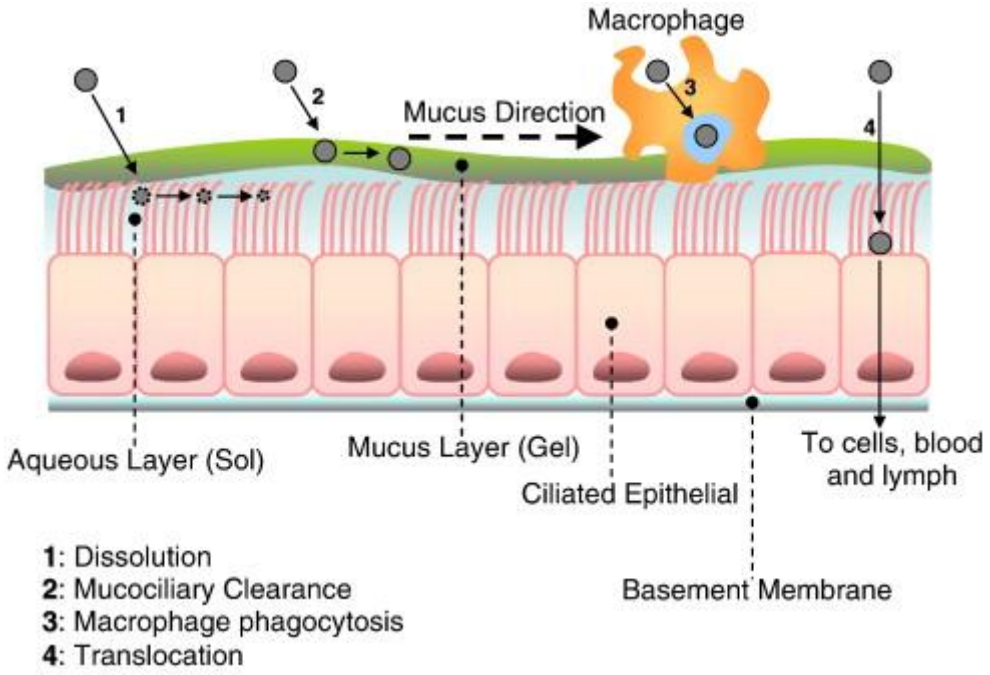

Figure 1.4: Potential pathways determining the fate of inhaled nanoparticles. (From Zhang et al., 2011)

The mucociliary escalator eliminates particles deposited in the airways. A major role of the respiratory mucus gel is to trap inhaled particles so that they can be swept from the airways by mucociliary clearance, thereby defending the lungs against pathogens and toxic materials. Mucus has been considered as a critical barrier to nanoparticle therapies (Lai et al., 2009). The primary mechanism by which mucus gels efficiently trap foreign particulates is the formation of polyvalent adhesive interactions (Lai et al., 2009). The high density of hydrophobic domains, coupled with the flexible nature of mucin fibers, allows efficient formation of multiple low-affinity adhesive interactions with hydrophobic regions on the surfaces of foreign particulates. Polyvalent adhesive interactions with mucus can be achieved via electrostatic interactions as well. Since the glycosylated regions of mucin fibers are densely coated with negative charges, mucus can also bind positively charged particles with high avidity. On the other hand, a size filtering mechanism stops the transport of particles with diameter larger than pore size.

The slow pulmonary clearance of inhaled particulates is usually attributed to phagocytic uptake by macrophages and their subsequent slow migration to the mucociliary escalator and lymph (Moller et al., 2008). However, macrophage mediated uptake of nanoparticles with a size of less than 100 nm is thought to be limited due to less efficient particle recognition (Geiser, 2010). In a study using 30 nm titanium nanoparticles, only 0.1 % of the particles

were found to be internalised by macrophages following bronchoalveolar lavage at 24 h (Geiser et al., 2008). Macrophage uptake by nanoparticles is also influenced by surface properties. *In vitro* investigations have shown that polymeric nanoparticles with high surface charge were phagocytized more efficiently by murine macrophage (He et al., 2010).

Nanocarriers that are not well cleared by phagocytic or mucociliary clearance have a greater opportunity to interact with the epithelial surface, where they may be retained, internalised or translocated. Although cellular uptake and/or epithelial translocation may be considered attractive for certain drug delivery applications, this raises concerns about the potential adverse effects and toxicities associated with nanoparticle use. Several routes for nanoparticle entry into non-professional phagocytic cells have been proposed (Chou et al., 2011). Internalisation may be receptor mediated (via clathrin or caveolin) or result from more passive interactions at the cell membrane surface (macropinocytosis, direct diffusion). The uptake of fluorescently labelled drug delivery nanoparticles by cultured airway epithelial cell layers has been reported to be up to 10% of the applied dose (Madlova et al., 2009). Nanoparticle translocation across the epithelial barrier may be a result of transcellular or paracellular transport, but the latter will probably be limited for drug delivery nanoparticles by their size. The tight junctions between adjacent cells are thought to restrict particle passage when they possess a size of > 10 nm (Lin et al., 2012). Pulmonary translocation has been demonstrated in animal models and it appears that smaller nanoparticles are translocated to a greater extent than larger nanoparticles (Kreyling et al., 2009).

1.8 Nanocarrier loading and release

When acting as vectors to facilitate the delivery of therapeutic agents, nanoparticles should display a high drug loading capacity, good drug retention during storage and transit, and effective drug release when at the intended site of residence/action. Normally the first important point to judge the suitability of a drug carrier system is its loading capacity. Drug loading into nanoparticles can be achieved by two methods: one by incorporating the drug at the time of nanoparticle production and second by adsorbing the drug after the formation of nanoparticles by incubating them in the drug solution (Soppimath et al., 2001). Several factors determine the loading capacity including solubility of drug in the selected matrix; miscibility of drug in the second phase and chemical and physical structure of the matrix (Müller et al., 2000). For example, the formation of highly crystalline particles with a perfect lattice has been demonstrated to lead to drug expulsion when the matrix was made of lipid

(Westesen et al., 1997). Although some strategies can be used to entrap more drugs within particle matrix physically or chemically, drug leaking during manufacture, storage and transit is still a major challenge (Emeje et al., 2012).

The kinetics of drug release from nanoparticles isan essential feature of their design (Modi and Anderson, 2013). However, there is no standardised release method that has been established to test nanocarrier drug release. Dialysis is one of the most commonly used methods for the determination of drug release from nanoparticles. The reason for the popularity of dialysis over other methods (e.g., ultracentrifugation and ultrafiltration) is that the additional step of separating nanoparticles from the free drug at various time points during the kinetic study is eliminated (Zambito et al., 2012). However, a major problem during the release with dialysis is the chemical stability of drug in dialysis medium. In terms of other methods, appropriate separation of the particles from the liquid phase in which they are suspended is necessary to distinguish the particle-bound and free drug. The most reliable way to separate the nanoparticles from the solution containing unbound drug is ultracentrifugation. This process can be achieved by ultracentrifugation or ultrafiltration (Cui et al., 2006). The external pressure applied for separation in other methods can disturb the equilibrium, and incomplete separation can lead to significant measurement errors (Wallace et al., 2012).

A major problem with nanoparticles as drug carriers is burst-release. In general drug release rate depends upon drug solubility, drug diffusion through the nanocarrier structure and biodegradation of the matrix materials. Passive drug release from nanoparticles can occur via desorption of surface bound drug, by drug diffusion through the carrier matrix/membrane, by carrier erosion, or via a mixture of these processes (Kumari et al., 2010). For a number of nanoparticles a burst-release phase can been observed followed by a slow-release phase, or phases, associated with drug diffusion or carrier erosion (Garc á-D áz et al., 2015). The drug release profiles are dependent on production parameters and also the nature of matrix. Premature release from nanoparticle systems is problematic as it means that the presentation of the drug molecules at the point of administration is different to that intended, i.e. the release drug will be free to be absorbed as a simple drug solution rather than drug-loaded nanoparticles, which can influence the resultant biopharmaceutical profile. Furthermore, the initial burst can liberate a significant portion of drug in a short period, which can lead to acute toxicity, and / or rapid clearance and thus a low bioavailability. Therefore a means to prevent

undesirable premature drug losses would be of considerable benefit to prolong the shelf life of nanoparticles. On the other hand, incomplete payload release can be an issue associated with nanoparticles. Although slow and sustained release profiles from nanoparticles are highly desirable, systems exhibiting close to zero release over a period of days would be unsuitable for pulmonary delivery where local inflammation is a concern (Shvedova et al., 2005). High drug concentration resulting from efficient drug liberation from carriers is a critical prerequisite to achieve pharmacological effects. Given the above, a strategic approach to controlled release appears to be the design of nanocarriers that display sufficient drug-carrier affinity to prevent premature drug leakage during manufacture, storage and transit, coupled with an efficient drug liberation mechanism to elicit release *in situ*.

1.8.1 Active drug release from nanocarriers

Nanoparticulate carriers could be beneficial in pulmonary drug delivery, but they must meet the conflicting demands of payload retention prior to dosing and effective release upon administration, especially when formulated as a nanosuspension (Sun et al., 2012). It has been suggested that this can be achieved by actively modifying the nanocarrier upon delivery so that drug release is optimised. Active drug release can be broadly classified into two categories: chemical or physical (Ganta et al., 2008). Active chemical triggers can induce a changeby modifying the functional groups of the material used to produce the nanocarrier and this can induce a range of subsequent events, e.g. it can stimulate the degradation of particles to cause the release of drug from the carrier (Chen et al., 2010; Du et al., 2011). The chemical that induces a change can be either exogenous or endogenous. Physical strategies in contrast often employ external devices to induce an environmental change such as a change in temperature, ultrasound or magnetic field (Oliveira et al., 2013; Wei et al., 2009; You et al., 2010). The most significant potential advantage of activenanocarrier delivery systems is better drug targeting compared to conventional systems, i.e. the drug is only released when needed.

In the context of inhaled medicines exogenously triggered active drug delivery systems seem preferable as they do not suffer from the inherent biological variability introduced by the patient. Several active drug release from nano-systems have been described in the literature, but their suitability for pulmonary delivery remains unclear (Al-Ahmady et al., 2012; Lo et al., 2010; Zhao et al., 2009). Particular consideration must be given to the biocompatibility of the active drug release trigger as the lung is susceptible to inflammation (Bhattacharya et al.,

2013; Shvedova et al., 2012). Furthermore, active drug release carrier systems must possess sufficient responsiveness to the release trigger to enable drug liberation. These two issues can generate a paradox for inhaled drug delivery as highly reactive nanoparticles can induce detrimental biological effects, for example by disrupting heomoeostasis or eliciting inflammatory responses whereas unreactive nanoparticle systems are poorly responsive to active release systems (Beyerle et al., 2011). It is difficult to find an existing nanosystem that satisfies the controlled release profile required for pulmonary airway administration.

1.8.2 Types of active drug release

The design of nanocarriers sensitive to stimuli may represent an attractive option for controlled drug delivery. The wide range of stimuli able to trigger the drug release at the right place and time, and the diversity of responsive materials that can be assembled in different architectures, allow great flexibility in the design of stimuli-responsive systems (Stuart et al., 2010).

a) Thermo responsive

Thermoresponsive drug delivery is among the most investigated stimuli-responsive strategies, and has been widely explored in oncology. Ideally, thermosensitive nanocarriers should retain their load at body temperature (~37 ℃), and rapidly deliver the drug within a locally heated tumour (~40–42 ℃). Thermoresponsive systems are generally liposomes, or polymer micelles or nanoparticles made of specific materials that exhibit a lower critical solution temperature (Al-Ahmady and Kostarelos, 2016). Liposomes are perhaps the most advanced thermoresponsive nanosystems, as shown by their use in several clinical trials. More recently, improved liposomal formulations have been shown to release their loads shortly after the onset of hyperthermia (~40–44 ℃) (Kono et al., 2015). The challenge in the design of thermoresponsive nanodevices lies in the use of materials that are both safe and sensitive enough to respond to slight temperature changes around the physiological temperature of 37 ℃.

b) pH responsive

pH variations have been exploited to control the delivery of drugs in specific organs (such as the gastrointestinal tract or the vagina) or intracellular compartments (such as endosomes or lysosomes), as well as to trigger the release of the drug when subtle environmental changes are associated with pathological situations, such as cancer or inflammation (Gerweck and Seetharaman, 1996). This strategy involves the use of polymers with ionizable groups that undergo conformational and/or solubility changes in response to environmental pH variation. For example, chitosan swelling induced on amino-group protonation (pka ~6.3) leads to the release of encapsulated tumour necrosis factor alpha (TNF-α) in the local acidic environment of tumour tissue (Deng et al., 2011). pH-mediated triggered delivery of proteins into ischemic areas was achieved with piperidine- and imidazole-modified PEG–poly(β-aminoester) micelles (Min et al., 2010). Because of the broad range of pH found throughout the gastrointestinal tract, pH-responsive systems for oral drug delivery have been designed to protect drugs from the harsh conditions found in the gastric region and to improve their absorption in the intestine (Wang and Zhang, 2012). At the cellular level, the acidification of endosomes (pH ~5–6) and their fusion with lysosomes (pH ~4–5) is another pH gradient that can be used for effective intracellular drug accumulation. Nanoplexes that expand in response to a mildly acidic pH to afford rapid release of peptides have been conceived using natural glycosides (Weng et al., 2015).

c) Redox responsive

Disulphide bonds, prone to rapid cleavageby glutathione (GSH), can be used to attain redox sensitivity as a high redox potential difference (∼ 100–1000 fold) exists between the reducing intracellular space and oxidizing extracellular space (Saito et al., 2003). For example, a thiomer-based nanoparticulate gene delivery system was developed (Schmitz et al., 2007). Thiol groups prone to oxidation were immobilized on the polymeric backbone of chitosan in order to incorporate the property of extracellular stability and intracellular gene release by forming reversible disulfide bonds. The highest efficiency was observed in transfection studies performed in a Caco-2 cell culture. GSH-sensitive crosslinking agents can be incorporated in the core of the micelles, leading to rapid micelle disassembly followed by specific intracellular release of hydrophobic drugs (Li et al., 2011). In addition, liposomes are the candidates for redox-sensitive systems as well (Ong et al., 2008). However, designing

these systems to be sensitive to discrete variations of pH and redox potential is not straightforward.

d) Chemical responsive

Triggered delivery systems that do not use specialist equipment for administration and where the process can be easily controlled, e.g. systems requiring co-administration of chemical triggers, offer a more convenient approach. Surfactant-induced leakage from liposomes has been studied. For example, Pluronic F127 (PF127) is a biocompatible tri-block copolymer, which can interact with lipid bilayer of liposomes and make leakage that allow the release of hydrophilic substance from liposome interior (Kim et al., 2014). Similarly, lipid nanoparticles engineered with a solid outer shell, could be selectively and rapidly permeabilised using the amphiphilic polymer Pluronic® L62D as a chemical trigger (Chana et al., 2015). Apart from surfactant, sugar can be used to trigger copolymers through hydrolysis (Roy et al., 2008). Similarly glucose-induced swelling attributed to the slow reaction between glucose and phenylboronic acid (PBA) groups enabled microgel suitable for sustained drug delivery (Xing et al., 2011). Some polymer films such as poly (2-vinylpyridine) is also responsive to cholesterol molecules, thus the material can be used to manufacture stimuli responsive nanomaterials for controlled release (Stuart et al., 2010). However only surfactant have been tested for pulmonary drug delivery.

1.9 Inhaled nanoparticle carriers used for anti-tuberculosis drugs

The advantages of local delivery to the primary site of infection, the lung, alongside the potential merits of nanotechnology make treatment of tuberculosis (TB) by inhalation of anti-TB drug-loaded nanocarriers an attractive prospect (Choudhary and Devi, 2015). TB is a highly contagious chronic granulomatous bacterial infection and is the second leading cause of death from an infectious disease worldwide after human immune virus (HIV) deficiency. Tuberculosisis a lethal infectious respiratory disorder which was considered a disease of the past, but about 30% of the world populations are afflicted with TB. According to The World Health Organization (WHO) guideline reports, the recent estimates in 2015 were 9 million incident cases of TB with 1.4 million TB deaths (Global Tuberculosis Report 2015).

TB is triggered by different strains of Mycobacteria, among them *Mycobacterium tuberculosis*, a slender, acid-fast, non-motile gram-positive bacilli being the most common

strain which may attack any part of body (Smith, 2003); 80% of infections are pulmonary TB and also advance as extrapulmonary TB in the central nervous or circulatory systems or elsewhere in the body (Dube et al., 2012). *Mycobacterium tuberculosis* has a complex cell wall, composed of long-chain fatt acids, glycolipids, peptidoglycan and proteins (Barry et al., 2009). Primary TB occurs within the first year or so after exposure and is the result of an uncontrolled initial infction. The majority (90%) of infected humans effectively contain the bacteria and are defined as having latent TB infection (Choudhary and Devi, 2015). A relatively smaller proportion of people who are infected with *M. tuberculosis* will develop TB disease. Risk of developing active disease varies conferring to time since exposure, age and host immunity (Newton et al., 2008). The lifetime risk of infection activation for a latently infected human has been estimated to be 2-23%.

Onced inhaled, most *M .tuberculosis* organisms will settle in the upper respiratory epithelium, where they are likely be expelled by the mucociliary escalator. The few bacteria reaching the deep lung are phagocytosed by alveolar macrophages and either killed or else survive to initate an infection (Ernst, 2012). The fate of the bacillus within the infected cell depends on the type and activation state of cell found. It is believed that a bacillus is able to survive within a macrophage if the phenotype of the phagocytic cell interacting with *M. tuberculosis* displays an anti-inflammatory phenotype also known as alternative activation state. Once inside the phagocyte, the mycobacteria modulate the behaviour of its phagosome by preventingits fusion with acidic, hydrolytically-active lysosomes (Smith, 2003).

Over the next 2 to 3 weeks, surviving organisms multiply, kill their host macrophages and release more bacillus infecting additional host cells. Pulmonary inflammation due to interaction of bacillus with macrophages and other cells results in recruitment of monocytes, neutrophils and primed T-cells and B-cells to lungs, culminatingin the formation of granulomatous lesions (Dartois, 2014). In its early stage, the granuloma has a core of infected macrophages enclosed by foamy macrophages and other monomuclear phagocytes, surrounded by lymphocytes. At the same time, there is a noticeable increase in the number of foamy macrophages responsible for the accumulation of casuous debris in the centre of the granuloma (Byrne et al., 2015).

Tuberculosis treatment represents a challenge which requires prolonged treatment times. Treatment may last for months especially in the case of immunosuppressive patients and those with multidrug-resistance tuberculosis (Mukherjee et al., 2004). Since the control of

bacterial resistance appears to be unsatisfactory, treatment with anti-tubercular (anti-TB) drugs is the only option available. The principal objective of chemotherapy in TB patients is the eradication of the whole bacillary load. Modern therapy relies on a combination of potent first-line antituberculosis drug which includes: isoniazid (INH), rifampicin (RIF), pyrazinamide (PZA) and ethambutol (EMB) (Table 1.4). In the case of multidrug-resistant (MDR-TB), in which the bacillus is resistant to these drugs, second-line drugs such as cycloserine, ethionamide and fluoroquinolones will be employed. Overall first line drugs are mainly bactericidal and combine a high degree of efficacy with a relative low toxicity to the patient during treatment, while second line drugs are mainly bacteriostatic and have lower efficacy and are usually more toxic. Thus, using second-line agents for TB treatment is not favored. Effective TB chemotherapy must include early bactericidal action against rapidly growing organisms and subsequent sterilization of dormant populations of bacillus. Multi-drug therapy is necessary for the treatment of active TB as single drug therapy of TB may result in development of drug resistance (Gandhi et al., 2010). According to WHO guidelines, the standard regimen for TB treatment uses a combination of rifampicin, isoniazid, pyrazinamide, and thambutol for 2 months followed by using rifampicin and isoniazid for further 4 months (Organization, 2015).

Table 1.4: Anti-tuberculosis drug regime (British National Formularly, 2015)

	Initial phase	**Continuous phase**
Duration	Two months	Four months
Antibiotics (Dose)	Rifampicin (450-600 mg) Isoniazid (300 mg) Ethambutol (15 mg/kg) Pyrazinamide (1.5-2 g)	Rifampicin (450-600 mg) Isoniazid (300 mg)
Frequency	Daily	Daily

To date the only routes of antituberculosis drug administration are the oral and parenteral routes. Although the oral and parenteral therapies are effective in treatment of TB, several studies reported some undesirable side effects leading to treatment interruption (Yee et al., 2003). Furthermore, prolonged administration of high doses is needed in the case of oral therapy as only small proportions of dose reach the lung, leading to side effects due to high

systemic exposure. For example, some side effects such as nausea, hepatotoxicity associated with acute renal failure have been reported by rifampicin when taken orally (Poole et al., 1971). In terms of parenteral route, the pain and inconvenient use make it not so highly acceptable. Consequently, the development of pulmonary anti-TB drug delivery systems with the ideal of increasing local drug concentration in the lungs and decreasing systemic side effects offers a potential value in TB treatment.

Several inhalable nanocarriers have been tested for local pulmonary delivery of drugs to treat tuberculosis (Costa et al., 2016). Polymeric nanoparticles have been tested for drug delivery to the lungs. A commonly investigated example of a natural polymer suitable for pulmonary delivery is PLGA, which has been greatly focused on as a carrier for anti TB drugs due to its high biodegradability and biocompatibility and low systemic toxicity. For example, Pandey et al. (2003) encapsulated anti-TB drugs into PLGA nanoparticles and evaluated their suitability for pulmonary delivery (Pandey et al., 2003). Prolonged drug retention in the lung and enhanced drug bioavailability of nebulized loaded nanoparticles was proved compared to oral administration of the drug. Similarly, porous nanoparticle-aggregate particles (PNAPs) were produced to examine the the encapsulation of rifampicin within PLGA nanoparticles and pharmacokinetic profiles (Sung et al., 2009). The results illustrated that rifampicin was released andmaintained its level in the lung over 8 h while free drug was cleared rapidly. Furthermore, a novel four-fluid nozzle spray drier has been established to produce rifampicin-PLGA microspheres.The results revealed that these carriers had good *in vitro* aerosol performance and enhanced uptake by alveolar macrophages compared to microspheres that were manufactured by a traditional two-fluid spray drier. Additionally, natural polymers, like chitosan and alginate have been employed to produce inhalable anti-TB drug delivery systems. *In vivo* pharmacokinetic and pharmacodynamic studies agree with previous data that respirable alginate nanoparticles had higher relative bioavailability compared to oral free drug (Zahoor et al., 2005). Thus, polymer based nanoparticles encapsulating anti-TB drugs have been demonstrated to be safely used for pulmonary tuberculosis treatment.

Liposomes are considered to be the simplest drug delivery systems for the treatment of pulmonary infections. The greatest advantage over other nanocarriers is the composition as they contain phospholipids similar in structure to that of pulmonary surfactants, resulting in high safety and decreased local irritation of the lung (Cipolla et al., 2014). Similary to

previously listed nanocarriers, liposomes are capable of increasing absolute bioavailability of aerosolised encapsulated drug and prolonging drug concentration in the lungs (Zaru et al., 2007). Furthermore, a higher antimycobacterial effect against *Mycobacterium bovis* was found by the encapsulation of isoniazid in liposomes compared to free drug (Rojanarat et al., 2011). However, the use of liposomes in TB inhalation therapy is limited by the lack of stability studies and clinical evaluation.

Although studies provided positive outcomes encouraging the use of nanocarriers in TB inhalation therapy, there are still some limitations and drawbacks in the application (Sosnik et al., 2010). None of the studies being tested now are dynamic systems, which makes the sustained release in the lungs unachieveable. Nanomaterial toxicity is another challenged concern. The interaction of nanoparticles with lung tissues and the long-term accumulation of inhaled nanocarriers in the lungs may lead to many toxic pulmonary issues such as pulmonary inflammation, fibrosis and lung cancer (Nel et al., 2006). Additionally, translocation and extrapulmonary delivery of inhaled nanocarrier may induce toxicity and adverse effects (Borm and Kreyling, 2004). On the other hand, cellular targeting delivery of anti-TB carriers is still a big challenge. Thus, it is of great importance to design a dynamic nanocarrier system suitable for controlled drug delivery to the lungs and thoroughly understand the complex nature of nanocarrier influence on biological systems.

1.10 Aims and scope of PhD

The overall aim of this thesis was to develop a new method to actively release drugs from nanoparticles intended for pulmonary delivery. Given the literature described in the introduction there are several key considerations when developing an active drug release nanoparticle system (Figure 1.5), for example, delivery of a drug to the airways using a nanoparticle system requires engineering of a micro-sized carrier in order to maximise deposition in the pulmonary tree (a), the liberation of the nanoparticles from the micro-sized carrier must occur efficiently after contact with the lung surface lining fluid (b), penetration of nanoparticles must occur through mucus in order to reach the epithelial surface (c), the nanoparticles must avoid clearance by the mucociliary escalator (d), the nanoparticles should reside at the epithelial barrier for a prolonged period of time (e), they should avoid rapid cell uptake (f). Ideally if the nanocarrier is to control drug release it should also aim to release the drug at the epithelial surface (e) and liberate their entrapped actives in a controlled manner.

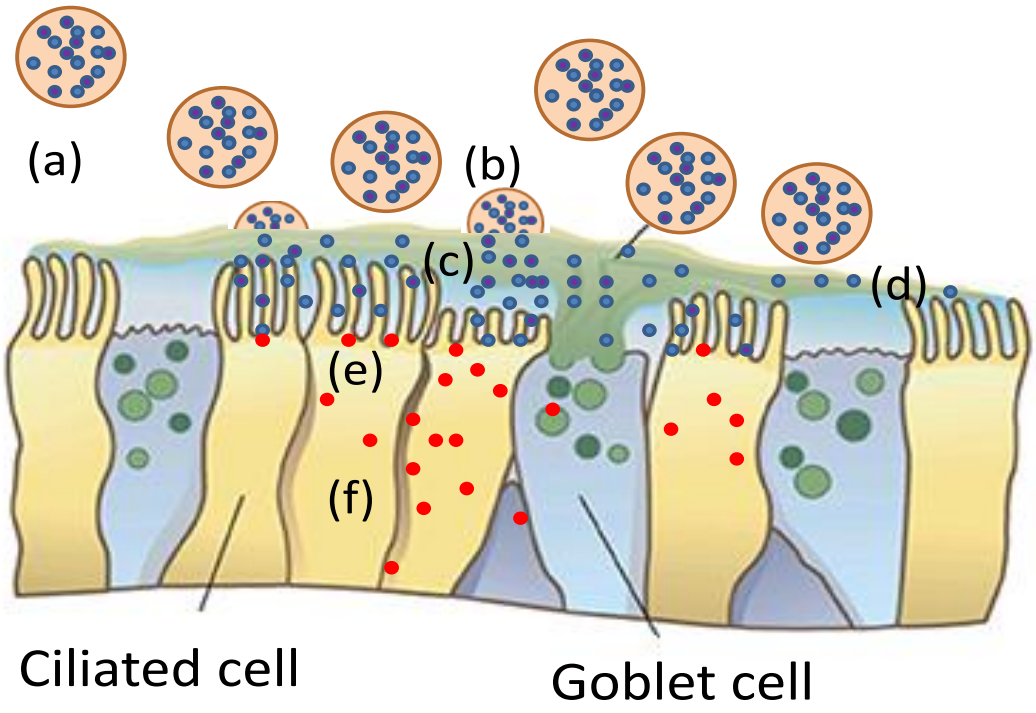

Figure 1.5: Considerations for an inhaled dynamic nanoparticle system: a) nanoparticle administration and b) liberation from a respiratory formulation, c) mucus permeation, d) mucociliary clearance, e) retention at mucus-epithelium interface and dynamic drug release and f) cell uptake.

It was anticipated that the delivery of nanoparticles to the lungs in this project would be achieved by incorporating a novel rifampicin-loaded nanosystem in an inert carrier to produce particles in inhalable size for deposition in the lungs. The formulation was designed such that after deposition within the pulmonary tract, the carrier matrix will readily release the nanoparticles. The nanoparticles should then penetrate through the mucus barrier rapidly and be retained at the mucus-epithelium interface, where the therapeutic payload can be released in a controlled manner at the targeted disease site.

The following objectives were set in order to help fulfil the overall aim:

- To manufacture nanoparticles that actively release their drug payloads in a controlled manner,
- To investigate the mechanisms of active release from nanoparticles,
- To assess nanoparticle diffusion through mucus barrier,
- To load nanoparticles into microparticles for inhalation,
- To track dynamic nanoparticles following administration to the respiratory tract

CHAPTER TWO

Active rifampicin release from nanoparticles using co-administered particle permeabilisers

2.1 Introduction

The potential of nanoparticles to function as carriers for drug delivery has received considerable interest over the last decade (Farokhzad and Langer, 2009; Parveen et al., 2012; Peer et al., 2007). It has been shown that they can act as an effective delivery system that provide opportunities to target the delivery of drugs, improve solubility of poorly-water-soluble drugs, enhance bioavailability and reduce immunogenicity (Park et al., 2009; Zhang et al., 2008).

The incorporation of inhaled drugs into nanoparticles has also been shown to solve some of the issues associated with the rapid clearance of agents delivered to the airways. For example, nanoparticles have been able to penetrate the mucus rapidly (Shan et al., 2015). Furthermore, nanoparticles may be able to evade clearance by macrophages and enter the respiratory epithelium more easily than larger-sized particles as alveolar macrophages are highly efficient at phagocytosing particles in the 1-3 μm range (Champion et al., 2008). But achieving a controlled drug release from the particles still remains problematic.

Currently available inhalation products on the market are mainly rapid release formulations, although numerous efforts have made to develop controlled release delivery systems (Loira-Pastoriza et al., 2014). Achieving controlled release in the lung using a non-toxic delivery system requires the nanoparticle to reside at the epithelial cell surface for a prolonged length of time. This is a challenge and as yet no commercial system has managed to achieve in the pulmonary system. One reason why this is the case is it is difficult to achieve payload retention prior to dosing and effective release upon administration, especially when nanoparticles are formulated as a nanosuspension (Zhao, 2010). The initial burst release is the most challenging problem in the development of controlled drug release using nanoparticles (Natarajan et al., 2014). It occurs during the first minutes of contact with the external medium and can liberate a significant portion of drug in a short period which can lead to acute toxicity, and / or rapid clearance and thus a low bioavailability. This rapid drug liberation from the nanoparticles can lead to acute toxicityand rapid clearance, thus a low bioavailability which is unhelpful *in vivo* (Danhier et al., 2009; Janes et al., 2001).

Improving the affinity of the drug for the carrier, e.g., by forming ion-pairs in the carrier matrix (Holmkvist et al., 2016; Natarajan et al., 2014; Pinkerton et al., 2012), can reduce the passive release and even facilitate drug release overseveral days (Mukherjee et al., 2008), but

such a slow release can lead another problem, incomplete drug liberation. If the drug release is too slow therapeutic index might be not maintained over a relatively long period. If nanoparticles do not liberate entire payload then this can also limit their applicability to only very potent molecules.

It has been shown that lipid nanocapsules can reside in the lung for up to 2 days (Patel et al., 2016). The ideal scenario for controlled drug to the lung is to use a system, which allows strong retention of the drug during formulation storage and complete liberation upon delivery. This is very difficult to achieve passively and hence there is a need to develop active release strategies that will facilitate controlled drug delivery from nanoparticles when they are administered to the lung.

Nanoparticles that respond to shell permeabilisation can provide active drug release and thus they provide one potential solution to the issues faced during the development of a controlled release nanoparticle for local delivery to the lung. The systems involve the modification of material properties by varying environmental conditions after administration using a chemical or physical stimulus to permeabilise the shell of the nanocarrier to facilitate drug release (Mura et al., 2013). The most significant advantage of active drug release nanoparticle systems is better drug delivery targeting compared to conventional system, i.e. the drug is only released when needed.

The aim of this Chapter was to investigate the drug release of rifampicin, a model drug, from two different nanoparticles that had the potential to display active drug release in response to a chemical permeabilisation process. A polymer shelled nanoparticle, constructed with a lipid benzyl benzoate core, a phospholipid intermediate layer and an outer poly(vinyl alcohol) (PVA) shell, was compared with alipidic shelled nanoparticle, which contained a triglyceride core and a semi-solid phosphatidylcholine / PEG hydroxystearateshell. Both nanoparticles have been shown to be biocompatible with lung airway cells (Chana et al., 2015; Madlova et al., 2009a) and their inflammatory potential *in vivo* has been assessed (Jones et al., 2014). The shell permeabiliser for the lipid nanoparticle was a Pluronic surfactant, which had previously been shown to induce distension of the carrier when a dye was loaded into it (Chana et al., 2015). To modify the PVA carrier an aliquot of an acidic buffer was incubated with the carrier in attempt to modify the hydrolysis of the polymer. To better understand how the model drug was released from the nanoparticles, two pH conditions 7.4 and 4.2 were selected as they had some relevance to *in vivo* conditions, i.e. they mimicked the

physiological pH of the lung airways and lysosomal compartments respectively (Mindell, 2012). In addition, the Chapter sought to investigate in detail how the particle modification changed the nanoparticle properties during drug release and test the robustness of the permeabilisation process to function in different environmental conditions.

2.2 Materials

Medium chain triglycerides (Labrafac® lipophile 1349), purified phosphatidylcholine (> 90 %) from soybean lecithin (Epikuron® 200) and PEG 15 hydroxystearate (Solutol® HS15) were kindly supplied by Gattefossé S.A. (Saint-Preist, France), Cargill GmbH (Germany), and BASF (Ludwigshafen, Germany), respectively. Pluronic® L62D was sourced from BASF (New Jersey, USA). Poloxamer 188 was from BASF (Ludwigshafen, Germany). Sodium chloride, sodium hydroxide, poly(vinyl acetate), benzyl benzoateand rifampicin (≥ 97%, high performance liquid chromatography HPLC grade) were purchased from Sigma Aldrich (Gillingham, UK). HPLC grade water, ethanol and methanol were obtained from Fischer Scientific (Leicestershire, UK).

2.3 Methods

2.3.1 Fabrication of lipid shell nanoparticles

Lipid shell nanoparticleswere manufactured via precipitation from a stable emulsion following repeated phase inversion, as previously described by Heurtault et al (Heurtault et al., 2002). Medium chain triglycerides (17% w/w), phosphatidylcholine (1.75% w/w), PEG hydroxystearate (17% w/w) and a 3% w/v sodium chloride aqueous solution (64.25% w/w) were mixed at room temperature and then heated to 85 ℃ at a rate of 4 ℃ per minute, with continuous magnetic stirring. The mixture was then allowed to cool to 60 ℃. The temperature of the mixture was cycled between 60 ℃ and 85 ℃ a total of three times. Within this temperature range phase inversion occurred, with an oil-in-water emulsion being converted to and from a water-in-oil emulsion. Following the final heating cycle, the emulsion was allowed to cool to 72 ℃, at which point 25 mL of ice-cold water was added, causing nanoparticle generation. The suspension was stirred for 5 min then made up to a final volume of 50 mL using deionised water. Lipid shell nanoparticle suspensions were purified of excess excipients and larger particulate matter via centrifugation (Beckman L8-80 ultracentrifuge, Beckman Coulter, Buckinghamshire, UK) at 110,000 *g* and 25 ℃ for 1 h. The suspension separated into three distinct layers; an upper gel like layer, a middle lipid shell nanoparticle suspension layer, and a bottom sediment layer. The purified suspension layer was used for further experimental work.

2.3.2 Synthesis of poly(vinyl alcohol)

The synthesis of PVA used to produce the nanoparticles was based on direct saponification method. PVA 32% hydrolysis was produced from a poly(vinyl acetate) via a stiochiometric reaction according to reaction (Chana et al., 2008). For 40% hydrolysis, for example, the starting mass of PVAc was 1 g, this provided 0.01163 moles of the vinyl acetate monomer and thus 0.004652 moles of NaOH was required to achieve 40% hydrolysis, assuming a 100% reaction efficiency. The concentration of NaOH solution was 0.18608 g/mL and this was added dropwise to 1 g of PVAc dissolved in 8 mL of acetone in a round bottom flask with a small 12 mm magnetic stirrer. The materials refluxed for a period of 1.5 hour (heating level 5, ~80 ℃) with continuous mild magnetic stirring and then the solution was transferred to a 50 mL beaker and placed in the fume hood to allow the organic solvent to evaporate overnight. A purification step was employed to remove sodium acetate by-product. Purification was conducted by adding 5 mL of preheated 80 ℃ deionised water and incubating the solution for 5 minutes, filtering through a 47-μm cellulose nitrate membrane under the vacuum and collecting the product. The purified polymer was placed on a grease proof paper weighed previously, dried at 80 ℃ overnight and the amount of product was weighed on the subsequent day to generate a yield.

2.3.3 ^{13}C nuclear magnetic resonance analysis of poly(vinyl alcohol)

To determine the percentage hydrolysis of the polymer nuclear magnetic resonance (NMR) analysis was performed on 60 mg of dried PVA sample dissolved in 660 μL of methanol-D4 and 330 μL of deionised water. Samples were heated gently at 60°C in water bath for a while to aid the solubility of PVA until the solution was totally transparent. A 600 μL aliquot of the sample was used for the measurements which were conducted at 100.61 MHz frequency using a temperature of 24 ℃. Triplet measurements were performed. The percentage hydrolysis was calculated according to the previously detailed method (Chana et al., 2008).

2.3.4 Fabrication of poly(vinyl alcohol) shell nanoparticles

Poly(vinyl alcohol) PVA shell nanoparticles were manufactured by nanoprecipitation. In order to optimise the formulation, the fabrication was conducted using different polymers. Briefly 20%, 40% and 80% hydrolyzed PVA was used with the amount ranging from 0 to 100 mg in the recipe. Citrate buffer was prepared by adding 40 mL of 0.1 M citric acid

solution to 60 mL of 0.1 M sodium citrate solution and adjusted to achieve a pH of 4.8. Poloxamer 188 (0.5 % w/v) was added to citrate buffer and made up to a volume of 100 ml. Methanol:water 9:1 was used as organic solvent. A mixture of 50 mg PVA and 75 mg of Epikuron phospholipids was dissolved in 5 mL and 10 mL of organic solvent respectively. An aliquot of 0.33 mL of benzyl benzoate was added to the methanol/water mixture to complete the organic dispersing phase. To fabricate the nanoparticles, the aqueous phase (30 mL) was homogenized at 5000 rpm for 2 minutes and then 15 mL of the organic phase was added drop-wise, at a speed of 8 mm/min, using a syringe pump. The homogenization process was continued for 10 minutes. The suspension produced was transferred to the fume hood and left to stir overnight to remove the organic solvent. The suspension was centrifuged at 4000 rcf for 5 minutes at 20 ℃ to remove large particle contamination.

2.3.5 Nanoparticle characterization

Nanoparticle size was analysed using photon correlation spectroscopy (PCS) (Zetasizer Nano, Malvern Instruments, Worcestershire, UK). All measurements were carried out at a scattering angle of 173 ° using water as the dispersant (refractive index 1.33, viscosity 0.8872 cP at 37 ℃). Each measurement comprised 10-14 runs and was performed in triplicate for each sample. Mean diameters obtained from the size-intensity frequency distributions were reported. To investigate the effect of suspension concentration on the accuracy of the size measurement, and to determine the absolute nanoparticle diameter, analyses were performed on particle suspensions serially diluted with HPLC grade water (n = 3). Mean diameter was plotted against suspension concentration, and the y-axis intercept following linear regression analysis was determined as the absolute diameter. The zeta potential of the nanoparticles was determined as a function of their electrophoretic mobility (Zetasizer Nano, Malvern Instruments, Worcestershire, UK). Samples were analysed following dilution with HPLC grade water. Each measurement comprised between 50 to 100 runs and was performed in triplicate at 37 ℃.In order to determine the solid content (mg/mL) of the purified nanoparticles, 0.5 mL aliquots were transferred to Amicon centrifuge tube and spin for 30 min. Then the inner cells were removed and dried in a fume hood until a constant mass was recorded.

2.3.6 HPLC analysis of rifampicin

HPLC quantification of rifampicin was performed using a Jasco HPLC pump and a dual absorbance detector. The column used was a reversed-phase C18. UV detection was performed at 335 nm. The mobile phase consisted of acetonitrile:PBS buffer (40:60 % v/v) pH 7.4 at a rate of 1 mL/min. 20 µl of sample injection volume was employed throughout. Calibration standards were produced using a 1 mg/mL rifampicin stock solution in methanol. Six serial dilution of the stock generated calibration standards in the range of 0.1-0.002 mg/mL. Calibration plots were constructed for rifampicin in standard solutionsby plotting the concentration verse peak area. The linearity of the calibration plots were evaluated using least square regression analysis. Intra-day and inter-day variation was assessed by determining the coefficient of variation (CV). The limit of detection (LOD) and the limit of quantification (LOQ) of the system were also determined.

2.3.7 Chemical stability of rifampicin

The chemical stability of rifampicin was determined by measuring the recovery of rifampicin from buffer solution. Briefly, solution of rifampicin in PBS buffer pH 7.4 was prepared and was constantly stirred at 37 ℃. At pre-determined time points, samples were withdrawn from the solution and analysed by HPLC and the recovery of rifampicin was evaluated.

2.3.8 Nanoparticle loading

For lipid shell nanoparticles, rifampicin was incorporated into the carriers by addition to the triglyceride phase as a 0.5% w/v acetonic solution. The acetone was removed by evaporation before continuing with the manufacture protocol. In order to try and enhance the interaction between rifampicin and oil, two counterions, sodium stearateand sodium ethyl acetate were combined with rifampicin at the molar ratio of 1:20 during the manufacture.For the fabrication of drug loaded PVA shell nanoparticles, 15 mg of rifampicin was dissolved in the organic phase and the manufacture was repeated as optimised previously. Amicon centrifugal device was used for loading assessment. The amount of each probe contained in a) the purified suspension as a whole, b) the nanoparticles only and c) the continuous phase was assayed by appropriate dilution of each compartment. The nanoparticles were separated from the continuous phase using Amicon ultra 0.5 centrifugal filter devices with ultracel 100 membranes (100 kDa molecular weight cut off) (Millipore, UK). Aliquots of 0.5 mL were

removed from the purified nanoparticle suspension and placed in the sample reservoir of the filter devices and centrifuged for 30 min at 14,000 *g* at ambient temperature (Biofuge Pico centrifuge, Heraeus, Buckinghamshire, UK). During this process any free drug in the continuous phase passed through the filter into the receiver chamber, and the nanoparticles were retained on the filter. The filtrate was diluted with water and subjected to HPLC analysis. The nanoparticles were dissolved in methanol and subjected to HPLC analysis. The drug recovery and loading efficiency of the purified nanosuspensions were calculatedusing Equations 2.1 and 2.2, respectively:

$$\text{Drug recovery} = \frac{\text{Mnanoparticle} + \text{Mfiltrate}}{\text{Msuspension}} \quad \text{Equation 2.1}$$

$$\text{Loading efficiency (\%)} = \frac{\text{Mnanoparticle}}{\text{Minput}} \quad \text{Equation 2.2}$$

Where $M_{suspension}$ was the mass of drug in the nanoparticle suspension; $M_{nanoparticle}$ was the mass of drug encapsulated into the nanoparticle; $M_{filtrate}$ was the mass of drug in aqueous filtrate and M_{input} was the mass of drug added during manufacture.

2.3.9 Release of rifampicin from nanoparticles

To characterize rifampicin release from the lipid shell nanoparticles, the drug remaining in the carrierswith and without prior exposure to shell permeabiliser Pluronic L62D was measured. When the lipid nanoparticle permeabliser was used it was mixed with the purified nanoparticle suspensions at a Pluronic: nanoparticle ratio of 1:0.5 w/w. The release of the lipid shell nanoparticles was determined by dialyzing the nanoparticle suspensions against PBS buffer (1.6 mg nanoparticle per mL buffer) either at pH 7.4 and 4.2, 37 ℃. For the PVA shell nanoparticles without the shell permeabiliser the suspensions generated by the manufacture method were mixed with PBS pH 7.4 in a 1:1 v/v and the drug release determined by dialysis. To permeabilise the PVA shell nanoparticles PBS pH 4.2 buffer was added to nanoparticle suspension in a 1:1 v/v and the mixture was transferred to a dialysis sac and dialysed against 500 mL of PBS buffer at either pH 7.4 or pH 4.2 to determine the drug release. The rifampicin solubility was measured to be 1550 μg/mL at pH 7.4 and 750 μg/mL at pH 4.2 and therefore sink conditions were maintained in all the release experiments (total loading per 500 mL was *ca.* 1.2 mg). To monitor the drug release from all the nanoparticle experiments 0.5 ml aliquots were removed from dialysis the tubing containing the suspensions (12-14 kDa molecular weight cut off) at a series of pre-determined time points and rifampicin content in the nanoparticles was measured by HPLC (as detailed in the

loading assessment method). The drug content remaining in the nanoparticles was calculated according to Equation 2.3:

$$\text{Release (\%)} = \frac{M0 - Mt}{M0} \quad \text{Equation 2.3}$$

Where M_0 was the mass of drug in nanoparticleat t_0 and M_t was the mass of drug in nanoparticle at a time point.

2.3.10 Size changes of permeabilised lipid nanoparticles

Changes in the size of the lipid nanocarries in response the shell permeabiliser were measured after the suspensions were exposed to Pluronic surfactant using identical conditions as in the release study. At regular intervals between 30 min and 24 h post permeabiliser exposure samples were taken from the dialysis tubing where the particles were being suspended and the particle size was measured. PCS was also used to study the effect of pH on the ability of surfactant to aggregate. Surfactant solutions of 1 to 100 mg/mL were prepared in PBS at the two pHs 7.4 and 4.2 as used in the release study. The derived count rate of the solutions were measured and the critical micelle concentration (CMC) of the surfactant in each of the pH conditions was determined by estimating where the two linear models applied to the derived count rate data intercepted. The lipid nanoparticles were also visualised using transmission electron microscopy (TEM) before and after exposure to the shell permeabiliser. The suspension (3 μL) was applied to a Pioloform-coated copper grid and allowed to settle for one min. Excess suspension was blotted away with filter paper and the grid washed twice over distilled water before negative staining with 3 μL of an aqueous 1% uranyl acetate solution. The grids were allowed to dry before examination with a Tecnai T12 electron microscope (FEI, Oregon, USA).

2.3.11 Size changes of permeabilised Poly(vinyl alcohol) nanoparticle

The particle size of the polymer nanoparticles had been previously determined not to change (~250 nm after permeabilisation) in preliminary work and hence changes in the chemical composition of the carrier matrix upon exposure to the shell permeabiliser were characterised using Fourier transform infrared spectroscopy (FTIR) (Perkin Elmer, Beaconsfield, UK). The FTIR spectrometer was fitted with a DuraSamplIRII diamond attenuated total reflectance attachment (Smiths detection, Warrington, UK). Each sample was applied in its liquid state to the diamond and 32 scans were performed to generate the spectra. Peak positions were

determined using Spectrum One software (version 6). Intensities of peaks referring to O-H and C-O bonds were specifically analysed in order to search for changes in the polymer hydrolysis over time. Nanoparticle size change before and after the shell permeabiliser were captured by TEM as described above.

2.3.12 Statistical analysis

SPSS version 20 (IBM, UK) was used for all statistical analyses. The normality (Sapiro-Wilk) and homogeneity of variances (Levene's test) of the data were assessed prior to statistical analysis. The transport data were analysed statistically using T-test or Mann-Whitney test. Differences were considered to be statistically significant at a level of $P < 0.05$.

2.4 Results

2.4.1 Nanoparticle characterization

NMR analysis of PVAc polymer showed mean hydroxylation values of 14.8 ± 2.0%, 31.9 ± 1.4% and 56.4 ± 3.3% for $PVA_{20\%,}$ $PVA_{40\%}$ and $PVA_{80\%}$ respectively, which were a slightly lower than targeted value (Figure 2.1). Different percentage polymer hydrolysis seemed to have no great effect on physiochemical properties of PVA shell nanoparticles (Table 2.1). PCS of the purified suspensions revealed a unimodal, normally distributed particle population in the nanometre size range (Figure 2.2). The blank lipid shell nanoparticles and the polymer shell nanoparticles had a mean diameter of ca. 50 and 250 nm and a polydispersity index of 0.074 ± 0.02 and 0.143 ± 0.02, respectively (Table 2.1). The lipid nanoparticles recorded a zeta potential of -3.46 ± 0.60 mV whilst the polymer nanoparticles had a zeta potential of-0.27 ± 0.45 mV. In order to investigate if the dispersion media was having a significant influence of the PCS data, the particle size measurements were repeated upon serial dilution of the nanoparticlesuspensions. The size measured upon dilution was consistent for the lipid shell nanoparticles over the tested dilution range, the effective diameter, i.e. the predicted size at infinite dilution was 49 nm (Figure 2.3). However, the size of the polymer shell nanoparticles reduced in size upon dilution due to the interference of the water soluble stabiliser with the size measurements and gave an effective hydrodynamic diameter of 204 nm (Figure 2.3).

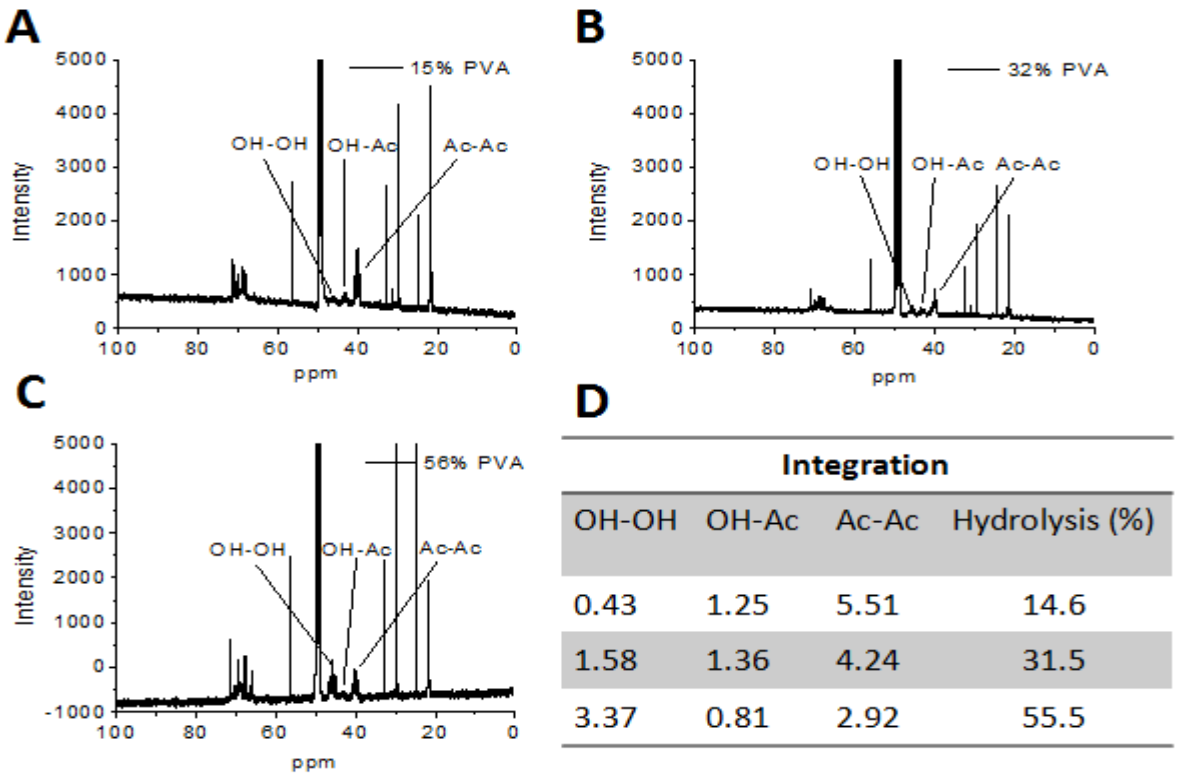

D

Integration			
OH-OH	OH-Ac	Ac-Ac	Hydrolysis (%)
0.43	1.25	5.51	14.6
1.58	1.36	4.24	31.5
3.37	0.81	2.92	55.5

Figure 2.1: NMR of 10%, 32% and 56% hydrolyzed PVA and corresponding calculation.

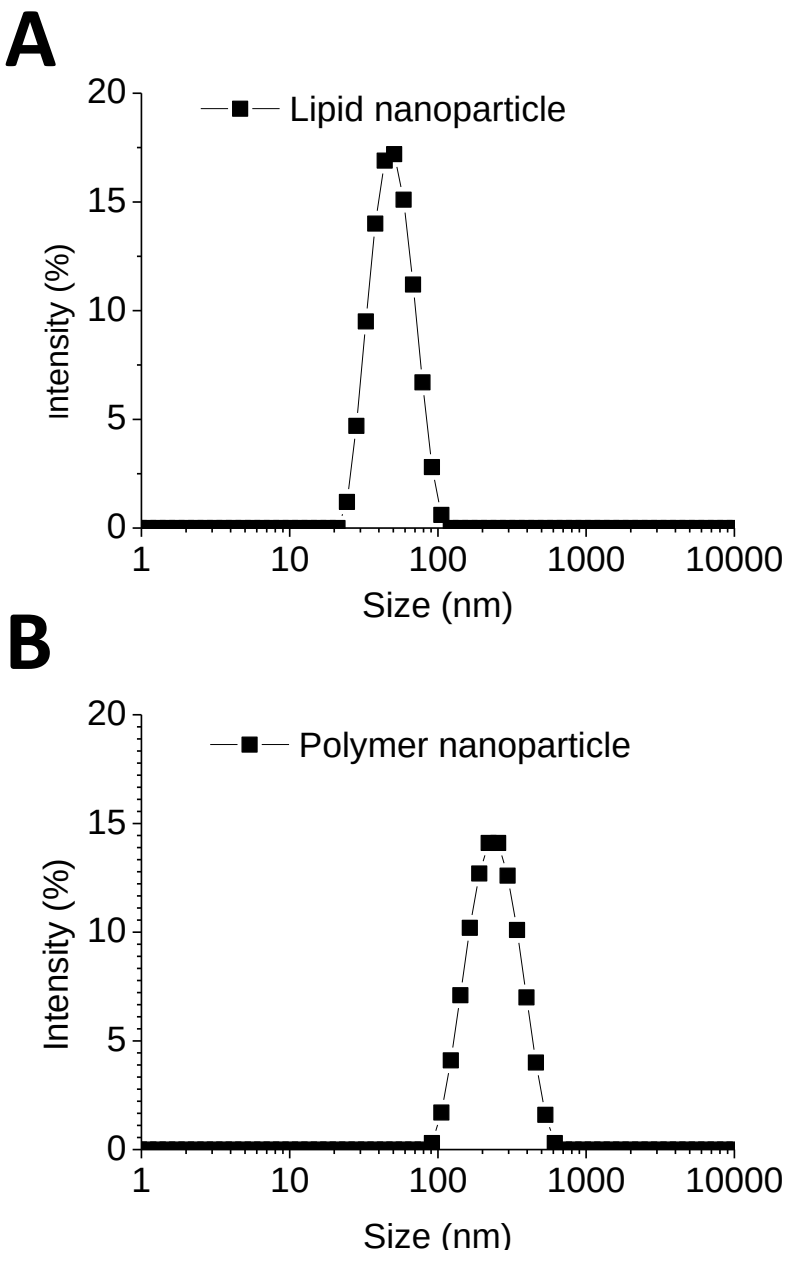

Figure 2.2: Representative size distribution (intensity weighted) of (A) lipid shell nanoparticles and (B) 32% PVA shell nanoparticles following 1/1 v/v dilution with water, as measured using photon correlation spectroscopy. Data represent mean ± standard deviation (n = 3).

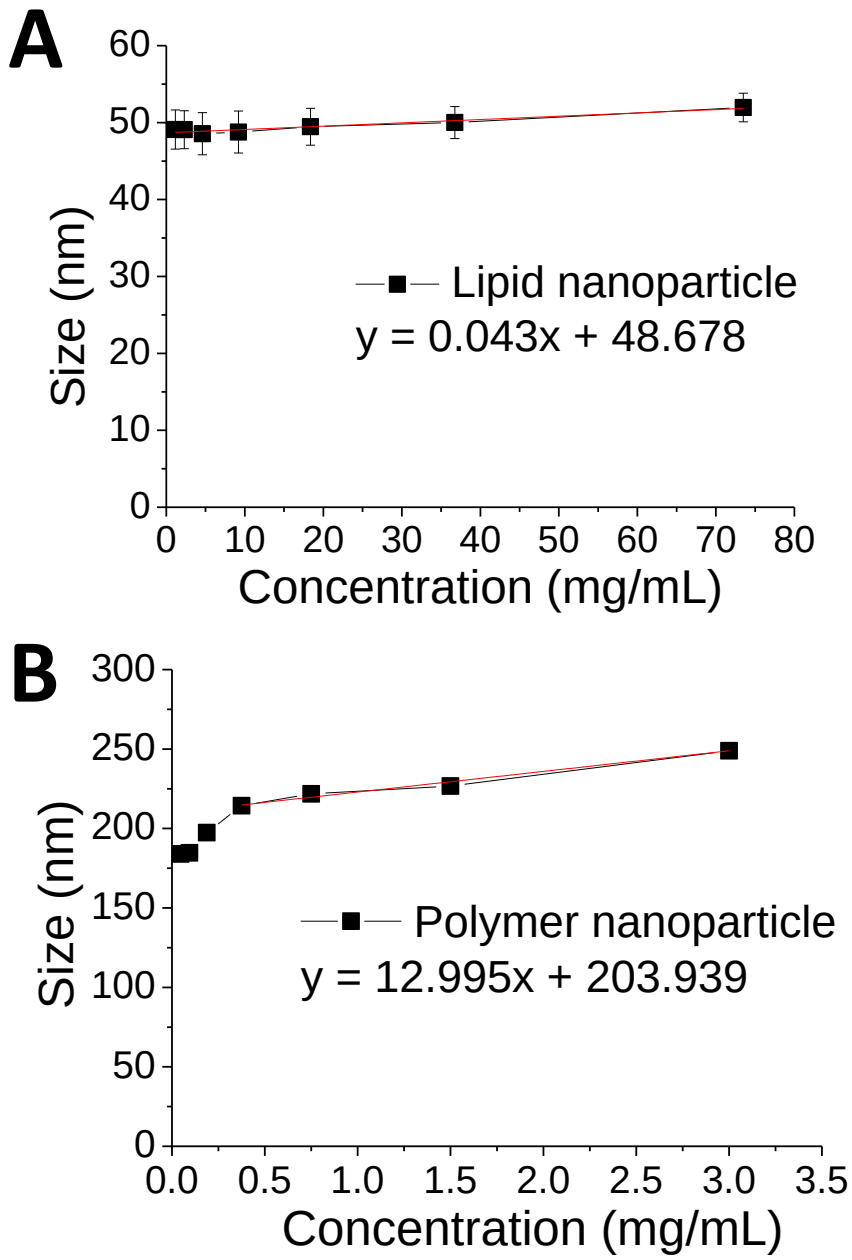

Figure 2.3: Determination of nanoparticle absolute hydrodynamic diameter following linear regression of nanoparticle size versus suspension concentration (mg/mL) using (A) lipid shell nanoparticles and (B) 32% PVA shell nanoparticles. Data represent mean ± standard deviation (n = 3).

Table 2.1: Size, polydispersity, zeta potential and solid content for unloaded (blank) and rifampicin-loaded lipid shell nanoparticles (LNP) and polymer shell nanoparticles (PVA). *Measured at nanoparticle concentration of 80 mg/mL and 3 mg/mL for LNP and PVA. Data represent mean ± standard deviation (n = 3).

NP type	Mean size (nm)*	Polydispersity* index	Zeta potential* (mV)	Solid content (mg/mL)
LNP_{blank}	52 ± 2	0.07 ± 0.02	-3.46 ± 0.60	146.7 ± 12.2
$LNP_{rifampicin}$	50 ± 3	0.07 ± 0.02	-2.07 ± 0.62	163.3 ± 7.0
$PVA10\%_{blank}$	248 ±7	0.12 ± 0.01	-0.21 ± 0.05	5.5 ± 1.2
$PVA10\%_{rifampicin}$	252 ± 7	0.22 ± 0.03	-0.17 ± 0.10	6.4 ± 1.1
$PVA32\%_{blank}$	249 ± 5	0.14 ± 0.02	-0.27 ± 0.45	5.9 ± 1.5
$PVA32\%_{rifampicin}$	261 ± 7	0.22 ± 0.02	-0.26 ± 0.37	6.0 ± 0.9
$PVA56\%_{blank}$	250 ±6	0.21 ± 0.02	-0.13 ± 0.21	4.7 ± 1.2
$PVA56\%_{rifampicin}$	258 ± 3	0.24 ± 0.04	-0.22 ± 0.03	5.2 ± 1.1

2.4.2 HPLC assay

Calibration curves constructed for rifampicin displayed a high degree of linearity (R^2> 0.999) in the concentration ranges tested (Figure 2.4). Intra-and inter-day variation data indicate the precision of the assay (Table 2.2). The average intra-day and inter-day variation data was 1.8% and 2.4%. Based on intraday data the limit of detection (LOD) and limit of quantification (LOQ) for the rifampicin assays were 2.5 and 8.4 µg/mL respectively.The developed assay was found to be fit for purpose in terms of precision and limits of detection and quantification.

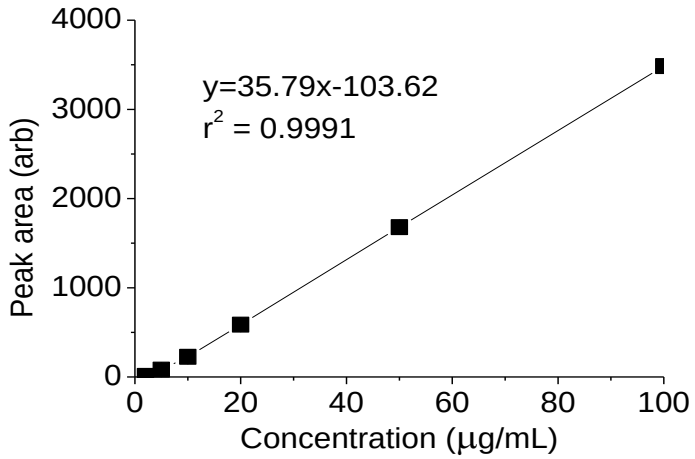

Figure 2.4: Representative calibration curve for rifampicin in methanol. Data represent mean ± standard deviation (n=3, error bars too small to be seen).

Table 2.2: Intra and inter-day variation in rifampicin peak area as a function of concentration in methanol. Intra-day variation data obtained from three days using the same standards (n=3). Inter-day variation data obtained over three days (n=9).

Concentration (µg/mL)	**Coefficient of Variation (%)**	
	Intraday	Interday
100	0.73	1.09
50	0.53	1.00
20	1.31	1.09
10	2.23	1.78
5	2.10	2.76
2	3.85	6.54

2.4.3 Rifampicin chemical stability

Although no significant peaks referring to degradants were found by HPLC assay, rifampicin recovery at PBS buffer 7.4 decreased by approximately 70% over 72 h (Figure 2.5). Therefore, rifampicin remaining in the nanoparticles was used to indicate the amount of drug release in the following work.

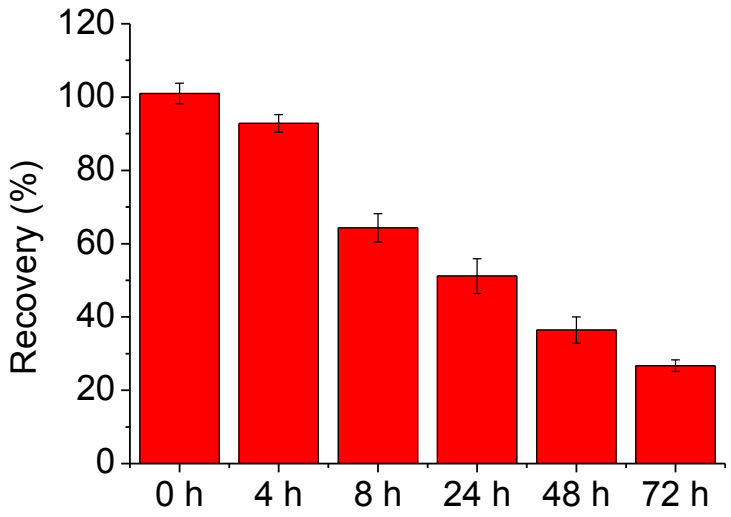

Figure 2.5: Recovery of rifampicin in PBS buffer pH 7.4 at 37 ℃ over 72 h. Data represent mean ± standard deviation (n = 3).

2.4.4 Optimisation of poly(vinyl alcohol) shell nanoparticles

As passive release was found in previous literatures, PVA shell nanoparticles with different formulations were manufactured to find the best formula. Nanoparticles made from 32% hydrolysed polymer had the highest loading efficiency compared to higher or lower hydrolysis degrees (Figure 2.6A). Different polymer amounts input also had great impact on the drug loading and release as shown in Figure 2.6A. When 50 mg of polymer was used in fabrication appeared to have a better formulation with a higher loading efficacy. Thus, 50 mg of 32% polymer would be used in the following nanoparticle manufacture to assess the drug loading and release.

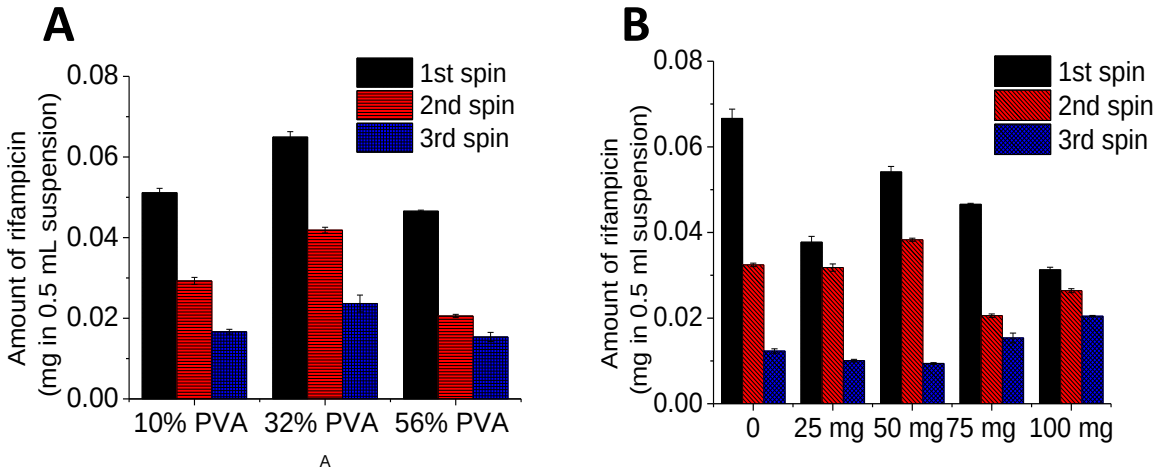

Figure 2.6: Passive release of rifampicin from different PVA shell nanoparticle formulations: (A) the effect of polymer hydrolysis degrees and (B) the effect of amount of 32% polymer in the recipe. Data represent mean ± standard deviation (n = 3).

2.4.5 Lipid shell nanoparticle drug release

Rifampicin was loaded into the lipid nanoparticles with an acceptable loading efficiency, 41.0 ± 11.4%. An average drug recovery of 90% was observed in the loading experiments. Continuous passive release from the lipid shell nanoparticles was observed at both pH 7.4 (A) and pH 4.2 (C) (Figure 2.7). This continuous release, which was presumably initiated immediately after manufacture, required the release testing be performed at an identical time post manufacture in all the studies. This strategy led to acceptable intra-batch variability across the experiments. The data demonstrated both in the presence and absence of the shell permeabilisers the drug release showed zero order kinetics (Figure 2.7B, D). However, the attempt to hold the drug in the oil to reduce the passive drug release using ion-pairing failed (Figure 2.8).

Despite the inability to prevent the continuous drug release from the lipid nanoparticles, there was still a significant increase in the extent of release at each time point when the shell permeabilisers were added to the nanoparticles at pH 7.4 ($P<0.05$). The drug release rates (k) for the lipid shell nanoparticlein the presence of the shell permeabiliser was double that of the control system ($P<0.05$), with the control and permeabilised nanoparticles releasing approximate 50% and 80% of their rifampicin load over 24 h. When PBS buffer at pH 4.2 was used as the release medium, there was no significant difference in release extents and rates between permeabilised and non-permeabilised nanoparticle test systems ($P>0.05$). The rate of drug release was suppressed at pH 4.2 compared to pH 7.4, i.e. it reduced from 0.0032 mg/h to 0.0030 mg/h.

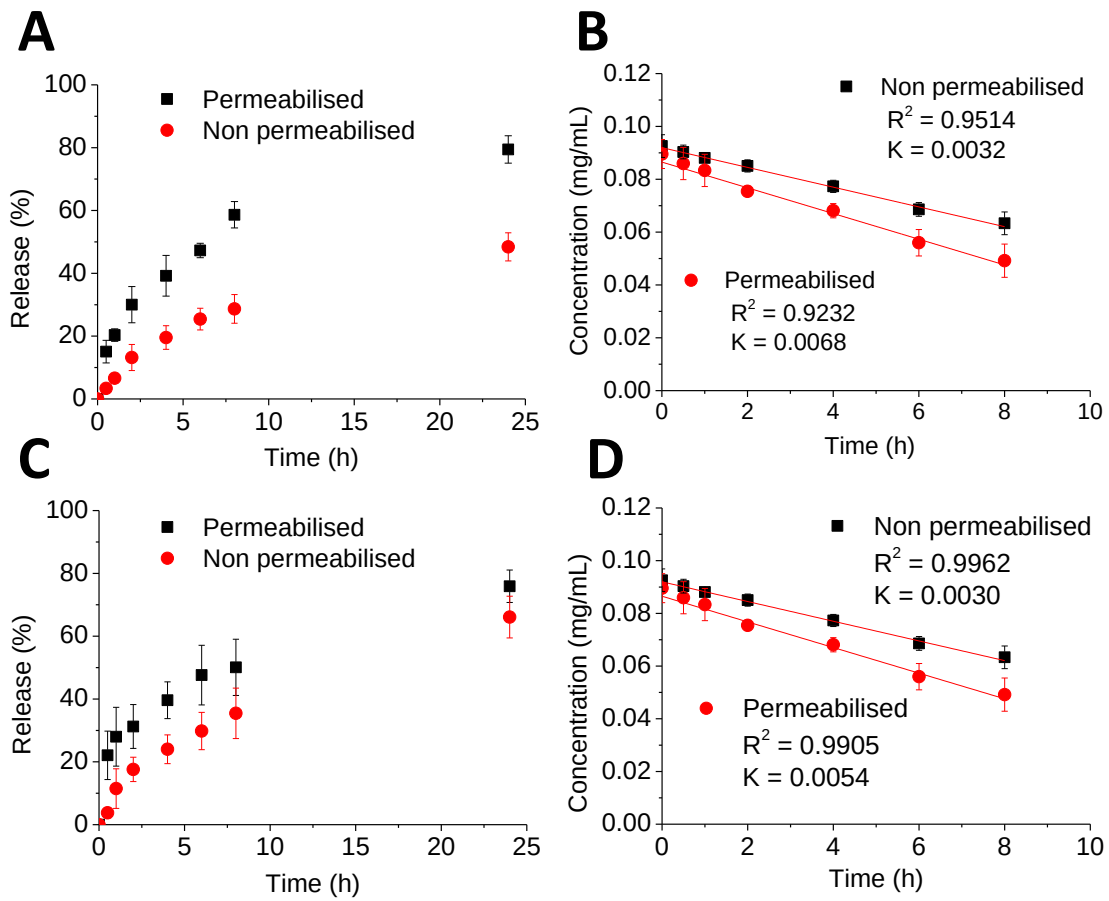

Figure 2.7: Release of rifampicin loaded lipid shell nanoparticles against (A) PBS buffer pH 7.4 and (C) PBS buffer pH 4.2. Graph (B) and (D) show the application of a linear model to the corresponding drug release. Data represent mean ± standard deviation (n = 3).

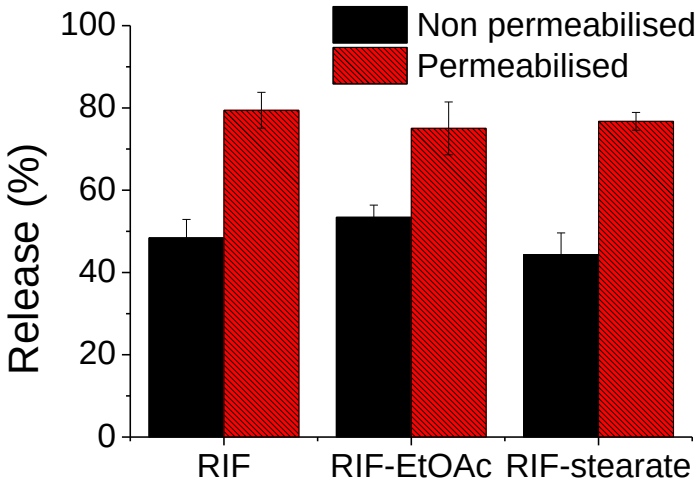

Figure 2.8: Release profiles of rifampicin-stearate and rifampicin – ethyl acetate ion paired lipid shell nanoparticles at 24 h against PBS buffer pH 7.4 compared to rifampicin loaded nanoparticles. Data represent mean ± standard deviation (n = 3).

2.4.6 Polymer shell nanoparticle drug release

The drug loading in the polymer shell nanoparticle was 25.9 ± 2.3%. In a similar manner to the lipid shell nanoparticles, at pH 7.4 continuous drug release (k=0.023 mg/h) was observed which was enhanced upon exposure to the shell permeabiliser (k=0.034 mg/h) ($p<0.05$, Fig.2.9). An 10% burst release was recorded in the release experiments which seemed low compared to previous reports of up 80% burst release with polymer nanoparticle. Almost 80% of drug came out the polymer shell nanoparticles which were subject to permeabilisation over 8 h, which was nearly double the control non-permeabilised system ($P<0.05$). When the release study was assessed in the pH 4.2 medium similar profiles were observed with and without the permeabiliser (no significant difference in drug release across the two sets of nanoparticles, $P>0.05$, Figure 2.9). The release rate of non-permeabilised nanoparticles in the acidic medium from 0.0023 mg/h to 0.0020 mg/h compared to the neutral release environment.

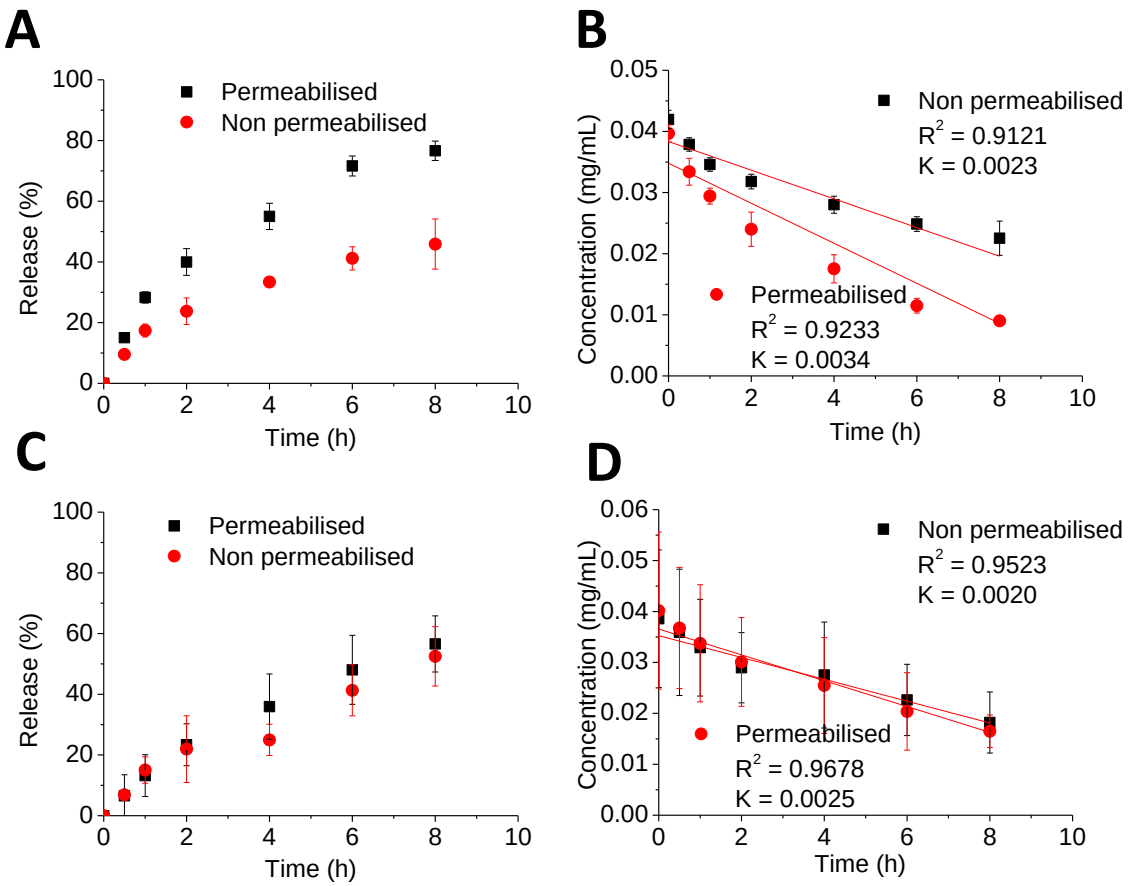

Figure2.9: Release of rifampicin loaded PVA shell nanoparticles against (A) PBS buffer pH 7.4 and (C) PBS buffer pH 4.2. Graph (B) and (D) show the application of a linear model to the corresponding drug release. Data represent mean ± standard deviation (n = 3).

2.4.7 Permeabilisation mechanism for lipid shell nanoparticles

The exposure of lipid shell nanoparticlesto the Pluronic surfactant permeabiliser at pH 7.4 induced a substantial increase in the carrier size over time ($P<0.05$), resulting in a mean size of 240 ± 1 nm at 24 h (Figure 2.10). No size change was recorded for the exposure at pH 4.2 compared to non-permeabilised nanoparticles. The light scattering data revealed that the Pluronic L62D surfactant displayed a significantly lower CMC (8.1 ± 1.4) at pH 4.2 compared to pH 7.4 (25.2 ± 2.1) ($p<0.05$, Figure 2.11), indicating the greater propensity for the surfactant to aggregate in the more acidic pH medium. TEM images of control lipid nanoparticle suspensions revealed the presence of spherical particles in the 50 nm size range (Figure 2.12). Following an 8 hour exposure to Pluronic L62D at pH 7.4 the lipid shell nanoparticles were larger (~200 nm), which agreed with the light scattering data (Figure 2.10).

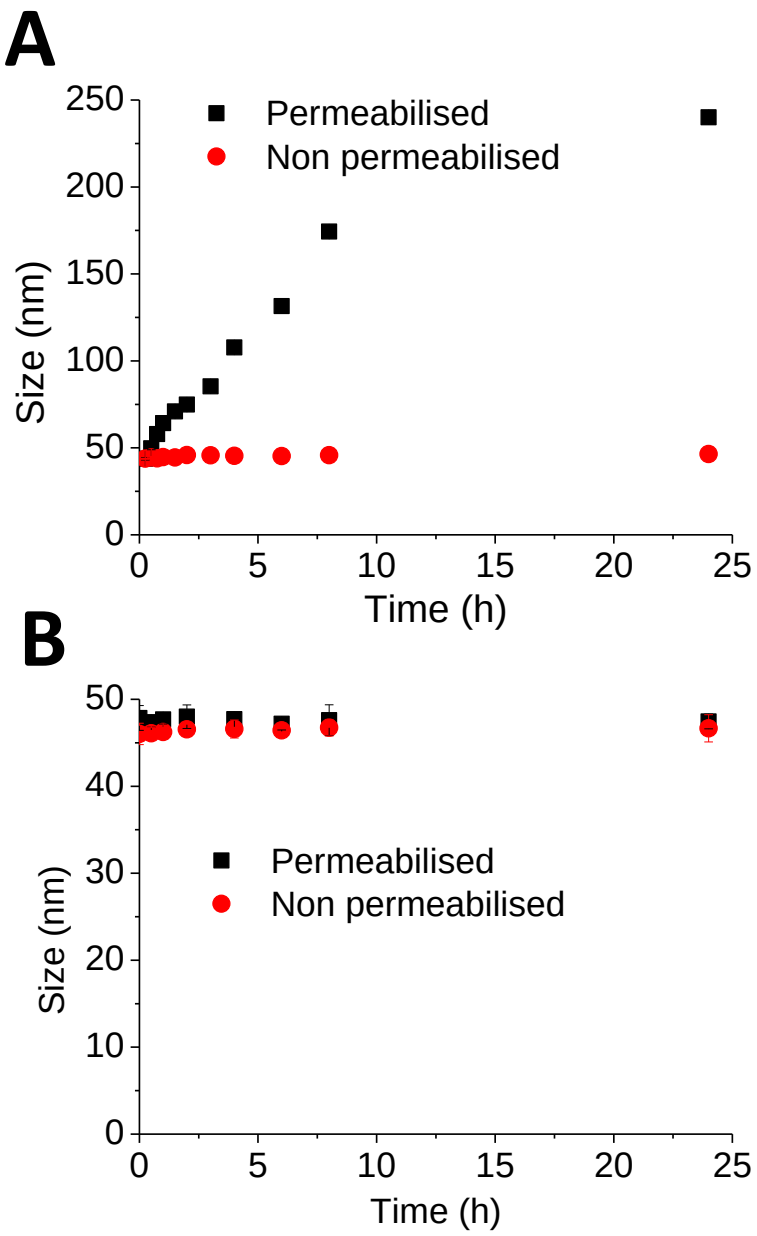

Figure2.10: Lipid shell nanoparticle permeabilisation over time following exposure to permeabiliser Pluronic L62D at (A) pH 7.4 and (B) pH4.2. Data represent mean ± standard deviation (n = 3).

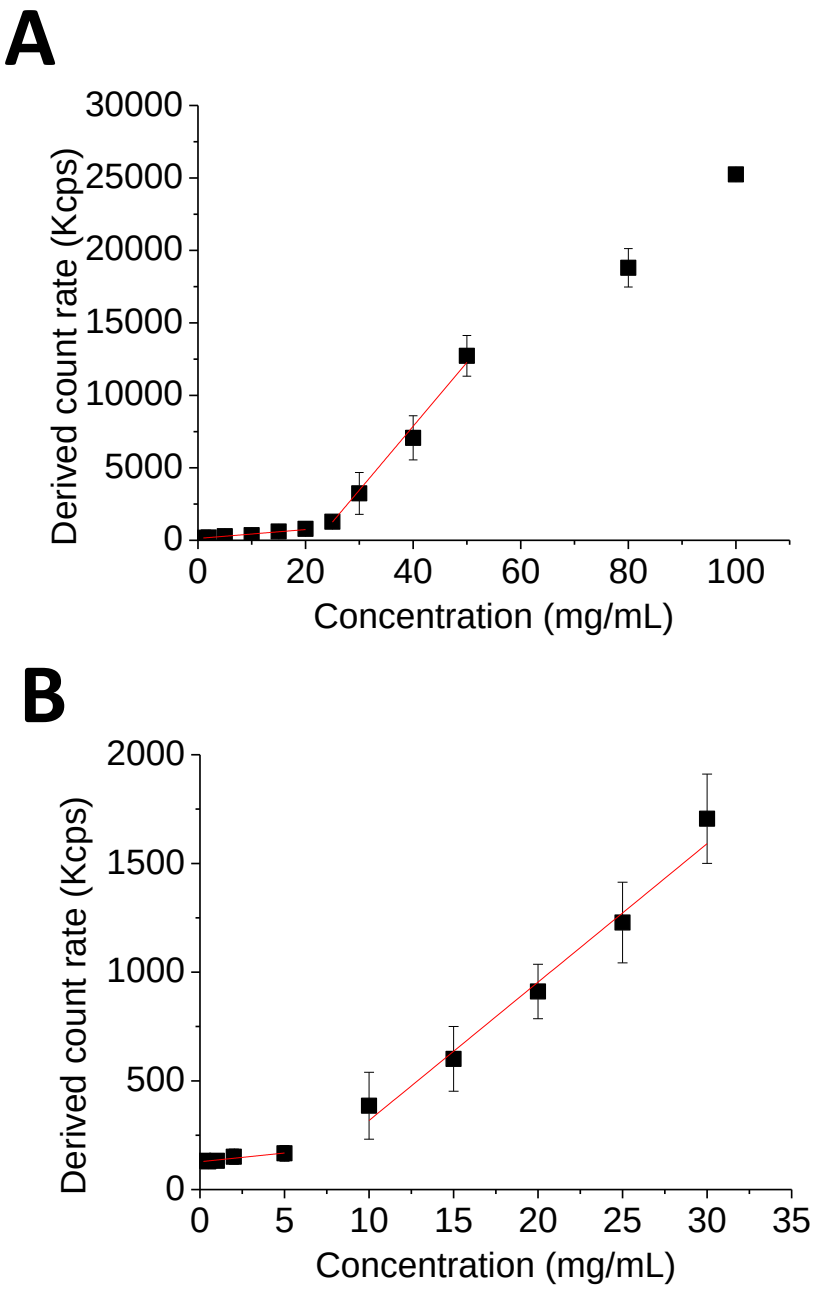

Figure 2.11: Critical micelle concentration (CMC) of surfactant Pluronic L62D in PBS buffer at (A) pH 7.4 and (B) 4.2. Data represent mean ± standard deviation (n = 3).

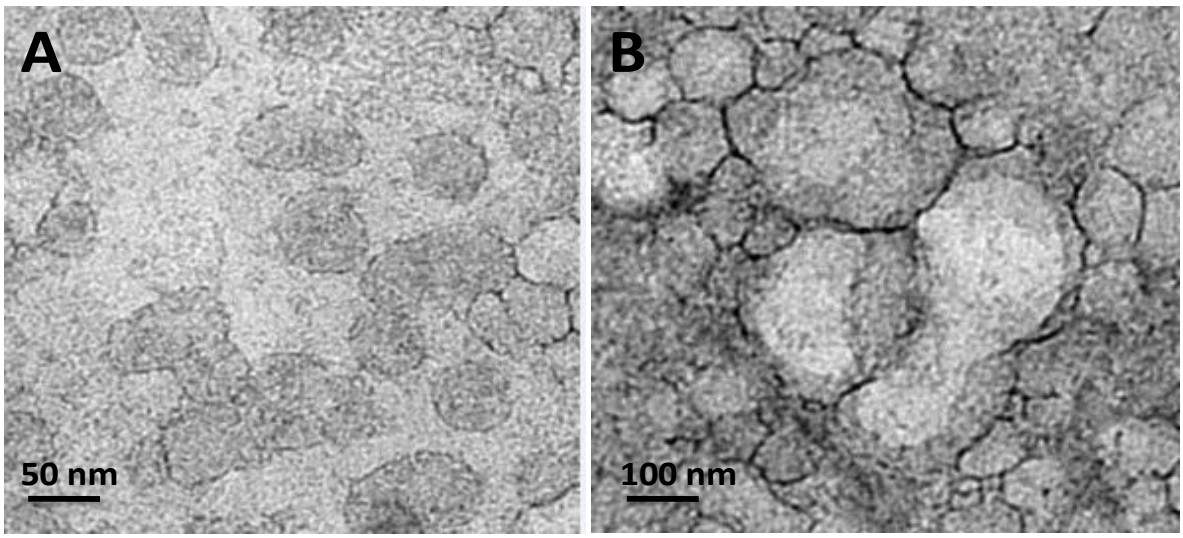

Figure 2.12: Transmission electron microscopy (TEM) images of lipid shell nanoparticle suspensions (A) before exposure to Pluronic L62D surfactant, (B) 8 h after exposure to Pluronic L62D surfactant.

2.4.8 Permeabilisation mechanism for the polymer shell nanoparticles

FTIR chemical analysis of the polymer shell nanoparticles showed that there was no difference in the intensity of OH peak over time when they were not exposed to the shell permeabiliser (Figure 2.13), which suggested the polymer's structure was unchanged. For the nanoparticle exposed to the shell permeabiliser the intensity of hydroxyl group increased over time. TEM showed that the shell permeabliser seemed to have no effect on particle size as illustrated in Figure 2.14. These results confirmed the mechanism of this dynamic nanosystem was carboxyl functional group hydrolysis caused by the acidic conditions.

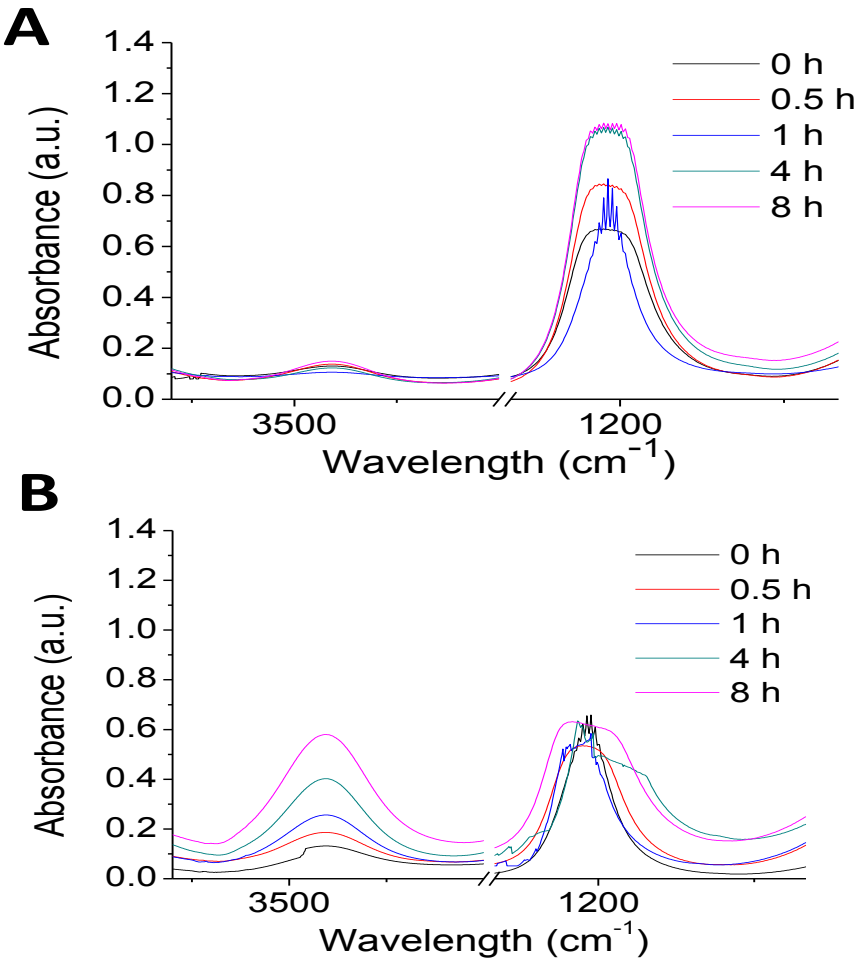

Figure 2.13: FTIR spectra for PVA shell nanoparticles permeabilised by (A) buffer pH 7.4 and (B) buffer pH 4.2. Regions of interest were the OH stretching region (3700-3200 cm^{-1}) and the C-O stretching region (1200-1000 cm^{-1}).

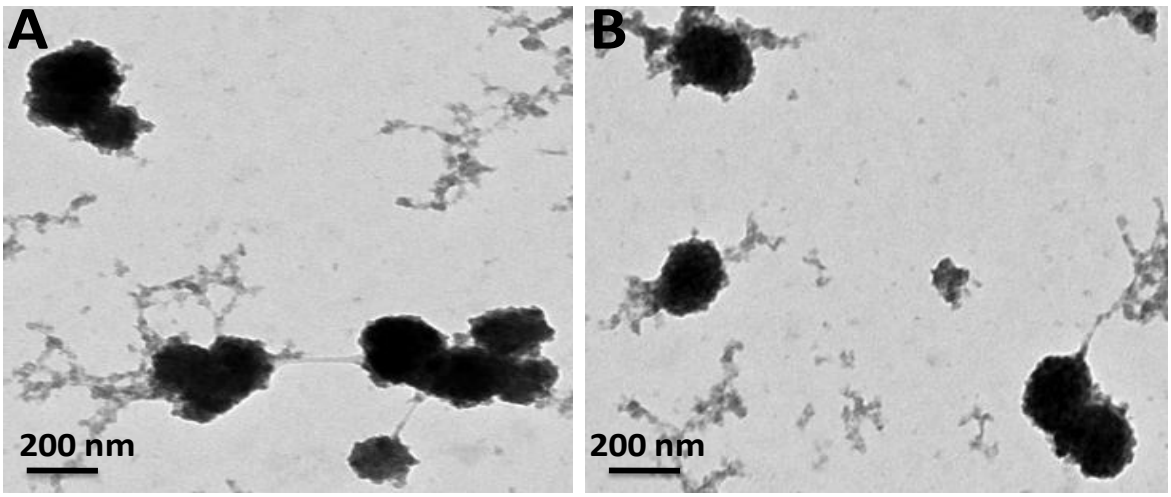

Figure 2.14: Transmission electron microscopy (TEM) images of (A) non-permeabilised polymer shell nanoparticles and (B) polymer nanoparticles permeabilised by the addition of an acid solution.

2.5 Discussion

The size and polydispersity of the lipid shell and polymer shell nanoparticles employed in this work were consistent with those previously reported using similar preparation methods (Chana et al., 2015; Madlova et al., 2009). The simplicity, rapidity and scalability of the process makes it well suited to the production of nanoparticles intended for inhaled drug delivery. The emulsion-precipitation method of nanoparticle fabrication was shown to generate a much higher nanoparticle solid content compared to the injection-precipitation method. As anticipated the technique produced a relatively high nanoparticle product yield (solid content 160 mg/mL) when compared to alternative fabrication methods (Grenha et al., 2007).

Lipid shell nanoparticles have previously been shown to exhibit zero-order drug release kinetics (Abdel-Mottaleb et al., 2010; Zhai et al., 2014). Zero-order release suggested that the drug release was limited by the nanopacrticle carrier and this provided evidence that the drug was encapsulated by the lipid components of the nanoparticle. According to the sizing data, in the absence of the Pluronic surfactant the control lipid shell nanoparticles did not change in size. Thus, the drug release of rifampicin from the carrier was assumed to be a consequence of drug diffusion through the nanoparticle's lipid shell. The marked differences in lipid shell nanoparticle size following exposure to the Pluronic surfactant suggested nanoparticle distension lead to an increase in shell permeability and it was this change in the carrier properties, which was responsible for the increase in drug release compared to the control nanoparticles.

However, the release of rifampicin from the lipid shell nanoparticles was much more efficient compared to that previous obtained with a rhodamine dye using the same carrier system (Chana et al., 2015). It is notable that there was a methodical difference in the two studies that determined release from the same lipid shell nanoparticles. Dialysis was used in the current study in order to ensure sink conditions were maintained whereas the previous study to measure drug release of rhodamine used direct extraction from a nanoparticle suspension. However, the difference in the two release profiles was probably not a result of the different drug release methodology rather it was probably a consequence of the different physicochemical properties of the two release agents. Rifampicin has pKas of 1.7 and 7.9 and a log P of 1.1 (Bhise et al., 2010) whilst rhodamine has a pKa of 4.2 and log P of 2.7

(Lahnstein et al., 2008). Hence rhodamine would be predicted to have a higher affinity to the oil core of the particles, which could result in less release of the dye from the nanoparticles.

Ion-pairing has been previously used to improve the retention of hydrophilic drugs in the lipid matrix (Zhao et al., 2016) and it has been shown to modify the drug release kinetics without changing the chemical structure of the drug in the nanoparticles (Song et al., 2016). However, there does not appear to be any previous work that attempted to apply this strategy to the release of rifampicin from nanoparticles. Theoretically rifampicin and the counterions are fully ionized at acidic condition respectively so that ion-pairs can be formed. The hydrophobicity of the complex should increase as the counterions (log P: ethyl acetate 0.28, sterate 3.62, calculated by Marvin Sketch, ChenAxon Ltd, Hungary) neutralise some of the polarity of the parent drug and thus increase its affinity for lipid nanoparticle oil core. The inability of the counterions used in this work to slow rifampicin diffusion out of the particles may have been because the drug did not reside preferentially in the oil core of the carrier. Perhaps the rifampicin was arranged at the oil capsule interface and the counterion was located in the oil core and it was the ability for these molecules to freely move to their most preferential environment within the lipid shell nanoparticle core that preventing them from interacting. Alternatively the complex structure of rifampicin may have caused steric hindrance that prevented ion-pair formation.

Even in the presence of the enhanced drug release rate it appeared that the lipid shell nanoparticle did not suffer from an initial burst release. There is not a standard method that that is used to determine burst release from nanoparticles. In this study the % of drug release at t=0.5 h was determined to be the burst release. The lipid shell nanoparticles showed a 5% release at t=0.5 h. The encapsulation of the counterions had no effect on this initial release percentage. Compared to previous studies using nanoparticles, which usually cite burst release to be an issue when they have rapid release of 30-50% of their drug payloads (Sun et al., 2013), the lipid shell nanoparticles in this work appeared not to have a significant issue of burst release.

The pH dependent triggering release was observed in this work, which could be due to the changes of Pluronic properties at different pHs. An increase in the PO block length and PO:EO ratio have been reported to increase the surfactant hydrophobicity and extent of lipid bilayer disruption (Firestone et al., 2003). For Pluronic with intermediate PO block lengths it is thought that insertion into bilayers is the primary means of membrane interaction. The lipid

nanoparticles have an external semisolid shell made from phospholipid and when Pluronic interacts with this external surface it is expected that the two EO segments of the surfactant reside on the apical side of the membrane and the PO chain protrudes into the hydrophobic domain (Firestone et al., 2003). The pH-dependent swelling responses to Pluronic L62D supported the shell insertion mechanism of action because the increase propensity for the PEO-PPO-PEO block copolymer to aggregate in the aqueous solution would diminish its affinity for the nanoparticle shell surface (Mao et al., 2001). Yang et al. (2006) investigated the effect of acid on the aggregation behaviour of Pluronic P123 (Yang et al., 2006) and showed that the PEO block was degraded in strong acids. It is possible that the greater acidity of the medium could have resulted in degradation in this work, but at a pH of 4.2, which is only mildly acidic compared to the previous work, this effect was thought not to be as significant compared to the changes in CMC demonstrated using the light scattering data.

Several new polymeric nanoparticle technologies have been developed recently that were thought to be suitable for drug delivery applications. These include ‘porous nanoparticle-aggregate particles, dynamic pH responsive nanoparticles and self-assembling nanoparticles, but the use of these systems in pharmaceutical products has been limited by scale up and toxicity concerns (Kean and Thanou, 2010). PVA is a water soluble synthetic polymer that is formed by full or partial hydrolysis of poly(vinyl acetate) (PVAc). It has been proved to be safe as a coating agent for pharmaceutical and dietary supplement products, it has a good compatibility with lung cells and in comparison to other polymeric systems it has a limited potential to cause local lung inflammation (DeMerlis and Schoneker, 2003). Furthermore, the production of the nanoparticles using PVA is easily scalable. Therefore, this material is well suited to the formation of nanoparticles for clinical applications (Madlova et al., 2009). The amphiphilic grades of the polymer (30–60% hydrolysis) are probably the most interesting in terms of drug delivery, but they are not readily available. Therefore, PVA was synthesised in this study to attain a degree of hydrolysis that would spontaneously generate nanoparticles in an aqueous solution (Chana et al., 2008; Madlova et al., 2009).

It is generally assumed that the main release process from polymeric nanoparticles is diffusion through the polymer matrix but release can also occur as a consequence of polymer degradation (Soppimath et al., 2001). In the case of the polymer shell nanoparticlesin this work the drug is placed in an oil core that is coated with the polymer and therefore the release from the carrier most probably occurs by diffusion of the drug through the polymeric shell. If

this mechanism works well then the drug release should follow the zero-order kinetics as observed in this study.

It was unusual that the low pH conditions, which had previously been shown to induce polymer hydrolysis, did not increase the rate of drug release. This result suggested that another factor was confounding the potential for enhanced drug release at pH 7.4. Just like for the lipid systems the lower aqueous solubility at pH 4.2 (0.75 mg/mL) compared to pH 7.4 (1.55 mg/mL) (data not shown graphically) could have been responsible for the inability for the permeabiliser to influence the drug release at pH 4.2.

It is well known that ester group of PVA can be hydrolysed to an alcohol under acidic conditions (Clayden et al., 2012). Increasing the amount of hydroxyl groups would enhance the affinity of the polymer membrane to water and increase surface film solvation, which would facilitate drug release via diffusion through membrane pores. It is also possible that the polymer molecular weight can be reduced due to hydrolysis which could facilitate drug release (Xu and Du, 2003). However, in the time frame of the release experiments it was thought that increased PVA film hydration was most probably the primary cause of the increase in drug release.

2.6 Conclusion

Rifampicin loaded lipid shell nanoparticles and polymer shell nanoparticles both provided controlled zero-order drug release. The carriers controlled release primarily through their outer shells. As a consequence when the nanoparticle shells were permeabilised greater quantities of drug diffused out of the carriers. However, although the lipid shell nanoparticles were permeabilised using a Pluronic surfactant which inserted into the outer shell, whilst the polymer shell carriers were permeabilised through polymer hydrolysis both mechanisms were ineffective at pH 4.2. This suggested that the drug solubility, which was lower at pH 4.2 was also an important factor in determining the release from these carriers. At the epithelial surface of the lung the pH is thought to range between 6.5-7.4. Within this pH range the carrier permeabilisation mechanism should result in enhanced drug release and therefore these nanoparticles present an attractive means to provide controlled release of drug to the airways of the lungs. Even though the nanoparticles showed an active release profile for the drug delivered to the lungs they should also penetrate through the mucus and this will be tested in Chapter 3.

CHAPTER THREE

Nanoparticle penetration through mucus

3.1 Introduction

When nanomedicines are administered via the airways the drug release kinetics and inflammatory potential are influence by their interaction with the mucus barrier. In order to reside in the airway for an adequate period of time to achieve sustained drug absorption, nanomaterials ideally should move rapidly towards the lung epithelial surfaces and avoid rapid mucocillary clearance and macrophage engulfment. The mucus in the lung airways is a semipermeable viscoelastic barrier that is continuously renewed. The major constituent of mucus is water (~ 95%). This solvent hydrates a network of crosslinked and entangled mucin fibers that are continuously secreted by goblets cells and sub mucosal glands of the epithelial barriers (Thornton and Sheehan, 2004). Mucins are glycoproteins with high molecular weight ranging from 0.5-40 MDa (Cone, 2009). The polypeptide backbone contains a large number of serine, threonine and proline (PTS repeats), making up around 20% of molecular mass (Bansil and Turner, 2006). Oligosaccharide side chains attach to serine or threonine along the backbone via O-glycosidic bonds (Figure 3.1). Usually the oligosaccharide has 8-10 monosaccharide residues such as fucose, galactose and sialic acid (Bromberg and Barr, 2000). Thus the PTS domains are negatively charged due to negatively charged carboxyl groups of sialic acid. Glycosylation is the most important feature of mucin, which governs the physiochemical properties of glycoprotein. Multimers can be formed via disulfide bonds in cysteine rich regions (Svensson and Arnebrant, 2010). Currently, more than 20 mucin glycoproteins have been assigned to the *MUC* gene family (Dekker et al., 2002). Mucins can be divided into two catalogues according to sequence homology: secreted mucins (i.e. MUC5AC) and membrane bound mucins (i.e. MUC 1) (Johansson et al., 2011). The MUC5AC gene product is a major mucin in the stomach and airways of both humans and pigs (Gendler and Spicer, 1995).

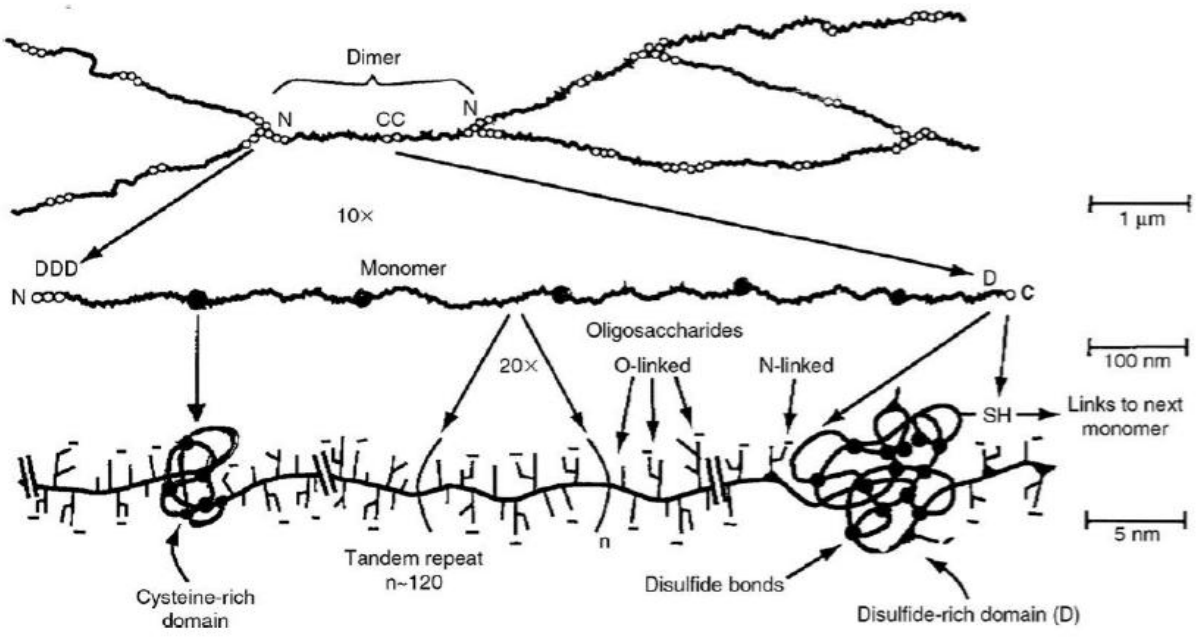

Figure 3.1: Summary of thestructure of mucin at three different magnifications (From Cone, 2009).

The thickness of mucus varies greatly depending on the anatomic site where it is produced. The stomach and colon have the thickest mucus blanket in the human GI tract, with barriers stretching 50-450 μm and 110-160 μm respectively *in vivo* (Pullan et al., 1994). It has been shown that digestive activity influences the thickness of mucus in the GI tract (Brownlee et al., 2003). The airway has a much thinner mucus blanket ranging from 5 to 55 μm (Clunes and Boucher, 2007), but this can change if the lungs are effects by a disease. In the case of cystic fibrosis, a much denser and more highly glycosylated mucus is present in the respiratory tract, resulting in increased viscoelasticity of the barrier. The lifetime of mucus is relatively short ranging from minutes to hours, due to its continuous secretion, digestion and recycling. The thin mucus layers typically show the fastest turnover at the epithelial surface. A relatively quick turnover time in the order of 10-20 min has been previously reported for the respiratory mucus (Ali and Pearson, 2007). In order to deliver drug molecules beyond the mucus barrier, a carrier must be capable of penetrating the mucus, hence particles must have a faster diffusion rate than mucus renewal and clearance or release their pay load prior to removal by this layer.

At the molecular level, mucus is an integrated structure of biopolymers. Its physical behaviour is complex (non-Newtonian), with highly variable properties that are between those of a viscous liquid and an elastic solid referred to as a viscoelastic gel because it

possesses both flow (viscosity) and deformation (elasticity) properties (Lai et al., 2009). Mucin content is the major determinant of mucus rheology as mucin exhibits a tendency to aggregate and form gels (mucus) (Bromberg and Barr, 2000). As the matrix of the gel is formed by relatively weak non-covalent and strong disulfide bonds between the glycoprotein, any factors affecting these linkages will influence the rheological properties of the mucus. For example, the strength of selectivity of both native and reconstituted mucin hydrogel can be modulated by pH and charged objects (Crater and Carrier, 2010). Experiments with negatively charged human immunodeficiency viruses have been shown to be less mobile in acidic cervicovaginal mucus (CVM) than at neutral pH (Suk et al., 2009). Similarly, a strong retention of charged particles has been observed in low pH mucus. By contrast, free diffusion through mucus of neutral particle has been shown at neutral pH (Lieleg et al., 2010). The characterization of the physical properties of mucus is often conducted from two different aspects: macrorheological and microrheological. The former provides measurements of bulk physical properties whereas the latteraffords detailed characterization of the special interactions within the biological fluids, accounting for both contributions from the fluid within the biopolymer network as well as the network mesh itself (Lai et al., 2009). Advances in the rheological characterization of mucus from the macroscopic to nanoscopic levels have contributed critical to a better understanding of mucus physiology, disease pathology but as yet it has not lead to the commercial development of a new type of drug delivery systems designed for use at mucosal surfaces. Nanoparticles seem to offer a means of controlled drug delivery in the airways and hence if mucus nanoparticles interactions could be understood perhaps these materials could facilitate the commercialization of an effective nanomedicine.

The diffusion of nanoparticles has been explored in a variety of human mucus secretions, including human CF sputum, human CVM and porcine gastric mucus (PGM) using various diffusion system (Abdulkarim et al., 2015; Kirch et al., 2012; Lai et al., 2007; Roblegg et al., 2012). Two major mechanisms namely size filtering and interaction filtering are considered to reduce the speed of penetration through mucus (Lieleg and Ribbeck, 2011). The size filtering mechanism hinders the diffusion of particles with diameters larger than the mesh size between the mucin fibers. Rapid penetration of Norwalk and human papilloma virus through cervical mucus suggested the diffusion capacity of particles through low viscosity pores within the highly elastic mucin fiber matrix was possible (Olmsted et al., 2001). However, the slow diffusion of 59 nm carboxyl-modified polystyrene nanoparticles (Diffusion in mucus, $D_{muc} = 0$), which were smaller than the average mucus mesh pore size in

the same experiment demonstrated size is not the only factor that determines penetration through mucus. The relatively rapid diffusion of nanoparticles as large as 500 nm through cervicovaginal mucus was observed (the ratio of diffusion in water and mucus, D_w/D_m= 12), if particles were densely coated with low molecular weight polyethylene glycol (PEG) (Tang et al., 2009). These results suggested that charge interactions between particles and mucus hydrogel play an important role in modulating penetration through mucus. The mucin mesh network is relatively dense and thus it slows to some extent most foreign particles, presumably due to the formation of polyvalent adhesive interactions via hydrophobic and anionic forces (Norris and Sinko, 1997). Alternatively, electrostatic interactions contribute to polyvalent adhesive interactions. Positively charged particles can form adhesive interactions with negative charges impacted by the presence of carboxyl or sulfate groups on the mucin proteogycans, resulting in anionic particles diffusing 20-30 times faster than cationic particles (Crater and Carrier, 2010). This is critical for the removal of foreign particles smaller than the average pore size. In addition to charge interactions there is the potential for hydrophobic interactions. The high density of hydrophobic domains, existing in the globular regions, allows efficient formation of multiple low-affinity adhesive interactions with hydrophobic regions on the surfaces of foreign particulates, which are strong enough to bundle mucin strands into thick cables (Lai et al., 2009). The interactions between hydrophobic molecules and hydrophobic mucus have been shown to result in significant decreases in the diffusion rate of both small and large molecules and this could also occur with particulates.

Diffusion chambers appear to be described most frequently in the previously published literature regarding methods to track nanoparticles translocation across mucus (Norris and Sinko, 1997). According to the position of compartments this methodology can be divided into two sub-categories: horizontal diffusion chambers such as Snapwell cell layer transport system (Sanders et al., 2000) and vertical diffusion chambers including Franz cell chamber and Transwell system (Broughton-Head et al., 2007). Both setups allow for quantification of diffused particle by measuring their concentration and this results in a concentration vs time profile from which a barrier diffusion rate can be obtained. Although the diffusion-chamber method is conceptually straightforward and easily set up, it is sensitive to a number of parameters that are difficult to control, such as the precise thickness of the mucus layer, the uniformity of the mucus distribution across the face of the filters, blockage of the filter pores by mucus, and alterations in mucus properties during preparation (Saltzman et al., 1994). Alternatively using a particle tracking technique, empirical data for the diffusion of particles

in mucus gel can be observed directly, which is usually depicted as one dimensional transport in a semi-infinite medium and recorded by an *in situ* analytical device. The availability and high sensitivity of fluorescence detection renders nanoparticle labelling and tracking the most repeated methods in recent studies. The subsequent development of multi-photon imaging has make particle tracking even more rapid and sensitive for example, multiple particle tracking (MPT) has shown excellent results (Olmsted et al., 2001; Suh et al., 2005). Particle tracking is valuable in obtaining information on how fast particles move through mucus, but it does not establish if a particle can translocate across a mucus barrier. As a consequence particle tracking studies have so far focused on how nanoparticle surface chemistry influences horizontal particle mobility, whereas vertical translocation was not described. The majority of these works employed unpurified mucus, thus the identity of the objects captured by the camera employed in particle tracking technique remain uncertain. A summary of previous study findings with regarding to particle translocation is highlighted in Table 3.1.

Table 3.1: Mucus particle diffusion study summary (D_{muc}: average diffusion coefficients in mucus; D_w: the theoretical diffusion coefficient in water; SPS: sulphate polystyrene particle; CPS: carboxylated polystyrene particle; APS: amine polystyrene particle; PEG-CPS: PEGylationcarboxylated polystyrene particle).

Experimental method	Mucus	Diffusion rate/percentage	Reference
Diffusion chamber	Cystic fibrosis sputum	0.24 ± 0.08 % (124 nm), 0.022 ± 0.008 % (270 nm), and 0.0017 ± 0.0009 % (560 nm) translocated after 150 min.	(Sanders et al., 2000)
Diffusion chamber	Porcine buccal mucosa	Translocation of 200 nm 100 μg/mL CPS and APS were 0.17 ± 0.02 % and 14.5 ± 0.44 % after 4 h.	(Roblegg et al., 2012)
Particle tracking	Human cervical mucus	Mucus diffusion rate of 150 nm NP and 150 nm PEG-NP = 2.5 ± 0.5 $\times 10^{-9}$ cm^2/s and 26.45 ± 3.9 $\times 10^{-9}$ cm^2/s.	(Cu and Saltzman, 2008)
Particle tracking	Chronic rhinosinusitis mucus	217 nm CPS D_w/D_m = 2300; 231 nm PEG-CPS D_w/D_m = 20	(Lai et al., 2011)
Particle tracking	Porcine intestinal mucus	Mucus diffusion rate of 200 nm CPS = 6.32 $\times 10^{-10}$ cm^2/s; mucus diffusion rate of 200 nm APS = 1.67 $\times 10^{-10}$ cm^2/s	(Crater and Carrier, 2010)

Different sourced mucus have similarities in mucins contents and biochemical properties (rheology) and have been tested for different administration routes. It is difficult to directly compare the results described in Table 3.1 as the methods were not consistent. However,

individually each report allows an understanding of the effects of surface chemistry on particle translocation. Some questions like do smaller particles diffuse faster than larger particles still remain unclear. Thus it is difficult to get a solid consensus due to the lack of method standardisation which needs to be addressed.

The main aimof this Chapter of the PhD thesis was to investigate the diffusivity in mucus and penetration through mucus by the lipid shell nanoparticles (LNP) and PVA shell nanoparticles (PVA). These two nanosystems have been shown good candidates for controlled release by permeabilisers in the previous Chapter. In order to achieve this aim a novel vertical Transwell diffusion cell system was developed and shown to be fit for purpose using polystyrene (PS) nanoparticle with diameters of 50, 200 and 750 nm as reference particles Table 3.2). Then the model was employed to study the movement of the dynamic nanoparticles through porcine gastric mucus, chosen to represent 'normal respiratory mucus' (Celli et al., 2005), and CF mucus harvested from cells derived from CF patients. The mucus harvested from the cell line has previously been shown to a good representation of the viscous respiratory human CF mucus from patients (Sajjan et al., 2004; Sheehan et al., 2000) and therefore although it was derived from a cell line it was termed as CF mucus in this work. These two model systems were selected rather than mucus samples directly from patients because previous work has shown the patient samples were too heterogeneous to enable accurate distinctions between the movement of different particles (Donaldson et al., 2006). Finally the multi particle tracking system with a flow cell was used to measure the horizontal movements of particles in the mobile mucus gel such that the multidimensional mucus diffusion modeling could be performed.

Table 3.2: Test of mucus penetration using different particles under variable conditions.

Nanoparticles	Size (nm)	pH condition
PS	50	8.5
LNP	50	8.5
PS	200	2.5
PS	200	6.5
PS	200	8.5
PVA	200	8.5
PLNP	250	8.5
PS	750	8.5

3.2 Materials

Porcine stomachs were purchased from Mutch Meats (Whitney, UK). The human mucus was from Epithelix (EpithelixSarl, Geneva, Switzerland). Fluoresbrite YG carboxylate polystyrene microspheres (0.05, 0.2 and 0.75 μm, 2.5% w/v) were sourced from Polysciences (Eppelheim, Germany). Materials for nanoparticle manufacture refered to Section 2.2. Sodium chloride, ethylene diamine tetra acetic acid (EDTA), phenylmethylsulfonyl fluoride (PMSF), sodium azide, N-methyl-2-pyrrolidone, sodium fluorescein salt, nile red, sodium phosphate dibasic heptahydrate, sodium phosphate monobasic monohydrate, thioglycolic acid, trypsin, lysozyme, bovine serum albumin (BSA), transferring and haemoglobin were purchased from Sigma-Aldrich (Dorset, UK).

3.3 Methods

3.3.1 Collection and purification of porcine gastric mucus

The stomachs of freshly slaughtered pigs were opened along their greater curvature, inverted, any food content removed mechanically and washed with double-distilled water. The mucus lining the stomachs was gently removed by scraping using a plastic spatula and transferred to a container, containing protease inhibiting buffer composed of 200 mM sodium chloride, 0.02 % (w/v), sodium azide, 5 mM EDTA and 1 mM PMSF. The mucus was mixed well with an equal volume of the protease inhibiting buffer to inhibit bacteria growth and homogenised with a mixer for 2 min. The mixture then was centrifuged at 11,200 *g* for 45 min at 4 ℃. The supernatant was poured into visking dialysis tubing (MWCO: 12-14 kDa, Fisher Scientific, Loughborough, UK) and dialysed against distilled-deionised water for 24 h. The dialysed mucus solution was concentrated in an Amicon ultra-filtration stirred cell (Model 8400, Merck Millipore, UK) under nitrogen at a pressure of 40 psi and temperature of 4 ℃. The purified and concentrated mucus was collected into a bottle and frozen at -20 ℃ until used (Figure 3.2).

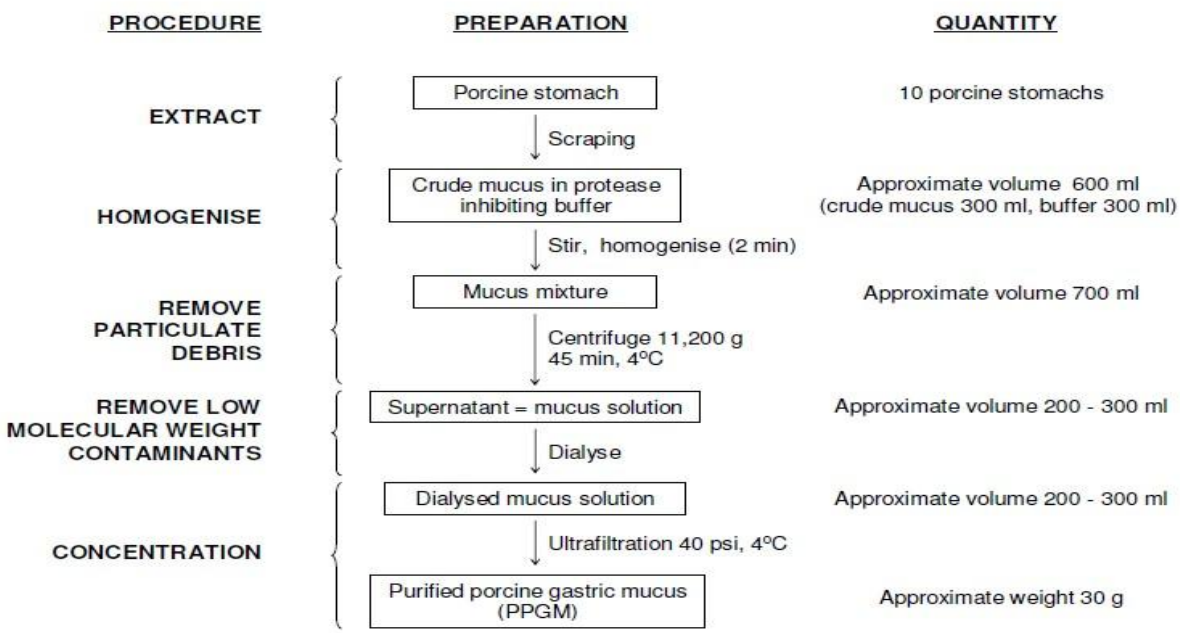

Figure 3.2: Schematic of the purification of the PGM (From Boontarika Boonyapiwat, 2005).

3.3.2 Respiratory mucus collection

The respiratory mucus was secreted by cells harvested from a CF patient that were cultured *in vitro* using MucilAir^{TM} cell model as illustrated in Figure 3.3.

Figure 3.3: Illustration of MucilAir cell model

3.3.3 Characterisation of purified mucus

The dry weight of mucus was determined by weighing a sample into a porcelain dish and placing it into an oven at 80 ℃ until a constant weight. The percentage of dry weight was calculated as the difference in the weight before and after heating. A known concentration

was used in all studied. The determination of both elastic modulus (G') and viscous modulus (G'') of collected mucus was performed on samples of approximately 2 g using the Carri-Med rheometer (TA Instruments, US). Viscous modulus is the extent to which the gel resists the tendency to flow and elastic modulus measures the tendency for the gel to recover its original shape following deformation. The viscoelastic properties of the mucus as a function of frequency were studied at a constant stress of 1.8 Pa. The purified mucus swelling was quantified by applying 1 µL mucus to Transwell insert with 1, 5 and 10 µL polystyrene nanosuspension on top and the weight of the donor compartment was measured at a number of time points by taking it out of contact with a Tris buffer (50mM, pH 8.5), carefully removing the fluid from the surface of the mucus by wicking with a towel and placing the mucus-containing Transwell on a balance. The swelling was calculated as the difference in the weight over the initial weight. To characterize the molecular weight of collected mucus a sample (100 µL, 1 mg/mL) was injected into size exclusion column (TSK Gel 3000 SW,Tosoh Bioscience LLC, Japan) at the flow rate of 1 mL/min using gel permeation chromatography machine equipped with refractive index detector (Malvern Instruments, Worcestershire, UK). Phosphate buffer 50 mM with 0.3 M sodium chloride at pH 7 was used as a mobile phase. Molecular weight was determined according to the plot of molecular weight against retention time obtained for standards (lysozyme, trypsin, peroxidase, BSA and thyroglobulin) using Ominsec software (Malvern Instruments, Worcestershire, UK). For CF mucus, only the molecular weight was measured.

3.3.4 Nanoparticle fabrication

The lipid shell nanoparticles and PVA shell nanoparticles were manufactured via precipitation from a stable emulsion following repeated phase inversion and nanoprecipitation method as previously described in Section 2.2.2. The freshly manufactured nanoparticles were prepared for all the experiments. For the particle tracking, nile red was loaded into both nanoparticles by dissolving nile red in organic phase.

3.3.5 Nanoparticle characterization

The size of nanoparticles were analysed by dynamic light scattering using a Zetasizer Nano ZS (Malvern, Worcestershire, UK). Nanoparticles (250 µg/mL) were suspended in Tris buffer solution (50 mM, pH 8.5) and sizes were measured at 37 ℃. All measurements were carried out at a scattering angle of 173 ° using water as the dispersant. Each measurement

comprised of 10 to 14 runs and was performed in triplicate for each sample. Zeta potential measurements were performed at 37℃ with all suspensions diluted in Tris buffer (50 mM, pH 8.5) solutions to a final concentration of 250 μg/mL. Each measurement was derived from between 50 to 100 runs and the measurements were performed in triplicate.

3.3.6 Radiolabelling of lipid shell nanoparticles

To incorporate a radiolabel chelator into the shell of the lipid nanoparticle systems, 0.1% w/w 1,2-dimyristoyl-sn-glycero-3-phosphoethanolamine-N-diethylene triaminepentaacetic acid (DMPE-DTPA) (Avanti Polar Lipids Inc, Alabama, USA) was added to the components during the coarse emulsion step and the lipid shell nanoparticles were prepared as described above (Rubin, 2007). Suspensions were diluted to 12 mg/mL with 0.1 M ammonium acetate (pH 6.6). Indium-111 chloride (Mallinckrodt Medical Inc, Petten, The Netherlands), ~50 MBq ($^{111}InCl_3$, half-life 2.83 days), was dissolved in 0.5 M ammonium acetate (pH 5.0) and mixed with lipid nanoparticles-DMPE-DTPA at a ratio of 1:2 v/v. The mixture was incubated at 37℃ for 45 min under gentle shaking. Radiolabeling efficiency was measured by quantifying the radioactivity in the supernatant of the washing solution and washed carrier residue after three cycles of washing using spin filtration with Amicon ultrafiltration centrifuge tubes (Millipore Ltd., Hertfordshire, UK; 30 kDa MWCO).

3.3.7 Nanoparticle fluorescence assay

Fluorescence intensities of nanoparticle suspensions were determined using a Perkin Elmer luminescence spectrometer LS50B (Cambridgeshire, UK). For polystyrene nanoparticles, maximum excitation of 441 nm and emission of 486 nm were used for subsequent analyses on standard solutions prepared in the range of 1 μg/mL to 50 μg/mL from a stock solution (100 μg/mL). For PVA nanoparticle, fluorescence intensities of nile red solutions in methanol were determined with an excitation of 469 nm and an emission of 529 nm. Intra-day, inter-day variation, LOD and LOQ were detected as described in Section 2.3.6.

3.3.8 Mucus penetration model set-up

3.3.8.1 The effect of barrier thickness

The mucus model was optimised using fluorescein transport to measure the barrier provided to small molecular weight solute permeability. The basic set up used a Transwell system (0.3

cm^2 polyester, 3 μm pore size, Corning, UK, Figure 3.3) to support a mucus layer which was inserted into a receiver chamber containing 600 μL of Tris buffer (50 mM, pH 8.5). In the fluorescein transport studies the mucus thickness was varied such that a barrier with a theoretical mucus thickness of 35, 180, 350, 500, 700, 1400, 2100 and 2800 μm was achieved by adding known volumes of mucus onto the insert membrane (calculated on the basis that the insert was a cylinder with a surface area of 0.3 cm^2). For the thickness measurement, mucus layer on top of the membrane was rapidly moulded and frozen in the liquid nitrogen. The block was fixed in the Cryostat (Leica CM3050, Leica Microsystems, UK) and sections were cut with a thickness of 30 μm. The actual mucus thickness was measured using a microscope (Leica DM2000, Leica Microsystems, UK). Prior to the initiation of the transport experiments the mucus was equilibrated in the Transwell at 37℃ for 1 h. Then a donor solution containing 100 μL of sodium fluorescein (100 μg/mL), in Tris buffer (50 mM, pH 8.5), was applied onto the surface of the mucus layer to initiate a transport experiment, t=0. At regular time points over 30 h, 50 μL samples were removed from the receiver chamber and the amount of fluorescein in the samples was determined. Samples were analysed using a 96-well plate reader (FLx800 Microplate Fluorescence Reader, Bio-TEK Instruments, UK), operated with an excitation of 460 nm and an emission of 515 nm. The assay methodology was shown to be fit for purpose in terms of precision and limit of detection in previous work (Chana et al., 2015). The cumulative mass of sodium fluorescein transferred to the receiver chamber per cm^2 of mucus area was calculated, plotted against the time and the transport rate (i.e. flux derived from the linear mass transported vs time graph) was calculated.

3.3.8.2 The effect of volume

Once the mucus barrier properties were characterised, the effect of donor solution volume on the mucus hydration was evaluated by applying 1, 5 or 10 μL of 10 mg/ml polystyrene (PS) nanoparticles to the 35 μm thick mucus barrier and measuring the particle transport rate. The effect of barrier thickness on the nanoparticle penetration was then evaluated by employing the thickest (2800 μm) and thinnest (35 μm) mucus layers in comparative studies with 1 μL of 10 mg/mL polystyrene nanoparticles. Fluorescence intensity was measured to quantify the nanoparticle transport. In order to verify that the particles were actually passing through the mucus a selected number of samples that were removed from receiver chamber and were analysed using Transmission Electron Microscopy (TEM). TEM required placing a 3 μl sample onto Formvar coated grid. It was washed with deionized water for 2 min three times

and then the sample was stained with 1% aqueous uranyl acetate for 3 min at 4^{o}C until dry. Images were obtained using a FEI Tecnai G^2 transmission electron microscope operated at 200 kV fitted with a GatanUltrascan US1000 (2kx2k) camera.

3.3.9 Tracking nanoparticle penetration through mucus

Using the optimal parameters for the mucus barrier transport (i.e., a 35 μm thick mucus barrier and a 1 μL donor solution) the diffusion of three different sized polystyrene nanoparticles (50 nm, 200 nm and 750 nm) and the two in-house manufactured nanoparticles was assessed. Again, 600 μL of Tris buffer (50 mM, pH 8.5) was used as the receiver fluid. A particle loading dose of 10 mg/mL was applied onto the surface of the barrier to allow for adequate detection in the receiver fluid. When characterising the transport of the distensible lipid shell nanoparticles, Pluronic (80 mg/mL) was first mixed with nanosuspension (160 mg/mL) with a ratio of 1:0.5 w/w to initiate the distension process and then the mixture was added on the barrier. Nile red was loaded into PVA shell nanoparticles for tracking. At appropriate intervals during an 8 h time course samples were removed and the fluorescence of polystyrene nanoparticles was quantified with an excitation of 441 nm and an emission of 486 nm at room temperature. The lipid shell nanoparticles were quantified by scintillation counting. Fluorescence of nile red encapsulated in PVA shell nanoparticles were quantified by dissolving particles in methanol and measured with an excitation of 469 nm and an emission of 529 nm. In order to study the effect of pH on the transport of 200 nm polystyrene nanoparticles, Tris buffer (50 mM) with pH of 2.5, 6.5 and 8.5 was used as the receiver fluid. Finally mucus penetration rates were calculated using steady-state flux equation as shown below (Equation 3.1):

$$\frac{\mathrm{dM}}{\mathrm{dt}} = \frac{\mathrm{DC}}{\mathrm{h}} \quad \text{Equation 3.1}$$

Where $\frac{dM}{dt}$ is flux, D is diffusion coefficient, C is concentration of the permeant in the donor solution and h is thickness of the membrane.

3.3.10 Multiparticle tracking using nanoparticle tracking analysis

Lateral nanoparticle diffusion through mucus was measured using a NanoSight LM10 (Malvern, UK) with an LM14 top-plate, equipped with a green 533 nm laser and syringe pump. All the samples used in the vertical diffusion cell were diluted by a factor of 100 (0.28%

w/w) before being injected into the system. An aliquot of 1 mL was injected into the NanoSight, with the 560 nm wavelength cut-off filter in place. Then 6×60 second videos were recorded for each particle type and measurements were performed in triplicate, whilst samples were being continuously pushed through the top-plate at a speed of 70 AU in order to minimise fluorescent bleaching. All measurements were conducted at 37 ℃. The raw diffusion coefficients were determined for each set of videos and averaged across the three repeats using NTAv3.0 (Malvern, UK). The diffusion of particles in the liquid was calculated using the Stokes-Einstein equation (Equation 3.2):

$$D = \frac{kT}{3\pi\eta d} \quad \text{Equation 3.2}$$

Where D is the diffusion coefficient, k is the Boltzmann constant, T is the absolute temperature, η is the dynamic viscosity, and d is the particle diameter.

3.3.11 Statistical analysis

SPSS version 20 (IBM, UK) was used for all statistical analyses. The transport data were analysed statistically using one way analysis of variance (ANOVA) testing for the normally distributed data and non-parametric Kruskal-Wallis tests for non-normally distributed data. Post hoc comparisons of the means of individual groups were performed when appropriate using Dunnet's test for normal distributed data and Games Howell test for non-Gaussian distributed data. For all pair-wise comparison of means, Student's independent T-test or Mann-Whitney test was applied. Differences were considered to be statistically significant at a level of $P < 0.05$.

3.4 Results

3.4.1 Mucus characterization

A single batch of porcine gastric mucus (PGM) was prepared for the vertical translocation studies. A total of 10 stomachs produced around 16 g of mucus with a solid content of 28% w/w. PGM had the molecular weight range of 14 to 860 kDa (Figure 3.4). The PGM showed viscoelastic properties with a G' (elastic modulus) = 100.3 Pa and G" (viscous modulus) = 57.5 Pa at 10 Hz (Figure 3.5). Cystic fibrosis mucus (CFM) had an average molecular weight of 412 kDa with a uniform distribution (Figure 3.6). Its viscoelastic properties could not be measured due to the limited sample volume that was available for the studies.

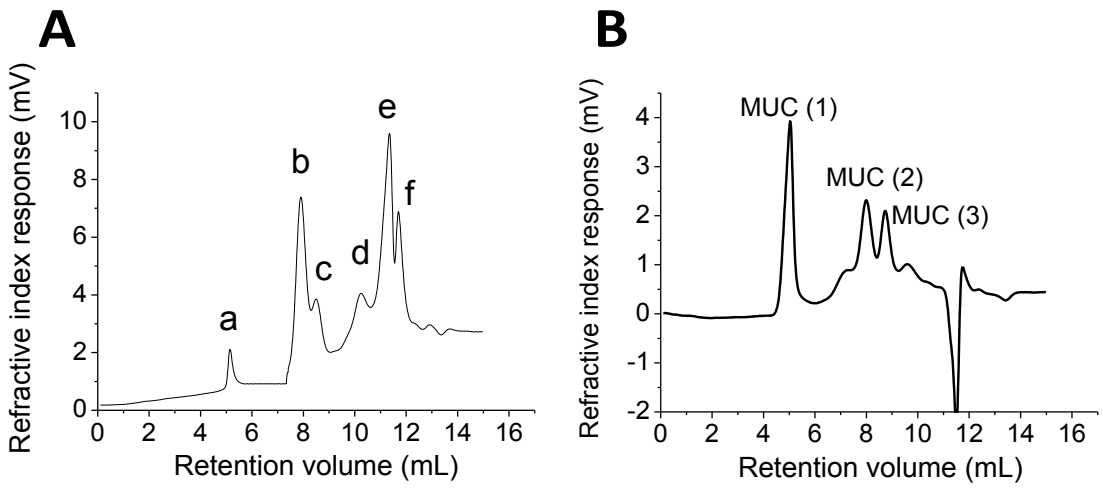

Elutes	Molecular weight (KDa)	Retention volume (mL)
Thyroglobulin (a)	660	5.2
Bovine serum albumin (b)	66	7.9
Peroxidase (c)	44	8.5
Trypsin (d)	23	10.2
Lysozyme (e)	14	11.4
Solvent (f)	0	11.8
MUC （1）	822	5.1
MUC （2）	59	7.9
MUC （3）	41	8.7

Figure 3.4: Molecular weight of (A) standards and (B) PGM determined by size exclusion chromatography. Mucin numbers (1-3) were assigned based on the sequence of eluates.

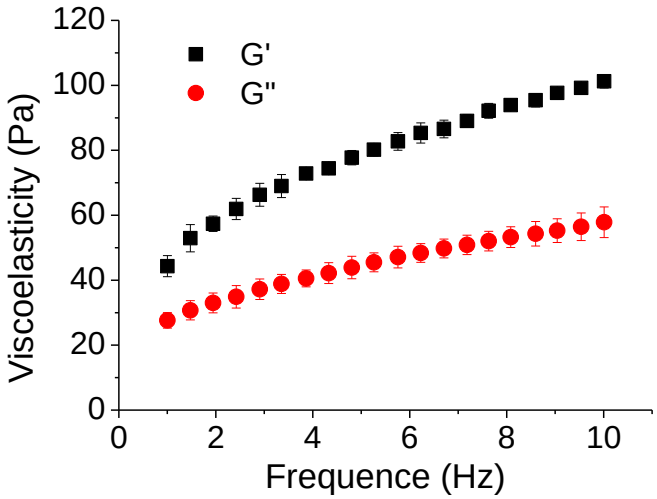

Figure 3.5: Elastic modulus (G') and viscous modulus (G") of PGM. Data represent mean ± standard deviation (n=3).

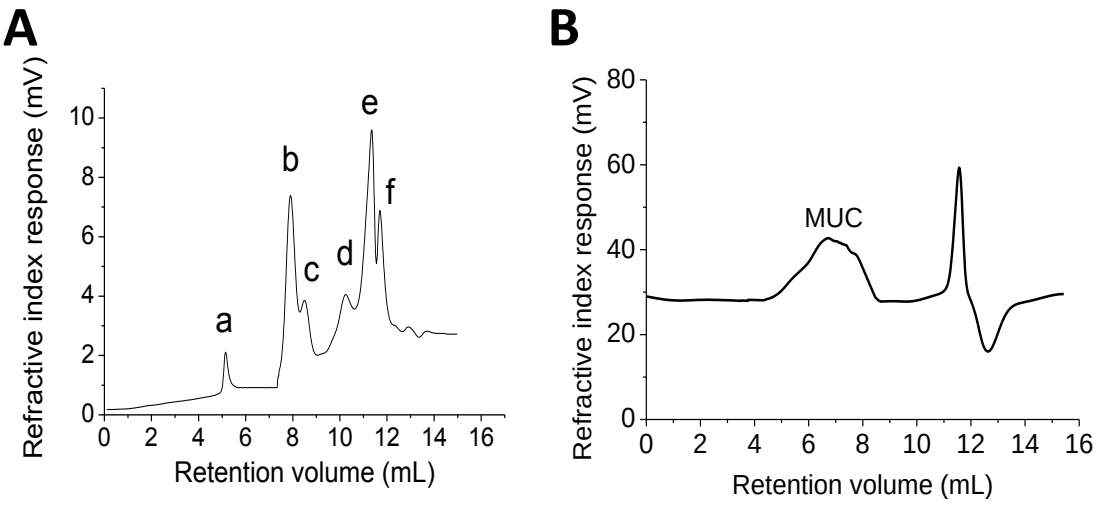

Elutes	Molecular weight (KDa)	Retention volume (mL)
Thyroglobulin (a)	660	5.2
Bovine serum albumin (b)	66	7.9
Peroxidase (c)	44	8.5
Trypsin (d)	23	10.2
Lysozyme (e)	14	11.4
Solvent (f)	0	11.8
MUC	412	6.9

Figure 3.6: Molecular weight of (A) standards and (B) cystic fibrosis mucus (CFM) determined by size exclusion chromatography.

3.4.2 Fluorescence assay

Calibration curves of all nanoparticles displayed a high degree of linearity (R^2> 0.999) in the concentration ranges tested. Average intra and inter day variation data (Table 3.3) indicate the precision of the assay. Intra-day variation in fluorescence intensities for the calibration standards was lower than inter-day variation. Based on intra-day data the LOD and LOQ for the all particle assays were summarized in Table 3.4.

Table 3.3: Average intra and inter-day variations in polystyrene (PS) and PVA particle fluorescence. Intra-day variation data obtained from measurements made in triplicate at each concentration (n=3). Inter-day variation data obtained over three days (n=9).

Nanosuspensions	**Coefficient of Variation (%)**	
	Intra-day	Inter-day
PS50 at pH 8.5	2.80 ± 2.31	3.65 ± 2.40
PS200 at pH 2.5	4.61 ± 3.30	4.24 ± 2.91
PS200 at pH 6.5	4.99 ± 3.71	5.65 ± 4.19
PS200 at pH 8.5	2.60 ± 3.06	3.33 ± 3.71
PVA200 at pH 8.5	5.52 ± 1.56	6.71 ± 2.86
PS750 at pH 8.5	4.03 ± 3.48	4.67 ± 4.50

Table 3.4: LOD and LOQ of different nanosuspensions

Nanosuspensions	**LOD (µg/mL)**	**LOQ (µg/mL)**
PS50 at pH 8.5	3.38	11.26
PS200 at pH 2.5	0.95	3.17
PS200 at pH 6.5	0.97	3.20
PS200 at pH 8.5	3.11	10.35
PVA200 at pH 8.5	1.87	2.43
PS750 at pH 8.5	0.57	1.89

3.4.3 *In vitro* mucus translocation model

Faster translocation rates of sodium fluorescein were observed when the barrier thickness was reduced as shown in Figure 3.7. Without applying any donor solution to the barrier the measured thickness was identical to the mathematical calculation (35 µm). The images of the Transwell supports showed that even the mucus layer that only measured 35 µm still appeared to form a confluent barrier. The fluorescein appeared to diffuse freely through the Transwell membrane system without significant binding as >95% of the applied dose appeared in the receiver chamber 2 h after the application of the sample.

In preliminary studies of particle penetration through the PGM, PS 200 nm particle translocation across thin (35 µm) and thick (2800 µm) mucus layers was measured. The measurement of fluorescence intensity in the receiver chamber after particle application to the surface of the 35 µm mucus layers indicated an initial rapid phase of particle translocation (0-0.5 h) followed by a slower phase plateauing towards 24 h (Figure 3.8A). TEM analysis confirmed the presence of 200 nm particles in the receiver chamber of the Transwell system when the thin layer was used (Figure 3.8A). When the experiment was conducted using the thicker mucus layer (2800 µm), the fluorescence signal in the receiver fluid was lower after application of the PS particles to the apical surface of the diffusion chamber compared to the thin mucus layer. There was also a high fluorescence reading when samples were taken from the basolateral side of the thick mucus when no fluorescent particles were applied to its apical surface. This fluorescence reading in the absence of particles for the thick mucus barrier was attributed to the fluorescence of mucus fragments that had leached into the receiver chamber of the Transwell from the barrier, which was confirmed by the TEM images (Figure 3.8B). The TEM measurements confirmed that the particle translocation was lower across the thick PGM barrier compared to the thin barrier as they showed that it was difficult to isolate images of the polystyrene in the receiver chamber fluid samples (Figure 3.8B).

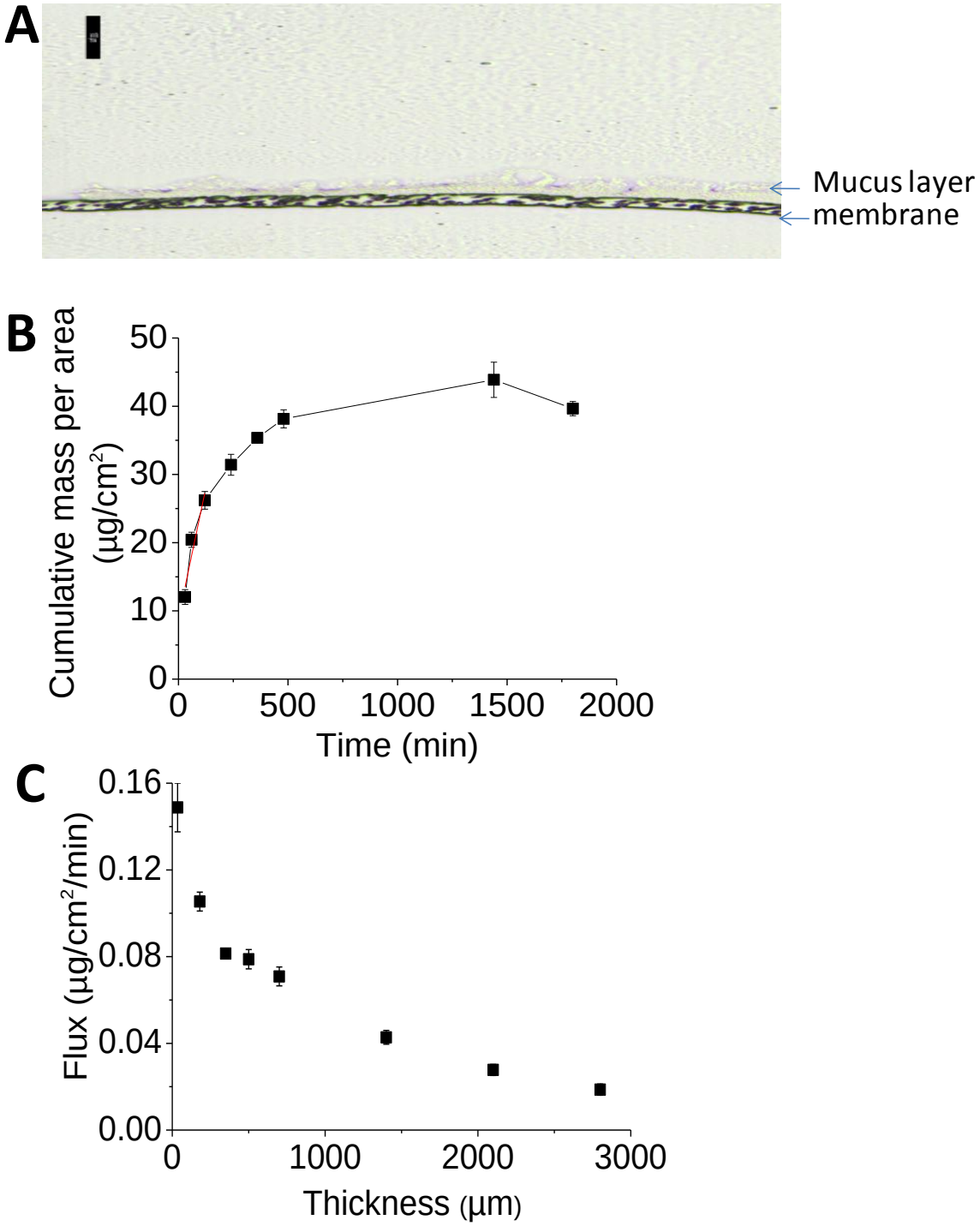

Figure 3.7: Porcine gastric mucus provides a barrier to the penetration of sodium fluorescein. (A) Illustrative micrograph showing the thickness of a PGM layer on the permeable membrane of a Transwell insert. Scale bar represents 100 µm. (B) Typical profile for cumulative mass transfer of sodium fluorescein across a 35 µm PGM layer lining a Transwell insert. (C) Flux of sodium fluorescein through PGM as a function of mucus layer thickness. Data represent mean ± standard deviation (n = 3).

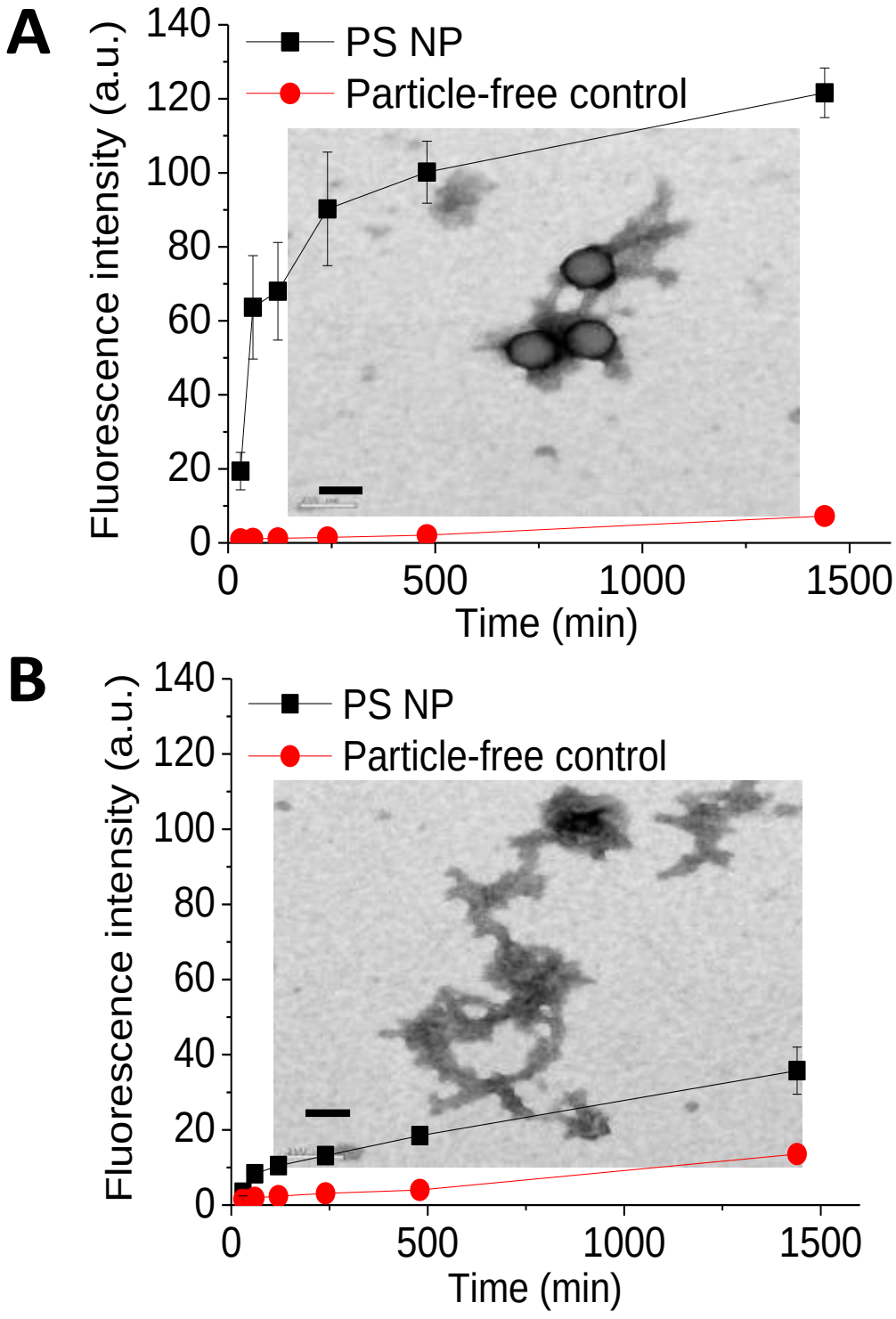

Figure 3.8: Fluorescence intensity and transmission electron micrograph (inset) of the material in the Transwell receiver chamber following the application of PS 200 nm nanoparticles or particle-free control Tris buffer pH 8.5 to mucus layers with a thickness of (A) 35 µm, and (B) 2800 µm. Data represent mean ± standard deviation (n = 3). The scale bar in the images represents 200 nm.

Both increasing the fluid application volume in which an increasing sodium fluorescein was applied to the surface of the mucus barrier and fixing the fluid volume whist increasing sodium fluorescein concentration led to a higher flux compared to the fixed concentration (Figure 3.9). Both profiles had linear portions when increased concentration was plotted against flux, but they displayed different patterns of data. When the concentration was fixed and the volume was variable, distinct linear portions of the graph can be observed, 1 to 10 and 10 to 75 µL, this suggested that the application fluid volume was swelling the barrier and having an influence onits function. The 10 µL was thought to be a critical point where in the fluid volume started to have a significant impact on the transport rate. The application of small volumes (1-10 µL) of particle suspension to the surface of a 35 µm mucus layer resulted in a similar extent of mucus gel swelling irrespective of the sample volume applied (Figure 3.10A). However, the volume in which the PS 200 nm particles were applied to the surface of the mucus layer greatly affected the rate of translocation of the material into the receiver fluid (Figure 3.10B). When applied in a 1 µL aliquot the nanoparticle translocation was complete within 8 h, whereas only 25-30% of particles transferred into the receiver chamber over the same time period when 5 or 10 µL sample volumes of the particles were applied to the surface of the mucus ($p<0.05$;Figure 3.10). For subsequent studies, the smallest sample volume (1 µL suspension) and the thinnest mucus layer (35 µm) were used as these conditions appeared to constitutea robust model for particle penetration and were thought to mimic the conditions *in vivo* (Mühlfeld et al., 2008).

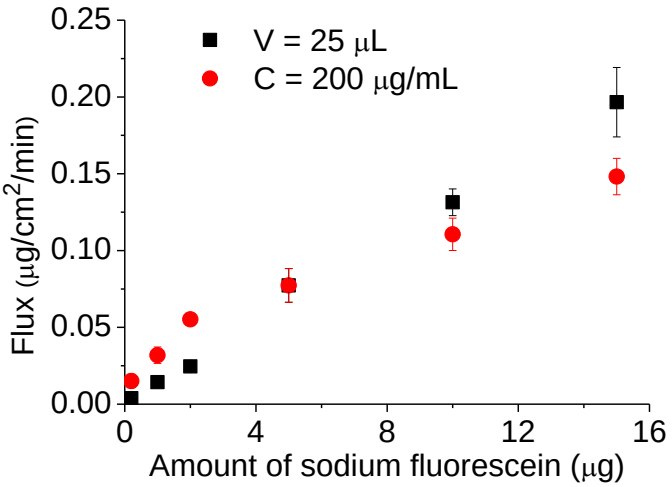

Figure 3.9: Transport of increased donor solution concentration (C) and volume (V) through PGM barrier. Data represent mean ± standard deviation (n = 3).

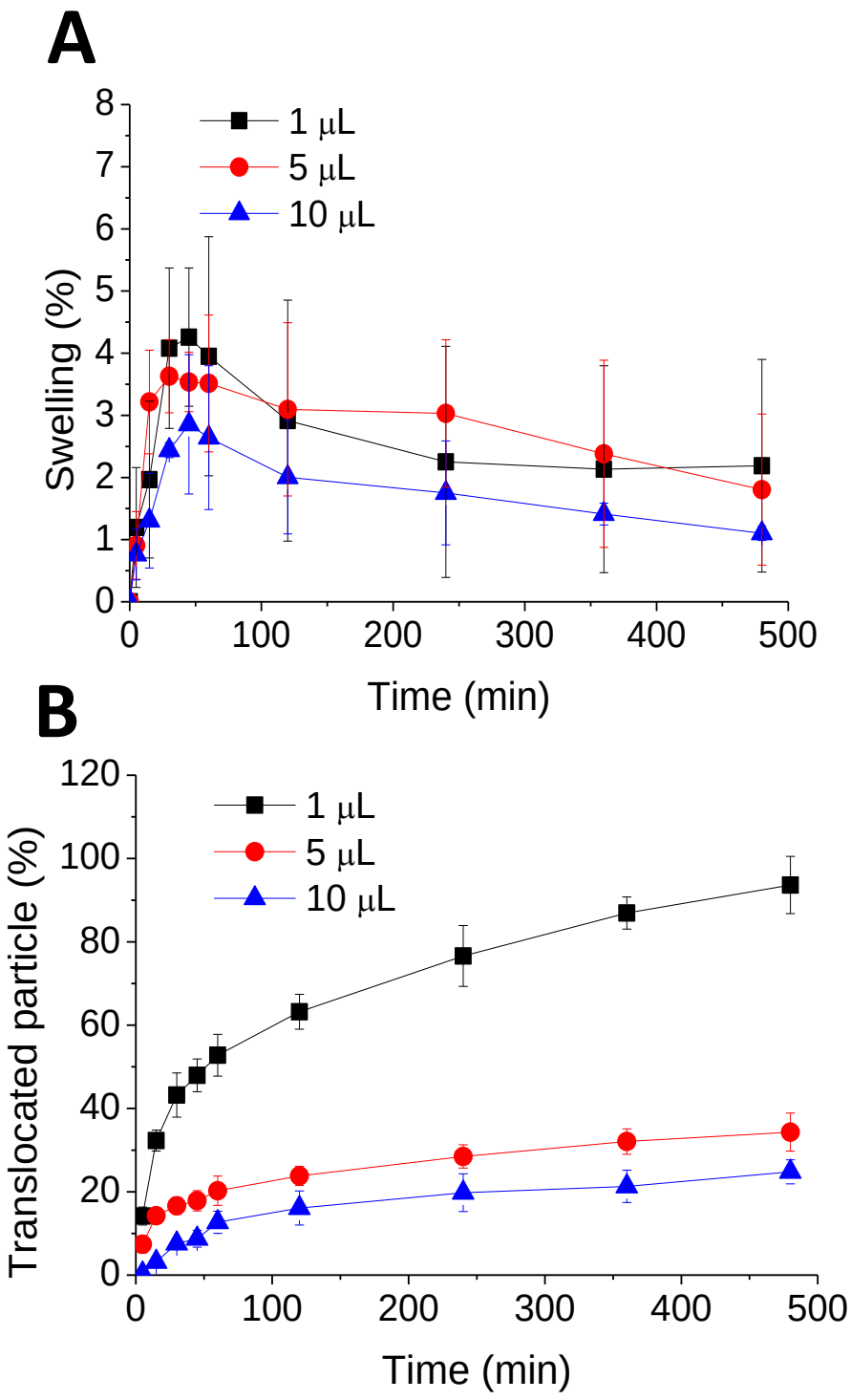

Figure 3.10: Effect of the volume (1-10 μL) of PS 200 nm nanoparticle suspension applied to the surface of a 35 μm porcine gastric mucus layers on (A) mucus swelling and (B) the translocation of PS particles across the mucus layer. Data represent mean ± standard deviation (n = 3).

3.4.4 Nanoparticle translocation through pig gastric mucus

The carboxylated polystyrene nanoparticles were verified to be of the size described by manufacturer's specification and they exhibited a negative charge (Table 3.4). Both particle size and pH of the applied vehicle were determinants in the rate of nanoparticle translocation through mucus (Figure 3.11). In order to compare with the data obtained from NanoSight, unit of nm^2/s was used for data obtained from static model. The particle transport rates showed that the 200 nm particles moved through the barrier three times faster than 50 and twice as fast as 750 nm particles ($p<0.05$; Figure 3.11A). According the polystyrene particle experiments the mucus barrier was more restrictive at acidic pH. The fastest penetration rate of 200 nm PS nanoparticles was observed at pH 8.5, which was 2- and 8-fold faster compared to pH 6.5 and pH 2.5, respectively ($p<0.05$; Figure 3.11B). Lipid shell nanoparticles had the fastest penetration rate through the mucus, translocating across the mucus barrier 3 times faster than equivalent sized negatively charged polystyrene particles ($p<0.05$; Figure 3.12A). The fabricated lipid shell nanoparticles were 50 nm in diameter with a neutral surface. However, the diffusion rate of 200 nm PVA shell nanoparticles was 10-fold lower than 200 nm PS nanoparticles ($p<0.05$; Figure 3.12B). When the lipid shell nanoparticle permeabilisation process was achieved the penetration rate was equivalent to controlled nanoparticles, indicating that surfactant-induced nanoparticle distension had little effect on mucus penetration (Figure 3.13).

Table 3.5: A summary of nanoparticle characteristics (PS: polystyrene; LNP: lipid nanoparticle; PLNP: permeabilised lipid nanoparticle; PVA: poly vinyl alcohol nanoparticle) and their diffusion through porcine gastric mucus (PGM) and cystic fibrosis mucus (CFM) using static and mobile mucus models. Data represent mean ± standard deviation (n = 3). Symbols indicate a statistical difference when comparing the results across the groups which differed in *particle size, #pH, and surface chemistry ($p<0.05$).

Test System	Diameter, (nm)	ξ-potential, (mV)	Diffusivity in PGM, $\times10^4$ nm^2/s (Transwell)	Diffusivity in PGM, $\times10^4$ nm^2/s (NanoSight)	Diffusivity in CFM, $\times10^4$ nm^2/s (Transwell)
PS50 in pH 8.5	53 ± 1	-35.9 ± 0.8	9.87 ± 0.61	329 ± 166	1.14 ± 0.20
PS200 in pH 8.5	187 ± 2	-48.4 ± 1.4	19.93 ± 5.47	267 ± 99	0.88 ± 0.10
PS750 in pH 8.5	778 ± 3	-61.5 ± 1.0	6.67 ± 1.28*	140 ± 77*	0.30 ± 0.02*
PS200 in pH 6.5	185 ± 2	-41.8 ± 3.9	9.54 ± 3.26	198 ± 34	0.38 ± 0.03
PS200 in pH 2.5	183 ± 2	-33.2 ± 1.1	2.98 ± 0.74#	107 ± 7#	0.18 ± 0.08#
LNP50 in pH 8.5	52 ± 2	-3.5 ± 0.6	30.08 ± 2.49△	494 ± 4	28.99 ± 3.28△
PLNP50 in pH 8.5	52 ± 2	-2.4 ± 1.0	27.10 ± 3.84△	397 ± 38	29.51 ± 2.13△
PVA200 in pH 8.5	225 ± 5	-1.5 ± 0.8	1.64 ± 0.37	N/A	N/A

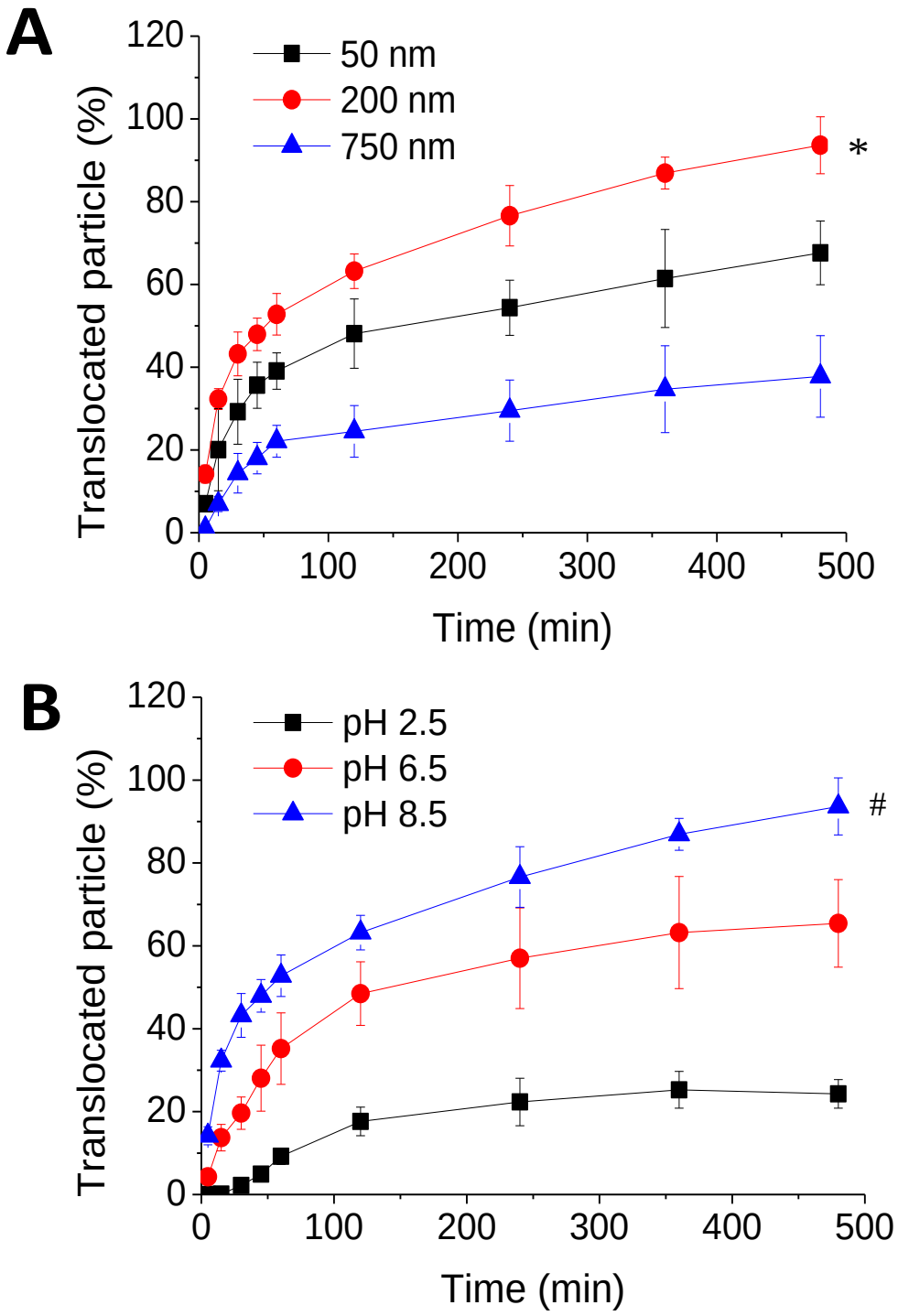

Figure 3.11: The transport of (A) 1 µL of 50, 200 and 750 nm PS NP at pH 8.5 through a 35 µm PGM barrier and (B) 1 µL of 200 nm PS NP at pH 2.5, 6.5 and 8.5 through a 35 µm PGM barrier. Data represent mean ± standard deviation (n = 3).

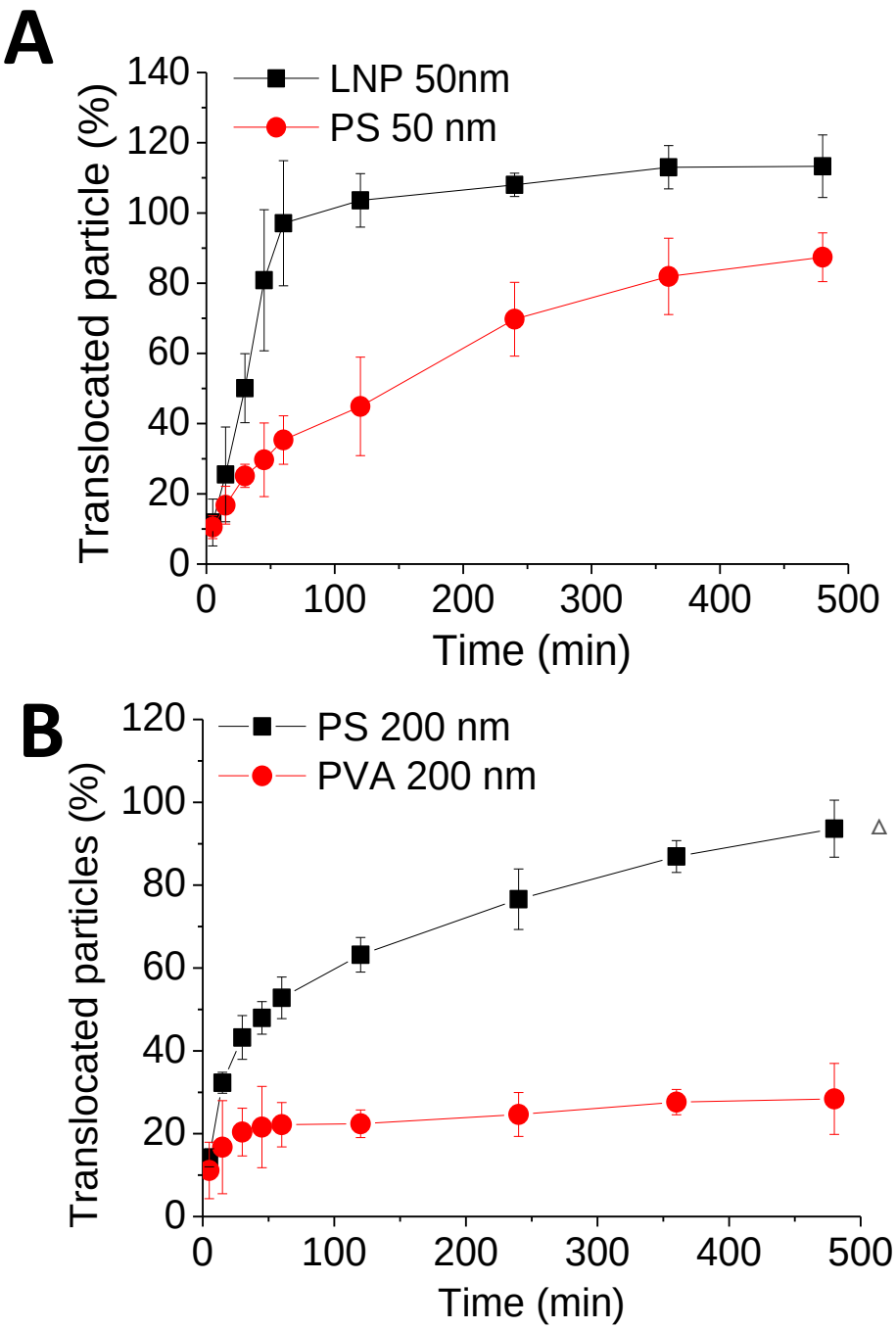

Figure 3.12: The translocation of (A) 50 nm lipid shell nanoparticles (LNP) through a 35 μm PGM barrier at pH 8.5 compared to 50 nm PS NP and (B) 200 nm PVA shell nanoparticles (PVA) compared to 200 nm PS NP. Data represent mean ± standard deviation (n = 3).

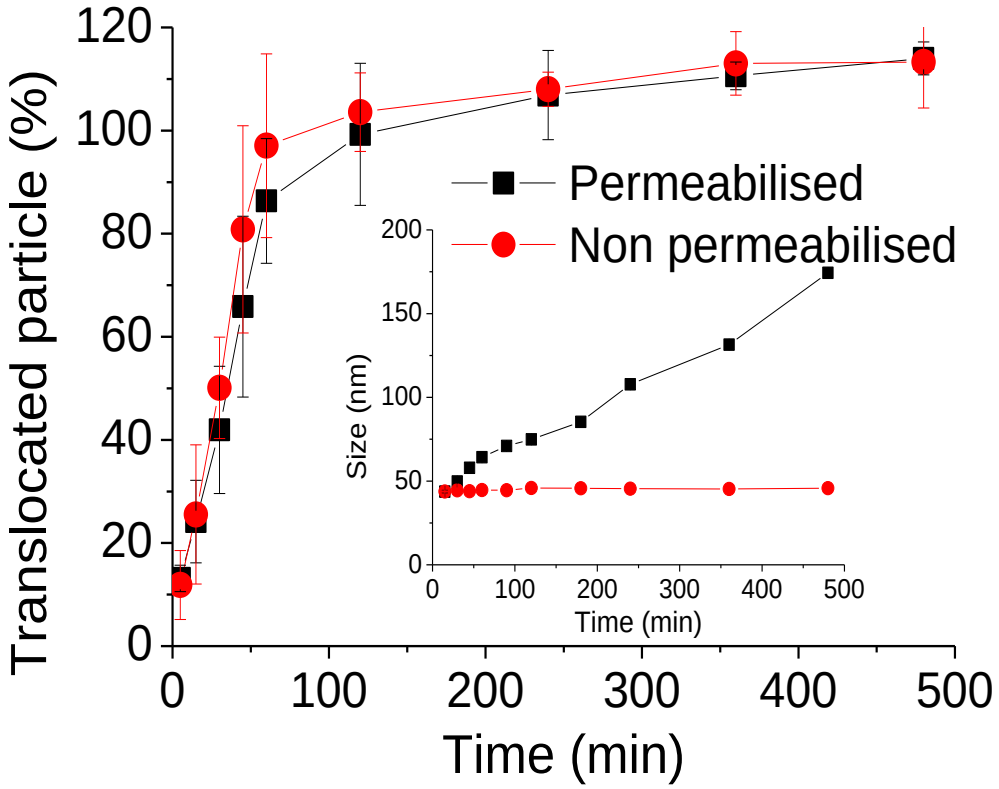

Figure 3.13: The translocation of permeabilised and non-permeabilised 50 nm lipid shell nanoparticles through a 35 µm PGM barrier at pH 8.5 with associated nanoparticle permeabilisation process (inset). Data represent mean ± standard deviation (n = 3).

3.4.5 Multiparticle tracking of lateral diffusion

When lateral particle diffusion was measured in mucus, the mean particle diffusion rates were up to thirty times greater compared to the diffusion calculated in the static model (Figure 3.14). This difference in the diffusivity when the particle tracking data and the Transwell data were compared was not consistent across the different particles types. Although both pH and particle size influenced the particle movement in both mucus diffusion systems, there were significant differences in the trends across the two data sets. Unlike the Transwell diffusion data in the horizontal studies the 50 nm sized nanoparticles moved through the gel at the fastest rate (329 ± 166 nm^2/s) and the 700 nm particles the slowest (140 ± 77 nm^2/s, $p<0.05$, Figure 3.14, Table 3.5). Furthermore, the mucus gel was sensitive to the lipid shell nanoparticle size distension process, with the distensible nanoparticles passing through the mobile mucus system at a slower rate (397 ± 38 nm^2/s) compared to the none-distending carriers (494 ± 4 nm^2/s, Figure 3.13, Table 3.4). The effects of pH were similar across the two different mucus model data sets (Figure 3.14, Table 3.5).

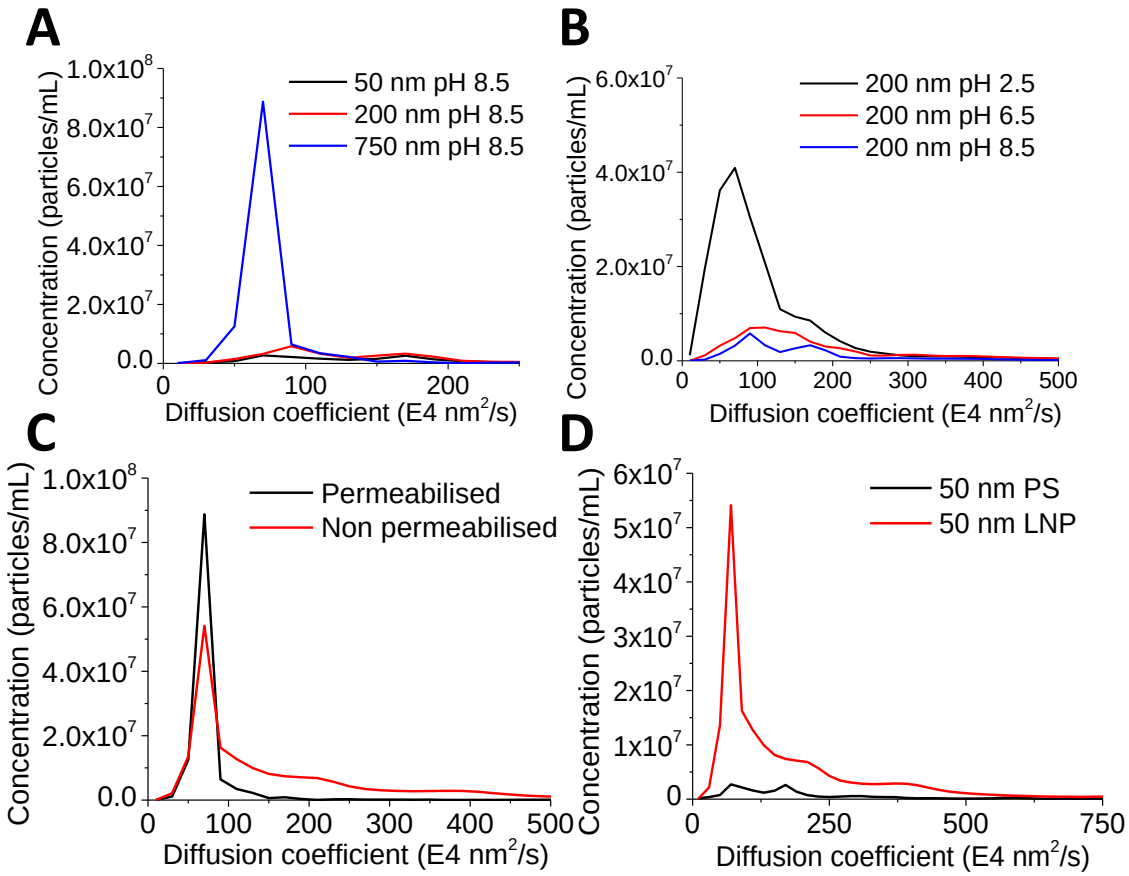

Figure 3.14: The lateral diffusion profiles of nanoparticles in porcine gastric mucus (PGM) displaying (A) the effect of polystyrene particle size, (B) effect of media pH on 200 nm polystyrene nanoparticles, (C) permeabilised and non-permeabilised lipid shell nanoparticles and (D) surface charge.

3.4.6 Nanoparticle diffusion through cystic fibrosis mucus

The diffusionof particles in cystic fibrosis mucus in the Transwell inserts was slower compared to PGM for all the polystyrene particles ($p<0.05$; Table 3.5; Figure 3.15A and B). The magnitude of diffusion retardation was between 10 to 20-fold compared to the rates recorded in PGM ($p<0.05$; Table 3.5). The pH had a similar effect on the mucus transport compared to the PGM, but interestingly the 50 nm particles permeated at the quickest rate compared to 200 and 750 nm particles ($p<0.05$; Table 3.5). The lipid shell nanoparticles again exhibited the most rapid translocation rates in the cystic fibrosis mucus, its diffusivity was ~ 25-fold higher compared to similar sized polystyrene particles ($p<0.05$), irrespective of the trigger conditions (Figure 3.15C and D). The lipid shell nanoparticle diffusivity was not slowed down in the cystic fibrosis mucus compared to the PGM like the polystyrene particles ($p>0.05$).

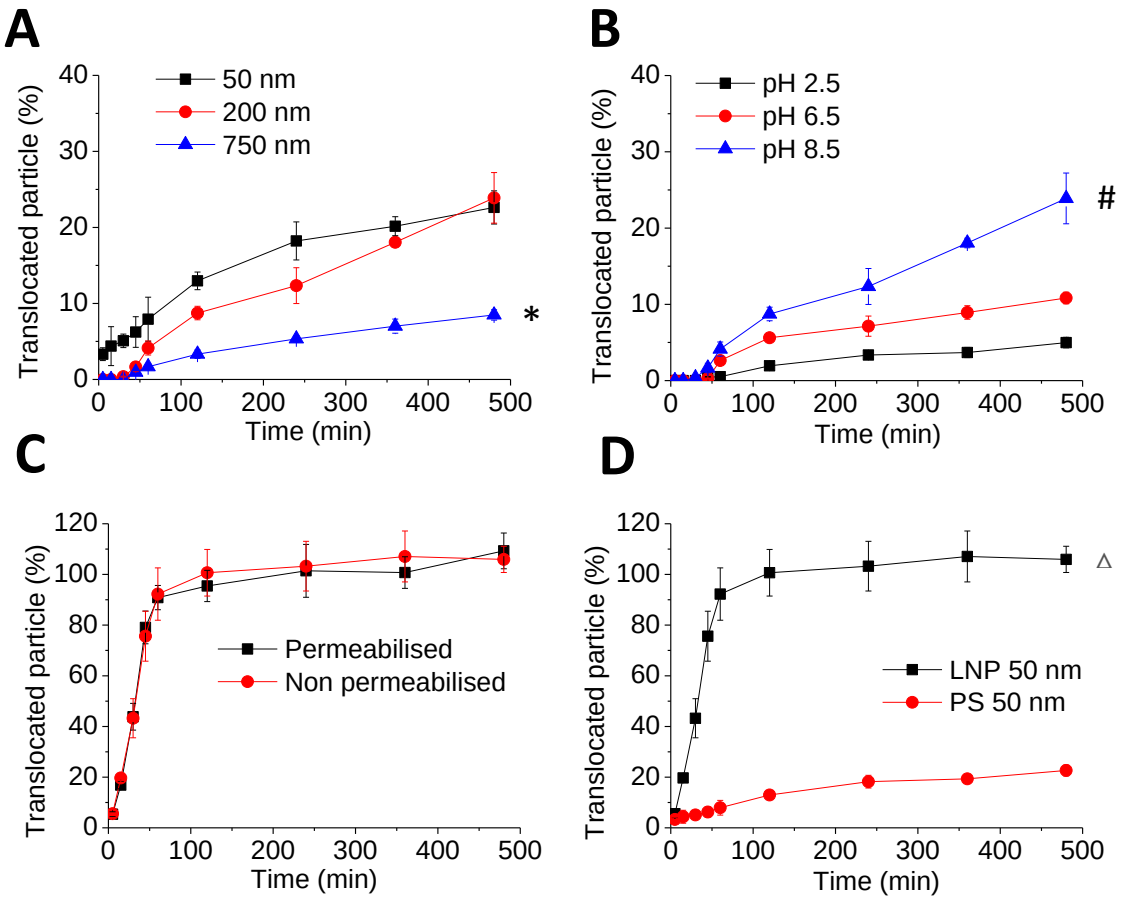

Figure 3.15: Nanoparticles penetration through respiratory cell-derived cystic fibrosis mucus, showing the effect of (A) polystyrene nanoparticle (PS) size at pH 8.5, (B) the pH of the vehicle in which PS 200 nm were applied, (C) permeabilisation of the lipid shell nanoparticles (LNP) at pH 8.5, and (D) the surface properties of the nanoparticles at pH 8.5. Data represent mean ± standard deviation (n = 3).

3.5 Discussion

In this Chaptera novel means to determine the manner in which nanoparticles translocate across a mucus barrier was developed in order to understand how dynamic nanoparticles passed through respiratory mucus.The mucus-particle interactions were understood through comparison of the lipid shell nanoparticles and PVA shell nanoparticles with polystyrene nanoparticles in two types of mucus.

A major role of the respiratory mucus gel is to trap inhaled particles so that they can be removed from the airways by mucocilliary clearance, thereby defending the lungs against inhaled pathogenic microorganisms and toxic materials (Thornton et al., 2008). The mucus that lines the airways provides a challenge to efficient nanoparticle delivery to the lungs due to the poor penetration of most conventional particle systems through this barrier. The particle systems developed in Chapter 2 therefore must cross the mucus barrier if they are to be effective drug delivery systems.

As in previously published studies the diffusion data in this Chapter indicated that the nanoparticles transport through the mucus barrier was influenced by particle size, surface charge and surface hydrophobicity (Lieleg and Ribbeck, 2011). In the Transwell mucus penetration assay, 200 nm PS particles translocated the mucus barrier at a much faster rate compared to the 50 and 750 nm particles. The 200 nm PS particlediffusion rate of 20×10^4 nm^2/s, was similar to a previous study,which measured the particle diffusion in human cervical mucus using a particle tracking technique (Cu and Saltzman, 2008). In the current study the particle tracking diffusivity was consistently approximately thirty times higher compared to the Transwell system diffusivity values. Although both techniques measured diffusivity, the particle tracking technique measured only horizontal movement. The Transwell system diffusivity was a consequence of three dimensional movement and hence accounts for any effects of gravity.

The fact that rank order of particle translocation rate based on size in the Transwell assay was different to that obtained from the particle tracking system suggests that the mucus barrier was different in the two techniques. The horizontal particle tracking system appeared to obey an ideal Stokes-Einstein equation type behaviour, i.e. that smaller particles were subject to faster diffusion. However, in the Transwell assay the 200 nm particle moved through the mucus more rapidly than the 50 nm particle and this suggests this diffusion was influenced by

other factors such as gravity and diffusion path tortuosity. Lai who studied the transport of particles ranging from 100 to 500 nm in human cervicovaginal mucus using particle tracking showed similar results to those recorded in this study (Lai et al., 2007). In that study 100 nm sized particles were found to be almost completely immobile in mucus, whereas 200 and 500 nm sized particles had a higher diffusion coefficient. The horizontal movement tracked by the camera was estimated to be around 20 μm and this was quite similar to the vertical translocation which was ca. 35 μm (although it is accepted there was some swelling of the barrier), therefore the difference was attributed to the dilution of the mucus sample and the application of shear breaking up the mucus structure in the horizontal particle tracking measurements (Lai et al., 2010). If the mucus is sensitive to dilution then each mucus which has a unique structure could be influenced by the total solid content of mucins in the test systems. This could be one explanation why the particle tracking data appears to be very heterogeneous when previous studies are reviewed. For example, particle tracking measurements have shownan ideal Stokes relationship between diffusion and particle size using human lung mucus (Schuster et al., 2013) and murine luminal mucus penetration (Maisel et al., 2015), but there are other works using pig intestinal mucus (Abdulkarim et al., 2015) and human chronic rhinosinusitis mucus (Lai et al., 2011) that do not show this relationship. In none of these studies has the effect of mucin concentration been studied.

When nanoparticle transport in mucus in alkaline conditions (pH 8.5) was investigated, the mucus gel was more permeable in both the penetration assay and lateral particle tracking. The results are consistent with the suggestion that pH regulates the electrostatic interactions between the mucin polymers and diffusing particles. Studies using different analytical methods have found that lower pH facilitates mucus-particle interaction (Svensson et al., 2008) and as a consequence more rigid mucus network is formed at acidic pH (Bromberg and Barr, 2000; Hong et al., 2005; Maleki et al., 2008). This was observed for both the porcine gastric mucus and the cystic fibrosis mucus in this study when tested in the Transwell insert.

Cystic fibrosis generally results in an increase in the viscoelasticity of mucus, owing in part to reduced water content and an increased fraction of glycoproteins (Boucher, 2004; Rubin, 2007). Cystic fibrosis sputum undergoes significant shear-thinning with representative steady shear viscosities of ~14 Pa-s at shear rates of $1s^{-1}$, whereas the viscosity of porcine gastric mucus has been reported to be only ~0.085 Pa-s at a shear rate of 1.15 s^{-1} (Lai et al., 2009). In this study, the transport of PS particles through mucus derived from a respiratory cell line

from a human donor with cystic fibrosis was 20 times slower than across PGM. The much slower movement of polymeric particles in the respiratory mucus compared to the PGM has previously been reported. It was demonstrated that diffusion coefficient of amine modified particles in native gastric mucus were 40-fold lower compared to the theoretical diffusivity of the same particles in water (Crater and Carrier, 2010), and 5600-fold lowerin CF sputum (Suk et al., 2009). These results corresponds to the findings here that the respiratory CF mucus was much more restrictive than PGM. The structure of CF sputum has previously been studied by scanning electron microscopy (SEM) and this has led to pore size estimates of 100-400 nm (Sanders et al., 2000). The SEM technique however has several limitations when trying to assess the pore size of mucus due to the manner in which the samples are prepared. The 3D mesh spacing of physiological human CF sputum with minimal perturbation during sample preparation was probed and an average mesh size of 200 nm was reported (Suk et al., 2009). This suggested very slow rate of 750 nm sized particle diffusion was most likely attributed to extensive steric obstruction imposed by the smaller mesh spacing of CF sputum.

It is believed that the primary mechanism by which mucus gels interact with particles is through the formation of polyvalent adhesive interactions (Cone, 2009). However, the high density of hydrophobic domains within mucin fibres can efficiently form multiple low-affinity adhesive interactions with hydrophobic regions on the surfaces of particulates. Theoretically negatively charged mucin fibers showhigh affinity with positively charged particles and thus negatively charged particles may favour particle transport in the relatively hydrophilic pores of the mucus mesh. However, the carboxylate groups of the particle will provide opportunity for hydrogen-bonding interactions with mucin (Peppas and Huang, 2004) and higher transport rates for cationic particles than anionic particle within intestinal mucus has been reported (Abdulkarim et al., 2015). Neutral particles have advantages over charged particles as the electrostatic interactions and hydrogen bonding can be greatly reduced. The slow movement of 50 nm carboxyl modified hydrophobic particles through both types of mucus in this study was consistent with this mechanism and similar conclusions made in previous studies (Olmsted et al., 2001). Interestingly, similarsized neutral lipid nanoparticles had higher diffusion rates compared to the polystyrene particles suggesting the particles have less interactions with the mucin fibres in the mucus which similar results were previously reported (Nafee et al., 2014). Lipid shell nanoparticles comprise triglycerides dispersed in a saline solution, stabilised at the droplet interface with phospholipids and a PEG based surfactant (Heurtault et al., 2002). Wang et al. (2008) reported that nanoparticles coated with

low molecular weight poly(ethylene glycol) (PEG) possess hydrophilic and near neutrally-charged surfaces that minimize mucoadhesion by reducing hydrophobic or electrostatic interactions (Wang et al., 2008). Low PEG MW and dense PEG surface coverage were both required for rapid mucus penetration of coated particles. This has recently been confirmed by Jones et al (2014) using the lipid nanoparticles employed in this study (Jones et al., 2014) who characterised the surface hydrophobicity of nanoparticles using hydrophobic interaction chromatography (HIC) and classified the particles using a developed hydrophobicity scale: the HIC index. The results demonstrated that polystyrene nanoparticles (0.96 ± 0.04) displayed a higher HIC index than that of lipid shell nanoparticles (0.50 ± 0.09). The results from this study confirm that hydrophobicity of nanoparticles is also a significant factor in transport through mucus.

It was hypothesized that permeabilized particles could be immobilised in the mucus due to their size distension process. However, no effect of the distension process was observed on the diffusion. This result may be related to the kinetics of the particle distension process. The permeabiliser allows the nanoparticles to swell from 50 to 200 nm over a period of 8 h. However, the mucus penetration was rapid and mainly occurred over the first hour after application to the mucus. Significant higher transport rates were obtained compared to polystyrene particles, indicating that this dynamic lipid shell nanoparticle system was a robust mucus penetrating nanosystem that could be used for the controlled drug delivery of antibiotics even when the airway mucus became viscous.

When polyvinyl alcohol (PVA), a relatively hydrophilic and uncharged polymer routinely used as a surfactant to formulate drug carriers weas used to manufacture the nanoparticles, their diffusion in PGM were severely retarded compared to lipid shell nanoparticles and PS NP. This suggests that incorporating PVA in the particle formulation process may lead to the formation of mucoadhesive carriers. The influence of surface coating by PVA on the transport of nanoparticles in fresh human cervicovaginal mucus was investigated (Yang et al., 2014). PVA-coated polystyrene (PS) particles were immobilized, with speeds at least 4000-fold lower in mucus than in water, regardless of the PVA molecular weight or incubation concentration tested. As partially hydrolyzed PVA was used during the particle fabrication, both the hydroxyl groups and the residual acetyl groups may form hydrogen bonds with mucus constituents. In addition, the residual acetyl groups are also capable of establishing

hydrophobic interactions with the mucus mesh due to the hydrophobic terminal methyl group. Thus it is believed that PVA could prevent particle diffusion in mucus.

3.6 Conclusion

In this Chapter lipid shell nanoparticles were shown to be capable of penetrating both PGM and CF mucus and PVA shell nanoparticles were shown to be immobilized in PGM. The multidimensional mucus diffusion modeling performed in this work was an easy and robust means to assess the movement of particles through mucus. The penetration of polystyrene particles suggests that particle size, hydrophobicity and medium pH are significant factors in nanoparticle translocation. The rapid transport of lipid nanoparticle system coupled with prior knowledge that they were slow to move into epithelial cells and well tolerated *in vivo* suggests that have the potential to be developed for the delivery of a drug in a controlled manner in the airways of the lungs. These nanoparticles must however be encapsulated into a carrier to be efficiently deposited in the lungs and this will be tested in the next Chapter.

CHAPTER FOUR

Co-administration of nanoparticles with a shell permeabiliser using a microparticle carrier

4.1 Introduction

There have been studies that have dosed RIF, INHand PZA to the lungs using solid lipid particles (SLPs) and that were incorporated into a powder with a favourable mass median aerodynamic diameter suitable for bronchoalveolar drug delivery (Pandey, 2005). Pandey et al. (2003) demonstrated that sustained therapeutic effect was obtained when anti-TB drugs were loaded into PLGA nanoparticles that were nebulised as micro-droplets into the lung (Pandey et al., 2003). Doan et al. (2011) has also shown that rifampicin-loaded microspheres are suitable for lung delivery as sustained-release microsphere aerosol (Doan et al., 2011). A mixture of these two systems, i.e., nanoparticle-aggregate particles (PNAP), containing rifampicin, have also produced beneficial effects (Sung et al., 2009). Alginate nanoparticles have been shown to be capable of encapsulating INH, RIF andPZAand the delivery of these agents has shown promise in *in-vivo* models (Zahoor et al., 2005). These studies have established the proof of principle data that ATD dosing is favourable and possible, but none of the previous work in the field has gone on to make products. One reason for this is that although these systems provide controlled release they still cannot achieve the required drug levels in the lung macrophages to cut down the length of clinical treatment with ATDs (Zahoor et al., 2005).

In Chapter 2, it was demonstrated that encapsulating rifampicin into lipid shell nanoparticles increased drug chemical stability and this drug delivery system was shown to have the potential to release drug in a controlled manner through a carrier distension process. These nanoparticles could provide a solution to the current issues with carriers designed to deliver ATDs to the lungs and target macrophages as if they are administered in a microparticle which quickly dissolves, the nanoparticles can be permeabilised and the growth of the carriers could facilitate uptake by macrophages once in the lung. A dry powder inhalation for ATDs seems to be the most sensible choice given the drug's potential to chemically degrade (Sosnik et al., 2010)

Several particle engineering technologies have been applied for pulmonary powder production such as milling, spray drying, spray freeze drying and supercritical fluid technology (Shoyele and Cawthorne, 2006),spray drying (SD) is probably the most well-established method in pharmaceutical applications (Abdelwahed et al., 2006; Malcolmson and Embleton, 1998). It is one of the most sophisticated drying techniques and offers many possibilities for modification to facilitate novel particle engineering (Vehring, 2008).

Furthermore, spray drying is applicable tomany different liquid systems including nanopartcile suspensions. For example, previous study produced rifampicin/PLGA nanoparticle-containing microspheres using a modified spray drier (Ohashi et al., 2009). Spray drying offers the possibility of mixing fluids immediately prior to particle formation during the atomization process (Vehring, 2008). Furthermore, spray drying permits the controlled production of particles of different morphologies by changing the spray drying process conditions (Chew et al., 2005).

As spray drying seemed like the most flexible particle fabrication process, it was thought beneficial to develop a spray drying method, which could hold the surfactant permeabiliser and the nanoparticles separately until the microparticle carrier dissolved and allowed the two to mix freely. It was hypothesized that developing rapidly dissolving nanoparticle-permeabiliser containing microparticles, with an aerodynamic diameter between 1 and 5 μm, would facilitate controlled drug release and macrophage recognition. Therefore, the aim of the work in this Chapter was to design a novel spray drying method for the microencapsulated lipid shell nanoparticles and then investigate the ability of the surfactant to permeabilise rifampicin release from microencapsulated lipid shell nanoparticles in simulated lung fluid. To achieve this aim the lipid nanoparticles were spray dried, they were characterize with respect to particle size, nanoparticle size recovery, drug content and morphology. Finally, the effect of permeabiliser inclusion in the dry powder formulation on the release of rifampicin from the nanoparticles-containing microparticles was assessed.

4.2 Materials

Lactose was purchased from Sigma-Aldrich, UK. Other materials were as described in Chapter 2.

4.3 Methods

4.3.1 Preparation of nanoparticle

Blank and rifampicin-loaded lipid shellnanoparticles were prepared and purified according to the methods detailed in Section 2.3.1.

4.3.2 Microparticle fabrication

Spray drying was performed with a mini-spray drier (Buchi Laboratoriums-Technik, Flawil, Switzerland), which operated using a twin nozzle of air and liquid spraying in a parallel flow. For the preparation of blank and rifampicin containing nanoparticles loaded microparticles, nanosuspensions (1 mL) were mixed with lactose solutions (3% w/v) using magnetic stirring for 10 min. The Pluronic L62D, used to permeabilise the nanoparticles was dissolved in the second feed solution. The two feed stocks were supplied to the spray drier at the same speed using a T shaped connector using the operational conditions detailed in Table 4.1. The dried powders were recovered and stored at room temperature, protected from light, in the presence of a dessicant potassium pentoxide.

Table 4.1: Operation conditions for the spray-drying technique

Spray drying parameters	Operational conditions
Inlet air temperature (C)	160
Aspiration setting (%)	85
Feed flow rate (mL/min)	2
Air flow rate (L/h)	700
Atomising air pressure (psi)	80

4.3.3 Particle size analysis

The particle size distribution (PSD) of each sample was evaluated using a SympatecHelos/Rodos laser diffraction particle size analyser (Sympatec, Germany). Approximately 20 mg of powder was introduced to the dry dispersion feeder system using a vibratory feed tray. The dispersion pressure was set at 4 Bar. The laser diffraction system, equipped with the appropriate lens for the sample's particle-size range was used to measure the PSD of the sample. The volume mean diameter (VMD), D10, D50 and D90 (cumulative undersize below 10%, 50% and 90% of the size frequency plot) were calculated using the Sympatec software.

4.3.4 Particle morphology

Microparticles were mounted on 0.5 inch aluminium stubs using double sided adhesive tap discs. The samples were spatter coated at an electrical potential of 2.0 kV, a current of 20 mA and at high vacuum (0.02 Torr) for 2 min. This procedure resulted in a film of gold, approximately 10 to 20 nm thick, being deposited on the specimen. The electron micrographs were recorded on 220 size Ilford FP4 film using a scanning electron microscope (SEM) (Zeiss, Germany).

4.3.5 Nanoparticle recovery from dry powders in aqueous medium

A 100 mg aliquot of spray dried powder was dispersed in a bottle containing 5 mL of PBS 7.4 under magnetic stirring at a temperature of 37 ℃. The particle size of released LNPs from each formulation was measured by PCS under the conditions previously stated in Section 2.3.5.

4.3.6 Encapsulation efficiency and release study

Drug uniformity content for each formulation was determined by dissolving the dry powder in PBS buffer at pH 7.4. An aliquot of this solution was transferred to an Amicon centrifuge tube to separate nanoparticles from dispersing medium (see the methodin Section 2.3.8). For the release study, the suspension was placed into dialysis tubing and it was dialysed against PBS buffer pH 7.4. At a number of different time intervals, samples were withdrawn from the tubing. The drug content remaining in the particles was analysed by HPLC and the drug

release was determined by difference (due to the chemical instability of rifampicin in aqueous media.

4.3.7 Statistical analysis

SPSS version 20 (IBM, UK) was used for all statistical analyses. The normality (Sapiro-Wilk) and homogeneity of variances (Levene's test) of the data were assessed prior to statistical analysis. The release data were analysed statistically using T-test or Mann-Whitney test. Differences were considered to be statistically significant at a level of $P < 0.05$.

4.4 Results

4.4.1 Characterization of spray dried microparticles

Microparticles fabricated by spray drying had a median size of approximately 4 μm as shown in Table 4.2. Incorporating lipid shell nanoparticles or rifampicin-loaded lipid shell nanoparticles into microparticles did not have effect on particle size.

Table 4.2: Particle sizes of different spray dried powders obtained by laser diffraction: B-LNP-MP (blank lipid shell nanoparticles contained microparticles); RIF-LNP-MP (rifampicin-lipid shell nanoparticles contained microparticles); B-PLNP-MP (blank lipid shell nanoparticles contained microparticles with permeabiliser); RIF-PLNP-MP (rifampicin-lipid shell nanoparticles contained microparticles with permeabiliser). Data represent mean ± standard deviation (n=3).

	Particle size (μm)			
Formulation	**X10**	**X50**	**X90**	**VMD**
B-LNP-MP	1.19 ± 0.02	3.36 ± 0.37	6.92 ± 0.88	3.80 ± 0.42
RIF-LNP-MP	1.32 ± 0.29	3.69 ± 0.23	7.45 ± 0.09	4.19 ± 0.14
B-PLNP-MP	1.21 ± 0.05	3.93 ± 0.26	7.84 ± 0.41	4.31 ± 0.24
RIF-PLNP-MP	1.47 ± 0.29	4.06 ± 0.06	8.36 ± 0.14	6.43 ± 0.69

4.4.2 Morphology of microparticles

Microspheres were obtained with yields of approximately 50%. As can be observed in the SEM microphotographs depicted in Figure 4.1, the spray drying technique led to the production of well-defined microspheres with spherical shape. The sizes observed in the SEM images were similar to those obtained by laser diffraction. The incorporation of the Pluronic surfactant permeabiliser in the powder had no effect on the morphology of microparticles.

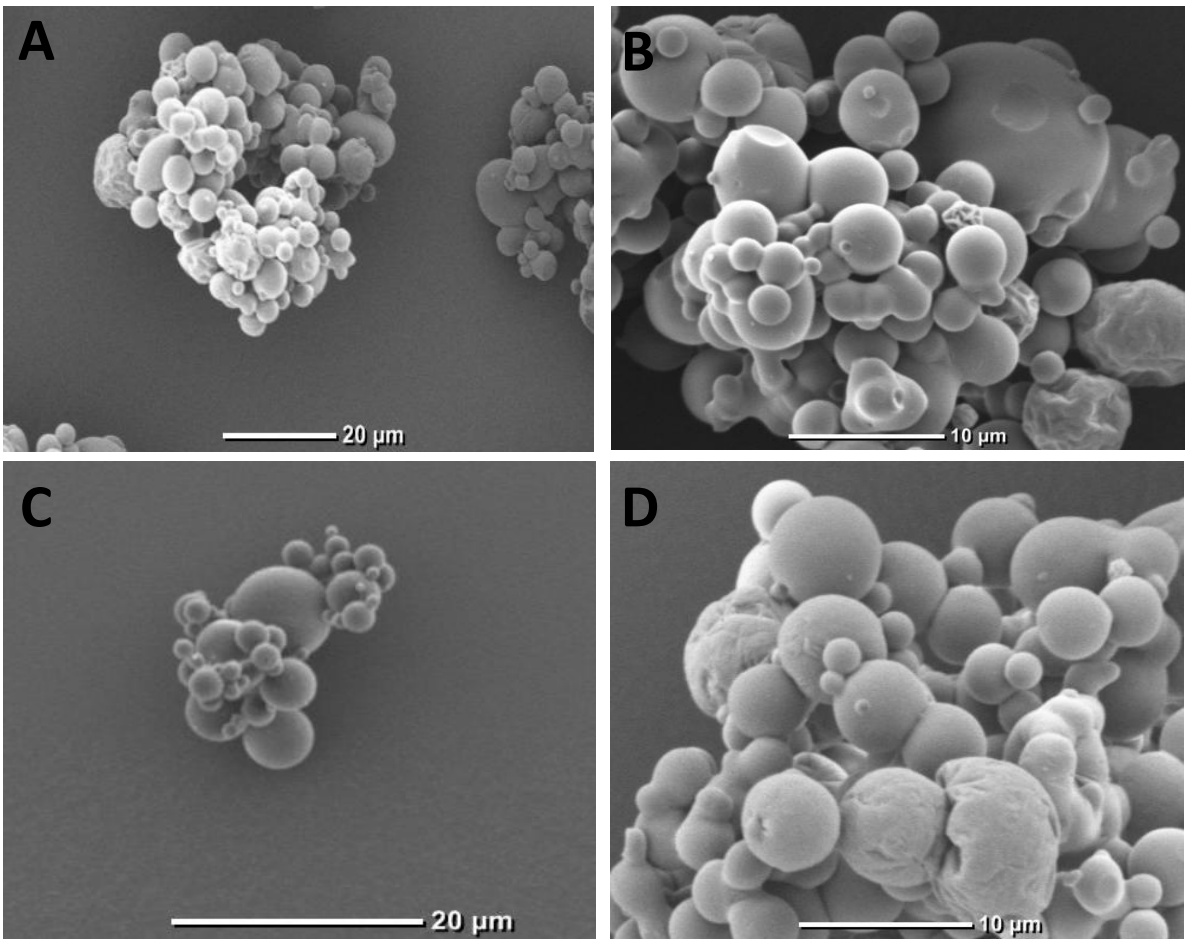

Figure 4.1: SEM microphotograph of representative microparticles prepared with (A) and (B) rifampicin-nanoparticles and (C) and (D) rifampicin-nanoparticles with permeabiliser.

4.4.3 Drug uniformity content and nanoparticles recovery from dry powders

The spray dried particles dissolved instantly when dispersed in aqueous solution. The mean particle size of the nanoparticles in the suspensions was found to increase by approximately 100% for both formulations without the addition of Pluronic (Table 4.3). Significantly swelled sizes were observed when Pluronic was included into the microparticles ($p<0.05$). The amount of rifampicin encapsulated in the microparticles was similar for the batches with and without Pluronic surfactant.

Table 4.3: Lipid shell nanoparticle size before spray drying and after microparticle dissolution in aqueous solution and rifampicin content in microparticles. Data represent mean ± standard deviation (n=3).

Formulation	Particle size before spray drying (nm)	Particle size after release (nm)	Amount of encapsulated rifampicin in 100 mg powder (μg)
B-LNP-MP	47 ± 1	95 ± 4	N/A
B-PLNP-MP	47 ± 1	198 ± 26	N/A
RIF-LNP-MP	49 ± 0	92 ± 5	135.7 ± 17.5
RIF-PLNP-MP	49 ± 0	202 ± 16	144.7 ± 10.8

4.4.4 Drug release

The incorporation of the Pluronic surfactant into the microparticles had a significant effect on the drug release from nanoparticles (Figure 4.2). The microparticle containing the Pluronic released almost 60% of its rifampicin load within 1 h, but after this time point the drug release was very gradual up to 8 h. To assess the stability of the microparticles, the release experiments were carried out at different time points post-manufacture (Figure 4.3). No signficant changes in release rates were found, from 0.0043 mg/h and 0.0244 mg/h for non-Pluronic permeabilised and Pluronic permeabilised groups initially to 0.0033 mg/h and 0.0213 mg/h respectively after 30 days when the nanoparticles were suspended in a microparticle ($p>0.05$). However, a significant difference was observed when the drug was stored as a simple nanosuspension in an aqueous vehicle over the same 30 day time period (Figure 4.3). More than 50% of rifampicin was lost from the nanoparticles upon storage in liquid ($p<0.05$). The release rates for non-permeabilised and permeabilised groups at day 1 were 0.1218 mg/h and 0.1688 mg/h respectively, which significantly reduced to 0.0716 mg/h and 0.0846 mg/h 30days after manufacture ($p<0.05$).

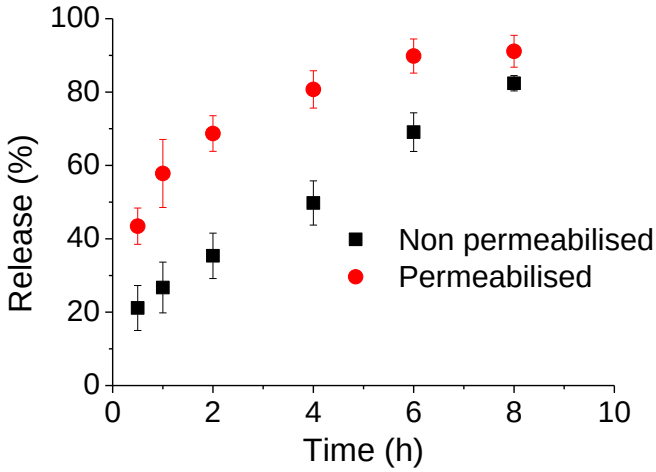

Figure 4.2: Rifampicin release from lipid shell nanoparticles included into microparticles with and without the permeabiliser. Data represent mean ± standard deviation (n=3).

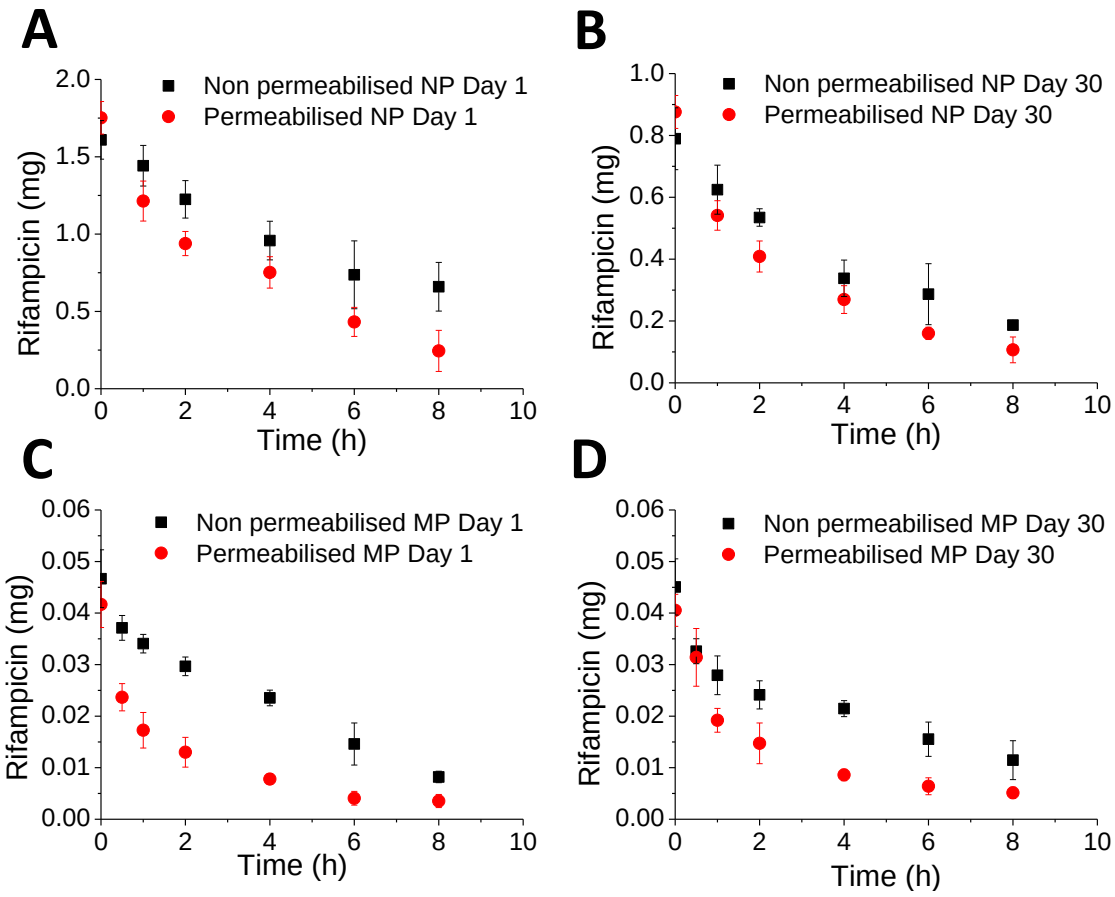

Figure 4.3: Rifampicin release from non-permeabilised and permeabilised lipid shell nanoparticles at day 1 (A) and day 30 (B). Graph (C) and (D) showed the release from microparticles over 30 days. Data represent mean ± standard deviation (n=3).

4.5 Discussion

It was previously demonstrated that rifampicin is prone to continuously diffuse out of lipid shell nanoparticles post manufacture when stored in an aqueous solution (Section 2.4.5). In this Chapter the incorporation of lipid shell nanoparticles in a dry powder formulation stabilised the nanoparticles, whilst still allowing the particle distension process to be triggered. Therefore, the data demonstrated that spray drying is a suitable method to load lipid shell nanoparticles into a lactose microparticle. A carbohydrate was selected for the microparticle matrix as it is approved by the Food and Drug Administration (FDA) for inhaled delivery and widely applied in aerosolised formulations (Ober et al., 2013). SEM micrographs revealed that lipid shell nanoparticles containing microparticles were spherical in shape and had a smooth surface. The aerodynamic diameter, which is a combination of the particle size and density, was not measured in this work because in previous work lactose microspheres have been shown to be easily aerosolised into the lungs when the particles are of a suitable size (Karavasili et al., 2016; Singh et al., 2015). The microspheres produced in this work had a diameter of 2 to 5 µm, which was considered to be suitable for delivery to the lower airways (Loira-Pastoriza et al., 2014). A similar sized microsphere has been previously engineered to deliver lipid nanoparticles using lactose (Freitas and Müller, 1998). However, the particles in the current work were different to the literature as they also contained the Pluronic surfactant in the microparticle matrix.

Drug content uniformity data showed that the encapsulation efficiency for both the distending lipid shell nanoparticles and non-distending lipid shell nanoparticles in the microparticles was high. However, the total drug loaded into the microparticles (~0.14% w/w) was still low compared to standard oral doses. A standard single adult oral dose is 600 mg (Donald et al., 2011). But there is some evidence that the inhaled dose would not need to match the oral dose. Directly exposing the alveolar macrophagesto the drug may improve its efficacy. In addition, the relative systemic bioavailability after inhaled nanoparticle-encapsulated microparticle delivery has previously been shown approximately 10-20 times higher than that of same dose of the orally dosed drug (Ahmad et al., 2006; Pandey et al., 2003; Sharma et al., 2004). There is also the possibility to improve the drug loading and or deposition efficiency in the lung using an advanced delivery device (Claus et al., 2014; Hoppentocht et al., 2014). This could be the subject of further work in this area.

In the current study, the ability of the obtained dry powder to deliver the lipid shell nanoparticles following incubation in PBS pH 7.4 was investigated. This pH was chosen in an attempt to perform the assay in a pH close to that of the airway surface liquid, which is approximately 7 (Walters, 2002). It was observed that after the microparticles incubation in aqueous medium under low stirring, the lactose dissolved, resulting in nanoparticle suspension which could be measured by light scattering. In spite of the slight enlargement of the nanoparticles after release from the microparticles they remain in the nano-range and thus retained the capacity to control drug release effectively. The swelling of particle size after spray drying was also found for powders prepared with lactose and gelatin nanoparticles in previous work, which attributed the changes the heat applied to the system during the spray drying process (Sham et al., 2004). When the permeabiliser was included in the microparticle it did not affect its stability, i.e., it did not induce drug release from the solid microparticle, but it still allowed the size distension process to occur according the particle sizing results. This suggested that it was possible to spray dry both drug and Pluronic permeabiliser simultaneously using the established method. From the results of this study it could be hypothesised that after reaching the lung, the lactose would dissolve in the lung lining fluid, releasing nanoparticles,which would release some drug, grow in size, as a result of the co dissolution of the Pluronic permeabiliser from the microparticle, release some drug prior to being engulfed by macrophages.

Considering the previous information on the release of lipid shell nanoparticles, it was expected that these would release rifampicin in a more controlled manner, in comparison to the nanoparticles, because of the extra barrier the drug has to overcome before release (Hasan et al., 2015). The introduction of the permeabiliser to the formulation successfully enhanced the release of the drug from the nanoparticles. There is a significant difference between the release profiles of permeabilised and non-permeabilised formulations. The pattern correlated well with the data obtained when the nanoparticles were presented as suspensions (see Section 2.4.5). There are some strategies that could be employed to try and improve the affinity between the nanoparticles and the loaded drug, including, changing the nanoparticle oil, adding a co-solvent or manipulating the properties of the drug through ion-pairing, these strategies could be employed in future work to try and optimise the system that has been developed in this work.

4.6 Conclusion

The data presented in this Chapter has demonstrated the feasibility of incorporating lipid shell nanoparticles into respirable micronized carrier particles. The spray dried powders had a suitable size and shape for airway deposition. After depositing and reaching lung surface, according to the *in vitro* data generated in this Chapter the carrier is expected to dissolve instantly in the surface lining fluid and release the nanoparticles. The microparticles seemed to stabilize nanoparticles removing the capability of the loaded drug to passively release upon storage. The results suggested that rifampicin could be formulated into nanoparticle-based inhalable sustained drug delivery system for better management of pulmonary tuberculosis, but to support this suggestion is important to understand the interaction of lipid shell nanoparticles with lung and this would be the focus of the next Chapter.

CHAPTER FIVE

Cellular bio-distribution of lipid shell nanoparticles in *in vitro* models of the airways of the lungs

5.1 Introduction

The fate of nanomedicines following inhalation is a major determinant of both their safety and efficacy (Nel et al., 2006). The administration of lipid shell nanoparticles to the airways of the lungs could potentially lead to the particles being distributed to a number of different biological compartments. The process of biodistribution of inhaled nanoparticles is heavily dependent on both mucociliary clearance and macrophageuptake. Mucociliary clearance is the predominant clearance mechanism for particulate matter in the tracheobronchial region and results in the upward movement of particles towards the larynx where they are eventually removed to the gastrointestinal tract (Lansley, 1993). Clearance of inhaled particulates by macrophages dominates in the alveolar regions but macrophage uptake also occurs in the ciliated airways (Zhang et al., 2011). Once internalised particles may undergo degradation within lysosomes or be transported by the macrophage to the lymphatic system or the mucociliary escalator (Oh and Swanson, 1996).

The nanoparticle fate following administration is critical to the delivery of its encapsulated therapeutic agent. The drug will be released following administration so it can reach its site of action but the release occurs optimally when it is proximal to its site of action whether this be at the epithelial surface for locally acting antibiotics or mucolytics (Ungaro et al., 2012), the underlying smooth muscle for beta agonists (Barnes, 2002) or the systemic circulation for proteins such as insulin (Yang et al., 2013). In order to achieve targeted delivery it is important to track the nanoparticle and the drug within the lung tissue.

The fate of the deposited nanoparticles is known to depend to a large extent on the physiochemical characteristics of the particles and the nature of their interaction with the surfactant film at the air-liquid interface. Previous work has shown particle hydrophobicity (Hu et al., 2007), particle size and surface charge (He et al., 2010) can all influence bio-distribution. Lipid shell nanoparticles have been shown to have surface properties that allow their preferential localisation in the lung rather than clearance into the gastrointestinal tract (Patel et al., 2016). However, there have not been any studies to date to investigate the cellular bio-distribution of the lipid shell nanoparticle system.

Lipid shell nanoparticles can be internalised by epithelial cells and translocated through the epithelial barrier. Non-phagocytic eukaryotic cells have also been shown to endocytose nanoparticles that do not possess specific targeting ligands via clathrin-coated pits and

caveolae in a size-dependent manner (Rejman et al., 2004). Therefore, even though there are almost 40 different cell types in the lung, it is reasonable to consider the epithelial cells and the macrophages to be two very important compartments into which molecules can distribute post-deposition.

Given the complex interaction of nanoparticles with the airway epithelium and the number of competing pathways that can occur *in vivo*, it is difficult to find a system capable of modelling all the processes in a manner that their effects on the nanoparticles fate can be elucidated. *In vitro* cell culture models offer simplicity and a high level of experimental control and they can therefore be powerful initial tools to assess selected nanoparticle-cell interactions. Nanoparticle internalization can be studied using monocultures, but the possibility of spatial interaction between cell types may change the observed effects. Therefore, co-cultures are preferred as they are thought to result in a more realistic evaluation of the potential fate of nanoparticles. As the pulmonary system is highly heterogeneous it is accepted that even a state-of-the-art co-culture system is still far from completely mimicking an *in vitro* tissue, but compared to monocultures, co-culture systems allow cell-to-cell communications to be factored into the particle distribution process (Klein et al., 2013). Two-dimensional (2D) culture systems have been used for *in vitro* studies though cell–cell and cell–matrix interaction are largely lost under these simplified conditions and therefore three-dimensional (3D) *in vitro* culture has emerged as a favoured approach to mimic the *in vivo* airway environment (Choe et al., 2006). 3D models have been shown to induce cells to behave in a manner that was a step closer to the natural conditions (Ravi et al., 2014). Compared to 2D model, cells grown in a 3D model have proven to be more physiologically relevant and showed improvements in several studies of biological mechanisms like: cell viability, morphology, proliferation, differentiation, response to stimuli, gene expression and general cell function (Zhang et al., 2016).

It was previously demonstrated that rifampicin released efficiently from lipid shell nanoparticles by Pluronic permeabilisation (Chapter 2) and the lipid nanoparticles can penetrate through mucus rapidly (Chapter 3). The aim of the work in this Chapter was to investigate the cellular bio-distribution of permeabilised lipid shell nanoparticles upon administration to the lung airways *in vitro*. A three-dimensional (3D) *in vitro* culture system was developed using the Calu-3 cell line, routinely used as an *in vitro* model of pulmonary human epithelium cell line (Forbes and Ehrhardt, 2005) and the human macrophage cell line

U937, which is widely used as model system for monocytes and macrophages. The system was setup using data from previous co-culture epithelial macrophage cell models which have been used to study bacterial infections (Bodet et al., 2006) and microparticle uptake (Rothen-Rutishauser et al., 2005). The co-culture uptake was compared to similar experiments in mono-cultures in order to understand the effects of the co-culture system. The uptake of lipid shell nanoparticles by single cells was studied in these mono-culture systems by fluorescence. The co-cultures were characterized prior to use and the distribution of lipid shell nanoparticles in this system was investigated with confocal laser scanning microscopy (CLSM) and flow cytometry in the presence and absence of the nanoparticle permeabilisation process.

5.2 Materials

Calu-3 human bronchial cells and U937 human macrophage cells were obtained from ATCC (Rockville, USA) and reagents for cell culture and the MTT cell viability assay were purchased from Sigma-Aldrich (Dorset, UK). These included Dulbecco's Modified Eagle's Medium/Nutrient F-12 Ham's 50/50, fetal bovine serum (FBS), L-glutamine, non-essential amino acids, gentamicin, trypsin-EDTA (0.25% trypsin, 0.05% EDTA), penicillin/streptomycin, RPMI medium, phorbol-12-myristate-13-acetate (PMA), MTT (3-4,5-dimethylthiazol-2-yl-2,5- diphenyltetrazolium), Hanks' Balanced Salt Solution (HBSS), trypan blue, dimethylformamide (DMF) and Triton X. Phosphate buffered saline (PBS) was prepared from PBS tablets (Oxoid, Hampshire, UK) using ultrapure water. Sodium dodecyl sulphate (SDS) solution (20% w/v) was purchased from Fisher Scientific (Leicestershire, UK). Rabbit anti-human CD11b (EPR1344) and rabbit IgG FITC isotype control (EPR25A) were from Abcam (Cambridge, UK). Goat anti-rabbit dylight 488 (ab96883) and Hoechst 33324 were from Thermo Fisher Scientific (Leicestershire, UK). Mouse IgG 1 k PE isotype control (P3.6.2.8.1) and CD326 antibodies (G8.8) were from eBioscience (Altrincham, UK). Materials for nanoparticle fabrication refer to Section 2.2.

5.3 Methods

5.3.1 Lipid shell nanoparticle fabrication, characterization and loading

Lipid shell nanoparticles were manufactured and characterized as previously described in Section 2.3.1. Rifampicin or nile red was loaded into nanoparticles and an Amicon centrifugal device was used to determine the loading efficiency referred to Section 2.3.8.

5.3.2 Calu-3 cell culture

The Calu-3 human bronchial epithelial cell line was used between passages 30-45 and cultures were maintained in a humidified 5% CO_2/ 95% atmospheric air incubator at 37℃. Cell culture medium comprised 50:50 Dulbecco's Modified Eagle's Medium/Nutrient F-12 Ham's (500 mL) supplemented with 10% FBS, 1% L-glutamine (200 mM) and 0.1% gentamicin. Medium was exchanged every 2-3 days and cells were passaged weekly at a 1:3 split ratio using trypsin-EDTA solution. Cell culture was carried out in a Class II safety cabinet.

Cells cultured on Transwell cell supports (0.33 cm^2, 3 μm pore size, Corning, UK) using air-interfaced conditions were seeded at a density of 1.65×10^6 cells/mL and were introduced into the apical surface of the Transwell cell culture support in 0.1 mL medium with 0.5 mL medium added to the basolateral chamber. The cells were incubated at 37 ℃, 5% CO_2 for 2 days. After this time, medium was replaced in the basolateral chamber and subsequently every 2 days.

5.3.3 Transepithelial electrical resistance (TER) measurements

Transepithelial electrical resistance (TER) measurements were made to check the cell line confluence on the Transwell inserts by using chopstick electrodes and an EVOM voltohmmeter (STX-2 and EvomG, World Precision Instruments, Stevenage, UK) on cells immediately upon removal from the incubator. Warmed medium (0.1 mL, 37 ℃) was added to the apical chamber before returning them to the incubator to equilibrate for a further 30 min, and then measuring the electrical resistance. TER was calculated by subtracting the resistance of a cell-free culture insert and correcting for the surface area of the Transwell cell culture support.

5.3.4 Permeability of Calu-3 cell layers

To prepare the cell layers on the day of transport studies, TER was taken and the medium on the apical and basolateral chambers was aspirated and the cell layers washed twice with warm HBSS (37 ℃). HBSS (0.1 mL pH 7.4) was introduced to the apical chamber and (0.5 mL) to the basolateral chamber. The cells were returned to the incubator at 37 ℃ for 1-2 h to equilibrate. The TER was measured after this equilibration period and immediately prior to experimentation.

For the drug transport studies rifampicin was dissolved in warm HBSS to produce a 0.75 mg/mL solution. Rifampicin loaded lipid shell nanoparticles were diluted in warm HBSS to obtain a suspension with the same concentration as the rifampicin solution. Rifampicin was chemically unstable and it degraded at a rate of 20 μg/h. During the time course of these experiments (8 hrs) the estimated loss due to chemical degradation when the drug was not encapsulated in the LNC was 0.3 %, this amount of degradation was not considered to have a significant effect on the study results. The HBSS in the apical chamber of each well was aspirated, and the experiment was initiated by introducing the test solution (200 μL). A

sample of this solution (100 µL) was then immediately removed for determination of the initial starting concentration. Basolateral sampling (100 µL) was carried out for 8 h, with samples being replaced with fresh warmed HBSS (37 ℃, 100 µL). At the final time point, a 100 µL sample was also removed from the apical chamber. TER was measured after the final sample was taken. All samples were transferred to HPLC vials and subject to HPLC assay Apparent permeability coefficients (P_{app}) were calculated by Equation 5.1, where F is flux (rate of change in cumulative mass transported), A is surface area of cell culture support, and C_0 is the initial concentration in donor chamber.

$$P\text{app} = \text{F}\left(\frac{1}{\text{AC0}}\right) \quad \text{Equation 5.1}$$

To assess the transport of the lipid shell nanoparticles, nile red loaded nanoparticles were used. Previously nile red had been shown not to be released from lipid shell nanoparticles both with and without the addition of the lipid shell permeabiliser (Chana et al., 2015). The transport of the nanoparticles through cell-free Transwell culture supports was investigated prior to them being evaluated in the epithelial cell lines. Particle suspensions (1 mg/mL in HBSS pH 7.4, 100 µL) were administered to the apical compartment (t_0) in triplicate, with 0.5 mL HBSS in the basolateral chamber, in a humidified incubator at 37 ℃. After 8 h the apical and basolateral chamber contents were removed for assay. Ethanol (200 µL) was added to the insert to recover any residual lipid shell nanoparticles and those trapped in the pores of the semi-permeable membrane of the Transwell culture support. Samples from the apical and basolateral chambers were diluted with ethanol to dissolve the lipid shell nanoparticles and they were assayed. To track the nile red loaded lipid shell nanoparticles after application to confluent Calu-3 cell layers a similar methodology was used. Cell culture medium in the basolateral chamber was first removed via aspiration and replaced with fresh medium (0.5 mL) pre-warmed to 37 ℃. The particle suspensions (1 mg/mL in HBSS pH 7.4, 100 µL) pre-warmed to 37 ℃ were administered to the apical compartment (t_0) of the Transwell chambers and the cell layers were then returned to the incubator. After 1 h the apical chamber contents were homogenised using a pipette taking care not to touch the cell layer, and the liquid was removed for assay. Fresh HBSS (100 µL) was added to wash the cell layer and recover any remaining nile red in the apical compartment. Basolateral chamber contents were aspirated and the cell layer was solubilised by applying 10% SDS (200 µL) and incubating overnight at 37 ℃. The process was repeated with replicate cell layers, with analysis at 8 time points up to

8 h exposure. To test the permeabilised nanoparticles the lipid shell nanoparticles were mixed with Pluronic L62D at the ratio of 1:0.5 w/w prior to application to the cells.

All samples from the nanoparticle transport studies were processed by mixing with an appropriate volume of ethanol to dissolve the nanoparticles and 200 μL aliquots were carefully transferred to black 96-well plates with clear flat bases suitable for fluorescence spectroscopy (Corning, through Sigma Aldrich, Gillingham, UK). Plates were read using an Infinite 200 Pro microplate reader (Tecan, Mannedorf, Switzerland) using excitation and emission wavelengths of 559 and 629 nm, respectively. The assay methodology was shown to be fit for purpose in terms of precision and limit of detection in previous work (Chana et al., 2015).

5.3.5 Macrophage U937 cell culture

The macrophage U937 cell line was used up to passage 24. The cells were grown in 162 cm^2 cell culture flasks using cell culture medium (RPMI supplemented with 10% v/v FBS, 1% v/v L- glutamine and 1% penicillin/streptomycin) within a humidified environment supplied with 5% CO_2 at 37 ℃. The cell culture medium was changed twice a week. Cells were subcultured when 90-100% confluency was reached at a split ration of 1:5. Differentiation of the U937 cells were achieved by incubating them in 8 nM PMA for 48 h in a 96-well plate, then adding fresh PMA medium and for culturing another 48 h, then finally adding fresh medium and culturing for 24 h to finish the differentiation.

5.3.6 Metabolic activity test (MTT)

Biocompatibility with the Calu-3 cell line had already been established in previous work (Chana et al., 2015). Therefore, only the U937 cell viability following exposure to the nanoparticles and surfactant used to permeabilise the particles was assessed using the MTT assay according to the methods of Grenhaet al.(Grenha et al., 2007). The U937 cells were seeded at a series of densities in 96-well plates and cultured for 24 h in cell culture medium (100 μL) to evaluate the optimum seeding density for the experiments. All test samples were prepared in pre-warmed cell culture medium prior to administration to the cells. Cells were either exposed to the test condition or control solutions (cell culture medium was the negative control, 1% Triton X-100 solution was the positive control) for 1 or 8 h. After this time all medium was removed from the wells, it was replaced with fresh cell culture medium (200

μL), the MTT solution was added (5 mg/mL in PBS pH 7.4, 50 μL) and the plates were placed in an incubator at 37 ℃. After 4 h the fluid was removed from all the wells and replaced with SDS solution (10% w/v in 50:50 DMF: water, 100 μL) to solubilise any formazan crystals generated. Absorbance from each well was measured 16 h later using a UV spectrophotometer (SpectraMax 190, Molecular Devices, USA) at 570 nm, and corrected for background absorbance at 650 nm. For each test well the absorbance of the corresponding cell free well was subtracted and the residual absorbance was used to determine the relative cell viability (%) by comparing to the negative and positive controls, as follows Equation 5.2:

$$\text{Viability (\%)} = \frac{\text{Abstest} - \text{Abspositive}}{\text{Absnegative} - \text{Abspositive}} \quad \text{Equation 5.2}$$

Where Abs_{test} is the absorbance corresponding to treated cell, $Abs_{positive}$ is the absorbance obtained for the positive control (Triton X-100 treated cells), $Abs_{negative}$ is the absorbance for the negative control (untreated cells).

5.3.7 Macrophage U937 cell uptake

Cells were differentiated in 96-well plates as described above at the density of 3.3×10^5 cells/mL. On day 6, the cell culture medium was removed and replenished with 100 μL fresh cell culture medium containing nile red loaded nanoparticles (1 mg/mL in HBSS pH 7.4) and nanoparticles mixed the permeabiliser Pluronic L62D with a ratio of 1:0.5 w/w. Negative controls comprised of cells treated with 100 μL fresh cell culture medium. Plates were incubated for different times over 8 h, after which the medium was removed, cells were washed three times with 1 mL PBS (37 ℃) per well to remove excess particles which were not strongly associated to the cells and the cell layer was solubilised by applying 10% SDS (200 μL) and leaving overnight in an incubator. The number of nanoparticles associated with the cell monolayer was calculated by quantifying the encapsulated nile red.

5.3.8 Co-culture model development

Calu-3 cells cultured on Transwell cell culture supports were seeded at a density of 1.65×10^6 cells/mL and were introduced into the apical surface of the Transwell cell culture support. Experiments were conducted between days 9 to 13. U937 cells were differentiated in the flask as previously described and added on the apical surface of the epithelial monolayer with a seeding density of 3.3×10^5 cells/mL based on the evaluation of their *in vivo* distributions (Stone et al., 1992). Cells were allowed to attach for 4 h. Upon attachment the medium was

removed from the upper compartment and the co-culture was cultivated for 24 h prior to exposure.

Transepithelial electrical resistance (TER) was measured with the Millicell-ERS system (MERS 000 01; Millipore AG, Volketswil, Switzerland) as previously described. In addition, the barrier of the epithelial cells in the presence of the U937 cells was determined using a solution of sodium fluorescein (10 μg/mL in HBSS pH 7.4) which added into the apical compartment of the Transwell holding the co-culture system. The cultures were then incubated for 240 min at 37 ℃. Empty inserts without cells served as a control. Basolateral sampling was carried out for 4 h, with samples being replaces with fresh warmed HBSS. All samples were transferred to a black 96-well plate. Fluorescence was measured via excitation and emission wavelengths of 495 and 520 nm by using a fluorometer (Cytoflour, Series 40000, Foster City, CA, USA) and the permeability was calculated using equation 5.1.

To verify the localisation of the cells in the 3D culture the cells were washed twice in PBS and fixed for 15 min at room temperature in 4% formaldehyde in PBS solution. Fixed cells were incubated for 30 min with 10% bovine serum albumin (BSA) in PBS to block unspecific binding. After blocking, rabbit anti-human CD11b and goat anti-rabbit daylight 488 (green) were diluted in PBS pH 7.4 (1:1000 v/v) and applied to the system to identify the differentiated macrophages cells (Klein et al., 2013). The cell nuclei were stained with Hoechst 33324 (blue) and the fluroscence images were taken with a Zeiss LSM 510 with an inverted Zeiss microscope (Zeiss, Germany).

5.3.9 Bio-distribution of lipid shell nanoparticles in co-culture model

Two methods were used to analyse the bio-distribution of lipid shell nanoparticles in the co-culture. First, the co-culture model was incubated for 1 h with 50 nm lipid shell nanoparticles suspended in HBSS medium. Then the cells were fixed and stained with Hoechst 33324 and anti-CD11b-antibody and analysed via CLSM imaging as described above. As with only imaging it has previously proven difficult quantify the particle uptake in cells, cell flow cytometry was used to quantify the cell uptake of the lipid shell nanoparticles in the co-culture. To facilitate the flow cytometry measurements after the cells had been exposed to the nanoparticle suspensions for 1 and 4 hour the apical solutions were removed and epithelial and macrophage cells were incubated with a 1:100 dilution of human CD326 and human CD11b antibodies, respectively. Two cell types were distinguished by specifically binding to

fluorescence labelled antibody. For the isotypic control rabbit IgG FITC and mouse IgG 1 k PE were used. After 1 h incubation at 37 ℃, samples were centrifuged to remove excess dye and subjected to flow cytometry (Epics XL; Beckman Coulter). Basically an unstained sample and appropriate isotype controls were included in each analysis to address autofluorescence and non-specific binding. Raw data were analysed using CXP software (Beckman Coulter). Internalization % was used to indicate the amount of cells associated with the nanoparticles.

5.3.10 Statistical analysis

SPSS version 20 (IBM, UK) was used for all statistical analyses. The normality (Sapiro-Wilk) and homogeneity of variances (Levene's test) of the data were assessed prior to statistical analysis. The data were analysed statistically using T-test or Mann-Whitney test. Differences were considered to be statistically significant at a level of $P < 0.05$.

5.4 Results

5.4.1 Nanoparticle characterization

The fabricated lipid shell nanoparticles had a mean diameter of ca. 50 nm with neutral surface charge (Table 5.1). Rifampicin was loaded into the lipid shell nanoparticles with a loading efficiency of 41.0 ± 11.4%.

Table 5.1: Size, polydispersity, zeta potential and solid content for unloaded and rifampicin-loaded lipid shell nanoparticles (LNP). Data represent mean ± standard deviation (n = 3).

NP type	Mean size (nm)	Polydispersity index	Zeta potential (mV)	Solid content (mg/mL)
LNP_{blank}	52 ± 2	0.07 ± 0.02	-3.46 ± 0.60	146.7 ± 12.2
$LNP_{rifampicin}$	50 ± 3	0.07 ± 0.02	-2.07 ± 0.62	163.3 ± 7.0

5.4.2 Calu-3 cell culture

By day 4, Calu-3 monoculture cell layers grown using air- interfaced conditions on Transwell inserts were confluent (Figure 5.1). They produced an effective barrier to the hydrostatically driven passage of the cell culture medium from the basolateral to apical well. The TER of cell layers increased above baseline values after 2-3 days in culture and reached a plateau of approximately 300 Ω cm^2 at around day 5 post-seeding which is in agree with previous study (Grainger et al., 2006). The maximum TER values occurred between days 11 and 13 and this was therefore selected as the timeframe in which to conduct the transport studies.

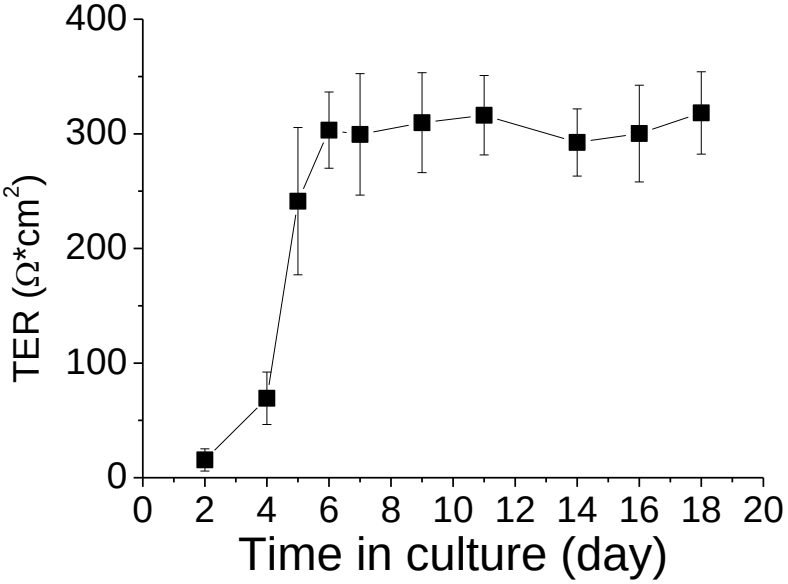

Figure 5.1: Transepithelial electrical resistance of Calu-3 cells cultured on 0.33 cm^2 cell culture supports as a function of time from three separate experiments. Data represent mean ± standard deviation (n=18).

5.4.3 Rifampicin transport across the Calu-3 cell lines

The rifampicin permeability, irrespective of the type of administration system, was similar for the first 7 hours of the transport study (Figure 5.2). The time points between 2 h to 8 h were used to calculate the permeability as the initial time period looked like lag time. After the 8 hour time point the permeation of rifampicin through the cells when administered as a solution appeared to deplete, but the nanoparticles provided a reservoir that prolonged the drug release ($p<0.05$). There was no significant difference between the drug release from the permeabilised and non-permeabilised nanoparticles throughout the experiment ($p>0.05$).

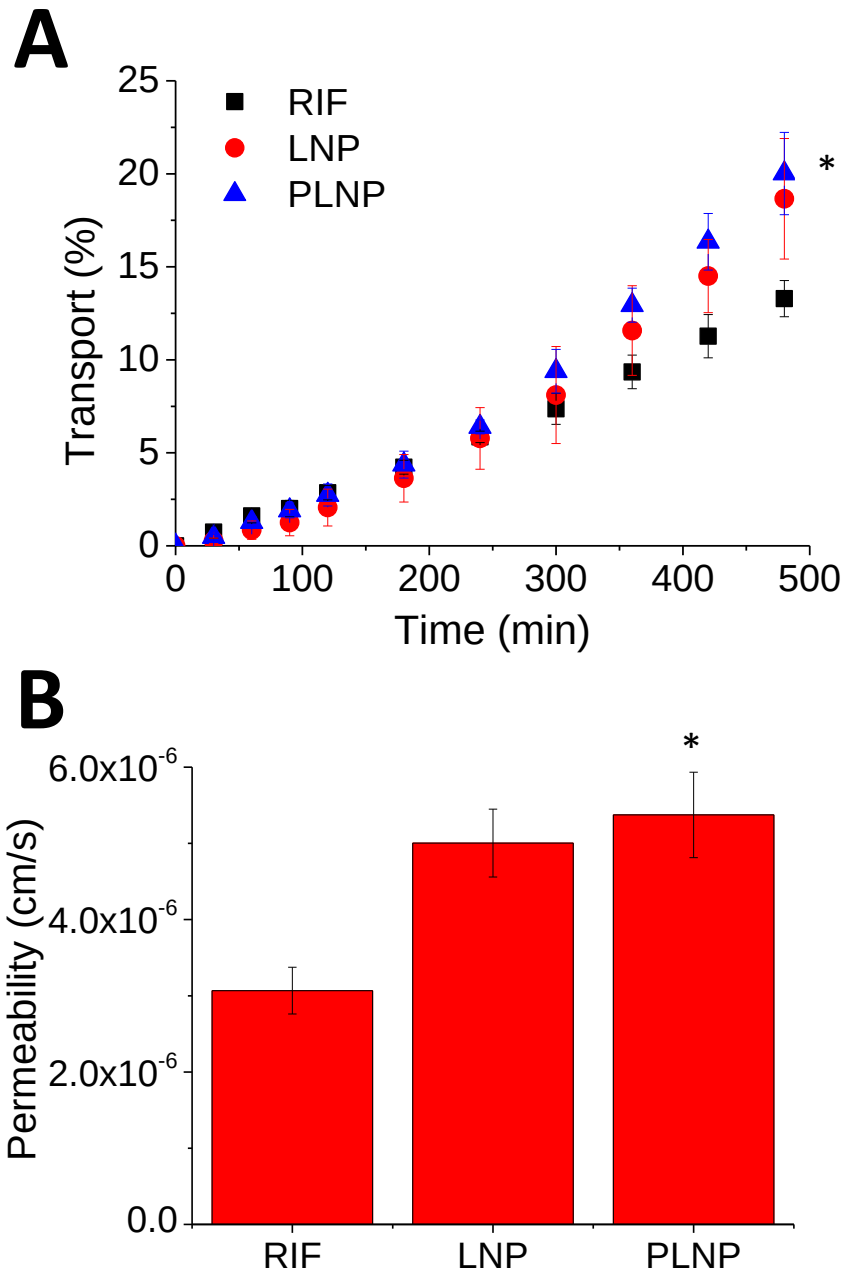

Figure 5.2: (A) Transport profiles and (B) permeability of rifampicin (RIF), non-permeabilised lipid shell nanoparticles (LNP) and rifampicin-loaded permeabilised lipid shell nanoparticles (PLNP) and across Calu-3 cell layers in mono-culture. Data represent mean ± standard deviation (n=12).

5.4.4 Lipid shell nanoparticle transport across Calu-3 cell lines

Following the application of nile red loaded lipid shell nanoparticles to cell-free Transwell culture supports for 8 h at 37 ℃, no penetration to the basolateral chamber was detected. After this period 82.3 ± 7.6% of the applied nile red was recovered from the apical compartment and 0.5 ± 0.4% was extracted from the culture support using ethanol. This is in line with previous reports of negligible nanoparticle penetration through Transwell using similar sized fluorescent polystyrene nanoparticles (Geys et al., 2006). On this basis the basolateral chamber was not sampled in the subsequent particle localisation experiments conducted with epithelial cell layers and a 90% recovery was set as an acceptable standard by which to gauge the subsequent experiments with the cells. When the transport of the nile red-loaded lipid nanoparticle suspensions was assessed over 8 h at 37 ℃ less than 10% of the applied particles moved into the cells (Figure 5.3). There was a significant increase ($p<0.05$) in cell associated nile red from 1% at 1 h to 3% at 8 h when the nanoparticles were added to the cell without the permeabiliser. Adding the Pluronic to the nanoparticles at the airway epithelial interface resulted in a significantly higher percentage of cell associated nile red being observed compared toan equivalent dose of controlled nanoparticles at all time points ($p<0.05$).

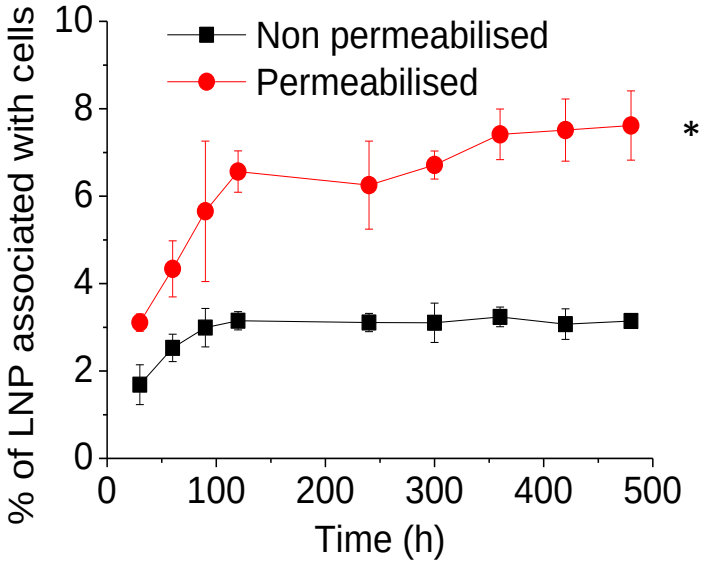

Figure 5.3: Amount of permeabilised and non-permeabilised lipid shell nanoparticles associated with Calu-3 cell layers over 8 h. Data represent the mean of three experiments. Data represent mean ± standard deviation (n=12).

5.4.5 Macrophage U937 cell viability

The macrophage U937 cell uptake experiments could not be conducted in Transwell plate in order to make it comparable to the uptake by Calu-3 cell because whilst the macrophage cells reside on the apical surface of the Transwell support membrane they do not form tight junctions and hence if a drug solution was applied to the U937 cells on the surface of the Transwell support the drug would rapidly pass through the membrane and only co-reside with the cells for a very short period of time. This does not represent *in vivo* conditions. As a consequence a 96-well plate was used to assess the lipid shell nanoparticle uptake in the U937 cell line. The cell concentration within the range at which MTT conversion was proportional to the number of viable cells was used to establish the optimum seeding density (3.3×10^5 cells/mL) for the experiments (Figure 5.4). The cells were found to be viable after exposure to lipid nanoparticles or permeabilised nanoparticles (Figure 5.5).

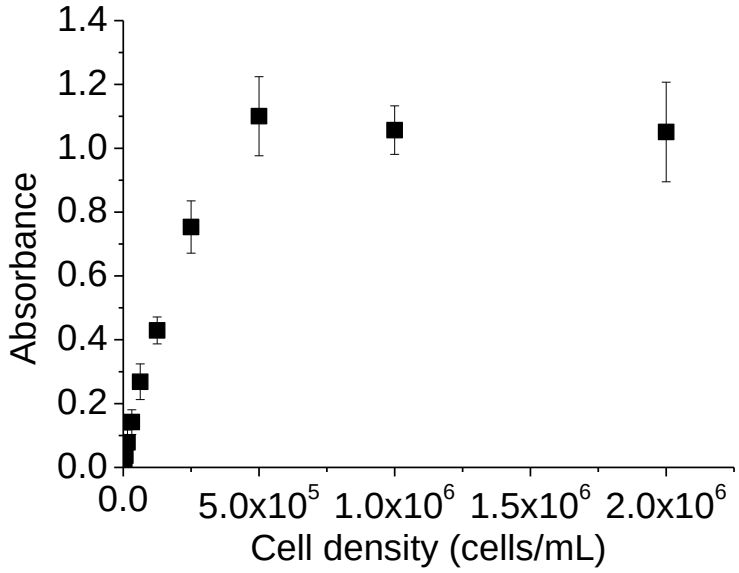

Figure 5.4: U937 seeding density in 96-well plate against absorbance using MTT assay. Data represent mean ± standard deviation (n=6).

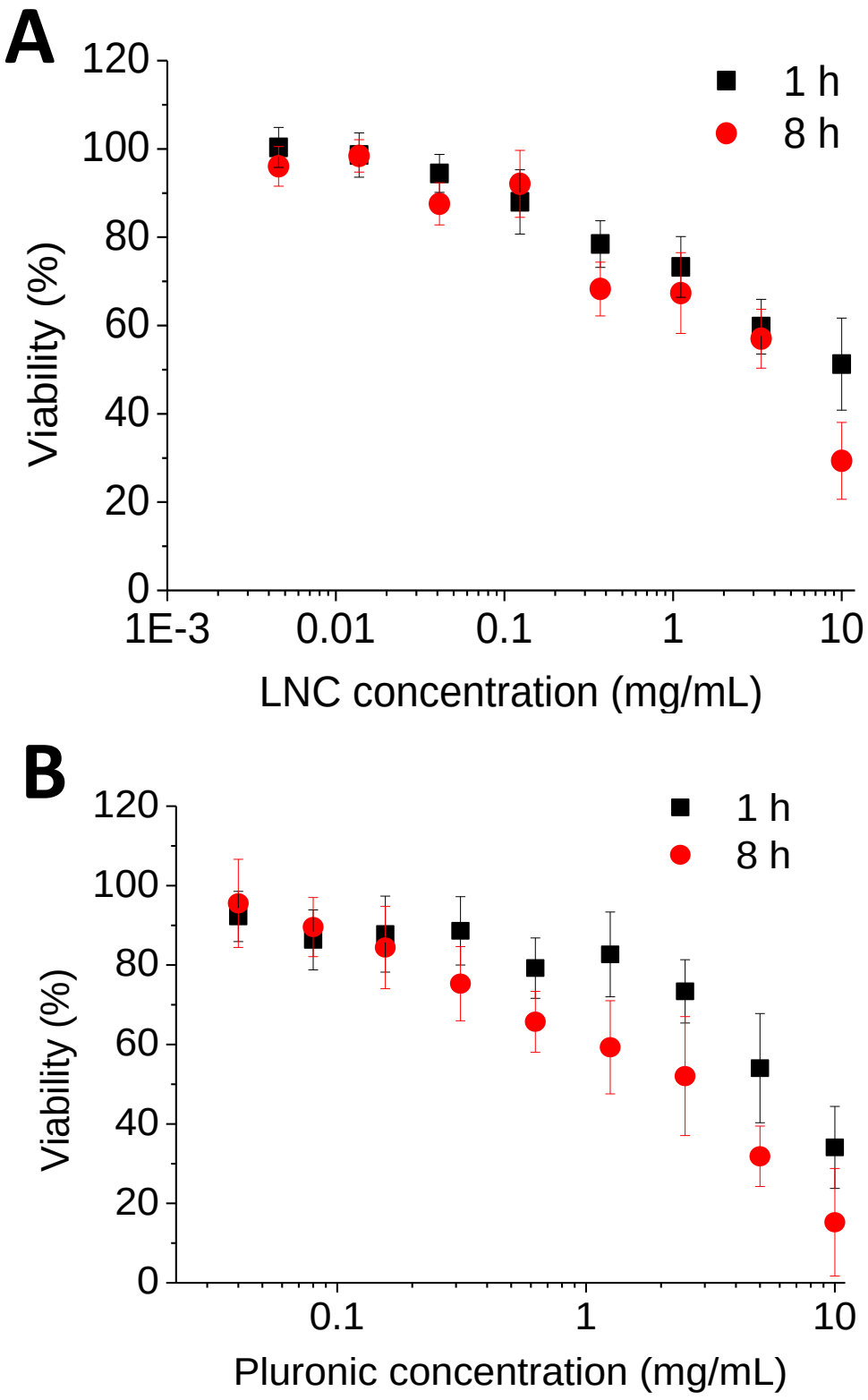

Figure 5.5 A: Relationship between applied lipid shell nanoparticles concentration and U937 cell viability (%) after 8 h exposure. B: Relationship between applied Pluronic L62D surfactant concentration and U937 cell viability (%) as in the presence of a fixed concentration of nanoparticles (1 mg/mL). Data represent mean ± standard deviation (n=6).

5.4.6 Lipid shell nanoparticle uptake by macrophage U937 cells

Association of lipid shell nanoparticleswith cells was found within 1 h, which was followed by a gradual increase during subsequent time points (Figure 5.6). There was a small but significantly different uptake of the non-permeabilised and permeabilised nanoparticles over 60 to 90 min time frame ($p<0.05$). The highest uptake of the permeabilised systems appeared to be within 2 h, which could have been related to the size growth. After the 2 h time point the system seemed to reach the equilibrium.

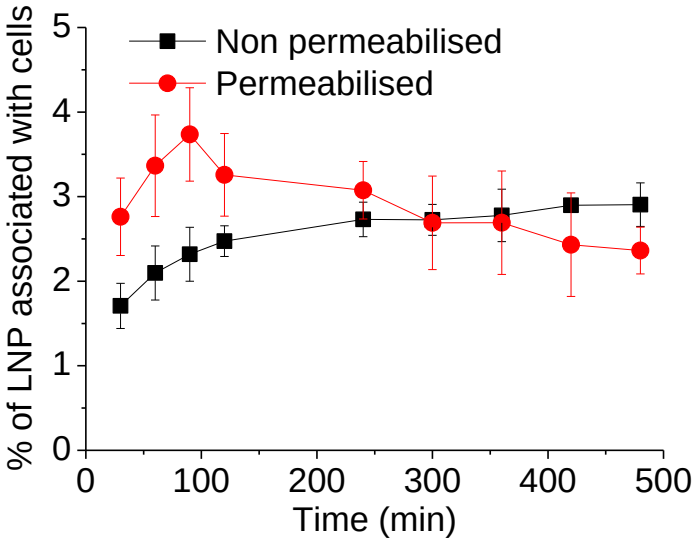

Figure 5.6: Amount of permeabilised and non-permeabilised lipid nanoparticles associated with U937 cell layers over 8 h. Data represent the mean of three experiments. Data represent mean ± standard deviation (n=12).

5.4.7 Co-culture development and characterization

At day 11, the cell layer TER of the Calu-3 cells reached a plateau of around 300 Ω cm^2. There was no difference between the TER of the Calu-3 monoculture and co-cultured systems (Figure 5.7). The penetration of Flu-Na through the bilayer showed no statistically significant differences between monolayer and co-culture systems (Figure 5.8). The epithelial cell nuclei, stained with blue Hoechst 33324 and the macrophage-like cells, which were counterstained with a green anti-CD11b-antibody, were both clearly visible in the images of the co-culture (Figure 5.9). Cross-section views of the image demonstrated that Calu-3 cells seeded on the bottom side of the insert covered the membrane and a small proportion of U937 cells were attached to the surface of epithelial cells (Figure 5.10).

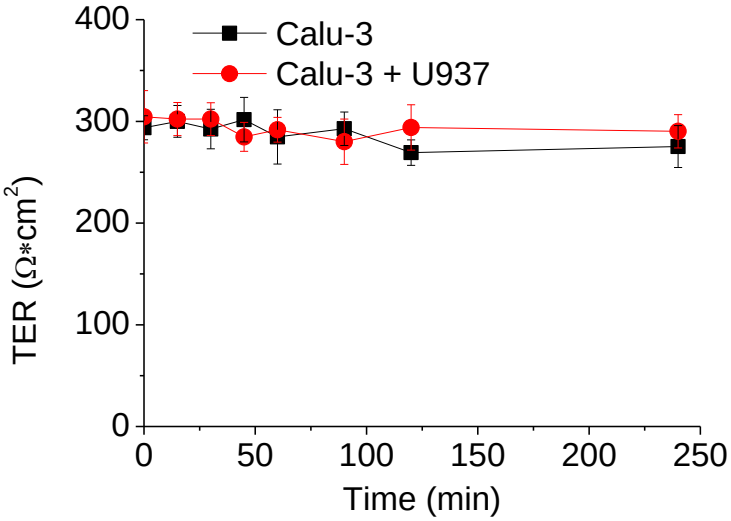

Figure 5.7: TER of monolayer and co-culture during experiments. Data represent the mean of three experiments. Data represent mean ± standard deviation (n=4).

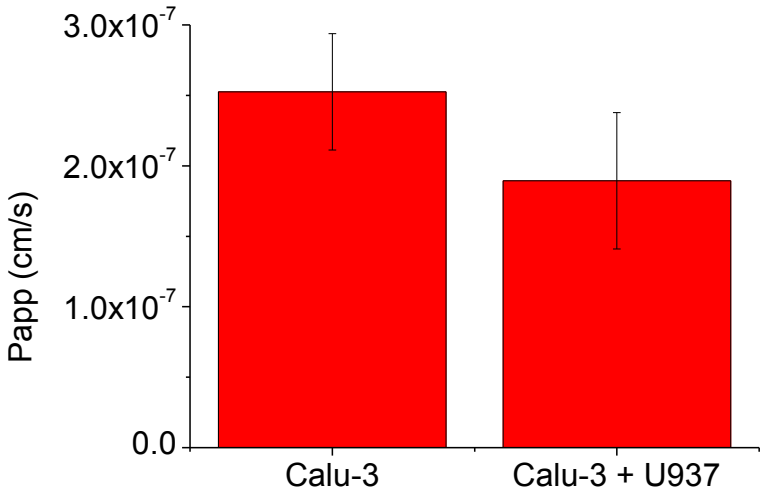

Figure 5.8: Permeability of sodium fluorescein through monolayer and co-culture. Data represent the mean of three experiments. Data represent mean ± standard deviation (n=4).

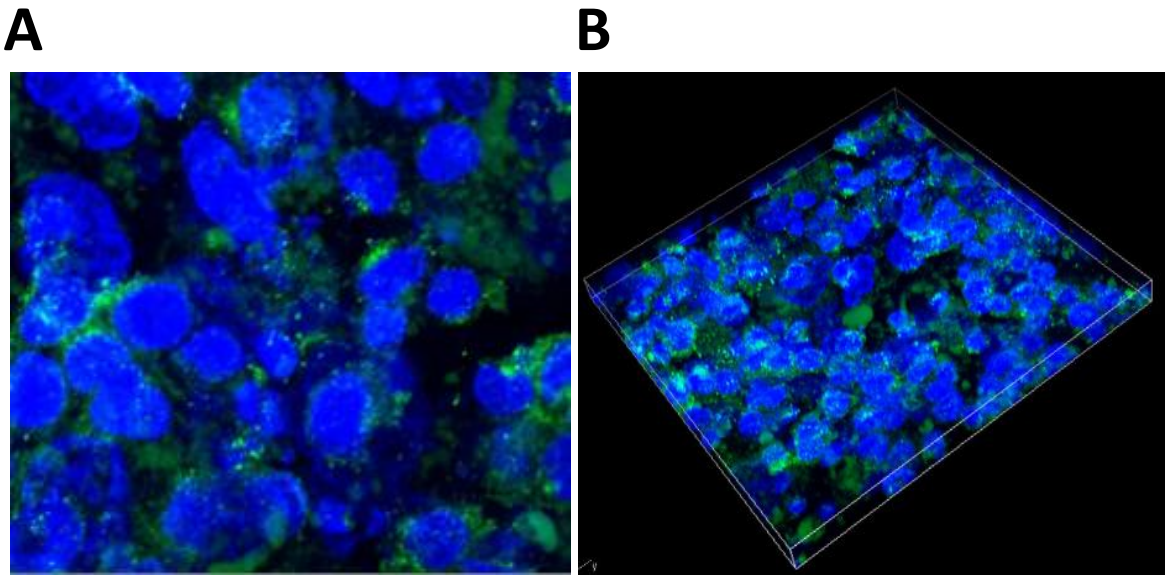

Figure 5.9: A: The staining of two types of cells in the co-culture system captured by inverted confocal. U937 cells are stained with anti-CD11b-antibody (green); nuclei are counterstained with Hoechst 33324 (blue). B: 3D reconstruction of the co-culture system based on the results of the z-stack image of series to analyse the distribution of U937 cells and Calu-3 cells in the co-culture present in the apical compartment of the insert.

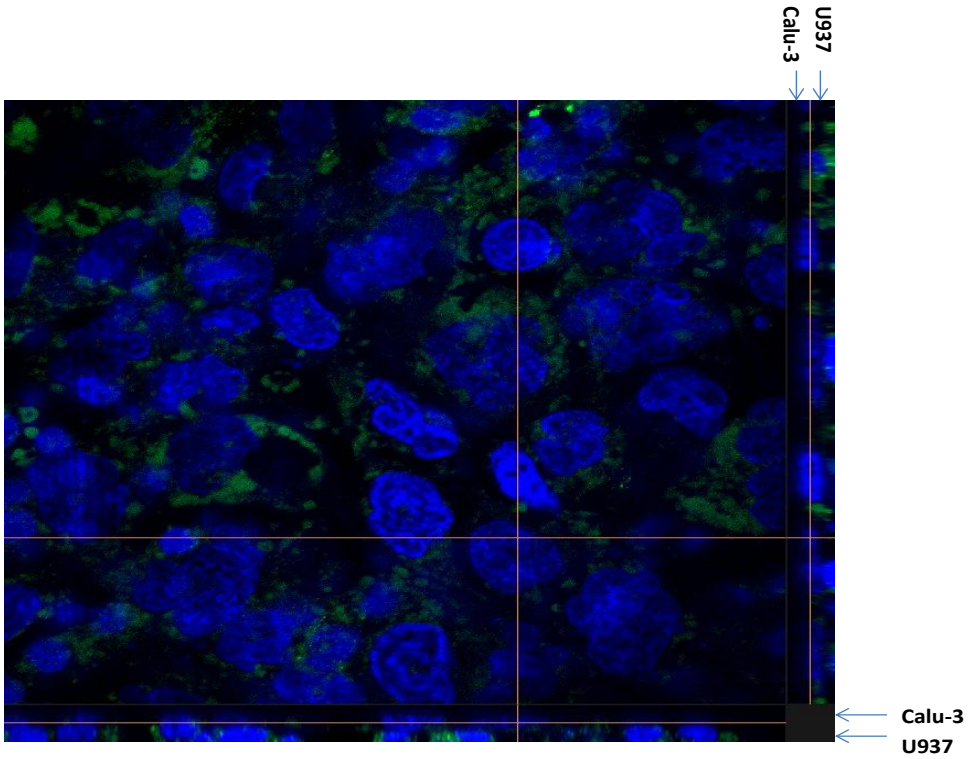

Figure 5.10: Respective side views of the distribution of Calu-3 and U937 cells on sides of a Transwell inserts using Z-stack image.

5.4.8 Bio-distribution of lipid shell nanoparticles

Images of the co-cultured system with the nanoparticles showed there are two ways that particles associated with the cells (inside the cells or attached to the cell surface) (Figure 5.11A). Some particles did not interact with the cells and seemed to aggregate to form clusters in the model. It seemed that there was no difference in the cell association between permeabilised and non-permeabilised systems captured by CLSM (Figure 5.11B).

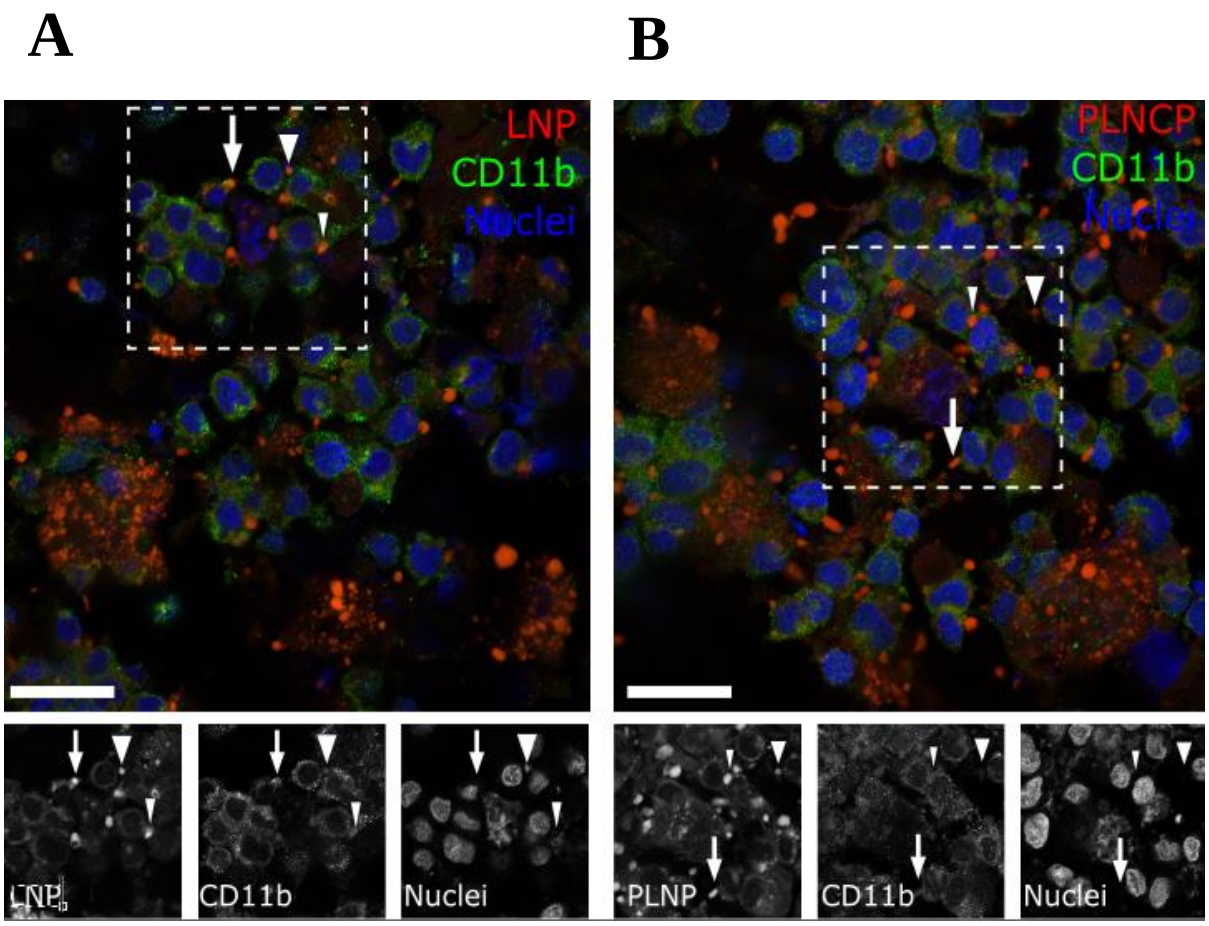

Figure 5.11: The bio-distribution of (A) lipid shell nanoparticles and (B) permeabilised lipid shell nanoparticles in the co-culture present in the apical compartment of the system. Three individual channels displayed at the bottom. Particles are found in (small triangle) or attached to (arrow) or detached to (big triangle) cells. Scale bar represents 20 μm.

To compliment the confocal images the distribution of nanoparticles in the co-culture model was also quantified by flow cytometry. From the quantitative interpretation of the flow cytometry data it was observed that the lipid shell nanoparticles preferentially distributed in macrophage cells rather than epithelial cells in the co-culture system, especially at the 1 h time point. The epithelial cell association with the nanoparticles increased during 4 h (Figure

5.12A). The permeabilisation significantly enhanced the epithelial cell association within first 1 h ($p<0.05$) compared to controlled system, but the distribution profile of the permeabilised and non-permeabilised particles were similar (Figure 5.12B).

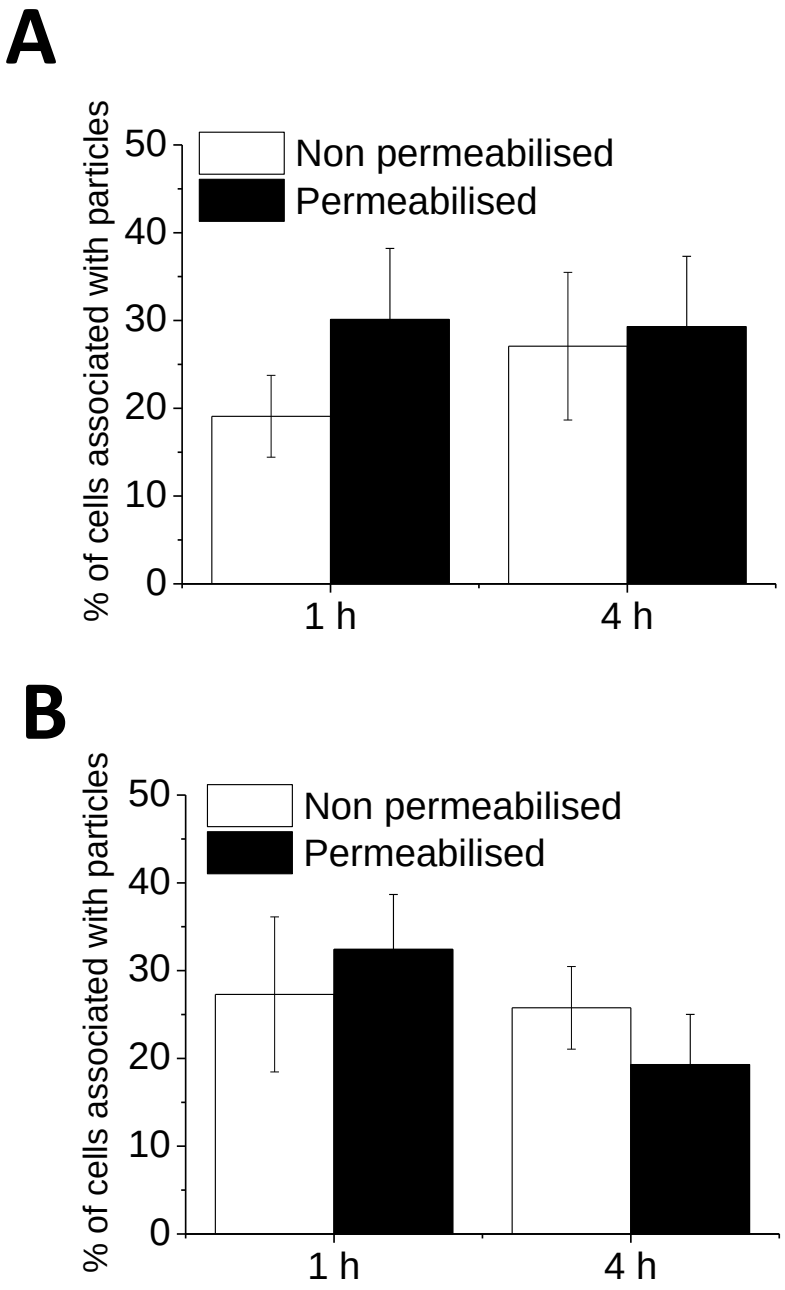

Figure 5.12: Amount of (A) epithelial cell and (B) macrophage cell associated with lipid shell nanoparticles in the co-culture model analysed by flow cytometry. Data represent the mean of three experiments. Data represent mean ± standard deviation (n=9).

5.5 Discussion

Knowledge of the cellular distribution is important when developing nanomedicines for pulmonary use because it can help evaluate the potential for long term toxicity issues (Nel et al., 2006) and it can inform strategies to load the carrier systems with the optimal therapeutic agents (Azarmi et al., 2008). In this work the cellular distribution of lipid shell nanoparticles was studied using rifampicin as a model drug. Drug distribution into both the epithelial cells and macrophages is thought to be beneficial in the treatment of pulmonary tuberculosis with rifampicin. As a consequence the distribution into both cell types was characterised.

The permeation rate of rifampicin when applied to Calu-3 airway epithelial cells as a solution was similar to values previously reported in literature (Tewes et al., 2008). The increase in permeation rate when rifampicin was incorporated into nanoparticles also accorded with the work of Roger et al. (2009) who found that paclitaxel-loaded lipid nanocarriers improved permeability of paclitaxel across intestinal epithelium (Roger et al., 2009). There have been several different reasons cited why lipid shell nanoparticles can improve the permeation of a drug across a cell layer (Beloqui et al., 2013). Usually the mechanism of action is specific to the drug. In this case rifampicin is known to be chemically unstable in water and it was thought that the most likely reason for the increase in the Calu-3 permeation was the protection of the drug inside the nanoparticles, which acted as a drug reservoir to release the drug across the cells.

In the Calu-3 monoculture model, lipid shell nanoparticles were found to persist at the epithelial surface over an 8 h period, less than 10% of the applied particles were associated with cells. The transport data suggested that the epithelial barrier remained resilient over the time course of the experiment when both permeabilised nanoparticle and non-permeabilised nanoparticle system were applied to the Calu-3 cells. This suggested that the non-ionic surfactant trigger had no deleterious effects on the cells. The data from other studies of uptake suggest that airway cells line have a limited capacity to take up nanoparticles. For example, 12% internalization by lung epithelial cells was observed over 8 h exposure to poly(lactide-co-glycolide) (PLGA) NPs (Mura et al., 2011) and 5% of fluorescently-labelled nanoparticles by airway epithelial cells (Vllasaliu et al., 2012). In the majority of studies that have reported upon the nanoparticle kinetics by airways cells it seems that the process proceeds until the cells reach a capacity, which is often < 10% of the applied dose. The

remaining 90% of the carriers reside on the cell surface and are available for macrophage engulfment.

Following lipid shell nanoparticle exposure to the Pluronic permeabiliser it appeared that epithelial cell uptake increased with approximately double the cell association of that observed for the equivalent controlled nanoparticle dose. This may be a result of the larger nanoparticles being more efficiently endocytosed by caveolae-mediated and clathrin dependent processes (Rejman et al., 2004). An alternative explanation is that the Pluronic molecules were acting as a cellular uptake enhancer. Pluronic block copolymers can incorporate into cell membranes (Batrakova and Kabanov, 2008), and this has previously been shown to be capable of enhancing cellular internalization *in vitro* (Park et al., 2013). Pluronic L62D used in this study has a small size of PEO block. It has been shown that the nanocarriers with shorter Pluronic PEO blocks were internalized by HeLa cells at a higher level than the carriers with larger PEO block length (Arranja et al., 2016). Therefore, it is likely the Pluronic had some effect on cell uptake, but it is difficult to say exactly how much of the overall enhancement was related to this effect.

Macrophages are one of the main hosts of pathogens in chronic infectious diseases, they represent a therapeutic target for intracellular delivery of anti-infective agents and thus there have been a number of studies that have monitored nanoparticle uptake (Pei et al., 2015). The data generated by these studies suggest that particle physicochemical properties such as size, surface charge and shape influence macrophage uptake of particles (Chou et al., 2011). The neutral non-distended 50 nm LNPs were associated to low extent (2-4%) by macrophage cells due to their small size (Chono et al., 2006). The LNPs contained a hydrophilic neutral PEG coating which is also thought to reduce recognition by phagocytic cells (Fromen et al., 2015; Walkey et al., 2012). When the size distension process was complete the particles displayed a size of 200 nm. In a previous study when LNPs were incubated at a high concentration with macrophages, an increased uptake rate was observed with increasing particle size (Vonarbourg et al., 2006). Although the distension process could increase the ability of macrophages to recognise these particles they are still quite small for macrophages to recognise and this may explain the only small change of particle association (2%) when the distending particles were applied to the cells (Hirsjärvi et al., 2013). However another study found that the surfactants of the lipid nanoparticles instead of size had an influence on macrophage uptake (Schöler et al., 2001). Interestingly the initial uptake of distensible

particles (50-100 nm) reached the peak within 2 h and a slight decrease was observed. The enhanced association was supported by previous work assessing the same particle uptake by RAW264.7 cells (Vonarbourg et al., 2006). The drop of uptake after 2 h suggests an optimal LNP size for cell internalisation. For example the uptake of 14, 50 and 74 nm gold nanoparticles was investigated in HeLa cells (Chithrani et al., 2006). It was found that the kinetics of uptake varied with the different-sized nanoparticles with 50 nm particles being the most efficient in their uptake, indicating that there might be an optimal size for efficient nanomaterial uptake into cells. On the other hand, the changed particle properties due to distension could also affect the uptake. Particle shape also plays a role in phagocytosis (Champion and Mitragotri, 2006). Upon distension, the Pluronic surfactant permeabilised the shell of the particle and it swelled by 4 times compared to original size. The shape of particles might change which influences phagocytosis by macrophages through varied cell attachment and internalization (Sharma et al., 2010). The overall process of phagocytosis is a result of the complex interplay between shape and size. The mechanism for shape and particle dependence of phagocytosis of LNPs requires further examination.

The distribution of some nanoparticlesat the surface of the cells and some within the cells agrees with previous work that evaluated nanomaterial uptake using a three-dimensional airway cellular model (Rothen-Rutishauser et al., 2005). Nanomaterial uptake begins with an initial adhesion of the materials to the cell via interactions with the lipids, proteins, and other components of the cell membrane. This is followed by the activation of an energy-dependent uptake mechanism (Chithrani et al., 2006), which allows the nanomaterials to be internalized into the cell. The initial nanomaterial adhesion to the cell membranehas been shown to be critical to uptake (Chithrani and Chan, 2007; Lesniak et al., 2013) and therefore the data in this study, which showed LNPs on the cell surface as well as inside the cells was expected.

As it was difficult to quantitatively visualize nanoparticle bio-distribution in the co-culture model using fluorescence microscopy, flow cytometry was used to quantify the particles. The uptake ratioof the nanoparticles by Calu-3 cells compared to macrophage cell in the monoculture system was approximately equivalent, but in the co-culture system more of the macrophage cells contained the particles compared to the Calu-3 cell. The permeabilised particles showed a different trend, as in the monoculture system the uptake was more extensive in the Calu-3 cells whereas in the co-culture system the uptake was even across both cell types. These interesting variations in bio-distribution profile could be due to the

cell-cell interactions in the co-culture model. Cell–cell contact in the pulmonary tract has previously been reported to play an important role in the mechanisms of particle cellular uptake (Blank et al., 2007). In our model, the interactions between macrophages and epithelial cells may therefore modulate responses to particle exposure. It has been proved that interaction of alveolar macrophages and airway epithelial cells following exposure to particulate matter produces mediators that stimulated the bone marrow (Fujii et al., 2002). Granulocyte macrophage colony stimulating factor (GM-CSF) expression was more rapidly induced in co-cultured cells compared with mono layers. Enhanced level of GM-CSF has also been observed in human alveolar macrophages and bronchial epithelial cells when exposed to ambient particles (Ishii et al., 2005). GM-CSF is an important factor determining the differentiation of macrophages *in vivo* and contributes to the macrophage activation (Gordon, 2003). This could be the reason more nanoparticles were associated with macrophages in co-cultured system compared to monolayers. Cell-cell communication may also have reduced the effect of permeabiliser on particle uptake in co-culture system. The uptake of hematite particles into human epithelial (A549) and macrophage (THP-1) cells was studied and results obtained from monoculture and co-culture was compared (Wottrich et al., 2004). The co-culture showed an increased sensitivity to particles concerning the cytokine release in comparison to the monocultures of each cell type. Similarly Muller et al. (2009) revealed an altered response of IL-8 release following particle exposure on a triple cell co-culture of A549 with macrophages and dendritic cells compared to the respective monocultures (Müller et al., 2009). The release of inflammatory markers could have impact on cytotoxicity especially when exposed to the permeabiliser for long period time. Thus co-culture model was better at simulating the real situation in the lung than monocultures as it reflects a synergistic effect between the different cell types owing to the interaction.

5.6 Conclusion

Using the co-culture and monoculture systems in this work it has shown that the kinetics of particle uptake were rapid and the particles retained in both the epithelial cell line compartments and the macrophage compartments, which enables the naosystem situable for controlled pulmonary drug delivery. Co-culture model provided a better tool to investigate the nanoparticle distribution at the cellular level compared to monoculture. Thus when cell distribution occurs rapidly with the lipid shell nanoparticle system *in vitro* cell culture is the only reliable method of tracking the kinetics of particle uptake. This relatively even distribution of the particles renders them particularly suitable for the delivery of anti-infective agents.

CHAPTER SIX

General Discussion

The lungs provide an attractive, non-invasive route for both local and systemic drug delivery. The high local concentrations of active agents that can be achieved rapidly following inhalation make it the mainstay of routine therapy for respiratory disorders such as asthma and COPD (Mansour et al., 2009). However, selecting this route for drug therapy can result in a short duration of clinical effect and thus a medicinal product with cumbersome multiple daily dosing regimens (Sung et al., 2007). This is in part attributable to the swift removal of aerosolised dosage forms from the respiratory tract, by rapid absorption of solubilised drugs or the indiscriminate action of innate defensive clearance mechanisms on particulate matter. These clearance pathways perform a vital function in removing the array of potentially noxious airborne particulates that penetrate into the lungs and should not themselves be disrupted. Therefore, when intending to design inhaled formulations with the objective of extending the biopharmaceutical profile of drugs the formulations must incorporate a specific strategy to avoid local clearance.

The use of nanoparticles as drug delivery vectors is one strategy that may be capable of increasing the residence time of drugs in the lungs. Nanoparticles could serve as a local reservoir to control the delivery of actives to the epithelial surface, sub-epithelial structures or the wider body via the circulation. The small size of nanoparticles is thought to confer the ability to reduce clearance by mucociliary and macrophage pathways (Geiser et al., 2008; Maisel et al., 2015; Moller et al., 2008). However, there are a number of technical challenges when developing nanoparticles to act as local drug reservoirs for pulmonary drug delivery. For example, a reproducible manufacturing technique, employing biocompatible excipients and generating high process yields for large scale pharmaceutical production (Petros and DeSimone, 2010; Riehemann et al., 2009). Drug loading and retention within the nanoparticles during storage must be optimised, but efficient release *in situ* must be realised to ensure adequate bioavailability (Sun et al., 2012). The simplest presentation of nanoparticles remains a nanosuspension, most often using water as the continuous phase. Such a system requires the active agent to have a high affinity to the carrier to prevent premature release, i.e. prior to being administered, but the drug must alsobe liberated at the site of action in order to be bioavailable and exert its pharmacological effects. The use of a nanoparticle permeabiliser can facilitate the switching of nanoparticles that is optimised for drug retention to a state that is optimised for drug release state. Nanoparticle permeabilisers could provide a practical approach to meeting the conflicting demands of good payload retention prior to dosing yet efficient *in situ* release following administration. If a co-

administered nanoparticle-permeabiliser system could be developed and the fate, safety and efficacy of nano-carriers could be determined then a nanoparticle may be able to generate a highly effective inhaled medicine.

The aim of the work presented in this thesis was to understand and explore the feasibility of developing an active drug release nanoparticle system for controlled pulmonary drug delivery. A simple, scaleable fabrication technique was employed to generate lipid shell nanoparticles and polymer shell nanoparticles. These two formulations were selected based on their biocompatible components, high process yields and desirable resultant particle characteristics. Active drug release from nanoparticles was achieved using a surfactant (lipid nanoparticles) and a pH-induced (polymer nanoparticles) shell permeabilisation. Upon administration it was envisaged that the engineered nanoparticles would be released from microparticles, they would translocate through mucus rapidly and they would be retained at the mucus-epithelium interface.

In this thesis the lipid shell nanoparticles were produced using a previously reported emulsion phase inversion-precipitation fabrication technique (Heurtault et al., 2002) and polymer shell nanoparticles were produced using a nanoprecipitation method (Madlova et al., 2009) (Chapter 2). Lipid shell nanoparticles had previously been shown to be biocompatible upon the deposition onto lung airway cells (Jones et al., 2014) and the PVA shell nanoparticles were found to retain their original size (ca. 220 nm), maintain a neutral surface charge in cell culture medium for 24 h and were not acutely toxic to respiratory cells *in vitro* (Madlova et al., 2009). Rifampicin was loaded into the nanoparticles as a model drug. The two formulation processes were capable of reproducibly generating nanoparticles with an average size of 50 and 250 nm respectively, low polydispersity, neutral surface and high loading efficiency (40% for lipid shell nanoparticles and 30% for polymer shell nanoparticles). The nanosuspensions generated in this work possessed a high solid content making them amenable for pharmaceutical use without the need for further ‘concentrating’ steps during large scale processing. Nanoparticle size was characterised using water in Chapter 2 just to investigate the properties, while this was carried out by different medium in the following work in a more speficid context. Data showed that medium had no effect on particle characterisation.

The materials used to generate the nanoparticles in this work were anticipated to facilitate the drug release in a controlled manner. Promisingly, the drug release profiles from two

nanoparticle formulations were enhanced by the application of the two different nanoparticle shell permeabilisers. This was in agreement with previous work which has demonstrated that lipid shell nanoparticles were able to release drug following exposure to Pluronic surfactant (Chana et al., 2015). Passive release was observed from both particle formulations which was a disadvantage of the systems.

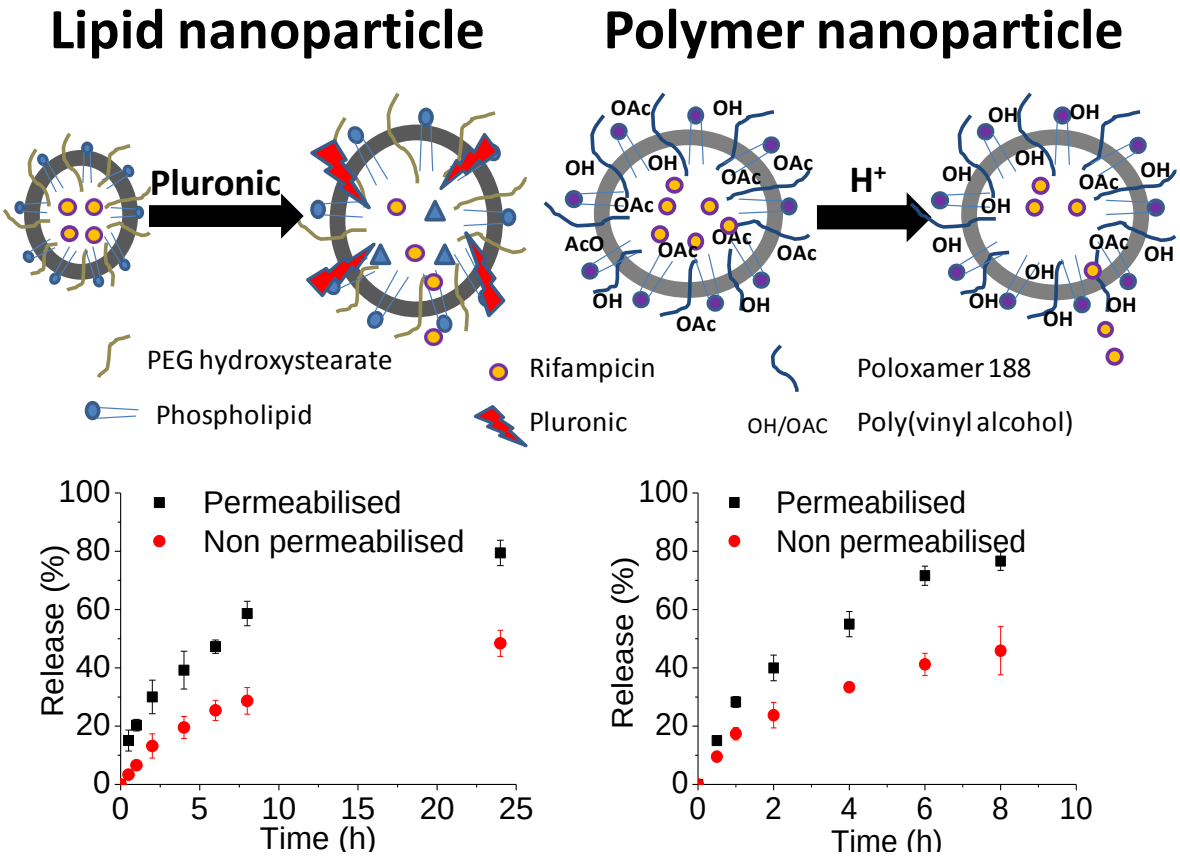

Figure 6.1: Permeabilisation mechanism for lipid shell and polymer shell nanoparticles and the corresponding release profiles.

Mucus is a complex viscoelastic, adhesive hydrogel that coversthe epithelial surfaces in the lungs. It is considered as a critical barrier that must be overcome to achieve effective controlled drug release (Cone, 2009). Trapped particles are typically removed from the mucosal tissue by mucuciliary clearance or macrophage engulfment, thereby strongly limiting the duration of sustained drug delivery to the lungs. Therefore it is important to understand the nanoparticle-mucus interaction (Lai et al., 2009). In this work a vertical translocation model was established to assess the penetration of fabricated nanoparticle through the mucus barrier (Chapter 3). To study how dynamic particles interact with mucus in three dimensions, a traditional diffusion chamber system could be the best available

method accordingly to the studies reviewed and discussed for this work (Chapter 3). Vertical particle transport across mucus is most relevant to the pharmaceutical context of drug delivery to the lungs as it best represents the mucus barrier *in vivo*. The data generated by this system indicated that the nanoparticle transport through the mucus barrier was influenced by both particle size, surfacecharge and hydrophobicity, which agreed with previous studies (Norris and Sinko, 1997; Svensson et al., 2008). Data generated from vertical model have been found to have similar trend to values obtained by nanoparticle tracking analysis. The diffusion model has an advantage over particle tracking as a small volume of sample is needed, which facilitated the performance of the study using a human CF cell-line derived mucus sample. Interestingly, the rank order of particle translocation rate in the mucus penetration assay was different to that obtained from the particle tracking system. This could be due to different measuring mechanisms as the particle tracking technique measured only lateral movement while the Transwell system permeation was a consequence of three-dimensional movement.

Permeabilised lipid shell nanoparticles were found to be capable of penetrating CF mucus much more rapidly compared to similar sized polystyrene nanoparticles (Figure 6.2). Lipid shell nanoparticles had higher diffusion rates probably because ofthe reduced hydrophobic adhesive interactions with mucin fibres. Lipid shell nanoparticles comprise triglycerides dispersed in a saline solution, stabilised at the droplet interface with phospholipids and a PEG based surfactant (Heurtault et al., 2002). This structure matches previous strategy for mucus penetrating particles design that nanoparticles coated with low molecular weight poly(ethylene glycol) (PEG) possess hydrophilic and near neutrally-charged surfaces that minimized mucoadhesion by reducing hydrophobic or electrostatic interactions (Wang et al., 2008b). It was hypothesized that permeabilised particles would have faster diffusion rate than non-permeabilised particles due to the permeabilisation generating 200 nm size particles that were shown to have the highest diffusion rate. However, no effect of the permeabiliser on the diffusion was observed. This was probably because the permeabilisation and subsequent particle swelling process occurred over 8 h and rapid mucus penetration was observed within initial 1 h. The PVA nanoparticle diffusion in PGM was severely retarded compared to lipid shell nanoparticles and PS NPs. This suggests that incorporating PVA in the particle formulation process may lead to the formation of mucoadhesive particles which had strong interactions with mucins through hydrogen bonding and hydrophobic interactions (Yang et al., 2014). Thus it is believed that PVA could inhibit particle diffusion in mucus. Although PVA

nanoparticles might be not a good carrier to meet the project criteria, the finding that PVA particles are strongly immobilized in PGM provides implications for developing new mucus penetrating particles. The rapid transport of dynamic lipid shell nanoparticle coupled with prior knowledge that they were slow to move into epithelial cells offers a potential for the development of controlled release formulations to provide prolonged residence times of the therapeutic agents within the respiratory tract. Thus lipid shell nanoparticles were selected for use in all the subsequent studies in the thesis.

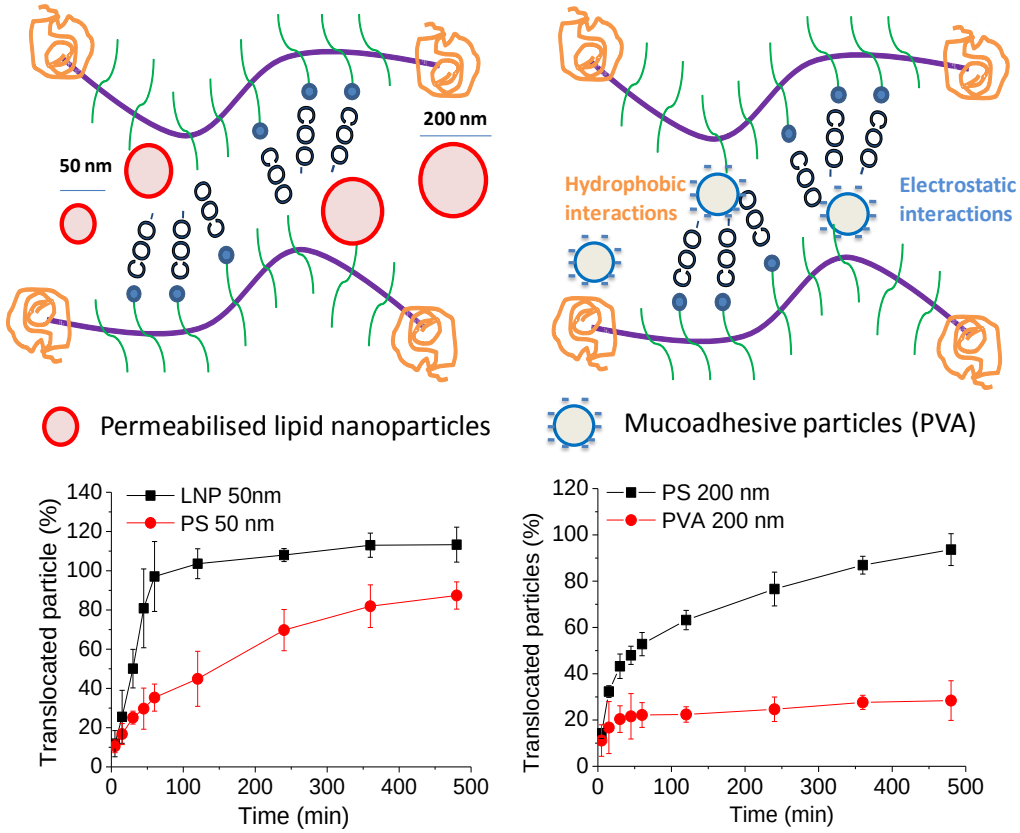

Figure 6.2: Interactions between permeabilised lipid nanoparticles and mucoadhesive PVA nanoparticles with mucus.

The feasibility of loading lipid shell nanoparticles into microparticle systems was assessed in Chapter 4. In this Chapter it was shown that the incorporation of lipid nanoparticles in a dry powder formulation increased the shelf life of the formulation during storage and minimized drug diffusion out of the nanoparticles before administration (release rate k = 0.071 mg/h for nanoparticles and 0.003 mg/h for microparticles). Spray drying was shown to be a suitable method to load lipid shell nanoparticles into lactose microparticles. The microspheres produced in this work had a diameter of 2 to 5 μm which was considered to be suitable for

delivery to the lower airways. Similar size particles havepreviously been reported for spray dried lipid nanocapsules with lactose (Freitas and Müller, 1998). Lipid shell nanoparticles were easily recovered from microparticles. The permeabiliser, nebulized into powder together with the nanoparticles, still functioned once mixed in the medium. This suggests that it is possible to spray dry both drug and permeabiliser simultaneously using the established method. From the results of this study it could be hypothesised that after reaching the lung, lactose will dissolve in the lung lining fluid, releasing nanoparticles which can be permeabilised at the same time.

The introduction of the permeabiliser to the formulation successfully enhanced the release of the drug from the nanoparticles as shown in Figure 6.3. There was a significant difference between the release profiles of permeabilised and non-permeabilised formulations. The release profiles correlated well with the data obtained when the nanoparticles were presented as suspensions (Chapter 2). Concerning the permeabilisation, the differences in release rates of microparticles over 30 days were much larger than those from nanosuspensions (Figure 6.3), proving that the release from the encapsulated carriers was much more controlled and the active drug release system was more effective in the microparticle formulation than in the nanosuspension due to the reduced passive release experienced by the latter. These results indicated the potential of rifampicin-loaded microparticle formulations delivered directly to the lungs for the treatment of tuberculosis. Although the loading of rifampicin is low compared to the usual oral dosage, considering the enhanced bioavailability of inhaled drug it would still be possible to deliver effective concentrations of rifampicin-loaded lipid shell nanoparticles to the lungs to increase local drug levels and reduce the dosing frequency for treatment of pulmonary tuberculosis.

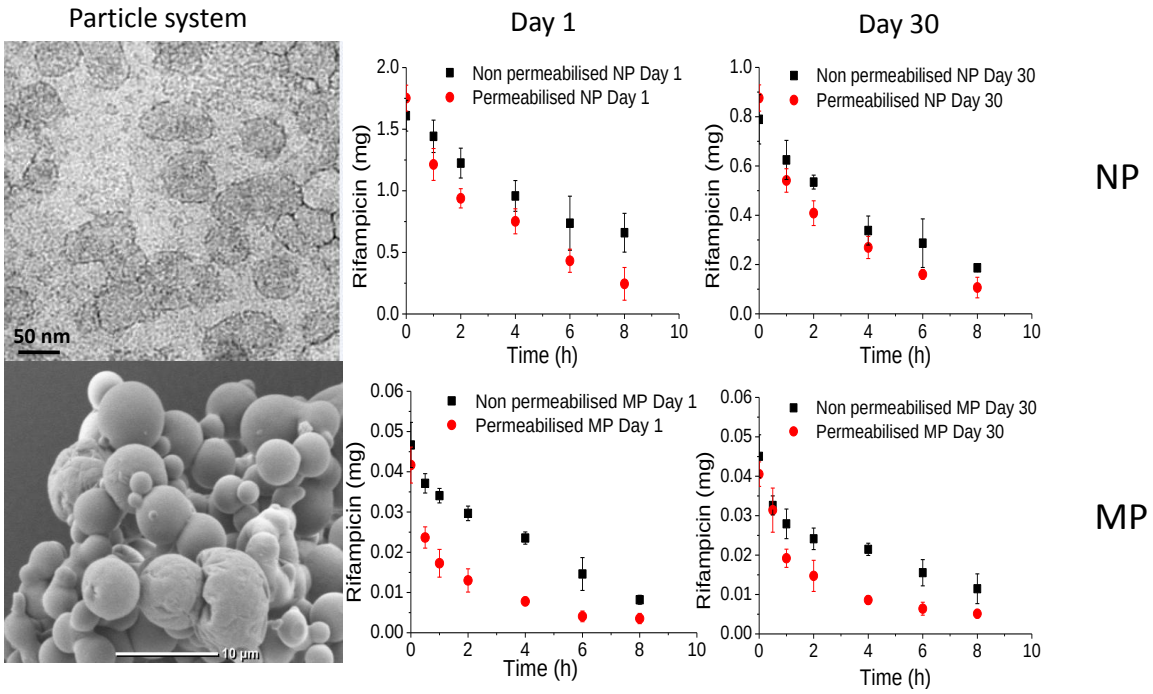

Figure 6.3: Imaging of lipid nanoparticles and lipid nanoparticles loaded-microparticles. Release profiles of rifampicn from lipid nanoparticles and lipid nanoparticles loaded-microparticle under permeabilised and non permeabilised conditions after 1 and 30 days.

Upon deposition on the lung lining surface, lipid nanoparticles can be released from microparticles and penetrate through the mucus rapidly. It is hypothesised that lipid nanoparticles can reside at the mucus-epithelium interface where upon triggered release can occur. Understanding the fate of nanomedicines in the lungs is important not only due to related toxicity, but also because the fate of the carrier and therapeutic action are closely linked. For instance, the rapid uptake of particles by alveolar macrophages can be a way of targeting anti-tuberculosis drugs to this cell type. Compared to an *in vivo* approach, *in vitro* methods offer the simplicity, robustness and better control in experiments and their data acquisition. In addition, considering the potential of the nanoparticles to rapidly distribute into cells the *in vitro* cell culture was considered to be the most reliable method of tracking the kinetics of particle uptake of the cellular distribution in the airways of the lung. An *in vitro* co-culture model was selected for these studies as it was thought to best mimic the *in vivo* cell environment.

In this work an *in vitro* human airway epithelial Calu-3 cells and macrophage U937 cells were used to represent the *in vivo* pulmonary epithelial barrier in mono and co-culture models (Forbes and Ehrhardt, 2005). Free rifampicin permeability across the epithelial cell was close

to values generally reported in the literature (Tewes et al., 2008). Encapsulation of rifampicin into nanoparticles resulted in an increase in rifampicin flux by 20% over 8 h. Lipid shell nanoparticles had been found to retain at the mucus epithelium interface after deposition, where drug can be liberated gradually from the reservoir provided by the nanocarriers (Chana et al., 2015). This result confirmed to previous studies that lipid nanoparticles could enhance the permeability of poorly water-soluble drugs across epithelium (Beloqui et al., 2013; Roger et al., 2009).

Following the application of labelled nanoparticles to the air-interfaced epithelial cell layers approximately 90 % of the administered dose was recovered from the apical cell surface over an 8 hour incubation period (Chapter 5). The observed retention of nanoparticles at the epithelial surface is highly desirable from the perspective of achieving sustained drug delivery as it offers the opportunity for these systems to act as reservoirs from which drug can be released in a controlled manner. Literature relating to nanoparticle fate following inhalation appears contradictory due to differences in the particle systems tested (size, materials), the lung models used (animal, human, *in vitro/in vivo*) as well as the scientific disciplines that have assessed these parameters. Very small nanoparticles have shown a propensity to translocate cell lines following inhalation (Choi et al., 2010). However, data from the majority of human studies suggests the translocated fraction is low (< 1 %) and that a large proportion of the inhaled dose can be retained for more than 24 h (Geiser and Kreyling, 2010; Kreyling et al., 2002). Hence it appears that nanoparticles uptake by lung epithelial cells has a saturation capacity. The lower internalization coupled with previous data that lipid nanoparticles penetrated the mucus rapidly suggested that they can reside in the lung airways for a period of time and as act as drug reservoirs.

In the current study the effect of the active drug release process on particle cellular uptake was considered important. The results showed the epithelial barrier was resilient against the permeabilised nanoparticle system and the permeabilisation process was robust enough to occur at this mucosal interface. Permeabiliser-responsive release was found to be efficacious following *in situ* testing at the air-epithelium interface.The ‘on-demand’ system resulted in more drugs being released from the nanoparticles and a greater extent (2X) of nanoparticles associated with the epithelial barriercompared to control lipid nanoparticles. This could be due to increased particle size (Rejman et al., 2004) or enhanced permeability induced by the Pluronic surfactant (Batrakova and Kabanov, 2008). Pluronic block copolymers with short

PEO block were shown to be potent biological response modifiers capable of enhancing cellular internalization *in vitro* (Park and Na, 2013). In light of the low cellular uptake, the efficacy of the permeabilised nanoparticle system demonstrates its potential for further development as a controlled inhaled pharmaceutical product.

When macrophage cells were exposed to lipid nanopaticles, similar results were obtained to the Calu-3 cell monocultures with less than 5% of the particles being internalized. The permeabilisation process had a small but significant effect on internalization in the *in vitro* macrophage system. Macrophages are one of the main hosts of pathogens in chronic infectious diseases and represent a therapeutic target for intracellular delivery of anti-infective agents and thus there have been a number of studies that have monitored nanoparticle uptake. The data generated by these studies suggests that particle physicochemical properties such as size, surface charge and shape influence macrophage uptake of particles (Chou et al., 2011). Lipid shell nanoparticles are not expected to be internalized by macrophage cells due to too small size (Chono et al., 2006). In spite of the particles swelling in size from 50 to 200 nm during the exposure to permeabiliser, they are still small for phagocytic uptake. Our findings are consistent with the literature (Hirsjärvi et al., 2013).

Overall lipid nanoparticles were found to be distributed in the Calu-3 cells and macrophage cells after administration (Figure 6.4). However the amounts of nanoparticles associated with epithelial cells and macrophage cells cultured as monocultures were similar while there were small differenties in the co-culture system. The effect of permeabiliser on nanoparticle internalisation was also differentin the co-culture system compared to the monoculture system. These interesting variations in distribution profile could be due to the cell-cell interactions in the co-culture model. Cell–cell contact in the pulmonary tract has previously been reported to play an important role in the mechanisms of particle cellular uptake (Blank et al., 2007). Response following particle exposure on a cell co-culture model compared to the monocultures is different due to the communication between cells. In the model, the interactions between macrophages and epithelial cells may therefore modulate responses to particle exposure. Thus a co-culture model is better at simulating the real situation in the lung than monocultures as it enables cross-talk between the different cell types which may affect outcomes.

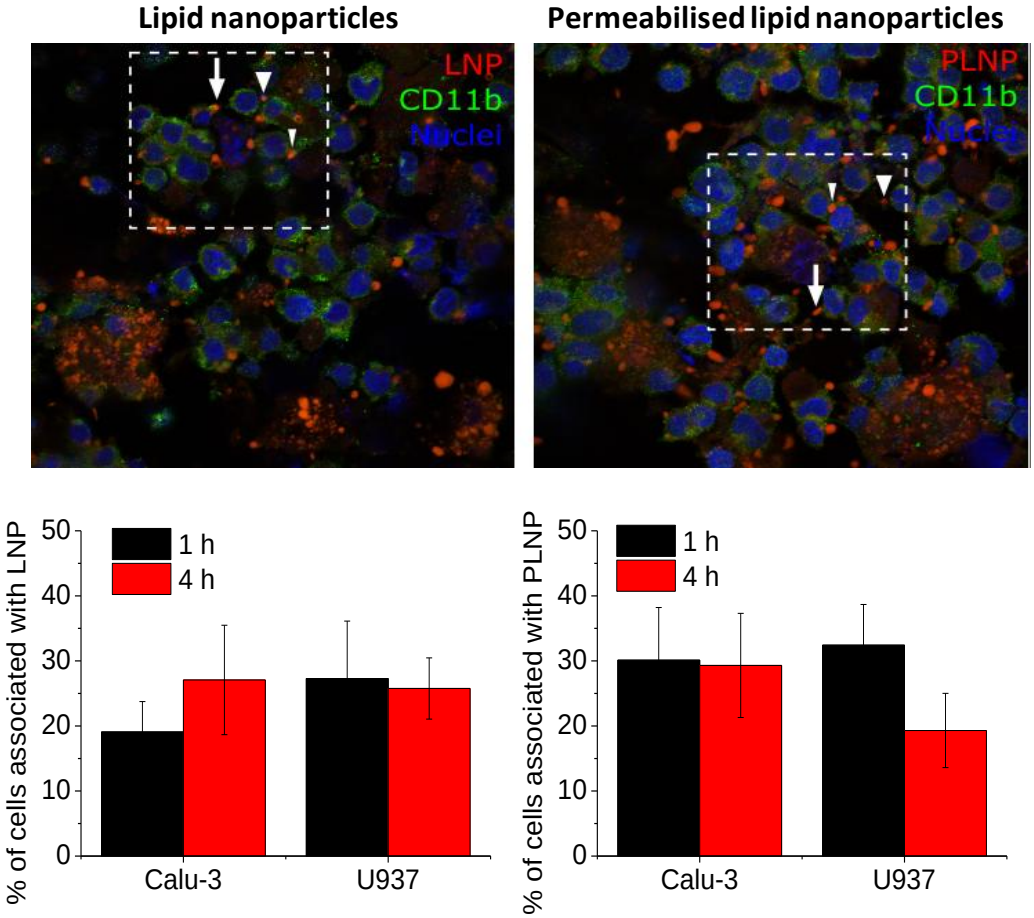

Figure 6.4: Bio-distribution of lipid nanoparticles (LNP) and permeabilised lipid nanoparticles (PLNP) in the co-culture lung cells model.

The main findings of the current work are depicted in Figure 6.5. The generated data contribute to the current understanding of the fate of inhaled permeabilised drug delivery nanoparticles. The apparent compatibility of lipid shell nanoparticles with the airway epithelium and macrophage supports the hypothesis that certain engineered nano-particulates do not cause acute orchronic toxic effects like those observed for inhaled environmental ultrafine particles and therefore may be suitable for biomedical applications. The permeabiliser-induced release from nanomedicines in the airways seemed to be useful. The encapsulation of nanoparticles into microparticles demonstrated that rifampicin could be formulated into nanoparticle-based inhalable sustained drug delivery system for better management of pulmonary tuberculosis. The preliminary localisation data obtained suggest that permeabilised lipid shell nanoparticles can be retained at the mucus epithelium interface over a considerable time period, which enhances their availability to serve as drug reservoirs for the purposes of sustained delivery.

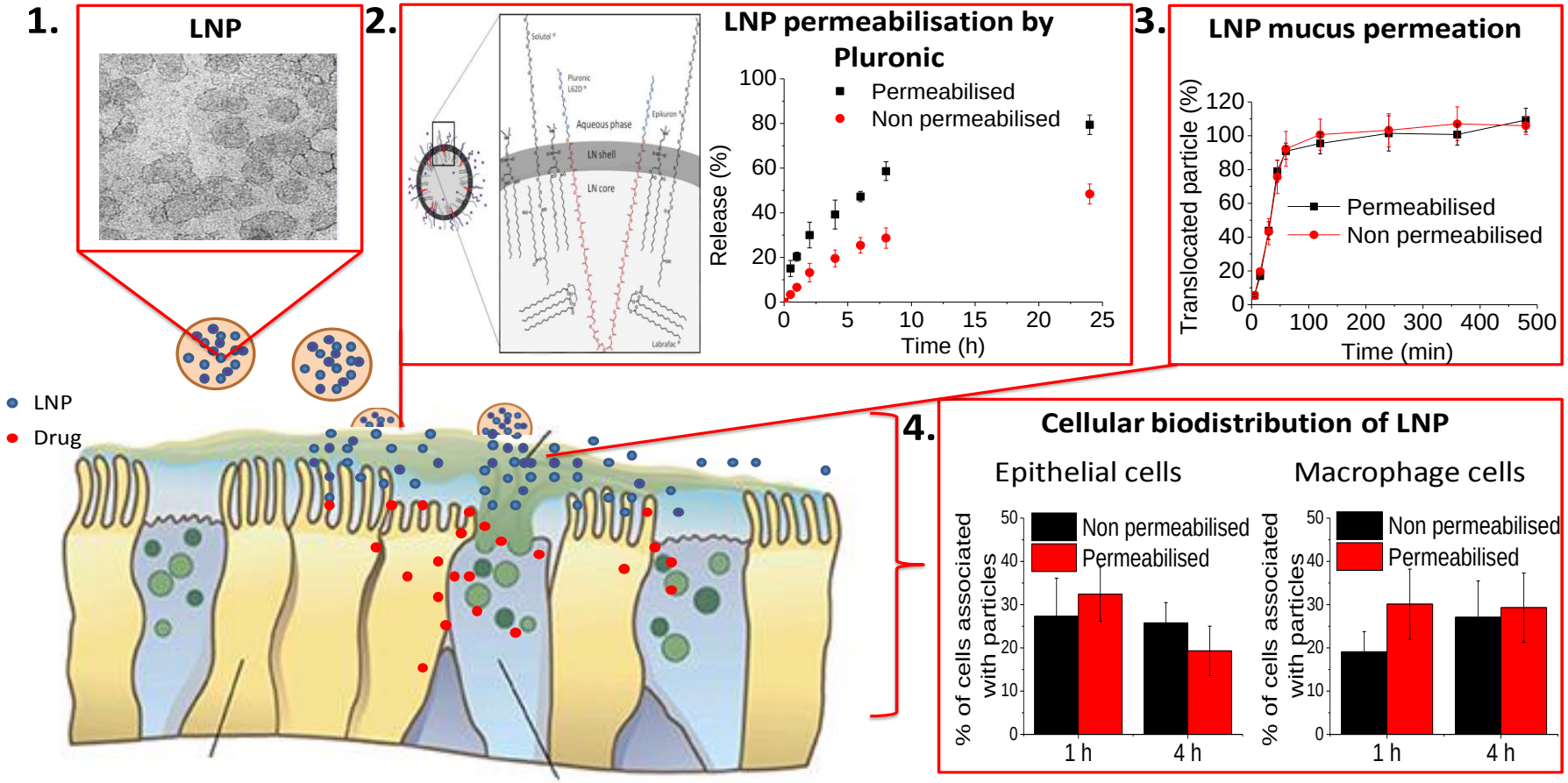

Figure 6.5: Schematic of main findings of current work: 1. Lipid nanoparticles (LNP); 2. Lipid nanoparticles permeabilised by Pluronic surfactant; 3. Mucus penetration of lipid nanoparticles; 4. Cellular bio-distribution of lipid nanoparticles.

Future work

The degradation pathways and clearance mechanisms of the lipid nanoparticles in the lung are unknown at present and warrants further investigation. Although the intention of the nanoparticle system developed in this work was its retention in order to facilitate sustained drug release at the respiratory epithelium its prolonged bio-persistence is undesirable as its potential for long-term toxicity is unknown. This is particularly important when considering the regular nature of dosing that would be required to manage a chronic disease state. It is a possibility that the nanoparticle permeabilisation by Pluronic surfactant may gradually transform the nanoparticles to a size range more amenable to phagocytic and mucociliary clearance, such that they are efficiently removed from the lungs following the delivery of their payload. Another hypothesis is that the nanoparticle permeabilisation will eventually be followed by particle fragmentation such that the lungs could clear the endogenous constituent components (i.e. phospholipids and triglycerides) through normal pathways.

Pre-clinical experiments would be the next logical step in confirming the fate and safety profiles of the inhaled dynamic nanosystem demonstrated in the current work. Preliminary *in vivo* investigations involving lipid nanoparticles intra-tracheal administration have been performed by the Drug Delivery and Pulmonary Pharmacology research groups at King's College London with promising results. In this ongoing study, lipid nanoparticles formed by the same emulsion phase inversion-precipitation process, followed by labelling with a radioactive tracer, were aerosolised in the trachea of mice using a microsprayer. These nanoparticles were found to be well distributed within the lungs where they were retained over a 24 h period. Small amounts of radioactivity were detected in the intestines, liver and faeces at 48 h, perhaps representing the portion cleared by mucociliary clearance and subsequently transferred to the gastrointestinal system organs (Patel et al., 2016). The lipid nanoparticles, administered in the absence of a permeabiliser, were found not to induce an inflammatory response in the lungs of mice or cause toxicity to macrophages (Jones et al., 2014). However, the effect of the permeabilisation process on the fate and safety of lipid nanoparticles needs to be investigated *in vivo* to enhance the understanding of the active release nanoparticle system biodistribution

Another relevant area of future investigation could be the further characterisation of nanoparticle loaded microparticles. Physicochemical properties such as crystallisation, solvent content and powder gravity could be further investigated. Also twin stage impinger

(TSI) could be used to study the aerosolisation property and microparticle deposition in the lungs. As rifampicin load in the particles used in the project probably needs to be increased which could be another area for development. A lot of strategies have been tested to bring high doses of drug to the lung (Claus et al., 2014). On the other hand, the development of novel inhaler devices facilitates the manufacture of improved inhalation formulations. For example, the TOBI® Podhaler® (Novartis AG, Basel, Switzerland) reached the market with the total amount of 112 mg of tobramycin formulation being administered by the inhalation of four capsules twice a day (German Summary of Product Characteristics). Thus the possibility to deliver high doses of lipid nanoparticles to the lung can be test using sophisticated systems.

It is possible that rifampicin might not be a good drug candidate for this formulation approach due to the low drug loading and passive release. It may be better to use a more hydrophobic drug that has a high affinity to nanoparticle core in order to reduce passive release.

Last but not least more biogical studies could be performed to enhance the understanding of the developed formulation. For example, mucus penetration study can be assessed at pH ~7.0 to more mimick the real situation and the system could be tested in vivo.

Conclusion

The data in this thesis have demonstrated that lipid shell nanoparticles formed by a simple, scalable technique have considerable potential as active delivery vectors for inhaled therapeutic agents. The nanoparticles can be loaded into microparticles. Upon deposition, they can penetrate through mucus rapidly and be retained at the epithelial cell surface, where they are available to serve as drug reservoirs. The release of drug from these reservoirs was increased by a co-administered Pluronic nanoparticle shell permeabiliser, which preferentially inserts into the lipid shell nanoparticles over cell membranes to fluidise them. Fluidisation leads to the enhanced release of entrapped drug, which is then available to performe a local action in the lungs. Therefore, the lipid shell nanoparticles developed in this work have the potential for targeted delivery to the lungs for the specific treatment of tuberculosis or other lung diseases.

References

Abdel-Mottaleb, M.M., Neumann, D., and Lamprecht, A. (2010). In vitro drug release mechanism from lipid nanocapsules (LNC). *International Journal of Pharmaceutics* **390**(2), 208-213.

Abdelwahed, W., Degobert, G., Stainmesse, S., and Fessi, H. (2006). Freeze-drying of nanoparticles: formulation, process and storage considerations. *Advanced Drug Delivery Reviews* **58**(15), 1688-1713.

Abdulkarim, M., Agulló, N., Cattoz, B., Griffiths, P., Bernkop-Schnürch, A., Borros, S.G., and Gumbleton, M. (2015). Nanoparticle diffusion within intestinal mucus: Three-dimensional response analysis dissecting the impact of particle surface charge, size and heterogeneity across polyelectrolyte, pegylated and viral particles. *European Journal of Pharmaceutics and Biopharmaceutics* **97**, 230-238.

Ahmad, Z., Pandey, R., Sharma, S., and Khuller, G. (2006). Alginate nanoparticles as antituberculosis drug carriers: formulation development, pharmacokinetics and therapeutic potential. *Indian Journal of Chest Diseases and Allied Sciences* **48**(3), 171.

Al-Ahmady, and Kostarelos, K. (2016). Chemical components for the design of temperature-responsive vesicles as cancer therapeutics. *Chemical Reviews* **116**(6), 3883-3918.

Al-Ahmady, Z.S., Al-Jamal, W.T., Bossche, J.V., Bui, T.T., Drake, A.F., Mason, A.J., and Kostarelos, K. (2012). Lipid–peptide vesicle nanoscale hybrids for triggered drug release by mild hyperthermia in vitro and in vivo. *ACS nano* **6**(10), 9335-9346.

Ali, M.S., and Pearson, J.P. (2007). Upper airway mucin gene expression: a review. *The Laryngoscope* **117**(5), 932-938.

Allen, T.M., and Cullis, P.R. (2013). Liposomal drug delivery systems: from concept to clinical applications. *Advanced Drug Delivery Reviews* **65**(1), 36-48.

Anderson, J.M., and Shive, M.S. (2012). Biodegradation and biocompatibility of PLA and PLGA microspheres. *Advanced Drug Delivery Reviews* **64**, 72-82.

Arnold, M.M., Gorman, E.M., Schieber, L.J., Munson, E.J., and Berkland, C. (2007). NanoCipro encapsulation in monodisperse large porous PLGA microparticles. *Journal of Controlled Release* **121**(1–2), 100-109.

Arranja, A., Denkova, A. G., Morawska, K., Waton, G., van Vlierberghe, S., Dubruel, P., Schosseler, F. and Mendes, E. (2016). Interactions of Pluronic nanocarriers with 2D and 3D cell cultures: Effects of PEO block length and aggregation state. *Journal of Controlled Release*.

Azarmi, S., Roa, W.H., and Löbenberg, R. (2008). Targeted delivery of nanoparticles for the treatment of lung diseases. *Advanced Drug Delivery Reviews* **60**(8), 863-875.

Bansil, R., and Turner, B.S. (2006). Mucin structure, aggregation, physiological functions and biomedical applications. *Current Opinion in Colloid & Interface Science* **11**(2), 164-170.

Barnes, P. (2002). Scientific rationale for inhaled combination therapy with long-acting β2-agonists and corticosteroids. *European Respiratory Journal* **19**(1), 182-191.

Barry, C.E., Boshoff, H.I., Dartois, V., Dick, T., Ehrt, S., Flynn, J., Schnappinger, D., Wilkinson, R.J., and Young, D. (2009). The spectrum of latent tuberculosis: rethinking the biology and intervention strategies. *Nature Reviews Microbiology* **7**(12), 845-855.

Batrakova, E.V., and Kabanov, A.V. (2008). Pluronic block copolymers: evolution of drug delivery concept from inert nanocarriers to biological response modifiers. *Journal of Controlled Release* **130**(2), 98-106.

Beck-Broichsitter, M., Merkel, O.M., and Kissel, T. (2012). Controlled pulmonary drug and gene delivery using polymeric nano-carriers. *Journal of Controlled Release* **161**(2), 214-224.

Beck-Broichsitter, M., Rieger, M., Reul, R., Gessler, T., Seeger, W., and Schmehl, T. (2013). Correlation of drug release with pulmonary drug absorption profiles for nebulizable liposomal formulations. *European Journal of Pharmaceutics and Biopharmaceutics* **84**(1), 106-114.

Beloqui, A., Solinís, M.Á., Gascón, A.R., del Pozo-Rodríguez, A., des Rieux, A., and Préat, V. (2013). Mechanism of transport of saquinavir-loaded nanostructured lipid carriers across the intestinal barrier. *Journal of Controlled Release* **166**(2), 115-123.

BéruBé, K., Prytherch, Z., Job, C., and Hughes, T. (2010). Human primary bronchial lung cell constructs: the new respiratory models. *Toxicology* **278**(3), 311-318.

Beyerle, A., Braun, A., Banerjee, A., Ercal, N., Eickelberg, O., Kissel, T.H., and Stoeger, T. (2011). Inflammatory responses to pulmonary application of PEI-based siRNA nanocarriers in mice. *Biomaterials* **32**(33), 8694-8701.

Bhattacharya, K., Andón, F.T., El-Sayed, R., and Fadeel, B. (2013). Mechanisms of carbon nanotube-induced toxicity: focus on pulmonary inflammation. *Advanced Drug Delivery Reviews* **65**(15), 2087-2097.

Bhise, S.B., More, A.B., and Malayandi, R. (2010). Formulation and in vitro evaluation of rifampicin loaded porous microspheres. *Scientia Pharmaceutica* **78**(2), 291.

Blank, F., Rothen-Rutishauser, B., and Gehr, P. (2007). Dendritic cells and macrophages form a transepithelial network against foreign particulate antigens. *American Journal of Respiratory Cell and Molecular Biology* **36**(6), 669-677.

Bodet, C., Chandad, F., and Grenier, D. (2006). Inflammatory responses of a macrophage/epithelial cell co-culture model to mono and mixed infections with Porphyromonas gingivalis, Treponema denticola, and Tannerella forsythia. *Microbes and Infection* **8**(1), 27-35.

Borm, P.J., and Kreyling, W. (2004). Toxicological hazards of inhaled nanoparticles—potential implications for drug delivery. *Journal of Nanoscience and Nanotechnology* **4**(5), 521-531.

Bosquillon, C. (2010). Drug transporters in the lung—do they play a role in the biopharmaceutics of inhaled drugs? *Journal of Pharmaceutical Sciences* **99**(5), 2240-2255.

Boucher, R. (2004). New concepts of the pathogenesis of cystic fibrosis lung disease. *European Respiratory Journal* **23**(1), 146-158.

British National Formularly 71, March 2016

Bromberg, L.E., and Barr, D.P. (2000). Self-association of mucin. *Biomacromolecules* **1**(3), 325-334.

Broughton-Head, V.J., Smith, J.R., Shur, J., and Shute, J.K. (2007). Actin limits enhancement of nanoparticle diffusion through cystic fibrosis sputum by mucolytics. *Pulmonary Pharmacology &Therapeutics* **20**(6), 708-717.

Brownlee, I.A., Havler, M.E., Dettmar, P.W., Allen, A., and Pearson, J.P. (2003). Colonic mucus: secretion and turnover in relation to dietary fibre intake. *Proceedings of the Nutrition Society* **62**(01), 245-249.

Byrne, Marais, B.J., Mitnick, C.D., Lecca, L., and Marks, G.B. (2015). Tuberculosis and chronic respiratory disease: a systematic review. *International Journal of Infectious Diseases* **32**, 138-146.

Byron, P.R. (1993). Physicochemical effects on lung disposition of pharmaceutical aerosols. *Aerosol Science and Technology* **18**(3), 223-229.

Byron, P.R., and Patton, J.S. (1994). Drug delivery via the respiratory tract. *Journal of Aerosol medicine* **7**(1), 49-75.

Carregal, S., Guardia, P., Yu, X., Hartmann, R., Pellegrino, T., and Parak, W.J. (2015). Magnetically triggered release of molecular cargo from iron oxide nanoparticle loaded microcapsules. *Nanoscale* **7**(2), 570-576.

Celli, J., Gregor, B., Turner, B., Afdhal, N.H., Bansil, R., and Erramilli, S. (2005). Viscoelastic properties and dynamics of porcine gastric mucin. *Biomacromolecules* **6**(3), 1329-1333.

Chalasani, K.B., Russell-Jones, G.J., Jain, A.K., Diwan, P.V., and Jain, S.K. (2007). Effective oral delivery of insulin in animal models using vitamin B12-coated dextran nanoparticles. *Journal of Controlled Release* **122**(2), 141-150.

Champion, J.A., and Mitragotri, S. (2006). Role of target geometry in phagocytosis. *Proceedings of the National Academy of Sciences of the United States of America* **103**(13), 4930-4934.

Champion, J.A., Walker, A., and Mitragotri, S. (2008). Role of particle size in phagocytosis of polymeric microspheres. *Pharmaceutical Research* **25**(8), 1815-1821.

Chana, J., Forbes, B., and Jones, S.A. (2008). The synthesis of high molecular weight partially hydrolysed poly (vinyl alcohol) grades suitable for nanoparticle fabrication. *Journal of Nanoscience and Nanotechnology* **8**(11), 5739-5747.

Chana, J., Forbes, B., and Jones, S.A. (2015). Triggered-release nanocapsules for drug delivery to the lungs. *Nanomedicine: Nanotechnology, Biology and Medicine* **11**(1), 89-97.

Chen, Huang, W., Wong, B.C., Yin, L., Wong, Y.F., Xu, M., and Yang, Z. (2012). Liposomes prolong the therapeutic effect of anti-asthmatic medication via pulmonary delivery. *International Journal of Nanomedicine* **7**, 1139.

Chen, Meng, F., Cheng, R., and Zhong, Z. (2010). pH-Sensitive degradable polymersomes for triggered release of anticancer drugs: A comparative study with micelles. *Journal of Controlled Release* **142**(1), 40-46.

Cheng, Y., Xu, Z., Ma, M., and Xu, T. (2008). Dendrimers as drug carriers: applications in different routes of drug administration. *Journal of Pharmaceutical Sciences* **97**(1), 123-143.

Chew, N.Y., Tang, P., Chan, H.-K., and Raper, J.A. (2005). How much particle surface corrugation is sufficient to improve aerosol performance of powders? *Pharmaceutical Research* **22**(1), 148-152.

Chithrani, B.D., and Chan, W.C. (2007). Elucidating the mechanism of cellular uptake and removal of protein-coated gold nanoparticles of different sizes and shapes. *Nano Letters* **7**(6), 1542-1550.

Chithrani, B.D., Ghazani, A.A., and Chan, W.C. (2006). Determining the size and shape dependence of gold nanoparticle uptake into mammalian cells. *Nano Letters* **6**(4), 662-668.

Choe, M.M., Sporn, P.H., and Swartz, M.A. (2006). Extracellular matrix remodeling by dynamic strain in a three-dimensional tissue-engineered human airway wall model. *American Journal of Respiratory Cell and Molecular Biology* **35**(3), 306-313.

Choi, H.S., Ashitate, Y., Lee, J.H., Kim, S.H., Matsui, A., Insin, N., Bawendi, M.G., Semmler-Behnke, M., Frangioni, J.V., and Tsuda, A. (2010). Rapid translocation of nanoparticles from the lung airspaces to the body. *Nature Biotechnology* **28**(12), 1300-1303.

Chono, S., Tanino, T., Seki, T., and Morimoto, K. (2006). Influence of particle size on drug delivery to rat alveolar macrophages following pulmonary administration of ciprofloxacin incorporated into liposomes. *Journal of Drug Targeting* **14**(8), 557-566.

Chou, L.Y., Ming, K., and Chan, W.C. (2011). Strategies for the intracellular delivery of nanoparticles. *Chemical Society Reviews* **40**(1), 233-245.

Choudhary, S., and Devi, V.K. (2015). Potential of nanotechnology as a delivery platform against tuberculosis: current research review. *Journal of Controlled Release* **202**, 65-75.

Cipolla, D., Shekunov, B., Blanchard, J., and Hickey, A. (2014). Lipid-based carriers for pulmonary products: preclinical development and case studies in humans. *Advanced Drug Delivery Reviews* **75**, 53-80.

Claus, S., Weiler, C., Schiewe, J., and Friess, W. (2014). How can we bring high drug doses to the lung? *European Journal of Pharmaceutics and Biopharmaceutics* **86**(1), 1-6.

Clayden, J., Greeves, N., and Warren, S. (2012). Organic Chemistry. 2nd (Oxford University Press. UK).

Clunes, M.T., and Boucher, R.C. (2007). Cystic fibrosis: the mechanisms of pathogenesis of an inherited lung disorder. *Drug Discovery Today: Disease Mechanisms* **4**(2), 63-72.

Cone, R.A. (2009). Barrier properties of mucus. *Advanced Drug Delivery Reviews* **61**(2), 75-85.

Cook, R.O., Pannu, R.K., and Kellaway, I.W. (2005). Novel sustained release microspheres for pulmonary drug delivery. *Journal of Controlled Release* **104**(1), 79-90.

Costa, A., Pinheiro, M., Magalhães, J., Ribeiro, R., Seabra, V., Reis, S., and Sarmento, B. (2016). The formulation of nanomedicines for treating tuberculosis. *Advanced Drug Delivery Reviews***102**, 103-115.

Courrier, H., Butz, N., and Vandamme, T.F. (2002). Pulmonary drug delivery systems: recent developments and prospects. *Critical Reviews™ in Therapeutic Drug Carrier Systems* **19**(4-5).

Crater, J.S., and Carrier, R.L. (2010). Barrier properties of gastrointestinal mucus to nanoparticle transport. *Macromolecular Bioscience* **10**(12), 1473-1483.

Cu, Y., and Saltzman, W.M. (2008). Controlled surface modification with poly (ethylene) glycol enhances diffusion of PLGA nanoparticles in human cervical mucus. *Molecular Pharmaceutics* **6**(1), 173-181.

Cui, F., Shi, K., Zhang, L., Tao, A., and Kawashima, Y. (2006). Biodegradable nanoparticles loaded with insulin–phospholipid complex for oral delivery: Preparation, in vitro characterization and in vivo evaluation. *Journal of Controlled Release* **114**(2), 242-250.

Dailey, L., Jekel, N., Fink, L., Gessler, T., Schmehl, T., Wittmar, M., Kissel, T., and Seeger, W. (2006). Investigation of the proinflammatory potential of biodegradable nanoparticle drug delivery systems in the lung. *Toxicology and Applied Pharmacology* **215**(1), 100-108.

Danhier, F., Lecouturier, N., Vroman, B., Jérôme, C., Marchand-Brynaert, J., Feron, O., and Préat, V. (2009). Paclitaxel-loaded PEGylated PLGA-based nanoparticles: in vitro and in vivo evaluation. *Journal of Controlled Release* **133**(1), 11-17.

Darquenne C, Paiva M, Prisk G K. (2000). Effect of gravity on aerosol dispersion and deposition in the human lung after periods of breath holding. *Journal of Applied Physiology* **89**(5), 1787-1792.

Dartois, V. (2014). The path of anti-tuberculosis drugs: from blood to lesions to mycobacterial cells. *Nature Reviews Microbiology* **12**(3), 159-167.

De Jong, W.H., and Borm, P.J. (2008). Drug delivery and nanoparticles: applications and hazards. *International Journal of Nanomedicine* **3**(2), 133.

DeFronzo, R.A., Bergenstal, R.M., Cefalu, W.T., Pullman, J., Lerman, S., Bode, B.W., and Phillips, L.S. (2005). Efficacy of inhaled insulin in patients with type 2 diabetes not controlled with diet and exercise a 12-week, randomized, comparative trial. *Diabetes Care* **28**(8), 1922-1928.

Dekker, J., Rossen, J.W., Büller, H.A., and Einerhand, A.W. (2002). The MUC family: an obituary. *Trends in Biochemical Sciences* **27**(3), 126-131.

DeMerlis, C., and Schoneker, D. (2003). Review of the oral toxicity of polyvinyl alcohol (PVA). *Food and Chemical Toxicology* **41**(3), 319-326.

Deng, Z., Zhen, Z., Hu, X., Wu, S., Xu, Z., and Chu, P.K. (2011). Hollow chitosan–silica nanospheres as pH-sensitive targeted delivery carriers in breast cancer therapy. *Biomaterials* **32**(21), 4976-4986.

Doan, T., Couet, W., and Olivier, J. (2011). Formulation and in vitro characterization of inhalable rifampicin-loaded PLGA microspheres for sustained lung delivery. *International Journal of Pharmaceutics* **414**(1), 112-117.

Dolovich, M.B., and Dhand, R. (2011). Aerosol drug delivery: developments in device design and clinical use. *The Lancet* **377**(9770), 1032-1045.

Donald, P., Maritz, J., and Diacon, A. (2011). The pharmacokinetics and pharmacodynamics of rifampicin in adults and children in relation to the dosage recommended for children. *Tuberculosis* **91**(3), 196-207.

Donaldson, S.H., Bennett, W.D., Zeman, K.L., Knowles, M.R., Tarran, R., and Boucher, R.C. (2006). Mucus clearance and lung function in cystic fibrosis with hypertonic saline. *New England Journal of Medicine* **354**(3), 241-250.

Du, J.-Z., Du, X.-J., Mao, C.-Q., and Wang, J. (2011). Tailor-made dual pH-sensitive polymer–doxorubicin nanoparticles for efficient anticancer drug delivery. *Journal of the American Chemical Society* **133**(44), 17560-17563.

Dube, D., Agrawal, G.P., and Vyas, S.P. (2012). Tuberculosis: from molecular pathogenesis to effective drug carrier design. *Drug Discovery Today* **17**(13), 760-773.

Duncan, R., and Gaspar, R. (2011). Nanomedicine (s) under the microscope. *Molecular Pharmaceutics* **8**(6), 2101-2141.

Edwards, D.A., Hanes, J., Caponetti, G., Hrkach, J., Ben-Jebria, A., Eskew, M.L., Mintzes, J., Deaver, D., Lotan, N., and Langer, R. (1997). Large porous particles for pulmonary drug delivery. *Science* **276**(5320), 1868-1871.

El-Sherbiny, I.M., and Smyth, H.D. (2010). Biodegradable nano-micro carrier systems for sustained pulmonary drug delivery:(I) self-assembled nanoparticles encapsulated in respirable/swellable semi-IPN microspheres. *International Journal of Pharmaceutics* **395**(1), 132-141.

Emeje, M.O., Akpabio, E.I., Obidike, I.C., and Ofoefule, S.I. (2012). *Nanotechnology in Drug Delivery* (INTECH Open Access Publisher).

Ensign, L.M., Cone, R., and Hanes, J. (2012). Oral drug delivery with polymeric nanoparticles: the gastrointestinal mucus barriers. *Advanced Drug Delivery Reviews* **64**(6), 557-570.

Ernst, J.D. (2012). The immunological life cycle of tuberculosis. *Nature Reviews Immunology* **12**(8), 581-591.

Farokhzad, O.C., and Langer, R. (2009). Impact of nanotechnology on drug delivery. *ACS Nano* **3**(1), 16-20.

Ferin, J., and Oberdörster, G. (1992). Translocation of Particles from Pulmonary Alveoli into the Interstitium*. *Journal of Aerosol Medicine* **5**(3), 179-187.

Firestone, M.A., Wolf, A.C., and Seifert, S. (2003). Small-angle X-ray scattering study of the interaction of poly (ethylene oxide)-b-poly (propylene oxide)-b-poly (ethylene oxide) triblock copolymers with lipid bilayers. *Biomacromolecules* **4**(6), 1539-1549.

Forbes, B., and Ehrhardt, C. (2005). Human respiratory epithelial cell culture for drug delivery applications. *European Journal of Pharmaceutics and Biopharmaceutics* **60**(2), 193-205.

Foster, K.A., Yazdanian, M., and Audus, K.L. (2001). Microparticulate uptake mechanisms of in-vitro cell culture models of the respiratory epithelium. *Journal of Pharmacy and Pharmacology* **53**(1), 57-66.

Freitas, C., and Müller, R.H. (1998). Spray-drying of solid lipid nanoparticles (SLN TM). *European Journal of Pharmaceutics and Biopharmaceutics* **46**(2), 145-151.

Fromen, C.A., Rahhal, T.B., Robbins, G.R., Kai, M.P., Shen, T.W., Luft, J.C., and DeSimone, J.M. (2015). Nanoparticle surface charge impacts distribution, uptake and lymph node trafficking by pulmonary antigen-presenting cells. *Nanomedicine: Nanotechnology, Biology and Medicine***12**(3), 677-687.

Fujii, T., Hayashi, S., Hogg, J.C., Mukae, H., Suwa, T., Goto, Y., Vincent, R., and van Eeden, S.F. (2002). Interaction of alveolar macrophages and airway epithelial cells following exposure to particulate matter produces mediators that stimulate the bone marrow. *American Journal of Respiratory Cell and Molecular Biology* **27**(1), 34-41.

Fulford, G., and Blake, J. (1986). Muco-ciliary transport in the lung. *Journal of theoretical Biology* **121**(4), 381-402.

Gandhi, N.R., Nunn, P., Dheda, K., Schaaf, H.S., Zignol, M., Van Soolingen, D., Jensen, P., and Bayona, J. (2010). Multidrug-resistant and extensively drug-resistant tuberculosis: a threat to global control of tuberculosis. *The Lancet* **375**(9728), 1830-1843.

Ganta, S., Devalapally, H., Shahiwala, A., and Amiji, M. (2008). A review of stimuli-responsive nanocarriers for drug and gene delivery. *Journal of Controlled Release* **126**(3), 187-204.

Garcá-Díaz, M., Foged, C., and Nielsen, H.M. (2015). Improved insulin loading in poly (lactic-co-glycolic) acid (PLGA) nanoparticles upon self-assembly with lipids. *International Journal of Pharmaceutics* **482**(1), 84-91.

Geiser, M. (2010). Update on macrophage clearance of inhaled micro-and nanoparticles. *Journal of Aerosol Medicine and Pulmonary Drug Delivery* **23**(4), 207-217.

Geiser, M., Casaulta, M., Kupferschmid, B., Schulz, H., Semmler-Behnke, M., and Kreyling, W. (2008). The role of macrophages in the clearance of inhaled ultrafine titanium dioxide particles. *American Journal of Respiratory Cell and Molecular Biology* **38**(3), 371-376.

Geiser, M., and Kreyling, W.G. (2010). Deposition and biokinetics of inhaled nanoparticles. *Particle and Fibre Toxicology* **7**(1), 1.

Geiser, M., Schürch, S., and Gehr, P. (2003). Influence of surface chemistry and topography of particles on their immersion into the lung's surface-lining layer. *Journal of Applied Physiology* **94**(5), 1793-1801.

Gendler, S.J., and Spicer, A. (1995). Epithelial mucin genes. *Annual Review of Physiology* **57**(1), 607-634.

Gerweck, L.E., and Seetharaman, K. (1996). Cellular pH gradient in tumor versus normal tissue: potential exploitation for the treatment of cancer. *Cancer research* **56**(6), 1194-1198.

Gessler, T., Seeger, W., and Schmehl, T. (2008). Inhaled prostanoids in the therapy of pulmonary hypertension. *Journal of Aerosol Medicine and Pulmonary Drug Delivery* **21**(1), 1-12.

Geys, J., Coenegrachts, L., Vercammen, J., Engelborghs, Y., Nemmar, A., Nemery, B., and Hoet, P. (2006). In vitro study of the pulmonary translocation of nanoparticles: a preliminary study. *Toxicology Letters* **160**(3), 218-226.

Gill, K.K., Nazzal, S., and Kaddoumi, A. (2011). Paclitaxel loaded PEG 5000–DSPE micelles as pulmonary delivery platform: formulation characterization, tissue distribution, plasma pharmacokinetics, and toxicological evaluation. *European Journal of Pharmaceutics and Biopharmaceutics* **79**(2), 276-284.

Gonçalves, Maestrelli, F., Mannelli, L., Ghelardini, C., Almeida, A., and Mura, P. (2016). Development of solid lipid nanoparticles as carriers for improving oral bioavailability of glibenclamide. *European Journal of Pharmaceutics and Biopharmaceutics* **102**, 41-50.

Gordon, S. (2003). Alternative activation of macrophages. *Nature Reviews Immunology* **3**(1), 23-35.

Grainger C I, Greenwell L L, Lockley D J, et al. (2006). Culture of Calu-3 cells at the air interface provides a representative model of the airway epithelial barrier. *Pharmaceutical Research* **23**(7), 1482-1490.

Grenha, A., Grainger, C.I., Dailey, L.A., Seijo, B., Martin, G.P., Remuñán-López, C., and Forbes, B. (2007). Chitosan nanoparticles are compatible with respiratory epithelial cells in vitro. *European Journal of Pharmaceutical Sciences* **31**(2), 73-84.

Griesinger, J., Dünnhaupt, S., Cattoz, B., Griffiths, P., Oh, S., i Gómez, S.B., Wilcox, M., Pearson, J., Gumbleton, M., and Abdulkarim, M. (2015). Methods to determine the interactions of micro-and nanoparticles with mucus. *European Journal of Pharmaceutics and Biopharmaceutics* **96**, 464-476.

Gu, F., Zhang, L., Teply, B.A., Mann, N., Wang, A., Radovic-Moreno, A.F., Langer, R., and Farokhzad, O.C. (2008). Precise engineering of targeted nanoparticles by using self-assembled biointegrated block copolymers. *Proceedings of the National Academy of Sciences* **105**(7), 2586-2591.

Gumbleton, M. (2001). Caveolae as potential macromolecule trafficking compartments within alveolar epithelium. *Advanced Drug Delivery Reviews* **49**(3), 281-300.

Hajos, F., Stark, B., Hensler, S., Prassl, R., and Mosgoeller, W. (2008). Inhalable liposomal formulation for vasoactive intestinal peptide. *International Journal of Pharmaceutics* **357**(1), 286-294.

Hans, M., and Lowman, A. (2002). Biodegradable nanoparticles for drug delivery and targeting. *Current Opinion in Solid State and Materials Science* **6**(4), 319-327.

Hasan, A.S., Sapin, A., Damgé, C., Leroy, P., Socha, M., and Maincent, P. (2015). Reduction of the in vivo burst release of insulin-loaded microparticles. *Journal of Drug Delivery Science and Technology* **30**, 486-493.

He, C., Hu, Y., Yin, L., Tang, C., and Yin, C. (2010). Effects of particle size and surface charge on cellular uptake and biodistribution of polymeric nanoparticles. *Biomaterials* **31**(13), 3657-3666.

Heurtault, B., Saulnier, P., Pech, B., Proust, J.-E., and Benoit, J.-P. (2002). A novel phase inversion-based process for the preparation of lipid nanocarriers. *Pharmaceutical Research* **19**(6), 875-880.

Heyder, Gebhart, J., Rudolf, G., Schiller, C.F., and Stahlhofen, W. (1986). Deposition of particles in the human respiratory tract in the size range 0.005–15 μm. *Journal of Aerosol Science* **17**(5), 811-825.

Hickey, A.J. (2014). Controlled delivery of inhaled therapeutic agents. *Journal of Controlled Release* **190**(0), 182-188.

Hinds, W.C. (2012). *Aerosol technology: properties, behavior, and measurement of airborne particles* (John Wiley & Sons).

Hirsjärvi, S., Dufort, S., Gravier, J., Texier, I., Yan, Q., Bibette, J., Sancey, L., Josserand, V., Passirani, C., and Benoit, J.-P. (2013). Influence of size, surface coating and fine chemical composition on the in vitro reactivity and in vivo biodistribution of lipid nanocapsules versus lipid nanoemulsions in cancer models. *Nanomedicine: Nanotechnology, Biology and Medicine* **9**(3), 375-387.

Holmkvist, A.D., Friberg, A., Nilsson, U.J., and Schouenborg, J. (2016). Hydrophobic ion pairing of a minocycline/Ca 2+/AOT complex for preparation of drug-loaded PLGA nanoparticles with improved sustained release. *International Journal of Pharmaceutics* **499**(1), 351-357.

Hong, Z., Chasan, B., Bansil, R., Turner, B.S., Bhaskar, K.R., and Afdhal, N.H. (2005). Atomic force microscopy reveals aggregation of gastric mucin at low pH. *Biomacromolecules* **6**(6), 3458-3466.

Hoppentocht, M., Hagedoorn, P., Frijlink, H., and de Boer, A. (2014). Technological and practical challenges of dry powder inhalers and formulations. *Advanced Drug Delivery Reviews* **75**, 18-31.

Hu, X., Yang, F.-F., Quan, L.-H., Liu, C.-Y., Liu, X.-M., Ehrhardt, C., and Liao, Y.-H. (2014). Pulmonary delivered polymeric micelles–Pharmacokinetic evaluation and

biodistribution studies. *European Journal of Pharmaceutics and Biopharmaceutics* **88**(3), 1064-1075.

Hu, Y., Xie, J., Tong, Y.W., and Wang, C.-H. (2007). Effect of PEG conformation and particle size on the cellular uptake efficiency of nanoparticles with the HepG2 cells. *Journal of Controlled Release* **118**(1), 7-17.

Huang, Barua, S., Sharma, G., Dey, S.K., and Rege, K. (2011). Inorganic nanoparticles for cancer imaging and therapy. *Journal of Controlled Release* **155**(3), 344-357.

Huang, El-Sayed, I.H., Qian, W., and El-Sayed, M.A. (2006). Cancer cell imaging and photothermal therapy in the near-infrared region by using gold nanorods. *Journal of the American Chemical Society* **128**(6), 2115-2120.

Huang, and Wang, C.-H. (2006). Pulmonary delivery of insulin by liposomal carriers. *Journal of Controlled Release* **113**(1), 9-14.

Ibrahim, M., and Garcia-Contreras, L. (2013). Mechanisms of absorption and elimination of drugs administered by inhalation. *TherapeuticDelivery* **4**(8), 1027-1045.

Ishii, H., Hayashi, S., Hogg, J.C., Fujii, T., Goto, Y., Sakamoto, N., Mukae, H., Vincent, R., and Van Eeden, S.F. (2005). Alveolar macrophage-epithelial cell interaction following exposure to atmospheric particles induces the release of mediators involved in monocyte mobilization and recruitment. *Respiratory Research* **6**(1), 87.

Jain, K.K. (2014). *Drug Delivery System* (Springer).

Janes, K.A., Fresneau, M.P., Marazuela, A., Fabra, A., and Alonso, M.a.J. (2001). Chitosan nanoparticles as delivery systems for doxorubicin. *Journal of Controlled Release* **73**(2), 255-267.

Johansson, M.E., Ambort, D., Pelaseyed, T., Schütte, A., Gustafsson, J.K., Ermund, A., Subramani, D.B., Holmén-Larsson, J.M., Thomsson, K.A., and Bergström, J.H. (2011). Composition and functional role of the mucus layers in the intestine. *Cellular and Molecular Life Sciences* **68**(22), 3635-3641.

Jones, M.-C., Jones, S.A., Riffo-Vasquez, Y., Spina, D., Hoffman, E., Morgan, A., Patel, A., Page, C., Forbes, B., and Dailey, L.A. (2014). Quantitative assessment of nanoparticle surface hydrophobicity and its influence on pulmonary biocompatibility. *Journal of Controlled Release* **183**, 94-104.

Kaminskas, L.M., McLeod, V.M., Ryan, G.M., Kelly, B.D., Haynes, J.M., Williamson, M., Thienthong, N., Owen, D.J., and Porter, C.J. (2014). Pulmonary administration of a doxorubicin-conjugated dendrimer enhances drug exposure to lung metastases and improves cancer therapy. *Journal of Controlled Release* **183**, 18-26.

Karavasili, C., Bouropoulos, N., Sygellou, L., Amanatiadou, E.P., Vizirianakis, I.S., and Fatouros, D.G. (2016). PLGA/DPPC/trimethylchitosan spray-dried microparticles for the nasal delivery of ropinirole hydrochloride: in vitro, ex vivo and cytocompatibility assessment. *Materials Science and Engineering: C* **59**, 1053-1062.

Kean, T., and Thanou, M. (2010). Biodegradation, biodistribution and toxicity of chitosan. *Advanced Drug Delivery Reviews* **62**(1), 3-11.

Kim, Byeon, H.J., Kim, T.H., Lee, E.S., Oh, K.T., Shin, B.S., Lee, K.C., and Youn, Y.S. (2012). Doxorubicin-loaded highly porous large PLGA microparticles as a sustained- release inhalation system for the treatment of metastatic lung cancer. *Biomaterials* **33**(22), 5574-5583.

Kim, Chung, H.J., and Park, T.G. (2006). Biodegradable polymeric microspheres with "open/closed" pores for sustained release of human growth hormone. *Journal of Controlled Release* **112**(2), 167-174.

Kim, Chung, Y.-I., Kim, Y.H., and Tae, G. (2014). The modulation of the permeability and the cellular uptake of liposome by stable anchoring of lipid-conjugated pluronic on liposome. *Journal of Biomedical Nanotechnology* **10**(1), 100-108.

Kips, J.C., and Pauwels, R.A. (2001). Long-acting inhaled β2-agonist therapy in asthma. *American Journal of Respiratory and Critical Care Medicine* **164**(6), 923-932.

Kirch, J., Schneider, A., Abou, B., Hopf, A., Schaefer, U.F., Schneider, M., Schall, C., Wagner, C., and Lehr, C.-M. (2012). Optical tweezers reveal relationship between

microstructure and nanoparticle penetration of pulmonary mucus. *Proceedings of the National Academy of Sciences* **109**(45), 18355-18360.

Klein, S.G., Serchi, T., Hoffmann, L., Blömeke, B., and Gutleb, A.C. (2013). An improved 3D tetraculture system mimicking the cellular organisation at the alveolar barrier to study the potential toxic effects of particles on the lung. *Particle and Fibre Toxicology* **10**(1), 1.

Knoch, M., and Keller, M. (2005). The customised electronic nebuliser: a new category of liquid aerosol drug delivery systems. *Expert Opinion on Drug Delivery* **2**(2), 377-390.

Kono, K., Takashima, M., Yuba, E., Harada, A., Hiramatsu, Y., Kitagawa, H., Otani, T., Maruyama, K., and Aoshima, S. (2015). Multifunctional liposomes having target specificity, temperature-triggered release, and near-infrared fluorescence imaging for tumor-specific chemotherapy. *Journal of Controlled Release* **216**, 69-77.

Koussoroplis, S.J., Paulissen, G., Tyteca, D., Goldansaz, H., Todoroff, J., Barilly, C., Uyttenhove, C., Van Snick, J., Cataldo, D., and Vanbever, R. (2014). PEGylation of antibody fragments greatly increases their local residence time following delivery to the respiratory tract. *Journal of Controlled Release* **187**, 91-100.

Kreyling, W., Semmler, M., Erbe, F., Mayer, P., Takenaka, S., Schulz, H., Oberdörster, G., and Ziesenis, A. (2002). Translocation of ultrafine insoluble iridium particles from lung epithelium to extrapulmonary organs is size dependent but very low. *Journal of Toxicology and Environmental Health Part A* **65**(20), 1513-1530.

Kreyling, W.G., Semmler-Behnke, M., and Möller, W. (2006). Ultrafine particle-lung interactions: does size matter? *Journal of Aerosol Medicine* **19**(1), 74-83.

Kreyling, W.G., Semmler-Behnke, M., Seitz, J., Scymczak, W., Wenk, A., Mayer, P., Takenaka, S., and Oberdörster, G. (2009). Size dependence of the translocation of inhaled iridium and carbon nanoparticle aggregates from the lung of rats to the blood and secondary target organs. *Inhalation Toxicology* **21**(sup1), 55-60.

Kumari, A., Yadav, S.K., and Yadav, S.C. (2010). Biodegradable polymeric nanoparticles based drug delivery systems. *Colloids and Surfaces B: Biointerfaces* **75**(1), 1-18.

Labiris, and Dolovich (2003a). Pulmonary drug delivery. Part I: physiological factors affecting therapeutic effectiveness of aerosolized medications. *British Journal of Clinical Pharmacology* **56**(6), 588-599.

Labiris, and Dolovich (2003b). Pulmonary drug delivery. Part II: the role of inhalant delivery devices and drug formulations in therapeutic effectiveness of aerosolized medications. *British Journal of Clinical Pharmacology* **56**(6), 600-612.

Lahnstein, K., Schmehl, T., Rüsch, U., Rieger, M., Seeger, W., and Gessler, T. (2008). Pulmonary absorption of aerosolized fluorescent markers in the isolated rabbit lung. *International Journal of Pharmaceutics* **351**(1), 158-164.

Lai, S.K., O'Hanlon, D.E., Harrold, S., Man, S.T., Wang, Y.-Y., Cone, R., and Hanes, J. (2007). Rapid transport of large polymeric nanoparticles in fresh undiluted human mucus. *Proceedings of the National Academy of Sciences* **104**(5), 1482-1487.

Lai, S.K., Suk, J.S., Pace, A., Wang, Y.-Y., Yang, M., Mert, O., Chen, J., Kim, J., and Hanes, J. (2011). Drug carrier nanoparticles that penetrate human chronic rhinosinusitis mucus. *Biomaterials* **32**(26), 6285-6290.

Lai, S.K., Wang, Y.-Y., and Hanes, J. (2009). Mucus-penetrating nanoparticles for drug and gene delivery to mucosal tissues. *Advanced Drug Delivery Reviews* **61**(2), 158-171.

Lai, S.K., Wang, Y.-Y., Hida, K., Cone, R., and Hanes, J. (2010). Nanoparticles reveal that human cervicovaginal mucus is riddled with pores larger than viruses. *Proceedings of the National Academy of Sciences* **107**(2), 598-603.

Lamprecht, A., Saumet, J.-L., Roux, J., and Benoit, J.-P. (2004). Lipid nanocarriers as drug delivery system for ibuprofen in pain treatment. *International Journal of Pharmaceutics* **278**(2), 407-414.

Lansley, A.B. (1993). Mucociliary clearance and drug delivery via the respiratory tract. *Advanced Drug Delivery Reviews* **11**(3), 299-327.

Learoyd, T.P., Burrows, J.L., French, E., and Seville, P.C. (2008). Chitosan-based spray-dried respirable powders for sustained delivery of terbutaline sulfate. *European Journal of Pharmaceutics and Biopharmaceutics* **68**(2), 224-234.

Lesniak, A., Salvati, A., Santos-Martinez, M.J., Radomski, M.W., Dawson, K.A., and Åberg, C. (2013). Nanoparticle adhesion to the cell membrane and its effect on nanoparticle uptake efficiency. *Journal of the American Chemical Society* **135**(4), 1438-1444.

Li, Y., Xiao, K., Luo, J., Xiao, W., Lee, J.S., Gonik, A.M., Kato, J., Dong, T.A., and Lam, K.S. (2011). Well-defined, reversible disulfide cross-linked micelles for on-demand paclitaxel delivery. *Biomaterials* **32**(27), 6633-6645.

Lieleg, O., and Ribbeck, K. (2011). Biological hydrogels as selective diffusion barriers. *Trends in Cell Biology* **21**(9), 543-551.

Lieleg, O., Vladescu, I., and Ribbeck, K. (2010). Characterization of particle translocation through mucin hydrogels. *Biophysical Journal* **98**(9), 1782-1789.

Limbach, L.K., Li, Y., Grass, R.N., Brunner, T.J., Hintermann, M.A., Muller, M., Gunther, D., and Stark, W.J. (2005). Oxide nanoparticle uptake in human lung fibroblasts: effects of particle size, agglomeration, and diffusion at low concentrations. *Environmental Science &Technology* **39**(23), 9370-9376.

Lin, I.-C., Liang, M., Liu, T.-Y., Monteiro, M.J., and Toth, I. (2012). Cellular transport pathways of polymer coated gold nanoparticles. *Nanomedicine: Nanotechnology, Biology and Medicine* **8**(1), 8-11.

Lo, P.K., Karam, P., Aldaye, F.A., McLaughlin, C.K., Hamblin, G.D., Cosa, G., and Sleiman, H.F. (2010). Loading and selective release of cargo in DNA nanotubes with longitudinal variation. *Nature Chemistry* **2**(4), 319-328.

Loira-Pastoriza, C., Todoroff, J., and Vanbever, R. (2014). Delivery strategies for sustained drug release in the lungs. *Advanced Drug Delivery Reviews* **75**, 81-91.

Madlova, M., Jones, S., Zwerschke, I., Ma, Y., Hider, R., and Forbes, B. (2009). Poly (vinyl alcohol) nanoparticle stability in biological media and uptake in respiratory epithelial cell layers in vitro. *European Journal of Pharmaceutics and Biopharmaceutics* **72**(2), 438-443.

Maisel, K., Ensign, L., Reddy, M., Cone, R., and Hanes, J. (2015). Effect of surface chemistry on nanoparticle interaction with gastrointestinal mucus and distribution in the gastrointestinal tract following oral and rectal administration in the mouse. *Journal of Controlled Release* **197**, 48-57.

Makino, K., Nakajima, T., Shikamura, M., Ito, F., Ando, S., Kochi, C., Inagawa, H., Soma, G.-I., and Terada, H. (2004). Efficient intracellular delivery of rifampicin to alveolar macrophages using rifampicin-loaded PLGA microspheres: effects of molecular weight and composition of PLGA on release of rifampicin. *Colloids and Surfaces B: Biointerfaces* **36**(1), 35-42.

Malcolmson, R.J., and Embleton, J.K. (1998). Dry powder formulations for pulmonary delivery. *Pharmaceutical Science & Technology Today* **1**(9), 394-398.

Maleki, A., Lafitte, G., Kjøniksen, A.-L., Thuresson, K., and Nyström, B. (2008). Effect of pH on the association behavior in aqueous solutions of pig gastric mucin. *Carbohydrate Research* **343**(2), 328-340.

Mansour, H.M., Rhee, Y.-S., and Wu, X. (2009). Nanomedicine in pulmonary delivery. *International Journal of Nanomedicine* **4**, 299-319.

Mao, G., Sukumaran, S., Beaucage, G., Sabourgi, M.-L., and Thiyagarajan, P. (2001). PEO-PPO-PEO block copolymer micelles in aqueous electrolyte solutions: Effect of carbonate anions and temperature on the micellar structure and interaction. *Macromolecules* **34**(3), 552-558.

Matthay, M.A., Robriquet, L., and Fang, X. (2005). Alveolar Epithelium. *Proceedings of the American Thoracic Society* **2**(3), 206-213.

McCallion, O., Taylor, K., Bridges, P., Thomas, M., and Taylor, A. (1996). Jet nebulisers for pulmonary drug delivery. *International Journal of Pharmaceutics* **130**(1), 1-11.

Min, K.H., Kim, J.-H., Bae, S.M., Shin, H., Kim, M.S., Park, S., Lee, H., Park, R.-W., Kim, I.-S., and Kim, K. (2010). Tumoral acidic pH-responsive MPEG-poly (β-amino ester) polymeric micelles for cancer targeting therapy. *Journal of Controlled Release* **144**(2), 259-266.

Mindell, J.A. (2012). Lysosomal Acidification Mechanisms*. *Annual Review of Physiology* **74**, 69-86.

Modi, S., and Anderson, B.D. (2013). Determination of drug release kinetics from nanoparticles: overcoming pitfalls of the dynamic dialysis method. *Molecular Pharmaceutics* **10**(8), 3076-3089.

Moller, W., Felten, K., Sommerer, K., Scheuch, G., Meyer, G., Meyer, P., Haussinger, K., and Kreyling, W.G. (2008). Deposition, retention, and translocation of ultrafine particles from the central airways and lung periphery. *American Journal of Respiratory and Critical Care Medicine* **177**(4), 426-432.

Morimoto, K., Metsugi, K., Katsumata, H., Iwanaga, K., and Kakemi, M. (2001). Effects of low-viscosity sodium hyaluronate preparation on the pulmonary absorption of rh-insulin in rats. *Drug Development and Industrial Pharmacy* **27**(4), 365-371.

Mühlfeld, C., Rothen-Rutishauser, B., Blank, F., Vanhecke, D., Ochs, M., and Gehr, P. (2008). Interactions of nanoparticles with pulmonary structures and cellular responses. *American Journal of Physiology-Lung Cellular and Molecular Physiology* **294**(5), L817-L829.

Mukherjee, B., Santra, K., Pattnaik, G., and Ghosh, S. (2008). Preparation, characterization and in-vitro evaluation of sustained release protein-loaded nanoparticles based on biodegradable polymers. *International Journal of Nanomedicine* **3**(4), 487.

Mukherjee, J.S., Rich, M.L., Socci, A.R., Joseph, J.K., Virú, F.A., Shin, S.S., Furin, J.J., Becerra, M.C., Barry, D.J., and Kim, J.Y. (2004). Programmes and principles in treatment of multidrug-resistant tuberculosis. *The Lancet* **363**(9407), 474-481.

Müller, L., Riediker, M., Wick, P., Mohr, M., Gehr, P., and Rothen-Rutishauser, B. (2009). Oxidative stress and inflammation response after nanoparticle exposure: differences between

human lung cell monocultures and an advanced three-dimensional model of the human epithelial airways. *Journal of the Royal Society Interface***7**, S27-S40.

Müller, R.H., Mäder, K., and Gohla, S. (2000). Solid lipid nanoparticles (SLN) for controlled drug delivery – a review of the state of the art. *European Journal of Pharmaceutics and Biopharmaceutics* **50**(1), 161-177.

Mura, S., Hillaireau, H., Nicolas, J., Kerdine-Römer, S., Le Droumaguet, B., Deloménie, C., Nicolas, V.r., Pallardy, M., Tsapis, N., and Fattal, E. (2011). Biodegradable nanoparticles meet the bronchial airway barrier: how surface properties affect their interaction with mucus and epithelial cells. *Biomacromolecules* **12**(11), 4136-4143.

Mura, S., Nicolas, J., and Couvreur, P. (2013). Stimuli-responsive nanocarriers for drug delivery. *Nature Materials* **12**(11), 991-1003.

Nafee, N., Husari, A., Maurer, C.K., Lu, C., de Rossi, C., Steinbach, A., Hartmann, R.W., Lehr, C.-M., and Schneider, M. (2014). Antibiotic-free nanotherapeutics: ultra-small, mucus-penetrating solid lipid nanoparticles enhance the pulmonary delivery and anti-virulence efficacy of novel quorum sensing inhibitors. *Journal of Controlled Release* **192**, 131-140.

Natarajan, J.V., Nugraha, C., Ng, X.W., and Venkatraman, S. (2014). Sustained-release from nanocarriers: a review. *Journal of Controlled Release* **193**, 122-138.

Nel, A., Xia, T., Mädler, L., and Li, N. (2006). Toxic potential of materials at the nanolevel. *Science* **311**(5761), 622-627.

Newton, S.M., Brent, A.J., Anderson, S., Whittaker, E., and Kampmann, B. (2008). Paediatric tuberculosis. *The Lancet Infectious Diseases* **8**(8), 498-510.

Ninane, V., Vandevoorde, J., Cataldo, D., Derom, E., Liistro, G., Munghen, E., Pechéé, R., Schlesser, M., Verleden, G., and Vincken, W. (2015). New developments in inhaler devices within pharmaceutical companies: A systematic review of the impact on clinical outcomes and patient preferences. *Respiratory Medicine* **109**(11), 1430-1438.

Norris, D.A., and Sinko, P.J. (1997). Effect of size, surface charge, and hydrophobicity on the translocation of polystyrene microspheres through gastrointestinal mucin. *Journal of Applied Polymer Science* **63**(11), 1481-1492.

Nyambura, B.K., Kellaway, I.W., and Taylor, K.M. (2009). Insulin nanoparticles: stability and aerosolization from pressurized metered dose inhalers. *International Journal of Pharmaceutics* **375**(1), 114-122.

Ober, C.A., Kalombo, L., Swai, H., and Gupta, R.B. (2013). Preparation of rifampicin/lactose microparticle composites by a supercritical antisolvent-drug excipient mixing technique for inhalation delivery. *Powder Technology* **236**, 132-138.

Oh, Y.-K., and Swanson, J.A. (1996). Different fates of phagocytosed particles after delivery into macrophage lysosomes. *The Journal of Cell Biology* **132**(4), 585-593.

Ohashi, K., Kabasawa, T., Ozeki, T., and Okada, H. (2009). One-step preparation of rifampicin/poly (lactic-co-glycolic acid) nanoparticle-containing mannitol microspheres using a four-fluid nozzle spray drier for inhalation therapy of tuberculosis. *Journal of Controlled Release* **135**(1), 19-24.

Oliveira, H., Perez-Andres, E., Thevenot, J., Sandre, O., Berra, E., and Lecommandoux, S. (2013). Magnetic field triggered drug release from polymersomes for cancer therapeutics. *Journal of Controlled Release* **169**(3), 165-170.

Olmsted, S.S., Padgett, J.L., Yudin, A.I., Whaley, K.J., Moench, T.R., and Cone, R.A. (2001). Diffusion of macromolecules and virus-like particles in human cervical mucus. *Biophysical Journal* **81**(4), 1930-1937.

Ong, W., Yang, Y., Cruciano, A.C., and McCarley, R.L. (2008). Redox-triggered contents release from liposomes. *Journal of the American Chemical Society* **130**(44), 14739-14744.

Organization, W.H. (2010). *Treatment of tuberculosis: guidelines* (World Health Organization).

Pandey, Sharma, A., Zahoor, A., Sharma, S., Khuller, G.K., and Prasad, B. (2003). Poly (dl-lactide-co-glycolide) nanoparticle-based inhalable sustained drug delivery system for experimental tuberculosis. *Journal of Antimicrobial Chemotherapy* **52**(6), 981-986.

Pandey, R., and Khuller, G. (2005). Antitubercular inhaled therapy: opportunities, progress and challenges. *Journal of Antimicrobial Chemotherapy* **55**(4), 430-435.

Panyam, J., and Labhasetwar, V. (2003). Biodegradable nanoparticles for drug and gene delivery to cells and tissue. *Advanced Drug Delivery Reviews* **55**(3), 329-347.

Park, Li, X., Vogt, F.G., Hayes, D., Zwischenberger, J.B., Park, E.-S., and Mansour, H.M. (2013). Advanced spray-dried design, physicochemical characterization, and aerosol dispersion performance of vancomycin and clarithromycin multifunctional controlled release particles for targeted respiratory delivery as dry powder inhalation aerosols. *International Journal of Pharmaceutics* **455**(1), 374-392.

Park, H., and Na, K. (2013). Conjugation of the photosensitizer Chlorin e6 to pluronic F127 for enhanced cellular internalization for photodynamic therapy. *Biomaterials* **34**(28), 6992-7000.

Park, J., Fong, P.M., Lu, J., Russell, K.S., Booth, C.J., Saltzman, W.M., and Fahmy, T.M. (2009). PEGylated PLGA nanoparticles for the improved delivery of doxorubicin. *Nanomedicine: Nanotechnology, Biology and Medicine* **5**(4), 410-418.

Park, K. (2014). Controlled drug delivery systems: past forward and future back. *Journal of Controlled Release* **190**, 3-8.

Parveen, S., Misra, R., and Sahoo, S.K. (2012). Nanoparticles: a boon to drug delivery, therapeutics, diagnostics and imaging. *Nanomedicine: Nanotechnology, Biology and Medicine* **8**(2), 147-166.

Patel, A., Woods, A., Riffo-Vasquez, Y., Babin-Morgan, A., Jones, M.-C., Jones, S., Sunassee, K., Clark, S., de Rosales, R.T., and Page, C. (2016). Lung inflammation does not affect the clearance kinetics of lipid nanocapsules following pulmonary administration. *Journal of Controlled Release* **235**, 24-33.

Patton, J.S. (1996). Mechanisms of macromolecule absorption by the lungs. *Advanced Drug Delivery Reviews* **19**(1), 3-36.

Patton, J.S., and Byron, P.R. (2007). Inhaling medicines: delivering drugs to the body through the lungs. *Nature Reviews Drug Discovery* **6**(1), 67-74.

Peer, D., Karp, J.M., Hong, S., Farokhzad, O.C., Margalit, R., and Langer, R. (2007). Nanocarriers as an emerging platform for cancer therapy. *Nature Nanotechnology* **2**(12), 751-760.

Pei, Y. and Yeo, Y. (2015). Drug delivery to macrophages: Challenges and opportunities. *Journal of Controlled Release*.

Peppas, N.A., and Huang, Y. (2004). Nanoscale technology of mucoadhesive interactions. *Advanced Drug Delivery Reviews* **56**(11), 1675-1687.

Pérez-Gil, J. (2008). Structure of pulmonary surfactant membranes and films: the role of proteins and lipid–protein interactions. *Biochimica et Biophysica acta (BBA)-Biomembranes* **1778**(7), 1676-1695.

Petros, R.A., and DeSimone, J.M. (2010). Strategies in the design of nanoparticles for therapeutic applications. *Nature Reviews Drug discovery* **9**(8), 615-627.

Pilcer, G., and Amighi, K. (2010). Formulation strategy and use of excipients in pulmonary drug delivery. *International Journal of Pharmaceutics* **392**(1), 1-19.

Pinkerton, N.M., Grandeury, A., Fisch, A., Brozio, J.r., Riebesehl, B.U., and Prud'homme, R.K. (2012). Formation of stable nanocarriers by in situ ion pairing during block-copolymer-directed rapid precipitation. *Molecular pharmaceutics* **10**(1), 319-328.

Poole, G., Stradling, P., and Worlledge, S. (1971). Potentially serious side effects of high-dose twice-weekly rifampicin. *British Medical Journal***3**(5770), 343-347.

Pullan, R., Thomas, G., Rhodes, M., Newcombe, R., Williams, G., Allen, A., and Rhodes, J. (1994). Thickness of adherent mucus gel on colonic mucosa in humans and its relevance to colitis. *Gut* **35**(3), 353-359.

Ravi M, Paramesh V, Kaviya S R, et al. (2015). 3D cell culture systems: advantages and applications. *Journal of Cellular Physiology* **230**(1), 16-26.

Rawat, A., Majumder, Q.H., and Ahsan, F. (2008). Inhalable large porous microspheres of low molecular weight heparin: in vitro and in vivo evaluation. *Journal of Controlled Release* **128**(3), 224-232.

Rejman, J., Oberle, V., Zuhorn, I.S., and Hoekstra, D. (2004). Size-dependent internalization of particles via the pathways of clathrin-and caveolae-mediated endocytosis. *Biochemical Journal* **377**(1), 159-169.

Riehemann, K., Schneider, S.W., Luger, T.A., Godin, B., Ferrari, M., and Fuchs, H. (2009). Nanomedicine—challenge and perspectives. *Angewandte Chemie International Edition* **48**(5), 872-897.

Roblegg, E., Fröhlich, E., Meindl, C., Teubl, B., Zaversky, M., and Zimmer, A. (2012). Evaluation of a physiological in vitro system to study the transport of nanoparticles through the buccal mucosa. *Nanotoxicology* **6**(4), 399-413.

Roger, E., Lagarce, F., Garcion, E., and Benoit, J.-P. (2009). Lipid nanocarriers improve paclitaxel transport throughout human intestinal epithelial cells by using vesicle-mediated transcytosis. *Journal of Controlled Release* **140**(2), 174-181.

Rojanarat, W., Changsan, N., Tawithong, E., Pinsuwan, S., Chan, H.-K., and Srichana, T. (2011). Isoniazid proliposome powders for inhalation—preparation, characterization and cell culture studies. *International Journal of Molecular Sciences* **12**(7), 4414-4434.

Rothen-Rutishauser, B.M., Kiama, S.G., and Gehr, P. (2005). A three-dimensional cellular model of the human respiratory tract to study the interaction with particles. *American Journal of Respiratory Cell and Molecular Biology* **32**(4), 281-289.

Roy D, Cambre J N, Sumerlin B S. (2008). Sugar-responsive block copolymers by direct RAFT polymerization of unprotected boronic acid monomers. *Chemical Communications*, (21), 2477-2479.

Rubin, B.K. (2007). Mucus structure and properties in cystic fibrosis. *Paediatric Respiratory Reviews* **8**(1), 4-7.

Sahoo, S.K., and Labhasetwar, V. (2003). Nanotech approaches to drug delivery and imaging. *Drug Discovery Today* **8**(24), 1112-1120.

Saito, G., Swanson, J.A., and Lee, K.-D. (2003). Drug delivery strategy utilizing conjugation via reversible disulfide linkages: role and site of cellular reducing activities. *Advanced Drug Delivery Reviews* **55**(2), 199-215.

Sajjan, U., Keshavjee, S., and Forstner, J. (2004). Responses of well-differentiated airway epithelial cell cultures from healthy donors and patients with cystic fibrosis to Burkholderia cenocepacia infection. *Infection and Immunity* **72**(7), 4188-4199.

Sakagami, M. (2006). In vivo, in vitro and ex vivo models to assess pulmonary absorption and disposition of inhaled therapeutics for systemic delivery. *Advanced Drug Delivery Reviews* **58**(9), 1030-1060.

Saltzman, W.M., Radomsky, M.L., Whaley, K.J., and Cone, R.A. (1994). Antibody diffusion in human cervical mucus. *Biophysical journal* **66**(2 Pt 1), 508.

Sanders, N.N., De Smedt, S.C., Van Rompaey, E., Simoens, P., De Baets, F., and Demeester, J. (2000). Cystic fibrosis sputum: a barrier to the transport of nanospheres. *American Journal of Respiratory and Critical Care Medicine* **162**(5), 1905-1911.

Schleh, C., and Hohlfeld, J.M. (2009). Interaction of nanoparticles with the pulmonary surfactant system. *Inhalation Toxicology* **21**(s1), 97-103.

Schmid, O., Möller, W., Semmler-Behnke, M., A. Ferron, G., Karg, E., Lipka, J., Schulz, H., Kreyling, W., and Stoeger, T. (2009). Dosimetry and toxicology of inhaled ultrafine particles. *Biomarkers* **14**(S1), 67-73.

Schmitz, T., Bravo-Osuna, I., Vauthier, C., Ponchel, G., Loretz, B., and Bernkop-Schnürch, A. (2007). Development and in vitro evaluation of a thiomer-based nanoparticulate gene delivery system. *Biomaterials* **28**(3), 524-531.

Schöler, N., Olbrich, C., Tabatt, K., Müller, R., Hahn, H., and Liesenfeld, O. (2001). Surfactant, but not the size of solid lipid nanoparticles (SLN) influences viability and cytokine production of macrophages. *International Journal of Pharmaceutics* **221**(1), 57-67.

Serisier, D.J., Bilton, D., De Soyza, A., Thompson, P.J., Kolbe, J., Greville, H.W., Cipolla, D., Bruinenberg, P., and Gonda, I. (2013). Inhaled, dual release liposomal ciprofloxacin in non-cystic fibrosis bronchiectasis (ORBIT-2): a randomised, double-blind, placebo-controlled trial. *Thorax*, thoraxjnl-2013-203207.

Sham, J.O.-H., Zhang, Y., Finlay, W.H., Roa, W.H., and Löbenberg, R. (2004). Formulation and characterization of spray-dried powders containing nanoparticles for aerosol delivery to the lung. *International Journal of Pharmaceutics* **269**(2), 457-467.

Shan, W., Zhu, X., Liu, M., Li, L., Zhong, J., Sun, W., Zhang, Z., and Huang, Y. (2015). Overcoming the diffusion barrier of mucus and absorption barrier of epithelium by self-assembled nanoparticles for oral delivery of insulin. *ACS Nano* **9**(3), 2345-2356.

Sharma, A., Sharma, S., and Khuller, G. (2004). Lectin-functionalized poly (lactide-co-glycolide) nanoparticles as oral/aerosolized antitubercular drug carriers for treatment of tuberculosis. *Journal of Antimicrobial Chemotherapy* **54**(4), 761-766.

Sharma, G., Valenta, D.T., Altman, Y., Harvey, S., Xie, H., Mitragotri, S., and Smith, J.W. (2010). Polymer particle shape independently influences binding and internalization by macrophages. *Journal of Controlled Release* **147**(3), 408-412.

Sheehan, J.K., Brazeau, C., Kutay, S., Pigeon, H., Kirkham, S., Howard, M., and Thornton, D.J. (2000). Physical characterization of the MUC5AC mucin: a highly oligomeric glycoprotein whether isolated from cell culture or in vivo from respiratory mucous secretions. *Biochemical Journal* **347**(1), 37-44.

Shoyele, S.A., and Cawthorne, S. (2006). Particle engineering techniques for inhaled biopharmaceuticals. *Advanced Drug Delivery Reviews* **58**(9–10), 1009-1029.

Shvedova, A.A., Kisin, E.R., Mercer, R., Murray, A.R., Johnson, V.J., Potapovich, A.I., Tyurina, Y.Y., Gorelik, O., Arepalli, S., and Schwegler-Berry, D. (2005). Unusual inflammatory and fibrogenic pulmonary responses to single-walled carbon nanotubes in mice.

American Journal of Physiology-Lung Cellular and Molecular Physiology **289**(5), L698-L708.

Shvedova, A.A., Pietroiusti, A., Fadeel, B., and Kagan, V.E. (2012). Mechanisms of carbon nanotube-induced toxicity: focus on oxidative stress. *Toxicology and Applied Pharmacology* **261**(2), 121-133.

Singh, Jain, R.R., Soni, P., Abdul, S., Darshana, H., Gaikwad, R.V., and Menon, M.D. (2015). Preparation and evaluation of surface modified lactose particles for improved performance of fluticasone propionate dry powder inhaler. *Journal of Aerosol Medicine and Pulmonary Drug Delivery* **28**(4), 254-267.

Sleigh, M.A., Blake, J.R., and Liron, N. (1988). The propulsion of mucus by cilia. *American Review of Respiratory Disease* **137**(3), 726-741.

Smith, I. (2003). Mycobacterium tuberculosis pathogenesis and molecular determinants of virulence. *Clinical Microbiology Reviews* **16**(3), 463-496.

Smyth, H.D. (2003). The influence of formulation variables on the performance of alternative propellant-driven metered dose inhalers. *Advanced Drug Delivery Reviews* **55**(7), 807-828.

Song, Y.H., Shin, E., Wang, H., Nolan, J., Low, S., Parsons, D., Zale, S., Ashton, S., Ashford, M., and Ali, M. (2016). A novel in situ hydrophobic ion paring (HIP) formulation strategy for clinical product selection of a nanoparticle drug delivery system. *Journal of Controlled Release* **229**, 106-119.

Soppimath, K.S., Aminabhavi, T.M., Kulkarni, A.R., and Rudzinski, W.E. (2001). Biodegradable polymeric nanoparticles as drug delivery devices. *Journal of Controlled Release* **70**(1), 1-20.

Sosnik, A., Carcaboso, Á.M., Glisoni, R.J., Moretton, M.A., and Chiappetta, D.A. (2010). New old challenges in tuberculosis: potentially effective nanotechnologies in drug delivery. *Advanced Drug Delivery Reviews* **62**(4), 547-559.

Stone, K.C., Mercer, R.R., Gehr, P., Stockstill, B., and Crapo, J.D. (1992). Allometric relationships of cell numbers and size in the mammalian lung. *American Journal of Respiratory Cell and Molecular Biology* **6**(2), 235-243.

Stuart, M.A.C., Huck, W.T., Genzer, J., Müller, M., Ober, C., Stamm, M., Sukhorukov, G.B., Szleifer, I., Tsukruk, V.V., and Urban, M. (2010). Emerging applications of stimuli-responsive polymer materials. *Nature Materials* **9**(2), 101-113.

Suh, J., Dawson, M., and Hanes, J. (2005). Real-time multiple-particle tracking: applications to drug and gene delivery. *Advanced Drug Delivery Reviews* **57**(1), 63-78.

Suk, J.S., Lai, S.K., Wang, Y.-Y., Ensign, L.M., Zeitlin, P.L., Boyle, M.P., and Hanes, J. (2009). The penetration of fresh undiluted sputum expectorated by cystic fibrosis patients by non-adhesive polymer nanoparticles. *Biomaterials* **30**(13), 2591-2597.

Sun, J., Bi, C., Chan, H.M., Sun, S., Zhang, Q., and Zheng, Y. (2013). Curcumin-loaded solid lipid nanoparticles have prolonged in vitro antitumour activity, cellular uptake and improved in vivo bioavailability. *Colloids and Surfaces B: Biointerfaces* **111**, 367-375.

Sun, Q., Radosz, M., and Shen, Y. (2012). Challenges in design of translational nanocarriers. *Journal of Controlled Release* **164**(2), 156-169.

Sung, J.C., Padilla, D.J., Garcia-Contreras, L., VerBerkmoes, J.L., Durbin, D., Peloquin, C.A., Elbert, K.J., Hickey, A.J., and Edwards, D.A. (2009). Formulation and pharmacokinetics of self-assembled rifampicin nanoparticle systems for pulmonary delivery. *Pharmaceutical Research* **26**(8), 1847-1855.

Sung, J.C., Pulliam, B.L., and Edwards, D.A. (2007). Nanoparticles for drug delivery to the lungs. *TRENDS in Biotechnology* **25**(12), 563-570.

Surendrakumar, K., Martyn, G., Hodgers, E., Jansen, M., and Blair, J. (2003). Sustained release of insulin from sodium hyaluronate based dry powder formulations after pulmonary delivery to beagle dogs. *Journal of Controlled Release* **91**(3), 385-394.

Suzanne, Chan, J.G.Y., Kwok, P.C.L., Benson, B.R., Prud'homme, R.K., and Chan, H.-K. (2013). Aerosol delivery of nanoparticles in uniform mannitol carriers formulated by ultrasonic spray freeze drying. *Pharmaceutical Research* **30**(11), 2891-2901.

Svensson, O., and Arnebrant, T. (2010). Mucin layers and multilayers—Physicochemical properties and applications. *Current Opinion in Colloid & Interface Science* **15**(6), 395-405.

Svensson, O., Thuresson, K., and Arnebrant, T. (2008). Interactions between drug delivery particles and mucin in solution and at interfaces. *Langmuir* **24**(6), 2573-2579.

Takeuchi, H., Yamamoto, H., and Kawashima, Y. (2001). Mucoadhesive nanoparticulate systems for peptide drug delivery. *Advanced Drug Delivery Reviews* **47**(1), 39-54.

Tang, B.C., Dawson, M., Lai, S.K., Wang, Y.-Y., Suk, J.S., Yang, M., Zeitlin, P., Boyle, M.P., Fu, J., and Hanes, J. (2009). Biodegradable polymer nanoparticles that rapidly penetrate the human mucus barrier. *Proceedings of the National Academy of Sciences* **106**(46), 19268-19273.

Tewes, F., Brillault, J., Couet, W., and Olivier, J.-C. (2008). Formulation of rifampicin–cyclodextrin complexes for lung nebulization. *Journal of Controlled Release* **129**(2), 93-99.

Thomas, M., and Klibanov, A.M. (2003). Conjugation to gold nanoparticles enhances polyethylenimine's transfer of plasmid DNA into mammalian cells. *Proceedings of the National Academy of Sciences* **100**(16), 9138-9143.

Thompson, P.J. (1998). Drug delivery to the small airways. *American Journal of Respiratory and Critical Care Medicine* **157**(5), S199-S202.

Thornton, D.J., Rousseau, K., and McGuckin, M.A. (2008). Structure and function of the polymeric mucins in airways mucus. *Annual Review of Physiology***70**, 459-486.

Thornton, D.J., and Sheehan, J.K. (2004). From mucins to mucus: toward a more coherent understanding of this essential barrier. *Proceedings of the American Thoracic Society* **1**(1), 54-61.

Torchilin, V.P. (2007). Micellar nanocarriers: pharmaceutical perspectives. *Pharmaceutical Research* **24**(1), 1-16.

Tsapis, N., Bennett, D., Jackson, B., Weitz, D.A., and Edwards, D. (2002). Trojan particles: large porous carriers of nanoparticles for drug delivery. *Proceedings of the National Academy of Sciences* **99**(19), 12001-12005.

Ungaro, F., d'Angelo, I., Coletta, C., di Villa Bianca, R.d.E., Sorrentino, R., Perfetto, B., Tufano, M.A., Miro, A., La Rotonda, M.I., and Quaglia, F. (2012a). Dry powders based on PLGA nanoparticles for pulmonary delivery of antibiotics: modulation of encapsulation efficiency, release rate and lung deposition pattern by hydrophilic polymers. *Journal of Controlled Release* **157**(1), 149-159.

Ungaro, F., d'Angelo, I., Miro, A., La Rotonda, M.I., and Quaglia, F. (2012b). Engineered PLGA nano-and micro-carriers for pulmonary delivery: challenges and promises. *Journal of Pharmacy and Pharmacology* **64**(9), 1217-1235.

Ungaro, F., De Rosa, G., Miro, A., Quaglia, F., and La Rotonda, M.I. (2006). Cyclodextrins in the production of large porous particles: development of dry powders for the sustained release of insulin to the lungs. *European Journal of Pharmaceutical Sciences* **28**(5), 423-432.

Vehring, R. (2008). Pharmaceutical particle engineering via spray drying. *Pharmaceutical Research* **25**(5), 999-1022.

Veronese, F.M., and Pasut, G. (2005). PEGylation, successful approach to drug delivery. *Drug Discovery Today* **10**(21), 1451-1458.

Vllasaliu, D., Alexander, C., Garnett, M., Eaton, M., and Stolnik, S. (2012). Fc-mediated transport of nanoparticles across airway epithelial cell layers. *Journal of Controlled Release* **158**(3), 479-486.

Vonarbourg, A., Passirani, C., Saulnier, P., Simard, P., Leroux, J., and Benoit, J. (2006). Evaluation of pegylated lipid nanocapsules versus complement system activation and macrophage uptake. *Journal of Biomedical Materials Research Part A* **78**(3), 620-628.

Walkey, C.D., Olsen, J.B., Guo, H., Emili, A., and Chan, W.C. (2012). Nanoparticle size and surface chemistry determine serum protein adsorption and macrophage uptake. *Journal of the American Chemical Society* **134**(4), 2139-2147.

Wallace, S., Li, J., Nation, R., and Boyd, B. (2012). Drug release from nanomedicines: selection of appropriate encapsulation and release methodology. *Drug Delivery and Translational Research***2**(4), 284-292.

Walters, D.V. (2002). Lung lining liquid–The hidden depths. *Neonatology* **81**(Suppl. 1), 2-5.

Wang, Lai, S.K., Suk, J.S., Pace, A., Cone, R., and Hanes, J. (2008). Addressing the PEG mucoadhesivity paradox to engineer nanoparticles that "slip" through the human mucus barrier. *Angewandte Chemie International Edition* **47**(50), 9726-9729.

Wang, and Zhang, Q. (2012). pH-sensitive polymeric nanoparticles to improve oral bioavailability of peptide/protein drugs and poorly water-soluble drugs. *European Journal of Pharmaceutics and Biopharmaceutics* **82**(2), 219-229.

Wang, Y.-B., Watts, A.B., Peters, J.I., and Williams, R.O. (2014). The impact of pulmonary diseases on the fate of inhaled medicines—A review. *International Journal of Pharmaceutics* **461**(1), 112-128.

Wei, H., Cheng, S.-X., Zhang, X.-Z., and Zhuo, R.-X. (2009). Thermo-sensitive polymeric micelles based on poly(N-isopropylacrylamide) as drug carriers. *Progress in Polymer Science* **34**(9), 893-910.

Weibel, E.R., and Gomez, D.M. (1962). Architecture of the Human Lung Use of quantitative methods establishes fundamental relations between size and number of lung structures. *Science* **137**(3530), 577-585.

Weng, A., Manunta, M.D., Thakur, M., Gilabert-Oriol, R., Tagalakis, A.D., Eddaoudi, A., Munye, M.M., Vink, C.A., Wiesner, B., and Eichhorst, J. (2015). Improved intracellular delivery of peptide-and lipid-nanoplexes by natural glycosides. *Journal of Controlled Release* **206**, 75-90.

Westesen, K., Bunjes, H., and Koch, M. (1997). Physicochemical characterization of lipid nanoparticles and evaluation of their drug loading capacity and sustained release potential. *Journal of Controlled Release* **48**(2), 223-236.

Widdicombe, J., and Widdicombe, J. (1995). Regulation of human airway surface liquid. *Respiration physiology* **99**(1), 3-12.

Winkler, J., Hochhaus, G., and Derendorf, H. (2004). How the lung handles drugs: pharmacokinetics and pharmacodynamics of inhaled corticosteroids. *Proceedings of the American Thoracic Society* **1**(4), 356-363.

Wottrich, R., Diabaté, S., and Krug, H.F. (2004). Biological effects of ultrafine model particles in human macrophages and epithelial cells in mono-and co-culture. *International Journal of Hygiene and Environmental Health* **207**(4), 353-361.

Xing S, Guan Y, Zhang Y. (2011). Kinetics of glucose-induced swelling of P (NIPAM-AAPBA) microgels. *Macromolecules* **44**(11), 4479-4486.

Xu, Y., and Du, Y. (2003). Effect of molecular structure of chitosan on protein delivery properties of chitosan nanoparticles. *International Journal of Pharmaceutics* **250**(1), 215-226.

Yan, F., Li, L., Deng, Z., Jin, Q., Chen, J., Yang, W., Yeh, C.-K., Wu, J., Shandas, R., and Liu, X. (2013). Paclitaxel-liposome–microbubble complexes as ultrasound-triggered therapeutic drug delivery carriers. *Journal of Controlled Release* **166**(3), 246-255.

Yang, Bajaj, N., Xu, P., Ohn, K., Tsifansky, M.D., and Yeo, Y. (2009). Development of highly porous large PLGA microparticles for pulmonary drug delivery. *Biomaterials* **30**(10), 1947-1953.

Yang, Luo, J., Shi, S., Zhang, Q., Sun, X., Zhang, Z., and Gong, T. (2013). Development of a pulmonary peptide delivery system using porous nanoparticle-aggregate particles for systemic application. *International Journal of Pharmaceutics* **451**(1), 104-111.

Yang, Peters, J.I., and Williams, R.O. (2008). Inhaled nanoparticles—a current review. *International Journal of Pharmaceutics* **356**(1), 239-247.

Yang, B., Guo, C., Chen, S., Ma, J., Wang, J., Liang, X., Zheng, L., and Liu, H. (2006). Effect of acid on the aggregation of poly (ethylene oxide)-poly (propylene oxide)-poly (ethylene oxide) block copolymers. *The Journal of Physical Chemistry B* **110**(46), 23068-23074.

Yang, M., Lai, S.K., Yu, T., Wang, Y.-Y., Happe, C., Zhong, W., Zhang, M., Anonuevo, A., Fridley, C., and Hung, A. (2014). Nanoparticle penetration of human cervicovaginal mucus: The effect of polyvinyl alcohol. *Journal of Controlled Release* **192**, 202-208.

Yeates, D., Aspin, N., Levison, H., Jones, M., and Bryan, A. (1975). Mucociliary tracheal transport rates in man. *Journal of Applied Physiology* **39**(3), 487-495.

Yee, D., Valiquette, C., Pelletier, M., Parisien, I., Rocher, I., and Menzies, D. (2003). Incidence of serious side effects from first-line antituberculosis drugs among patients treated for active tuberculosis. *American Journal of Respiratory and Critical Care Medicine* **167**(11), 1472-1477.

You, J., Zhang, G., and Li, C. (2010). Exceptionally high payload of doxorubicin in hollow gold nanospheres for near-infrared light-triggered drug release. *ACS Nano* **4**(2), 1033-1041.

Young, P.M., Crapper, J., Philips, G., Sharma, K., Chan, H.-K., and Traini, D. (2014). Overcoming dose limitations using the Orbital® multi-breath dry powder inhaler. *Journal of Aerosol Medicine and Pulmonary Drug Delivery* **27**(2), 138-147.

Zahoor, A., Sharma, S., and Khuller, G. (2005). Inhalable alginate nanoparticles as antitubercular drug carriers against experimental tuberculosis. *International Journal of Antimicrobial Agents* **26**(4), 298-303.

Zambito, Y., Pedreschi, E., and Di Colo, G. (2012). Is dialysis a reliable method for studying drug release from nanoparticulate systems?—A case study. *International Journal of Pharmaceutics* **434**(1), 28-34.

Zaru, M., Mourtas, S., Klepetsanis, P., Fadda, A.M., and Antimisiaris, S.G. (2007). Liposomes for drug delivery to the lungs by nebulization. *European Journal of Pharmaceutics and Biopharmaceutics* **67**(3), 655-666.

Zhai, Y., Yang, X., Zhao, L., Wang, Z., and Zhai, G. (2014). Lipid nanocapsules for transdermal delivery of ropivacaine: in vitro and in vivo evaluation. *International Journal of Pharmaceutics* **471**(1), 103-111.

Zhang, J., Wu, L., Chan, H.-K., and Watanabe, W. (2011). Formation, characterization, and fate of inhaled drug nanoparticles. *Advanced Drug Delivery Reviews* **63**(6), 441-455.

Zhang, L., Gu, F., Chan, J., Wang, A., Langer, R., and Farokhzad, O. (2008). Nanoparticles in medicine: therapeutic applications and developments. *Clinical Pharmacology &Therapeutics* **83**(5), 761-769.

Zhang W, Zhuang A, Gu P, et al. (2016). A Review of the Three-Dimensional Cell Culture Technique: Approaches, Advantages and Applications. *Current Stem Cell Research & Therapy* **11**(4), 370-380.

Zhao (2010). Pharmaceutical foams: are they the answer to the dilemma of topical nanoparticles? *Nanomedicine: Nanotechnology, Biology and Medicine* **6**(2), 227-236.

Zhao, Li, N., Garamus, V.M., Handge, U.A., Liu, J., Zhang, R., Willumeit-Römer, R., and Zou, A. (2016). Doxorubicinhydrochloride-oleic acid conjugate loaded nanostructured lipid carriers for tumor specific drug release. *Colloids and Surfaces B: Biointerfaces*.

Zhao, Y., Moddaresi, M., Jones, S.A., and Brown, M.B. (2009). A dynamic topical hydrofluoroalkane foam to induce nanoparticle modification and drug release in situ. *European Journal of Pharmaceutics and Biopharmaceutics* **72**(3), 521-528.

Zhou, Q.T., Leung, S.S.Y., Tang, P., Parumasivam, T., Loh, Z.H., and Chan, H.-K. (2015). Inhaled formulations and pulmonary drug delivery systems for respiratory infections. *Advanced Drug Delivery Reviews* **85**, 83-99.